DIRECTING THE PARACRINE ACTIONS OF ADIPOSE STEM

CELLS FOR CARTILAGE REGENERATION

A Dissertation
Presented to
The Academic Faculty

by

Christopher S. D. Lee

In Partial Fulfillment
of the Requirements for the Degree
Doctor of Philosophy in the
Wallace H. Coulter Department of Biomedical Engineering

Georgia Institute of Technology
August 2012

DIRECTING THE PARACRINE ACTIONS OF ADIPOSE STEM CELL FOR CARTILAGE REGENERATION

Approved by:

Dr. Barbara D. Boyan, Advisor
Department of Biomedical Engineering
Georgia Institute of Technology

Dr. Robert E. Guldberg
School of Mechanical Engineering
Georgia Institute of Technology

Dr. Mary Murphy
Department of Medicine
National University Ireland Galway

Dr. Zvi Schwartz
Department of Biomedical Engineering
Georgia Institute of Technology

Dr. Anthanassios Sambanis
School of Chemical Engineering
Georgia Institute of Technology

Date Approved: April 09, 2012

ACKNOWLEDGEMENTS

I first want to thank Dr. Boyan and Dr. Schwartz for their guidance and continued support over the past four and a half years. Their mentorship was not only limited to the research bench but also directed my future career aspirations and personal life. I also want to thank my committee members: Dr. Guldberg, Dr. Murphy, and Dr. Sambanis. I especially want to thank Dr. Barry and Dr. Murphy for being such great hosts during the summer of 2008 and for imparting upon me a special appreciation for mesenchymal stem cell biology. I thank my collaborators as well: Dr. Ranly for helping me develop a better understanding of synchondrosis development, Dr. Boskey for her insights in understanding alginate calcification, Drs. Alicia and Greg Ford (Morehouse School of Medicine) with their assistance in the microarray study, Sha'Aqua Ashbury with her assistance with histology, and Angela Lin with her assistance in preparing μCT evaluation scripts for assessing growth plate morphology and cartilage regeneration.

Next I want to thank all of the graduate students, visiting doctors and faculty, and staff, many of whom have come and gone. Dr. Kinney's and Dr. Moyer's prior work was the basis for my microbead studies and Dr. Chen's and Dr. Yao's work paved the way for studying tether formation within the growth plate. Although they did not directly contribute to my Ph.D. research, I especially want to thank Dr. Bell, Dr. Raines, Dr. Wang, Dr. Olivares-Navarrete, Jamie Lazin, Reyhaan Chaudhri, Jiaxun Chen, Maryam Doroudi, Rolando Gittens, Chris Hermann, Shirae Leslie, and Jung Hwa Park for their guidance, input, assistance, and support. I also want to thank Crystal Branan Raines, Leang Chhun, Sri Vermula for their assistance with cell culture; Jamie Lazin for his assistance with many of the molecular biology assays; and Dr. Kaye and Dr. Kalisvaart

with their assistance in surgeries. I also thank Christopher Erdman, Megan Merritt, and Sharon Hyzy for their help with various assays and lab management and thank Maribel Baker and Brentis Henderson for all of their administrative help.

I must thank the research mentors I had prior to starting my Ph.D. Dr. Bonassar and Dr. Stroock took a huge risk by taking a freshman to help start their new labs. Dr. Gleghorn, Dr. Ballyns, and Dr. Kopesky were great mentors and Dr. Grodzinsky further inspired me to pursue a graduate degree in biomedical engineering. I also must thank the high school and undergraduate students who have worked for me over the years: Alex Akins, Olivia Burnsed, Siddharth Gaedpalli, Vineeth Raghuram, Elyse Watkins, and Abigail Williams. Although much of their work did not directly contribute to my Ph.D. research, I appreciate their hard work and dedication. I especially want to thank Olivia Burnsed and Elyse Watkins. Their contributions are why I am able to write this dissertation and their intellectual curiosity and passion have been inspiring. I am extremely proud of their accomplishments and future career aspirations.

I acknowledge the funding sources for my research which include the National Science Foundation Graduate Research Program, the TI:GER Program, and grants from the Price Gilbert, Jr. Foundation, Children's Healthcare of Atlanta, the Georgia Tech/Emory Center for the Engineering of Living Tissues (NSF EEC 9731643), and Department of Defense (W81XWH-11-1-0306).

Most of all, I want to thank my parents and brother for their continued support, guidance, and inspiration.

TABLE OF CONTENTS

LIST OF TABLES

LIST OF FIGURES

LIST OF ABBREVIATIONS

$1\alpha,25(OH)_2D_3$	lα,25-dihydroxy vitamin D_3
$24R,25(OH)_2D_3$	24R,25-dihydroxy vitamin D_3
AA2P	ascorbic acid 2-phosphate
ACI	autologous chondrocyte implantation
ACAN	aggrecan
Ang	angiopoietin
ANOVA	analysis of variance
ASCs	adipose stem cells
ATP	adenosine-5'-triphosphate
Bax	Bcl-2–associated X protein
Bcl2	B-cell lymphoma 2
BDNF	brain-derived neurotrophic factors
BIO	6-bromoindirubin-3'-oxime
BMP	bone morphogenetic protein
cDNA	complementary deoxyribonucleic acid
CM	chondrogenic medium
COL2	type-II collagen
COL10	type-X collagen
COMP	cartilage oligomeric matrix protein
CSF	colony stimulating factor
Dex	dexamethasone

DMEM	Dulbecco's modified Eagle's medium
DMSO	dimethyl sulfoxide
ECM	extracellular matrix
ELISA	enzyme-linked immunosorbent assay
eNOS	enzyme endothelial nitric oxide synthase
EPIC-μCT	equilibrium partitioning of an ionic contrast agent via micro-computed tomography
FBS	fetal bovine serum
FGF	fibroblast growth factor
GDNF	glial cell neurotrophic factor
GF	growth factor
GH	growth hormone
GM	growth medium
GP	growth plate
GSK-3	glycogen synthase kinase-3
GvHD	graft-versus-host disease
HGF	hepatocyte growth factor
HIF	hypoxia inducible factor
HLA	human leukocyte antigen
Hsp	heat shock protein
IDO	indoleamine 2,3-dioxygenase
IFN-γ	interferon-gammaMM
IGF	insulin-like growth factor

Ihh	Indian hedgehog
IL	interleukin
MAPK	mitogen-activated protein kinases
MMP	matrix metalloproteinase
mRNA	messenger ribonucleic acid
MSCs	mesenchymal stem cells
PBS	phosphate buffered saline
PCR	polymerase chain reaction
PDGF	platelet derived growth factor
PGE2	prostaglandin E2
PTHrP	parathyroid hormone-related peptide
PTHLH	parathyroid hormone linked hormone
RGD	arginine-glycine-aspartic acid
RT	reverse transcription
TIMP	tissue inhibitor of metalloproteinase
TGF-β	transforming growth factor-beta
RPS18	ribosomal protein S18
RUNX2	runt-related transcription factor 2
SDF	stem cell-derived factor
SOS	spheno-occipital synchondrosis
SOX9	sex determining region Y-box containing gene 9
VEGF-A	vascular endothelial growth factor-A

SUMMARY

Current cartilage regeneration techniques are ineffective in directly restoring the mechanical and biological functions of native hyaline cartilage. Therefore, using the paracrine actions of stem cell therapies to stimulate endogenous cartilage regeneration has gained momentum. Adipose stem cells (ASCs) are an attractive option for this endeavor because of their accessibility, chondrogenic potential, and secretion of factors that promote connective tissue repair. In order to use the factors secreted by ASCs to stimulate cartilage regeneration, the molecular signaling mechanisms that affect postnatal cartilage development and changes in morphology need to be understood. Next, approaches need to be developed to tailor the secretory profile of ASCs and to evaluate their effect on cartilage regeneration. Finally, delivery methods that localize ASCs within a defect site while facilitating paracrine factor secretion need to be optimized.

The growth plate is a unique model for understanding cartilage development because the different temporal stages of chondrogenesis are spatially organized in hierarchical zones within this tissue. Counter-intuitively though, X-ray opaque tethers that link the epiphysis and metaphysis have previously been observed in rat tibial growth plates and increase with age as the growth plate (GP) becomes thinner. To determine if tether formation is a regulated process of GP maturation, we tested the hypotheses that tether properties and distribution can be quantified by µCT, that rachitic growth plates typical of vitamin D receptor knockout (VDR-/-) mice have fewer tethers and altered tether distribution, and that tether formation is regulated by signaling via the VDR. Distal femoral GPs from VDR+/+ and VDR-/- 8-week old C57Bl/6 mice were analyzed

with μCT and then processed for decalcified and undecalcified histomorphometry. A wide range of parameters that assessed GP and tether geometry and morphology, along with tether distribution, was measured using both μCT and histology. Growth plates of 10 week old VDR+/+ and VDR-/- mice on a high calcium, phosphorus, lactose, and vitamin D3 rescue diet were also analyzed. Both microCT and histology showed tethers present throughout normal mice GPs, while reduction in tether number and volume percentage occurred in VDR-/- GPs with localization to the central region. Decreased shrinkage in the axial direction during decalcified histological processing correlated with tether formation, suggesting mechanical stability due to tethers. Tether formation increased greatly between 8 and 10 weeks. Rescue diets restored VDR-/- GP size but not tether volume percentage. Overall, these results demonstrated μCT imaging's utility for analyzing tether formation and suggested that signaling via the vitamin D receptor plays a pivotal role in tether formation.

Although observed in the growth plate, it is unknown if tethers are present in other growth centers, if they are regulated in a comparable manner, or if they have a functional role in skeletal development or stability. To address this, distal femoral growth plates (GPs) and spheno-occipital synchondroses (SOSs) of wild-type C57Bl/6 mice from 2 to 15 weeks of age were analyzed using μCT scans. The GPs and SOSs of VDR+/+ and VDR-/- mice fed regular or rescue diets to restore mineral homeostasis until 10 weeks of age were also scanned. Tethers in GPs and SOSs both thickened and accumulated in number as these growth centers decreased in size. Ablating the VDR made GPs and SOSs rachitic and nearly eliminated tether formation. Rescue diets restored the volume of both growth centers but only partially restored growth center

thickness and tether formation, suggesting that $1\alpha,25$-dihydroxy vitamin-D_3 partially regulates tether formation in these growth centers via its receptor. In VDR+/+ mice 2-15 weeks in age, growth center thickness was inversely correlated to animal weight whereas tether phenotype (tether volume/growth center volume, tether number/mm, tether width, tether spacing) was significantly related to animal weight. In both 2-15 week old VDR+/+ and 10 week old VDR+/+ and VDR-/- mice on normal and rescue diets, tether phenotype (tether number/mm, tether spacing) had strikingly similar relationships to growth center thickness. These results showed that tethers are present in growth centers in different anatomic and undergo developmental changes in a comparable manner; in both sites, VDR-regulated tether formation is strongly linked to growth center morphology; and tether formation is associated with body weight, suggesting a role in maintaining growth plate stability during growth.

After developing a better intuition of the signaling mechanisms that regulate cartilage formation, effective strategies are needed to direct the secretion of multiple growth factors from ASCs. ASCs differentiated in chondrogenic medium have previously been used to directly replace chondrocytes, but it is unknown if chondrogenic treatment alone can optimize ASC growth factor secretion for cartilage regeneration. The objective of this next study was to determine the effects chondrogenic medium and its components have on growth factor production from ASCs in order to promote cartilage regeneration. ASCs isolate from male Sprague Dawley rats and cultured in monolayer or alginate microbeads were treated with growth (GM) or chondrogenic medium (CM) for 5 days. In subsequent studies, ASC monolayers were treated with GM supplemented with different combinations of 50 µg/mL ascorbic acid-2-phosphate (AA2P), 100 nM

dexamethasone (Dex), 10 ng/mL TGF-β1, and 100 ng/mL BMP-6 or CM excluding different combinations of AA2P, Dex, TGF-β1, and BMP-6. Gene expression 8 hours after the last media change and growth factor production over 24 hours were quantified. Gene array analysis showed that ASCs had high mRNA levels of signaling molecules in the TGF-β and MAPK signaling pathways compared to liver mRNA. CM increased mRNA levels and secretion of TGF- β2, TGF- β3, and IGF-I, and decreased mRNA levels and secretion of VEGF-A and FGF-2 while microencapsulation in GM increased production of IGF-I, TGF- β2, and VEGF-A. In both GM and CM, AA2P increased IGF-I and TGF-β2 secretion and decreased FGF-18 mRNA levels and VEGF-A secretion, Dex increased BMP-2 and FGF-18 mRNA levels and decreased VEGF-A secretion, TGF-β1 increased FGF-2 and VEGF-A secretion and decreased IGF-I and PTHrP mRNA levels, and BMP-6 increased noggin and FGF-18 gene mRNA levels and TGF-β2 secretion. These results showed that differentiation media components have distinct effects on ASCs and can be used to tailor ASC trophic factor secretion to regenerate different musculoskeletal tissues.

After observing these findings in rat-derived ASCs, human ASCs were investigated. Microencapsulating human ASCs in injectable microbeads can enhance the delivery and localization of these therapies, but their ability to act as growth factor production sources are still unknown. To address this concern, the effects of microencapsulation in both GM and CM on ASC growth factor expression and secretion from 6 donors were studied. Additionally, the effects of crosslinking and alginate compositions on growth factor expression and production were determined. For ASCs derived from different donors, microencapsulation increased PTHrP mRNA levels and

secretion of IGF-I and TGF-β3. Meanwhile, CM decreased FGF-2 mRNA levels and VEGF-A secretion from ASC microbeads derived from the same donor population. Crosslinking microbeads in $BaCl_2$ instead of $CaCl_2$ did not eliminate the beneficial effects of microencapsulation, but did decrease IGF-I mRNA levels and production. Increasing the guluronate content of the alginate microbead increased TGF-β3 mRNA levels and IGF-I maintained within the microbeads. Decreasing the molecular weight of the alginate used eliminated the effects microencapsulation had on increasing IGF-I secretion while increasing the molecular weight of alginate used decreased PTHrP mRNA levels. This study demonstrated that microbeads can enhance growth factor secretion from human ASCs and may serve as a reliable source for delivering multiple growth factors to regenerate cartilage.

After thorough characterization of ASCs' secretory profiles under different preconditioning treatments, a better understanding of how ASCs and their secreted factors influence cartilage regeneration was needed. Therefore, the effects ASC-secreted factors have in repairing chondral defects were studied. ASCs isolated from male Sprague Dawley rats were cultured in monolayer or alginate microbeads supplemented with GM or CM. Subsequent co-culture, conditioned media, and in vivo cartilage defect studies were performed. ASC monolayers and microbeads cultured in CM had decreased FGF-2 mRNA levels and VEGF-A secretion compared to ASCs cultured in GM. Chondrocytes co-cultured with GM-cultured ASCs for 7 days had decreased mRNAs for col2, comp, and runx2. Chondrocytes treated for 12 or 24 hours with conditioned medium from GM-cultured ASCs had reduced sox9, acan, and col2 mRNAs; reduced proliferation and proteoglycan synthesis; and increased apoptosis. ASC-conditioned

medium also increased endothelial cell tube lengthening whereas conditioned medium from CM-cultured ASCs had no effect. Treating ASCs with CM reduced or abolished these deleterious effects while adding a neutralizing antibody for VEGF-A eliminated ASC-conditioned medium induced chondrocyte apoptosis and restored proteoglycan synthesis. FGF-2 also mitigated the deleterious effects VEGF-A had on chondrocyte apoptosis and phenotype. When GM-grown ASC pellets were implanted in 1 mm non-critical hyaline cartilage defects *in vivo*, cartilage regeneration was inhibited as evaluated by radiographic and equilibrium partitioning of an ionic contrast agent via μCT imaging. Histology revealed that defects with GM-cultured ASCs had no tissue ingrowth from the edges of the defect whereas empty defects and defects with CM-grown ASCs had similar amounts of neocartilage formation. Based on these findings, ASCs must be treated to reduce the secretion of VEGF-A and other factors that inhibit cartilage regeneration, which can significantly influence how ASCs are used for repairing hyaline cartilage.

Before the modified paracrine actions of ASCs can be used to repair cartilage, delivery within alginate microbeads needs to be optimized. Alginate calcification has been previously reported clinically and during preclinical studies; however no study has investigated the mechanism, extensively characterized the mineral, or evaluated multiple methods to regulate or eliminate mineralization. In the present study, alginate calcification was first studied *in vitro*: calcium-crosslinked alginate beads sequestered surrounding phosphate while forming traces of hydroxyapatite. Calcification *in vivo* was then examined in nude mice using alginate microbeads with and without ASCs. Variables included the delivery method, site of delivery, sex of the animal, time *in vivo*, crosslinking solution, and method of storage prior to delivery. Calcium-crosslinked

alginate microbeads mineralized when injected subcutaneously or implanted intramuscularly after 1 to 6 months. More extensive analysis with histology, μCT, FTIR, XRD, and EDS showed calcium phosphate deposits throughout the microbeads with surface mineralization that closely matched hydroxyapatite found in bone. Incorporating 25μM bisphosphonate reduced alginate calcification whereas using barium chloride eliminated mineralization. Buffering the crosslinking solution with HEPES at pH 7.3 while washing and storing samples in basal media prior to implantation also eliminated calcification *in vivo*. This study showed that alginate processing prior to implantation can significantly influence bulk hydroxyapatite formation and presents a method to regulate alginate calcification.

Finally, once the formulation of alginate microbeads was optimized, the method in which they were delivered into cartilage focal defects needed to be modified to promote cartilaginous tissue infiltration. ASC microbeads preconditioned with GM and CM were implanted into 3 mm critically-sized xiphoid defects. In a separate study, ASC microbeads preconditioned in GM and CM and immobilized in an RGD-conjugated hydrogel mixture were implanted into 2 mm critically-sized defects. ASC microbeads implanted without the hydrogel mixture did not promote cartilage regeneration within the defect after 35 days and performed no better than empty microbeads. ASC microbeads preconditioned with GM and immobilized within a RGD-conjugated hydrogel promoted limited tissue infiltration and perichondrium formation after 35 days. Meanwhile, ASC microbeads preconditioned with CM and immobilized within a RGD-conjugated hydrogel promoted tissue infiltration from the edges of the defect and perichondrium. The RGD-conjugated hydrogel alone did not promote any tissue deposition within the

defect. The results from this study showed that both the paracrine actions of ASC microbeads and a biomimetic scaffold that facilitates cell migration may be needed to facilitate focal cartilage defect regeneration.

This work was innovative because it developed a novel micro-CT evaluation method to study 3D tether morphology within anatomically distinct growth centers. This work also established a new set of criteria to investigate the therapeutic potential of stem cell therapies while developing methods to control the paracrine actions of ASCs for cartilage regeneration. Furthermore, this work created new formulations and methods to control the extent of alginate calcification *in vivo* and tissue infiltration within a focal cartilage defect. This work was significant because it determined the molecular mechanism that regulates tether formation within the growth plate and proposed the functional role these mineralized structures may have in cartilage and bone development. Additionally, this work showed that VEGF-A secreted by ASCs can inhibit cartilage regeneration and that preconditioning methods can reduce secretion of this angiogenic growth factor while increasing secretion of chondrogenic growth factors. Finally, this work showed that alginate can form hydroxyapatite *in vivo* via its calcium crosslinks and that both paracrine actions of ASCs and biomaterials that promote cell migration are needed to promote cartilage regeneration.

CHAPTER 1

SPECIFIC AIMS

Current cartilage repair methods are ineffective in restoring the mechanical and biological functions of native hyaline cartilage. Therefore, using the paracrine actions of stem cell therapies to stimulate endogenous cartilage regeneration has gained momentum. Adipose stem cells (ASCs) are an attractive option for this endeavor because of their accessibility, chondrogenic potential, and secretion of factors that promote connective tissue repair. In order to use the factors secreted by ASCs to stimulate cartilage regeneration, the signaling pathways that affect postnatal cartilage development and morphology need to be understood. Next, approaches need to be developed to tailor the secretory profile of ASCs to promote cartilage regeneration. Finally, delivery methods that localize ASCs within a defect site while facilitating paracrine factor secretion need to be optimized.

The *overall objective* of this thesis was to develop an ASC therapy that could be effectively delivered in cartilage defects and stimulate regeneration via its paracrine actions. The *general hypothesis* was that the secretory profile of ASCs can be tailored to enhance cartilage regeneration and be effectively delivered to regenerate cartilage *in vivo*. The *overall approach* used the growth plate as an initial model to study changes in postnatal cartilage morphology and the molecular mechanisms that regulate it, different media treatments and microencapsulation to tailor growth factor production, and alginate microbeads to deliver ASCs *in vivo* to repair cartilage focal defects.

1

SPECIFIC AIM 1: Determine the molecular mechanism that regulates morphology of a model cartilaginous tissue.

The growth plate is a well-defined model for understanding the molecular mechanisms involved in post-natal cartilage development and may elucidate the paracrine factors needed for cartilage regeneration. However, the three-dimensional temporal morphology of the growth plate and the signaling pathways involved in regulating morphology are not well-characterized. Previous studies described the presence of tethers that link the epiphysis and metaphysis of the growth plate, but it is not known if tether formation is a regulated process of growth plate maturation and needs to be taken into account when designing regeneration therapies. The *objectives* were to determine how the three dimensional morphology of the growth plate changes over time and to determine the molecular mechanism that regulates morphology. The *hypothesis* was that the decrease in growth plate size is correlated to the increase in tether formation with time and that tether formation is regulated, in part, by vitamin D receptor-mediated signaling. Histology and µCT reconstructions were used to study growth plate morphology and tether formation in different murine models.

SPECIFIC AIM 2: Determine if ASCs can be manipulated to secrete paracrine factors that can promote cartilage regeneration.

ASCs produce a wide array of growth factors and it is unknown what effects these molecules may have in cartilage regeneration. Additionally, techniques that enhance secretion of favorable growth factors and inhibit production of unfavorable ones can

improve the therapeutic potential of ASCs. The *objectives* were to determine what growth factors ASCs produce, to determine how microencapsulation and media treatments can be used to tailor growth factor secretion, and to investigate how the paracrine actions of these ASCs may affect chondrocytic behavior and cartilage regeneration. The *hypotheses* were that media treatments and microencapsulation have distinct effects on ASC growth factor production and that these secreted factors can enhance chondrocytic behavior and cartilage regeneration. Gene expression and protein production of growth factors from ASCs under different treatments were quantified, the influence ASC secreted factors had on chondrocytic behavior were studied in a series of co-culture and conditioned media experiments, and the effect ASCs had on cartilage regeneration was studied in a non-critical focal cartilage defect.

SPECIFIC AIM 3: Determine if ASC microbeads can be effectively delivered to regenerate cartilage in vivo.

A delivery method that localizes ASCs within a defect site, facilitates the long-term secretion of ASC-produced factors, and promotes cartilage infiltration is needed to effectively use the paracrine actions of ASCs to regenerate cartilage. We have previously developed an injectable microbead technology that can localize ASCs inside the body, however, it is unknown if it can facilitate mass transfer of therapeutic factors or promote tissue ingrowth into defects. The *objective* was to determine if ASC microbeads can facilitate the secretion of ASC-produced therapeutic factors to promote cartilage regeneration in a defect. The *hypothesis* was that microbeads can be used to deliver ASCs into cartilage defects and promote cartilage regeneration. The performance of

different alginate microbead formulations were evaluated *in vivo* and implanted into cartilage focal defects made in the xiphoid.

The outcomes of this study were expected to show that ASC microbeads secrete factors that can influence cartilage regeneration. In addition, this study provided a new set of criteria to evaluate the therapeutic potential of stem cell therapies. The research was significant because it provided greater insight into cartilage and adult stem cell biology while addressing problems with current cartilage repair techniques. This insight has the potential to create better cell therapies.

CHAPTER 2

BACKGROUND AND LITERATURE REVIEW

CURRENT CARTILAGE REGENERATION METHODS

There is a large and growing demand to develop effective cartilage regeneration methods. Approximately 1.5 million arthroscopic surgical procedures are performed on the knee each year [1], many of which aim to repair histologic and macroscopic lesions in articular cartilage [2]. These lesions are generated during the course of many joint diseases, most notably osteoarthritis, the largest form of disability in the industrialized world [3]. Current treatments for these types of tissue damage involve drug therapy and reparative surgeries like microfracture to manage the pain. However, patients treated with these techniques often experience short-term pain relief and develop progressive symptoms because of continued tissue deterioration [4-6]. Eventually, patients with osteoarthritis receive a total joint replacement. Although these procedures are relatively successful in alleviating pain and restoring partial function, total joint replacements typically need implant revision surgeries every 10 to 20 years and have significantly higher morbidity and mortality with each subsequent procedure [7, 8].

Because of these treatment options' shortcomings, regenerative medicine is viewed by many clinicians as the ultimate goal for treating cartilage damage and disease. Autologous chondrocyte implantation (ACI) was the first FDA-approved therapy aimed to regenerative cartilage lesions before the need for total joint arthroplasty and has gained scientific and clinical support [9, 10]. However, high variability in cartilage quality and

functional outcomes, possibly due to low cell retention in the defect site and dedifferentiation of chondrocytes during *in vitro* expansion, have led to limited adoption [11, 12]. Therefore, second generation cell implantation therapies for cartilage regeneration have implemented scaffolds [13, 14] along with characterized or modified chondrocytes [15, 16] in clinical studies.

The objective of scaffolds for second generation cell therapies approved in Europe is to keep cells localized within the defect site while providing a template for extracellular matrix (ECM) deposition. However, preclinical trials have suggested that cell viability on scaffolds is low once implanted [17, 18]. Genetically-modified chondrocytes or selected chondrocytes are undergoing pre-clinical and human trials to see if these cells can maintain their chondrocytic phenotype and create more functional cartilage [19-21]. However, due to donor site morbidity, the supply of reliable autologous chondrocytes is limited. At the same time, the clinical efficacy and consistency of any allogeneic graft or cell therapy is questionable due to possible disease transmission and immune rejection [22, 23]. Therefore, cell therapies using autologous adult stem cells to regenerate cartilage are being investigated.

Mesenchymal stem cells derived from bone marrow (MSCs) and adult stem cells derived from adipose tissue (ASCs) are the two most commonly used stem cells for pre-clinical and clinical trials to regenerate cartilage [24, 25]. They have a greater clinical potential compared to autologous chondrocytes because they provide a larger and more easily accessible pool of cells that can be differentiated into chondrocytes. However, current stem cell therapies have critical shortcomings. First, once implanted, these cells are known to have homing capabilities and migrate through the vasculature to different

6

sites in the body [26-30]. Additionally, it is difficult to control stem cell chondrogenesis. Under-differentiated stem cells form fibrous tissue whereas overstimulated cells easily undergo hypertrophic differentiation, leading to calcification and osteophyte formation [31]. Finally, these cells have yet to form tissue with comparable biological and mechanical properties to native cartilage [24]. Therefore, a new paradigm in using stem cell therapies to regenerate cartilage needs to be developed.

Both MSCs and ASCs are known to secrete a wide range of paracrine factors that can be used to direct tissue development [32, 33]. Additionally, these cells can be easily modified to secrete the appropriate signaling factors to regenerate different types of tissues. Using the paracrine actions of stem cells to stimulate endogenous tissue regeneration eliminates the need for these cells to directly differentiate into chondrocytes and replace damaged or diseased cartilage. At the same time, this new paradigm for stem cell therapies provides a new set of criteria for scientists and clinicians to investigate the therapeutic potential of stem cell therapies.

In order to use the factors secreted by stem cells to stimulate cartilage regeneration, a thorough understanding of the signaling molecules and pathways involved in directing cartilage formation is first needed. Next, different techniques that match the secretory profile of stem cells to that seen during cartilage development need to be developed. Finally, delivery methods that localize stem cells within a defect site while facilitating paracrine factor secretion need to be optimized. The remainder of this literature review will highlight current developments in these areas of cell biology and engineering and discuss the remaining challenges to effectively integrate these distinct concepts to use stem cell paracrine factors for regenerate cartilage.

SIGNALING MOLECUES REGULATING CHONDROGENESIS

It is generally accepted that natural tissue regeneration often recapitulates developmental processes [34]. The growth plate is a unique model for understanding cartilage development because the different temporal stages of developmental chondrogenesis are spatially organized in hierarchical zones within this tissue. Proliferation and differentiation between these different zones is tightly orchestrated by numerous paracrine and endocrine signaling molecules. To understand the actions of these factors, an overview of the morphological organization of the growth plate is needed.

Morphological Organization of the Growth Plate

Resting Zone

The resting zone consists of cells that are in a relatively quiescent state with a large amount of surrounding matrix rich in aggrecan and type II collagen. This zone is also thought to provide 'stem-like' cells that supply the reserve of cells for later proliferation and subsequent growth plate expansion [35]. However, these stem-like cells have a defined proliferative capacity that is gradually exhausted and is thought to lead to growth plate fusion [36]. Therefore, epiphyseal fusion is thought to be the result, not the cause, of skeletal maturation and the term 'growth plate senescence' has been introduced [37]. Although endocrine signaling via hormones like estrogen is conventionally thought to cause growth plate senescence [38], Stevens et al. showed in transplanted growth plate studies that the growth rate of these transplanted tissues were independent of the recipient age but dependent on the donor age [39]. This finding by Stevens et al. suggests that

'growth plate senescence' may actually be regulated by paracrine signaling intrinsic to growth plate cells. It is also thought that chondrocytes in the resting zone secrete growth plate-orientating factor (GPOF), a morphogen that directs alignment of proliferative cells into their columnar structures along the axial direction of bone [35]. Although the underlying mechanism behind this cellular organization is still unknown, it is believed that the GPOF concentration gradient within the proliferative zone guides the orientation of proliferative chondrocytes [35].

Proliferative Zone

As mentioned previously, chondrocytes in the proliferative zone organize as columns and undergo mitosis. These cells are the only ones that divide in the growth plate and are also referred to being at the top of the growth zone (which also includes the prehypertrophic and upper hypertrophic zones). The columnar structures are separated from each other by ECM with large amounts of type II collagen. At the same time, this zone has relatively high oxygen and glycogen content as well as increased mitochondrial ATP production in chondrocytes [40]. At the bottom of this zone, chondrocytes increase in volume and begin to undergo hypertrophic differentiation.

Hypertrophic Zone

At the top of the hypertrophic zone, chondrocytes are well in the process of terminal differentiation and have increased their volumes by 5-10 folds, making a significant contribution to bone lengthening (bottom of the growth zone) [36]. This differentiation is associated with hypertrophy accompanied by a large increase in matrix vesicle associated alkaline phosphatase (ALP) activity and type X collagen secretion [36, 41]. The chondrocytes in this zone also have large amounts of intracellular calcium,

which is essential for the production of the aforementioned matrix vesicles [42]. The secretion of these matrix vesicles results in proteolytic remodeling and mineralization of the surrounding matrix [43, 44]. At the bottom of this zone, many of the chondrocytes undergo apoptosis as the extracellular matrix becomes calcified. Additionally, this calcified matrix becomes vascularized and is invaded with osteoblastic cells, chondroclasts, and osteoclasts [36]. All of these actions are orchestrated by an array of growth factors and signaling molecules.

PTHrP, Ihh, and TGF-β Signaling Loop

Cell proliferation within the growth plate is controlled, in part, by a local negative feedback loop involving parathyroid hormone related protein (PTHrP), Indian hedgehog (Ihh), and transforming growth factor beta (TGF-β). Cells in the peri-articular region of long bones produce PTHrP, which then delays hypertrophic differentiation by acting on cells in the lower proliferative/prehypertrophic zones. These chondrocytes have high levels of PTH/PTHrP receptors and continue to proliferate due to the binding of PTHrP to these receptors [45]. When prehypertrophic chondrocytes are too far away from PTHrP-producing cells near the bone ends, they stop proliferating, begin to undergo hypertrophic differentiation, and secrete Ihh. Ihh can then act on perichondral cells to convert them into osteoblasts and is required for sustaining endochondral ossification [46]. Ihh also stimulates cells in the perichondrium to release TGF-β1. TGF-β1 then acts upon perichondral and peri-articular cells to increase PTHrP synthesis, completing the loop [41, 47-50]. TGF-β1, 2, and 3 can also act directly on chondrocytes to directly inhibit hypertrophy and promote the synthesis of cartilaginous ECM [6, 11].

BMPs

Bone morphogenic proteins (BMPs) are a subset of the TGFβ superfamily and are well known to stimulate ectopic cartilage and bone formation [51]. They also play important roles in both the early and later stages of chondrogenesis and skeletal development. Specifically, BMPs have crucial roles in the aggregation of mesenchymal cells during limb bud development, but are also involved in the complex mechanisms in bone development [52, 53]. Furthermore, BMPs have distinct spatial expression patterns with BMP-2, -3, -4, -5, and -6 being expressed in the perichondrium; BMP-2 and -6 being expressed in hypertrophic chondrocytes; and BMP-7 being expressed in proliferating chondrocytes [36]. BMPs are also integrated into the PTHrP, Ihh, and TGF-β signaling loop by inducing Ihh expression and subsequent chondrocyte proliferation [54]. Additionally, BMP signaling pathways may inhibit FGF signaling by inhibiting FGFR1 expression [55] and BMP concentration gradients may play a role in the spatial regulation and chondrocyte proliferation and differentiation within the growth plate [37].

IGFs

Insulin-like growth factor-1 (IGF-1) is the main IGF that acts on the growth plate. It is an autocrine and paracrine factor that increase proliferation of chondrocytes [56] and is involved in bone growth pre- and postnatal [57]. Local IGF-1 synthesis in chondrocytes can be stimulated by growth hormone (GH), forming the GF/IGF-1 axis. Based on studies investigating IGF-1 null mice, it is widely believed that GH's actions on the growth plate are mainly dependent on IGF-1 [58]. Additionally, IGF-1 produced locally by growth plate chondrocytes, and not systemic IGF-1 produced by the liver, is the critical source for maintaining normal skeletal growth [59]. IGF-1 may also mediate

11

some of its effects through other growth factors since it has been show to enhance TGF-β mediated proliferation [60].

<u>FGFs</u>

Fibroblastic growth factors (FGFs) are important modulators at all stages of chondrogenesis and bone formation within the growth plate by binding to at least four different types of FGF receptors (FGFRs). At the earliest stage of chondrogenesis, multiple FGFs and FGFR2 are expressed and is thought to stimulate SOX9 gene expression [61]. FGFR2 is also expressed on perichondral cells [36]. Additionally, FGFR3 is expressed in proliferating chondrocytes while FGFR1 is expressed in prehypertrophic and hypertrophic chondrocytes [53]. Meanwhile, signaling through the FGFR3 receptor inhibits chondrocyte proliferation and down regulates Ihh expression in hypertrophic chondrocytes, therefore shortening the proliferative columns [62]. Meanwhile FGF-18 binding to FGFR3 is suggested to facilitate hypertrophic differentiation and regulate skeletal vascularization [63]. FGF-2 is involved in both the early and later stages of growth plate development by stimulating chondroprogenitor proliferation and vascular invasion [53].

<u>VEGF</u>

Vascular endothelial growth factor (VEGF), a potent mitogen for endothelial cells and initiator of angiogenesis [64, 65], is expressed in hypertrophic chondrocytes [66]. The blood vessels formed in this region enables the ingrowth of osteoblasts, which leads to ossification. An absence of VEGF causes disturbances in growth plate architecture and longitudinal growth. Specifically, calcified cartilage remains due to a decrease in osteoblast and chondroblast recruitment and differentiation, which leads to a widen

hypertrophic region and decreased trabecular bone formation [66]. Angiopoietin-1 and 2 are also expressed by hypertrophic chondrocytes of the growth plate and may modulate the effects of VEGF [67]. VEGF-signaling is also known to enhance catabolic effects on chondrocytes and cartilage such as increased MMP expression, osteophyte formation, and osteoarthritis progression in articular cartilage [68-71].

MMPs and TIMPs

Along with VEGF, MMPs are important for the later stages of hypertrophic differentiation, matrix remodeling, and vascular invasion, all of which are prerequisites to migration and differentiation of osteoclasts and osteoblasts that remove mineralized cartilage and replace it with bone. MMP-13, a downstream target of RUNX2, is expressed by terminal hypertrophic chondrocytes [53]. Deficiencies in MMP-13 lead to interstitial collagen accumulation and delayed endochondral ossification of the growth plate with a hypertrophic zone of increased size [72, 73]. MMP-9 is expressed in endothelial cells that migrate into the central region of hypertrophic cartilage. Additionally, both MMP-9 and MMP-13 are involved in degrading non-mineralized matrix during primary and secondary ossification [44, 74]. Meanwhile, membrane-bound MT1-MMP (MMP-14) is essential for chondrocyte proliferation and secondary ossification [75]. Although not studied in detail within the growth plate, tissue inhibitors of MMPs (TIMPs) also play a role in articular cartilage development, mesenchymal stem cell chondrogenesis, and osteoarthritis progression [76-78].

Other Signaling Molecules

Cartilage development and endochondral ossification are not limited to the growth factors and proteases just discussed. Wnts are another class of signaling molecules that

are involved in chondrogenesis at two distinct stages. Initially, Wnt/β-catenin acts at low levels to promote chondroprogenitor differentiation, while at later stages, high levels of Wnt act via the canonical pathway to promote hypertrophic differentiation and subsequent endochondral ossification [79, 80]. Meanwhile, hormones like vitamin D metabolite $24R,25(OH)_2D_3$ has been shown to increase resting zone chondrocyte proliferation while inhibiting the activity of processing enzymes and imparting cytoprotective effects [81, 82]. Additionally, this metabolite reduces levels of arachidonic acid and ultimately prostaglandins [83]. Prostaglandins are a class of autocrine and paracrine lipid compounds that are produced in response to proinflammatory cytokines and regulate cartilage formation and bone repair [84-87]. Meanwhile, $1\alpha,25(OH)_2D_3$ has been shown to increase maturation of growth zone chondrocytes and subsequent matrix formation [88-90]. Other hormone metabolites such as 17β-Estradiol regulates proliferation and differentiation of female chondrocytes [91] while dihydrotestosterone increases proliferation and maturation of male growth zone chondrocytes [92].
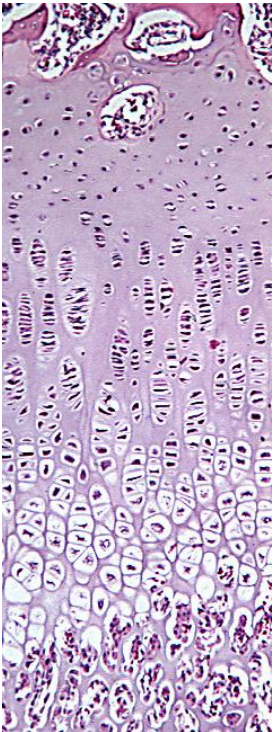
Endocrine	Paracrine		Zones
$24R,25(OH)_2D_3$	TGF-β1 Wnt-3A, 7A FGF-2/FGFR2 BMP-2,-4,-7 PTHrP		Resting
Growth Hormone 17β-Estradiol Dihydrotestosterone $1\alpha,25(OH)_2D_3$	IGF-1 FGF-2/FGFR3 BMP-2,-4, -7,-14 Ihh PGE$_2$		Proliferating
	FGF-18/FGFR3 BMP-2, -6		Hypertrophic
	FGF-2/FGFR1 Ang-1, -2 VEGF Wnt-14/β-catenin		Ossification

Figure 2.1: Signaling Molecules Regulating Chondrogenesis
Endocrine factors include hormones that can stimulate the production of paracrine factors or can directly influence proliferation and differentiation. Paracrine factors can act within specific zones or can have differential actions in multiple stages of chondrogenesis.

PARACRINE ACTIONS OF STEM CELL THERAPIES

The signaling molecules that regulate cartilage formation are numerous and have differential actions depending on the differentiation state of the recipient cell. Specifically, these factors promote and inhibit proliferation, chondrogenesis, hypertrophic differentiation, and vascular invasion. In order to use the paracrine actions of stem cell therapies to regenerate cartilage, the secretory profile of stem cells and their effects on general tissue regeneration first need to be understood. Methods then need to be developed to enhance the secretion of favorable factors while decreasing the secretion of unfavorable ones.

Stem Cell Secretory Profile and Paracrine Effects

Inflammation and Immune Modulation

Adult stem cells like MSCs and ASCs are well known to secrete a wide range of cytokines that can reduce inflammation and adaptive immunity responses [93-97]. For example, these cells secrete indoleamine 2,3-dioxygenase (IDO), TGF-β, human leukocyte antigen-G (HLA-G), and prostaglandin E2 (PGE2) to inhibit natural killer cell function [98-101]. Data also suggests that MSCs can modulate dendritic cell maturation via interleukin-6 (IL-6), M-colony stimulating factor (M-CSF), and PGE2 secretion [102-105]. Furthermore, these cells can suppress allogeneic T-cell response [99] via the secretion of TGF-β1, hepatocyte growth factor (HGF), nitric oxide, PGE2, and IDO [106-110]. Both MSCs and ASCs can also regulate hematopoietic cell production by secreting various hematopoietic cytokines such as G-CSF, M-CSF, GM-CSF, IL-7, and FMS-like tyrosine kinase 3 ligand [111, 112]. Although MSCs have underwent clinical trials for treating acute graft-versus-host disease (GvHD) by reducing severe inflammation, the results have been conflicting, possibly because the paracrine factors these cells secrete may depend on the inflammatory environment in the host [113, 114]. MSCs, ASCs, and other adult stem cell sources are also being investigated in treating autoimmune diseases such as diabetes, rheumatoid arthritis, Crohn's disease, inflammatory bowel disease, systemic lupus erythematosus, autoimmune encephalomyelitis, systemic sclerosis, and multiple sclerosis, through several ongoing preclinical, phase I, and phase II clinical trials [115-122].

Tissue Regeneration

Adult stem cells are also known enhance tissue regeneration via their paracrine actions. Specifically, they support cell survival and vascularization by secreting angiogenic and cytoprotective factors such as VEGFs, FGFs, IGF-1 and HGF [123-125]. Stem cells derived from different populations also have different secretory profiles as ASCs express IGF-1, VEGF-D, and IL-8 at higher levels than MSCs and other stem cells isolate from dermal sheath and dermal papilla [33]. MSCs and ASCs also secrete molecules such as FGF-2, VEGF, platelet-derived growth factors (PDGFs), IL-1β, IL-10, stem cell-derived factor-1 (SDF-1), HGF, IGF-1, thymosin-β4, and Wnt5a, that reduce apoptosis and necrosis in cardiomyocytes *in vitro* and *in vivo* [126-131]. These MSC and ASC-secreted factors, in addition to angiopoietin-1 and -2 (Ang-1 and -2), have also increased vascular density and blood flow in ischemic myocardium, increased cardiac function and perfusion [112, 132, 133], enhanced granulation tissue thickness, and improved epithelialization and capillary formation in chronic dermal wounds [32, 134, 135]. MSCs and other adult stem cell populations also secrete glial cell and brain-derived neurotrophic factors (GDNF and BDNF), and have been shown to increase neuron survival, differentiation, and growth in models of amyotrophic lateral sclerosis, Parkinson's Disease, and Huntington's disease [136-142].

Genetic Manipulation

MSCs and ASCs have been genetically modified to increase secretion of trophic factors via a number of different approaches, including viral and non-viral delivery of plasmids and switches for conditional gene expression [23, 143]. MSCs, ASCs, and muscle-derived stem cells have been modified to overexpress BMP-2, -4, -7, and -9, LIM

mineralization protein-1 and IGF-1 to repair critical size bone defects [144-146] while VEGF-A has also been overexpressed in ASCs to promote angiogenesis for bone repair [147]. Over expression of genes to improve stem cell graft survival has also had non-specific effects on growth factor production. MSCs overexpressed with Bcl-2 had increased VEGF-A secretion, which lead to increased capillary density and augmented functional recovery in ischemic myocardium *in vivo* [148]. Meanwhile, Akt-modified MSCs had increased secretion of VEGF, IGF-1, secreted fizzled-related protein 2, and FGF-2, which led to enhanced cardioprotective and inotropic effects on ischemic cardiomyocytes [129, 149-151].

Although genetic manipulation of stem cells can increase cell survival when delivered *in vivo* and enhance growth factor secretion, this approach also has several shortcomings. First, the ability to only target one gene at a time limits the therapeutic potential of this approach since cartilage formation is orchestrated by numerous growth factors and other signaling molecules [32, 53]. Furthermore, the potentially harmful side effects of genetic manipulation have hindered the clinical potential of these techniques [32, 152]. It is also unknown how long genetically modified stem cells can maintain their therapeutic potential *in vivo*.

Preconditioning

Preconditioning stem cells by intentionally exposing them to a specific stimulus at a defined intensity for a controlled amount of time has possible utility in enhancing the paracrine actions of these cells. Unlike genetic manipulation, preconditioning can affect production of a more global set of different trophic factors. For cartilage, this means enhancing the secretion of factors that promote chondrocyte and progenitor cell

proliferation and chondrogenesis while reducing the secretion of factors that promote hypertrophic differentiation and vascular invasion.

Hypoxic Exposure

In vitro pretreatment with hypoxic or anoxic exposure relative to normoxic atmospheric conditions (<5% O_2) provides an efficient method to precondition stem cells. These conditions up-regulate hypoxia-inducible factor-1α (HIF-1α), which then binds to the hypoxia response elements in a number of target genes, including several angiogenic growth factors [153, 154]. Although temporary exposure to hypoxic conditions had no effect on cell survival, it did increase expression of VEGF, FGF-2, IGF-1, thymosin-β4, and HGF in MSCs [148, 150, 153, 154] and secretion of VEGF-A in ASCs [155]. Additionally, hypoxic preconditioning increases expression of enzyme endothelial nitric oxide synthase (eNOS) [127, 149] and enhances the protective effects of MSCs on cardiomyocytes when transplanted into an infarcted myocardium [156].

Thermal Shock Induction

Considering the role heat shock proteins (Hsp) have in immune modulation and tissue development, thermal shock induction may be an effective method to enhance the paracrine actions of stem cells. Transient exposure to increased temperatures between 39 to 45°C increases secretion of Hsp molecules, which in turn negatively regulate Fas-mediated apoptosis and prevent proinflammatory cytokine production [157-159]. Additionally, Hsps are important in various stages of chondrogenesis. Hsp47 is a collagen-specific molecular chaperon that facilitates intracellular procollagen polypeptide synthesis and type II collagen triple helix assembly [160, 161]. Meanwhile, Hsp90 is abundant in a subpopulation of chondrocytes that are highly responsive to hormones like

GH while Hsp25 is deleterious to cartilage differentiation [161-163]. Although exposing dental pulp stem cells to hyperthermic conditions enhanced production of inflammatory modulator leukotriene B4 [164], extensive characterization of trophic factor production from various stem cell populations when exposed to thermal shock has yet to be vigorously tested.

Physical Environment

The ability of stem cells to interact with their environment to direct differentiation may also provide another method to direct growth factor production. MSCs grown on rough and hydrophilic titanium surfaces had increased secretion of TGF-β1, osteocalcin, and osteoprotegerin compared to smooth tissue culture polystyrene [165]. These same microstructured surfaces also increased expression of calcium-dependent Wnt5a and decreased expression of canonical Wnt ligands in a time-dependent manner [166]. Additionally, osteoblasts have a similar response to surface roughness and hydrophilicity, which is mediated by α2β1 integrin signaling and Dkk2 paracrine signaling [165-167]. Nanoscale features added to these microstructured Ti surfaces further increased the production of osteocalcin, osteoprotegerin, and VEGF-A from osteoblastic cells [168]. Biomimetic ligands may also be used to control growth factor production as MSCs microencapsulated in alginate microbeads modified with arginine-glycine-aspartic acid (RGD) peptides increased expression of FGF-2 compared to unmodified alginate [169]. Additionally, osteoblasts cultured on surfaces with lysine-arginine-serine-arginine (KRSR) had decreased secretion of TGF-β1 and PGE2 compared to unmodified surfaces whereas surfaces with lysine-serine-serine-lysine (KSSR) had increased levels of osteocalcin and PGE2 [170].

Mechanical and Biophysical Stimulation

Given the role mechanical loading and other biophysical stimuli have in stem cell differentiation, chondrogenesis, and cartilage homeostasis, mechanical preconditioning may serve as another mechanism to tailor the secretory profile of stem cells. Cyclic strain on MSCs increased MMP-2, -3,-13, and TIMP-2 secretion but not their mRNA levels, indicating that mechanical stimulation may have a post-translational regulatory role in paracrine factor production [171]. Subsequent actions of MMPs include modulating TGF-β1, VEGF, and FGFs in MSCs and displacing VEGF and members of the TGF-β family from extracellular matrix [53, 171, 172]. Mechanical preconditioning may also have direct effects on growth factor production as cyclic stretching of tendon fibroblasts increased secretion of TGF-β1, FGF-2, and PDGF-AB [173]. Low intensity ultrasound has been shown to increase PDGF-AB production from osteoblasts and endothelial cell lines [174] while enhancing transforming growth factor-beta 1 (TGF-β1) mediate chondrogenesis of MSCs [175], providing another viable method for preconditioning stem cells. Additionally, lasers extensively used by orthopaedic surgeons, have been shown to induce expression of Hsp70 in neural cells [176].

Pharmacologic Treatment

The cellular effects of various pharmacological agents are well characterized and may provide a viable and controllable method to tailor stem cell growth factor secretion. Dexamethasone, a potent anti-inflammatory and immunosuppressant corticosteroid, has been shown to decrease VEGF-A secretion for hemangioma-derived stem cells [177] and increase FGF-18 expression in MSCs [178]. Additionally, treating MSCs with β-mercaptoethanol increased Hsp72 expression and subsequently increased resistance to

oxidative stress [179]. MSCs and skeletal myoblasts treated with diazoxide, a potassium channel activator, enhance cell survival when implanted into ischemic environments. Specifically, diazoxide increased Akt phosphorylation, cyclooxygenase-2 and IL-11 expression levels, and secretion of Ang-1, VEGF, HGF, and FGF-2 in skeletal myoblasts [180, 181]. Verapamil, an L-type calcium channel blocker, has been shown to decrease IL-6 and VEGF production in keloid fibroblasts [182], and calcium has been shown to increase secretion of PTHrP from a variety of cell types including lung epithelial cells and human prostate and cancer cell lines [183, 184]. Other inhibitors such as 6-bromoindirubin-3'-oxime (BIO), a specific pharmacological inhibitor of glycogen synthase kinase-3 (GSK-3), has been shown to activate Wnt signaling in embryonic stem cells and help maintain their pluripotent state [185].

Biological Treatment

With the increasing number of recombinant cytokines, growth factors, hormones, and other proteins being approved as clinical therapies, preconditioning stem cells with this class of molecules may have promising results. Treating MSCs with interferon-gamma (IFN-γ) increased these cells immunosuppressive effects on T-cells and in patients with GvHD [113, 114]. Additionally, TNF-α enhanced IFN- γ induced immunosuppression activation [107, 113]. Growth factors and hormones are well-known to induce proliferation and differentiation of stem cells, but their actions on trophic factor production are only starting to become more well-defined. Injecting VEGF-A intramuscularly has been shown to increase circulating and myocardial levels of stromal-derived factor-1 (SDF-1) [186]. Additionally, both IL-6 and TGF-α have been shown to increase VEGF production from MSCs [187]. Though the effect of growth hormone on

22

IGF-1 secretion has been well-characterized, thyroid-stimulating hormone was more recently shown to up-regulate noncanonical Wnt components such as frizzled and Wnt5a and increase secretion of osteoprotegerin to attenuate bone resorption [188]. Estrogen treatments have also been shown to decrease levels of Wnt agonist sclerostin in osteoprogenitor cells in postmenopausal women [189].

DELIVERY METHODS FOR STEM CELLS AND SECRETED FACTORS

Cell encapsulation technology used to create 'living cell medicines' to provide long term drug delivery is a relatively old concept pioneered over 50 years ago [190]. The objective behind this concept was to isolate allogeneic or xenogeneic cells from the host's immune response by embedding them within permeable microcapsules that facilitated the outward diffusion of therapeutic molecules and inward diffusion of nutrients. This approach has been used as treatments for diseases of deficient hormone production such as insulin in diabetes [191], erythropoietin in anemia [192], and factors VIII and IC in hemophilia [193]. Although the optimal surface area-to-volume ratio for protein and nutrient diffusion make microcapsules the ideal candidate to deliver the paracrine actions of stem cell therapies, several modifications need to be made. First, microcapsules must improve cell protection and localization to the targeted tissue during initial delivery *in vivo*. Afterwards, microcapsules must control the temporal secretory profile of a wide range of different paracrine signaling molecules. Finally, microcapsules must have biomimetic characteristics to control cell release and engraftment and subsequent tissue integration. Possible parameters that can be adjusted to fulfill these

requirements include the biomaterials used for microencapsulation, the fabrication method, and subsequent biomimetic functionalization.

<u>Biomaterials</u>

Numerous biomaterials have been used for tissue engineering and regenerative medicine applications, but few of them are suitable for microencapsulating cells into microcapsules. Not only must they have favorable mass transfer properties, but they also must have favorable and repeatable gelation characteristics for forming microcapsules consistent in size and shape. Additionally, these materials should have parameters that are tailorable to adapt these microcapsules for different stem cell therapies.

<u>Alginate</u>

Alginate is a family of unbranched binary copolymers derived from brown seaweed and bacterium that consists of β-D-mannuronic acid (M) and α-L-guluronic acid (G) dimers that vary in proportions depending upon the source from which the alginate was isolated [194]. Specifically, the G dimers are responsible for crosslinking by sequestering divalent ions and affect the mechanical stiffness, diffusivity, biodegradability, swelling behavior, stability, and biocompatibility of alginate hydrogels [194-196]. Alginate has been the most prominent microencapsulation polymer because it has favorable mass transfer properties [197], can be molded into specific shapes [198, 199], has adjustable degradation kinetics [200-202], supports a range of different cell phenotypes [203-205], can be mechanically and biochemically modified [196, 206, 207], supports cell differentiation in large animal models [208], and is biocompatible for delivery of cells in human trials [6, 209]. Additionally, most studies use alginate in

combination with other materials. Poly-L-lysine as a polycationic shell to enhance the immunoisolation properties of microcapsules is the most common addition [204, 210].

Agarose

Agarose, a modified form of the agar material used for bacteria cell culture, is a polysaccharide derived from seaweed. Unlike alginate, agarose has the ability to form thermally reversible gels. Agarose has previously been used for cartilage tissue engineering [211, 212] and for submicron encapsulation of proteins [194]. Agarose microcapsules can be formed by using a reduction in temperature [213]. One disadvantage of using agarose for delivery of autologous stem cells is its unfavorable biodegradative properties.

Chitosan

Chitosan is a biodegradable polysaccharide derived from the deacetylation of chitin found in crustacean shells, fungi, insects, and molluscs. Chitosan forms hydrogels by ionic or chemical cross-linking with glutaraldehyde and degrades via enzymatic hydrolysis. Chitosan has been used in a number of biomedical applications such as wound dressings, drug delivery, and space-filling implants [214-216]. Because of its weak meachanical properties and limited bioactivity, it is often combined with other materials such as polyglicolic acid, calcium phosphate, and collagen [194].

Other Materials

Collagen, fibrin, and hyaluronic acid are naturally derived polymers with favorable mass transfer and gelation characteristics to deliver cells for regenerating tissues [194, 217]. Collagen gelation is controlled by changes in pH whereas fibrin is formed from the reaction between fibrinogen and thrombin. Synthetic poly (ethylene

glycol) functionalized with vinyl end groups, such as methacrylates and acrylates, employs a radical cross-linking approach involving two or more polymerizable moieties to encapsulate cells [218]. Self-assembling peptides, characterized by amino acid sequences of alternating hydrophobic and hydrophilic side groups, are a promising class of biomaterials for cell encapsulation due to the flexibility of manipulating peptide sequences to control cell adhesion and differentiation [219], scaffold degradation [220, 221], and delivery of stimulatory growth factors [222].

Fabrication Methods

Microcapsules can be classified into 3 main categories: matrix core, liquid or hollow core/shell, and cell-core shell. Matrix cores, or microbeads, consist of a porous hydrogel or polymer with cells seeded uniformly within and may have an outer shell to enhance delivery and biocompatibility. Liquid or hollow core/shells consists of a permeable protective membrane with cells suspended in liquid or adhered to the inner membrane. Cell-core shell or conformal coating consists of a cell mass surrounded by a permeable membrane. Microbeads are by far the most investigate microcapsule in preclinical and clinical studies because of their long term stability and various methods to fabricate them [217].

Extrusion

Extrusion is the most common method of forming microbeads as a viscous polymer-cell suspension – almost always consistent of alginate – is fed through a needle to form droplets that fall into a crosslinking solution containing a divalent cation. To counteract the capillary surface interactions between the extruded droplet and needle, vibration, mechanical disruption with air flow, and application of an electrostatic

potential can be used to form microbeads 25 to 500μm in diameter [194, 217].

Microencapsulation with an electrostatic potential is favorable because of the consistent

size, shape, and uniformity [223], but are not effective in forming microbeads under 100

μm. To form smaller microbeads with high mechanical stability and controlled size,

spraying techniques have been developed to encapsulate MSCs and monocytes [224].

Emulsion

Emulsion techniques are also used to encapsulate cells in agarose and alginate.

These methods involve the aqueous form of the biomaterial to be mixed and dispersed in

an immiscible organic phase, such as oil, which is often facilitated by a surfactant. When

the dispersion reaches equilibrium, microbead formation is initiated by cooling or adding

a gelling agent. Although this method has been used to encapsulate pancreatic islets

[213, 225-227], its feasibility for stem cell delivery is unknown. Despite its

advantageous scalability, large microbead size distributions and shear stress applied to

cells have limited the use of this technique.

Microfluidics

Over the past decade, the manipulation of multiphase flows in microfluidic

devices has created a new method to generate polymer particles, emulsions, and foams of

uniform shape and size [228]. This method exploits the fluid dynamics within

microchannels, such as laminar flow, to better control microbead characteristics. By

varying the flow rates of the different liquid phases, various microfluidic devices have

been able to make alginate microbeads 50 to 200μm in size [229-232]. All of these

devices extrude alginate or other hydrogels under the laminar flow of an oil phase. More

recently, this method has been combined with a bio-electrospraying technique to maintain

cell viability of microbeads containing single or multiple cells [233]. However, the use of organic solvents and surfactants and the shear forces induced by microchannels, make this approach less favorable for stem cell delivery.

Microlithography and Micromolding

In addition to forming microfluidic devices for microencapsulation, a lithographic approach has also been used directly to form alginate microcapsules with various shapes and sizes [234]. Using standard soft lithography techniques, a polydimethylsiloxane template with arrays of microwells on its surface is fabricated, filled with alginate solution, and crosslinked in $CaCl_2$, resulting into free standing alginate microcapsules. Continuous-flow microlithography processes have been proposed to increase microbead fabrication output, but none have been successful in microencapsulating cells [235]. In a similar approach to microlithography, micromolding has also been used to form microbeads. A layer of hyaluronic acid monomer and photoinitiator are place on a methacrylate glass slide and a polydimethylsiloxane stamp with void regions is placed on top. This mold is then exposed to ultraviolet light to cure the hyaluronic acid, which has successfully microencapsulated NIH-3T3 cells [236]. Although innovative, these processes have had limited use due to their limited scalability [237].

Biomimetic Functionalization

For cell microencapsulation, the biomaterial used has always been considered a simple device to entrap the cells. In order to harness the full regenerative capacity of stem cells' paracrine actions, microbeads must be able to direct stem cell behavior and the subsequent secretion profile of multiple growth factors. Therefore, microbeads must have parameters that can adjust cell adhesion to direct cell proliferation and

28

differentiation, growth factor retention to control growth factor localization and secretion, and degradation to promote cellular release and tissue regeneration.

Cell Adhesion

Biomimetic peptides modified to the polymer backbone can be used to promote cell adhesion and subsequent proliferation and differentiation. RGD in alginate hydrogels is well known to promote cell adhesion, proliferation, and FGF-2 expression [169, 205-207], but has also been shown to inhibit chondrogenesis [238]. Other peptide moieties such as IKLLI, IKVAV, LRE, PDSGR, and YIGSR have also been used to promote cell focal adhesions, which then trigger a cascade of intracellular signaling events [239-242], which can also affect trophic factor secretion from stem cells. In addition to biomimetic peptides, incorporating natural ECM components, like hyaluronic acid, for cells to adhere on has been shown to increase chondrogenesis of MSCs in alginate cultures [243].

Growth Factor Retention

ECM components and binding proteins are well known to bind growth factors, store otherwise rapidly degraded proteins, present them in a localized fashion, and release them to regulate soluble distribution [244]. A common method for controlling growth factor retention and release kinetics in biomaterials involves pre-encapsulating therapeutic proteins into PLGA microspheres which gradually releases growth factor via degradation [245]. However, this strategy does not directly control the paracrine actions of microencapsulate stem cells. An example of an alternative approach is the peptide GGWSHW derived from thrombospondin-1, which mimics its ability to bind TGF-β1 [246, 247]. Additionally, other studies suggest further biomimetic sequences that can

29

bind IL-1α [248, 249]. Methods to reversibly bind growth factors directly to fibrin scaffolds have also been investigated [250]. In spite of these potential strategies, none have been successfully implemented to control the secretory profile of microencapsulate stem cells.

Biodegradation

Strategies to promote degradation of large biomaterial and alginate constructs have been successful in decreasing mechanical properties and increasing cell proliferation and migration. Several studies by Mooney et al. have shown that oxidizing alginate polymers alters the chain conformation and promotes hydrolysis in aqueous solutions, which decreases construct compressive modulus and subsequently facilitates the deposition of cartilaginous extracellular matrix in chondrocyte seeded constructs [202, 251]. Alternatively, modifying alginate with matrix metalloproteinase (MMP)-cleavable peptides facilitated human mesenchymal stem cells (MSCs) to migrate and form cellular networks as constructs visibly decreased in size *in vitro* [252]. For specific degradation, Sarkar et al. discovered a collagen mimetic peptide containing GIAGQ that is exclusively cleaved by MMP-9 and not by trypsin or other general enzymes [253]. Additionally, poly(lactide-*co*-glycolide) (PLGA) microspheres loaded with alginate lyase have been able to degrade hydrogels, leading to a significant increase in expansion rate of encapsulated neural progenitor cells [254]. Despite these efforts, no reported strategy has been successful to control the release of cells or biologics from microbeads

CONCLUSION

Methods that direct the paracrine actions of adult stem cells to regenerate cartilage will need to integrate the latest discoveries and innovations in both cell biology and engineering. Cartilage formation, maturation, and subsequent endochondral ossification are orchestrated, in part, by a network of paracrine factors. Not only are these growth factors' actions dependent on each other, but their actions are also contingent upon the differentiation state of the recipient cell. Just as numerous and complex are the paracrine actions of adult stem cells, which naturally modulate inflammation and adaptive immunity while promoting cell survival and angiogenesis. For cartilage regeneration, different forms of genetic manipulation or preconditioning are needed to make stem cells secrete factors that cause chondroprogenitor proliferation, chondrogenesis, and matrix deposition while preventing hypertrophic differentiation and vascular ingrowth. Finally, to improve localization and viability of stem cells *in vivo* while maximizing mass transfer of their secreted factors, microbeads appear to be a promising candidate. However, modifications to the materials used, the fabrication method, and biomimetic functionalization are needed to control the spatial and temporal secretion profiles of different factors. Meanwhile, these modifications are also needed to promote cartilage infiltration and regeneration.

CHAPTER 3

FORMATION OF TETHERS LINKING THE EPIPHYSIS AND METAPHYSIS IS REGULATED BY VITAMIN D RECEPTOR-MEDIATE SIGNALING

INTRODUCTION

Vitamin D deficiency during long bone growth results in development of rickets, a condition in which the growth plate becomes extended due to a failure of the hypertrophic chondrocytes to calcify their extracellular matrix [255]. Cartilage cells within the growth plate continue to enter the zone of hypertrophy, but because there is not a concomitant removal of calcified cartilage at the metaphysis, hypertrophic cells pile up onto each other, causing the growth plate to thicken and the tissue eventually becomes deformed, leading to structural deformities in the bone.

Rachitic growth plates are also seen in mouse models that lack functional vitamin D receptors (VDR) [256, 257]. The defect can be treated by restoring serum calcium concentration [258, 259], supporting the hypothesis that rickets is due to defective calcium ion homeostasis [260]. However, vitamin D metabolites also contribute to growth plate development via mechanisms that are not directly associated with the rapid stimulation of intestinal Ca^{++} transport by the steroid hormone, $1\alpha,25$-dihydroxy vitamin D_3 [$1\alpha,25(OH)_2D_3$][83, 261].

MicroCT images of rat tibial growth plates show that the natural process of growth plate closure is marked by an accumulation of mineralized struts termed "tethers"

[262]. The tethers form perpendicular to the plane of the growth plate, connecting the epiphyseal and metaphyseal bone surfaces. Tether formation has been noted on histological sections of fusing dog, pig, and human epiphyses and has been described in the metatarsus of calves as multiple perforations of the growth plate [263]. Although the rat growth plate never fully fuses, it becomes thinner and the number and volume of these tethers rapidly increase starting at adolescence, following a sigmoidal manner over the average rat life span [262]. Investigators have used three dimensional (3D) magnetic resonance imaging (MRI) to examine human growth plates during premature closure, and have reported the presence of large bone bridges [264, 265], but it appears likely that these bone bars were due to trauma and may not be comparable to the tethers seen during normal growth plate closure.

The long bones of active adolescent animals including humans undergo an array of different directional and dynamic loading patterns with, at times, large magnitudes. In addition to absorbing these loads, the growth plate must facilitate rapid bone growth. It has been shown in 1 day old chick tibias that external loading can alter growth plate shape and gene expression while negatively impacting bone biomechanics and formation [266]. Additionally, relative mechanical behavior among the three zones of neonatal and 5 week old rat growth plates appear to be vastly different [267, 268], suggesting that growth plate composition changes significantly between birth and adolescence. Tethers that appear in the growth plate before skeletal maturation may provide the needed stability to protect the growth plate from deleterious loading while contributing to its changing mechanical behavior. Before this functional role of tethers can be investigated, however, it must first be determined if tether formation is a regulated characteristic of

normal growth plate maturation or if it is just a coincidental artifact of extracellular matrix calcification. Figuring out the mechanism controlling tether formation will be essential in developing tissue engineering or regenerative medicine strategies for treating diseased and damaged growth plates.

In order to glean further insight into how tethers originate, it would be advantageous to assess growth plates from an animal model where the genotype can be modified such as the mouse. The benefit of using microCT imaging over histology is the ability to quantitatively evaluate the growth plate and tether formation via three dimensional reconstructions without destroying the actual tissue. No study, however, has yet investigated tether formation in the growth plate in long bones of mice using microCT imaging or investigated tether formation in an animal model with an altered genotype that would affect bone development. Therefore, we took advantage of the vitamin D receptor knockout mouse model (VDR-/-) in which structural stability of the growth plate is compromised due to rickets [269] and abnormal mineral homeostasis is exhibited [256]. Symptoms of rickets and osteomalacia in VDR-/- mice are well established by 8 weeks of age with almost their entire bone surface covered with osteoid by 10 weeks of age [259]. When VDR-/- mice are fed a high calcium, phosphorus, lactose, and vitamin D_3 rescue diet, normal growth plate volume, bone mineralization, and bone mechanical properties are restored while eliminating secondary hyperparathyroidism and osteomalacia [258, 259].

We imaged the growth plates of 8-week old rachitic VDR-/- mice and their normal VDR+/+ littermates by microCT and histomorphometry to determine if microCT was an effective method for analyzing tether formation in mice. To determine if any

changes in tether formation or distribution were due to altered calcium ion homeostasis or other VDR-dependent signaling we used microCT imaging to quantify tether formation in 10-week old VDR+/+ and VDR-/- mice fed a rescue diet high in lactose, calcium, phosphate, and vitamin D_3. We hypothesized that microCT imaging would be an accurate and effective method to study tether formation in mice with different genotypes and that altered growth plate morphology associated with a nonfunctional VDR will have decreased tether formation and altered distribution. We also hypothesized that tether formation is strongly influenced by signaling via the VDR and is not an artifact of tissue calcification; therefore normal mineral homeostasis alone would not fully restore their presence in animals lacking a functional VDR.

METHODS AND MATERIALS

Animal Maintenance

Male and female VDR-/- mice and their VDR+/+ littermates were used as the animal model. The phenotypic characteristics of the VDR-/- mice have been described in detail in a series of publications [256, 269, 270]. Although the $1\alpha,25(OH)_2D_3$-dependent membrane associated PDIA3 signaling pathway is still functional in growth plate chondrocytes from these mice [271], they develop rickets due to reduced serum Ca^{++} [259]. A heterozygous [VDR+/-] breeding pair was obtained as a gift from Dr. Marie Demay (Harvard Medical School, Massachusetts General Hospital, Boston, MA), and a mouse colony was established in the Physiology Research Laboratory in the Institute of Bioengineering and Bioscience at the Georgia Institute of Technology under an Institutional Animal Care and Use Committee approved protocol. Offspring were

genotyped at two weeks after birth. VDR+/- mice were allowed to breed. Homozygous

VDR+/+ and VDR-/- mice were euthanized when 8 weeks old. This age was chosen to

ensure that the rachitic pathology was fully developed in VDR-/- mice since osteomalacia

is not observed in these mice until at least 35 days of age [259]. In addition to

genotyping, homozygotes were assessed for evidence of rickets by histologic analysis of

the costochondral cartilages. VDR-/- mice exhibited phenotypic markers of vitamin D

deficiency, including rachitic growth plates with expanded hypertrophic cell zones.

In a subsequent study, homozygous VDR+/+ and VDR null mice were also fed a

rescue diet containing 20% lactose, 2% calcium, 1.25% phosphorus, and 2200IU vitamin

D_3/kg (TD96348, Teklad, Madison, WI) from 22 days of age. These mice were then

euthanized at 10 weeks of age. This different age was selected to accurately assess the

rescue diet's effect on mineralization since over 85% of the bone surface is covered with

osteoid in VDR-/- mice fed a regular diet at this time [259].

Sample Preparation

A total of 30 animals (15 mice each for VDR+/+ and VDR-/-) were used in the

initial study and 24 more (6 mice for each genotype and diet) were used in the subsequent

study. Following euthanasia by CO_2 asphyxiation, the right femurs were disarticulated

from pelvic bone and tibia and cleaned of soft tissues by sharp dissection. The bones

were soaked in phosphate buffered saline and stored at -20ºC until used. Prior to

microCT scanning, the femurs were thawed at room temperature. After scanning, 9

specimens from the VDR+/+ and VDR-/- groups on a regular diet were randomly chosen

and fixed in 10% buffered formalin for 24 hours with post fixation in 70% ethanol and

processed for histology. One specimen from each group was used for undecalcified bone

histology and the remaining eight specimens were decalcified and embedded in paraffin ad described below.

MicroCT Processing

The VDR-/- mouse was generated in a C57BL/6 background [269]; accordingly, in a preliminary study, C57BL/6 mice were used to verify that mice also possess growth plate tethers (data not shown). Based on these observations, the distal portion of the right femurs of VDR-/- mice and their VDR+/+ littermates were scanned by microCT (μCT 40, Scanco Medical, Switzerland) with a voxel size of 16μm. The growth plate was contoured and isolated from the microCT scan by reconstructing the image at a specific value identified to threshold out all soft tissue including the growth plate (Figure 3.1A). Scanco software was used to invert the image and contour out the growth plate while calculating the average thickness and growth plate volume along with the tether volume within the growth plate. 3D color images representing the range of X-ray attenuation values were generated to visualize growth plate morphology and distribution of X-ray opaque regions signifying calcified tethers. Projections of these images were then used to measure projected growth plate and tether area using Image Pro Plus software (MediaCybernetics, Bethesda, MD). To assess tether distribution, a 3D color image derived from the microCT scan of a representative VDR+/+ growth plate was marked with ellipses coded from 1 to 12 to form a distribution map based on the distribution of tethers (Figure 3.1B). This map was then overlaid on all 3D color images of both VDR+/+ and VDR-/- growth plates to assess the distribution of the tethers within each region. The probability of finding tethers in any one region of the growth plate was determined by counting the tethers within each of the 12 ellipses on the growth plate

map. The probability index was defined as the percentage of samples with tethers in each area.

Histological Processing

One specimen in each group was fixed and processed for undecalcified histomorphometry. Sagittal sections were stained with silver nitrate to detect the presence of tethers in growth plate. Undecalcified specimens were used to orient histological sections in order to compare different measured parameters from histological analysis to 3D reconstruction of microCT images (Figure 3.1A).

Because of the difficulties associated with doing serial sectioning on undecalcified samples, eight femurs in each group were then decalcified and processed for histologic analysis. Paraffin-embedded sagittal sections 4μm in thickness were consecutively sliced with a microtome (Micom HM 355s Rotary microtome, Germany), and every fourth section was stained with haematoxylin and eosin. VDR-/- growth plates averaged 400 slices, whereas VDR+/+ growth plates averaged 300 slices. The growth plates of microscope images (Leica DMLB, Germany) of each stained section were outlined and tethers, defined as sharp changes in texture and color that span the growth plate and resembled the bordering bone, were subsequently outlined for histomorphometric analysis (Figure 3.1C). After marking the tethers directly on each serial micrograph, a 3D reconstruction of tether dimension was generated so that each tether was counted only once in the overall assessment of the growth plate. Moreover, this allowed us to directly compare the histological image with the corresponding three-dimensional microCT image.

Comparing MicroCT Assessment to Histology

To determine whether microCT images of tethers based on X-ray refraction correlated with histological micrographs of bone-like tissue bridging the growth plate, we rotated the 3D microCT image and created secondary ISQ images using Scanco software to match the orientation of histological images and aligned the microCT image accordingly (Figure 3.1A). In order to do this, it was necessary to calculate a shrinkage percentage for the VDR-/- and VDR+/+ tissues following histological processing using morphometric data from the histological and microCT images of the same orientation. Shrinkage percentage was determined in part by normalizing the difference between the microCT and histological values to the microCT value.

After alignment of the microCT image with the histological image, the vertical height (GP thickness), horizontal length, and number of tether were determined on histology sections using Image Pro Plus. In histology images, growth plate volume was calculated by equation 1:

GP Volume $= \Sigma A_i \times 16\mu m$ (1)

where A_i is the growth plate area of a particular serial section in the sagittal direction, i is the total number of serial sections of the growth plate, and 16µm is the interval between each serial section.

Tether volume within the growth plate was approximated in a similar manner for each tether detected in histology sections. Tether volume percentage for each growth plate was then calculated by dividing tether volume by growth plate volume for both

histological and microCT analysis. Projected growth plate area was calculated utilizing equation 2:

Projected GP Area = Σ $L_i \times$ 16µm (2)

where L_i is the growth plate length in the horizontal direction, i is the total number of serial sections of the growth plate, and 16µm is the interval between each serial section. Tether projected area was calculated in a similar fashion. Additionally, tether area percentage for each growth plate was calculated by dividing tether projection area by growth plate projection area for both histological and microCT analysis.

<u>Statistical Analysis</u>

There were no statistically significance differences between male and female samples for all measured parameters so data for each measurement were expressed as overall means ± standard errors. Student's t-test comparing VDR+/+ to VDR-/- mice and 2-way ANOVA comparing VDR+/+ to VDR-/- on regular and rescue diets were performed with Statistix (Analytical Software, FL, USA) using a post-hoc Tukey test for pairwise comparison (p<0.05) to determine statistical differences. The correlations between histological measurements and microCT measurements were investigated by linear regression in Minitab 15 (Minitab Inc., State College, PA, USA). The correlation coefficient for each parameter was compared with a critical value for the number of corresponding measurements in the study to determine statistical significance (2-tail analysis, p<0.05) [272].
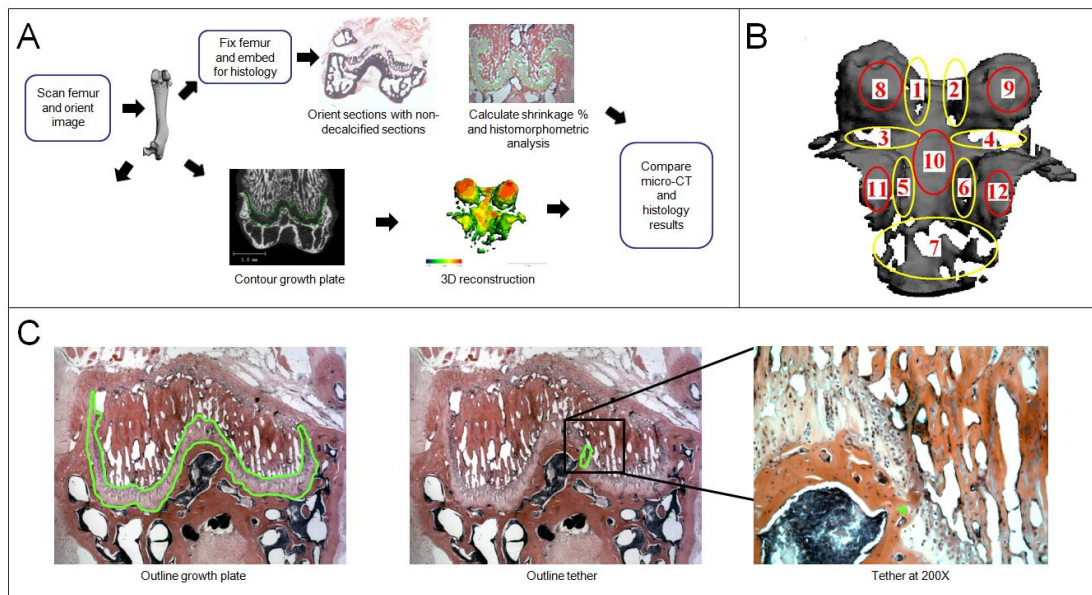
Figure 3.1: Micro-CT and Histological Evaluations of the Growth Plate
(A) Schematic of growth plate morphology and tether distribution analysis with both micro-computed topography and (B) Outline of how tethers were quantified using histomorphometric analysis (C)Tether distribution map overlaid on a typical VDR+/+ mouse distal femoral growth plate used to assess the distribution of the tethers within each region of all growth plates.

RESULTS

Micro-Computed Tomography Analysis

Analysis of the microCT images showed that the projected growth plate area in the VDR-/- mice was more than twice that seen in VDR+/+ growth plates (Figure 3.2A). Moreover, microCT analysis revealed that average growth plate thickness was more than five times greater in VDR-/- femurs compared to VDR+/+ controls (Figure 3.2B) and growth plate volume was more than six times greater in VDR-/- animals than VDR+/+ mice (Figure 3.2C). Serial microCT images showed significant differences between VDR+/+ and VDR-/- growth plates (Figure 3.3A-F). In general, serial images separated by 40µm showed that VDR+/+ mice had narrow growth plates, thin distinct tethers distributed throughout the length of the growth plate, and frequent changes in both

growth plate morphology and tether distribution along the sagittal direction (Figure 3.3A-C). Meanwhile, serial sections separated by 70μm showed that VDR-/- femurs had large growth plates, a large and weakly visible tether localized to the center of the growth plate, and relatively few changes in both growth plate morphology and tether distribution along the sagittal axis (Figure 3.3D-F).
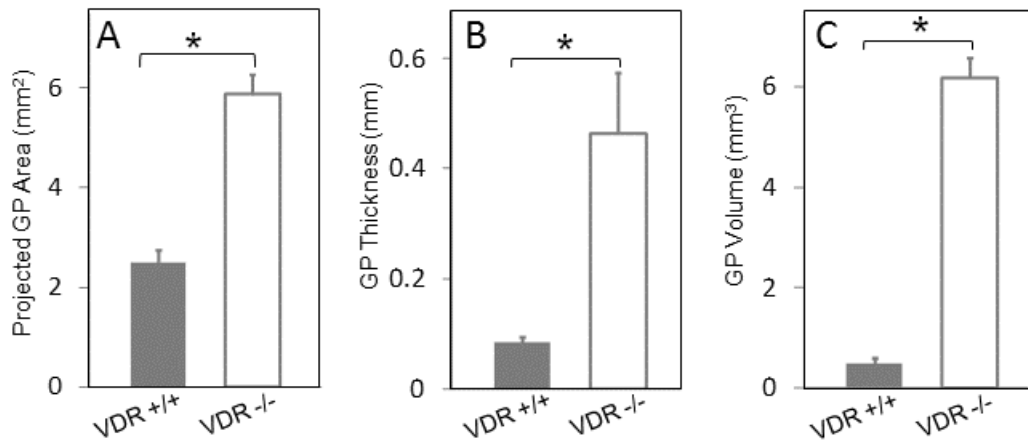
Figure 3.2: Parameters of 3-D Morphology of VDR+/+ and VDR-/- Growth Plates
(A) Projected growth plate area, (B) average growth plate thickness, and (C) growth plate volume for VDR+/+ and VDR-/- femurs calculated from 3D micro-CT images; For each measured parameter, n=15±SE. (*) $p < 0.05$ for VDR-/- compared to VDR+/+.

Distribution of tethers in the VDR -/- growth plates also differed from their distribution in VDR+/+ animals as seen in 3D color images of the growth plate (Figure 3.3G, H) and highlighted by the table of probability indexes for each region (Table 3.1). Tethers most frequently occurred throughout peripheral regions of 1 to 7 in VDR+/+ growth plates, while most tethers in VDR-/- mice were in the central part in region 10. Probability indexes also indicate that whereas tethers were present in all VDR+/+ growth plates, not all VDR-/- growth plates had tethers. The number of tethers in femoral growth plates experienced a 20-fold reduction when VDR was knocked out (Figure 3.4B). At the same time, projected tether area percentage decreased by 99% (Figure

3.4C) and projected tether area per growth plate in VDR-/- mice was one quarter of the projected tether area in VDR+/+ mice (Figure 3.4D). Tether volume percentage had a 92% reduction when VDR was knocked out (Figure 3.4E); however, the tether volume per growth plate remained about the same regardless of VDR genotype (Figure 3.4F).
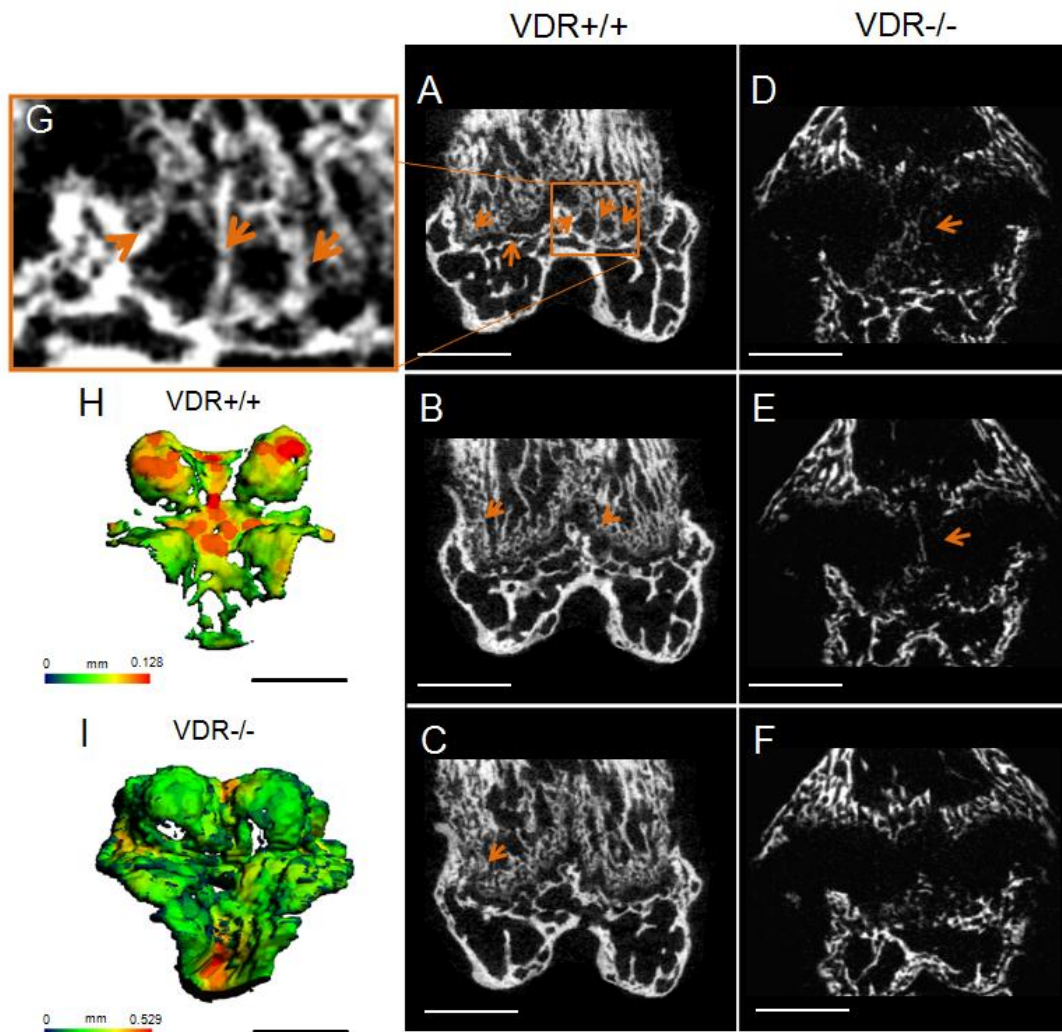
Figure 3.3 Micro-CT 3-D Evaluation of VDR+/1+ and VDR-/- Growth Plates
(A-C) Serial micro-CT images of a VDR+/+ growth plate separated by 40µm. (D-F) Serial micro-CT images of a VDR-/- growth plate separated by 70µm. Orange arrows point to tethers crossing the growth plate. (G) Magnified micro-CT image of tethers (H) 3-D micro-CT color image of a VDR+/+ growth plate and (I) VDR-/- growth plate. White spots represent X-ray opaque tethers. For all images, bar represents 1mm.

Table 3.1: Tether Probability Index and Distribution in the Growth Plate

Region	VDR+/+ (%)	VDR-/- (%)
1	93.3	0
2	100	6.7
3	100	6.7
4	100	6.7
5	93.3	0
6	86.7	0
7	100	0
8	13.1	0
9	47.4	6.7
10	13.3	2
11	26.7	0
12	60	0

Histological Analysis

Growth plates in the distal femurs of VDR-/- and VDR+/+ mice exhibited differences in their shrinkage properties following decalcified histological processing (Figure 3.4A). While no differences in projected growth plate area shrinkage were seen in VDR-/- and VDR+/+ specimens following histological processing, there was a greater loss of growth plate volume and growth plate thickness in mice lacking a functional VDR. Histological sections indicate that knocking out VDR incurs a 5.5 fold reduction in the number of tethers present in the growth plate (Figure 3.4B). In addition, projection tether area percentage was decreased by 63% (Figure 4C) but projected tether area per growth plate was 2.7 times larger in VDR-/- femurs (Figure 3.4D). Tether volume percentage decreased by 84% (Figure 3.4E) but tether volume per growth plate was statistically the same for both VDR+/+ and VDR -/- growth plates (Figure 3.4F).
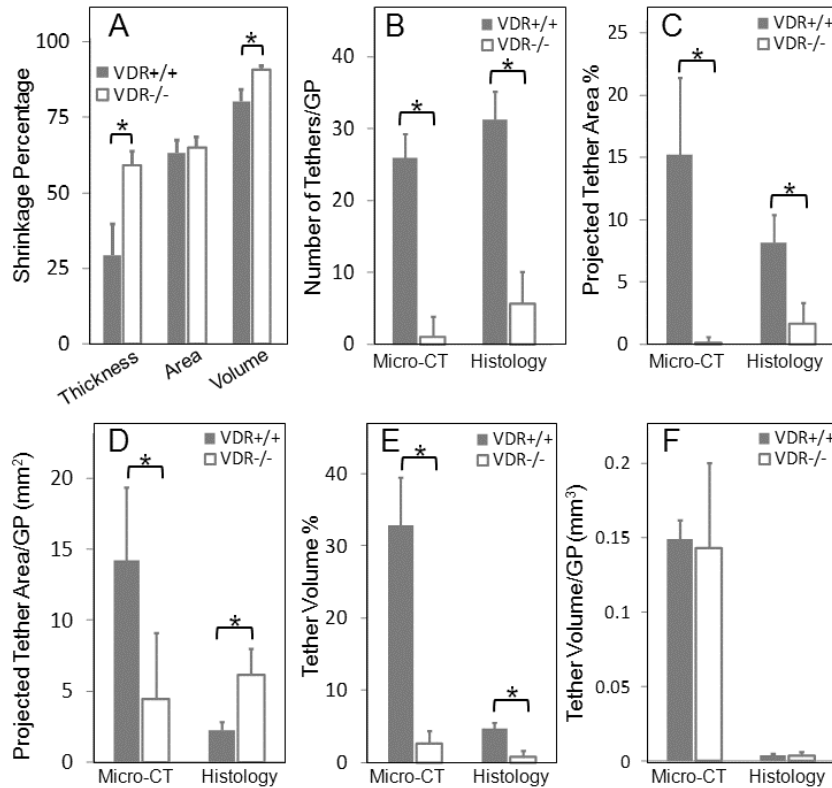
Figure 3.4: Parameters of Tethers in VDR+/+ and VDR-/- Growth Plates
(A) Shrinkage percentages for VDR+/+ and VDR-/- growth plates during histological processing (n=8±StDev). (B) Number of tethers, (C) projected tether area percentage, (D) projected tether area per growth plate, (E) tether volume percentage, (F) tether volume per growth plate for VDR+/+ and VDR-/- femurs measured from micro-CT images and histology sections. n=15±SE for micro-CT and n=8±SE for histology. (*) p<0.05 for VDR-/- compared to VDR+/+.

Decalcified histology showed VDR-/- mice exhibited changes in their femoral epiphyses characteristic of rickets. Serial sections of VDR-/- mice had expanded growth plates and the epiphyseal bone contained enlarged marrow spaces and thin trabeculae in comparison with VDR+/+ mice (Figure 3.5D-F). Additionally, growth plates in the VDR-/- femurs had an expanded hypertrophic cell zone and the tissue was malformed and disorganized. Rather than the well-defined W-shaped morphology seen in the VDR+/+ animals, the VDR-/- growth plates were distended, resulting in a wider metaphysis. This was reflected in the need to cut 400 serial sections for the VDR-/-

growth plates versus 300 sections for the VDR+/+ specimens. Tethers in haematoxylin and eosin stained sections were defined as regions of darker staining that span the growth plate and resembled the surrounding metaphyseal and epiphyseal bone they linked. Tethers were evident in the undecalcified histologic images of the VDR+/+ growth plates and evolved quickly in the sagital direction (Figure 3.5A-C), but few, if any, were seen in the VDR-/- growth plates and were mainly localized to the center of the growth plate (Figure 3.5D-F).
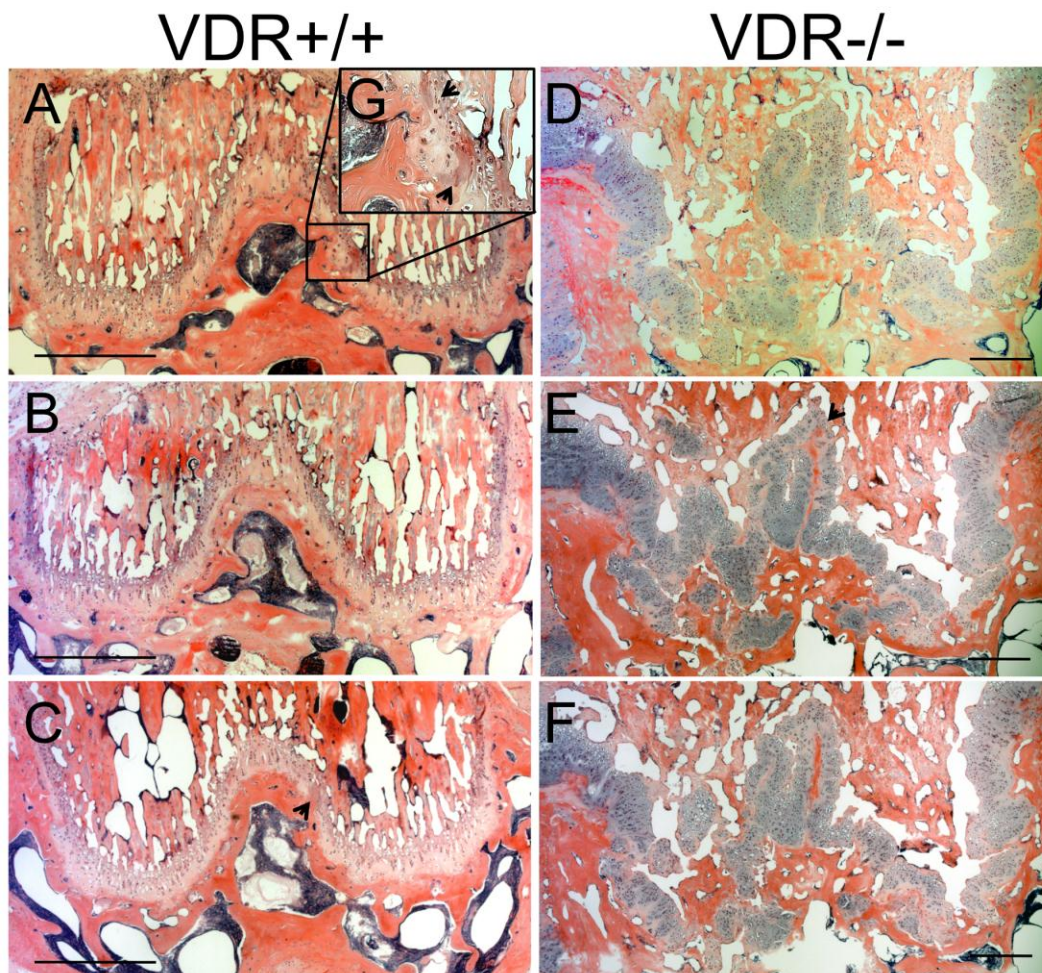
Figure 3.5: Serial Histology of VDR+/+ and VDR-/- Growth Plates
(A-C) Serial decalcified histological micrographs of a VDR+/+ growth plate separated by 48μm. (D-F) Serial decalcified histological micrographs of a VDR-/- growth plate separated by 48μm. Black arrows point to tethers crossing the growth plate. For all micrographs, bar represents 100μm.

<u>Comparison between Histological and MicroCT Analyses</u>

Measurements by histological and microCT analyses exhibited similar trends when comparing VDR+/+ femurs to VDR-/- femurs for all tether parameters except for projected tether area per growth plate (Figure 3.4B-F). When analyzed by linear regression, histological and microCT measurements of growth plate thickness, projected area, and volume were highly correlated (Figure 3.6A-C) with microCT measurements being 2-9 times larger due to shrinkage during decalcified histological processing (Figure 3.4A). The number of tethers per growth plate measurements were correlated between the two analytical techniques (Figure 3.6D), whereas measurements for the tether area percentage and tether volume percentage had lower correlation coefficients (Figure 3.6E, F). Measurements from histology sections and microCT imaging were not correlated for either tether area per growth plate nor bone volume per growth plate (Data not shown).
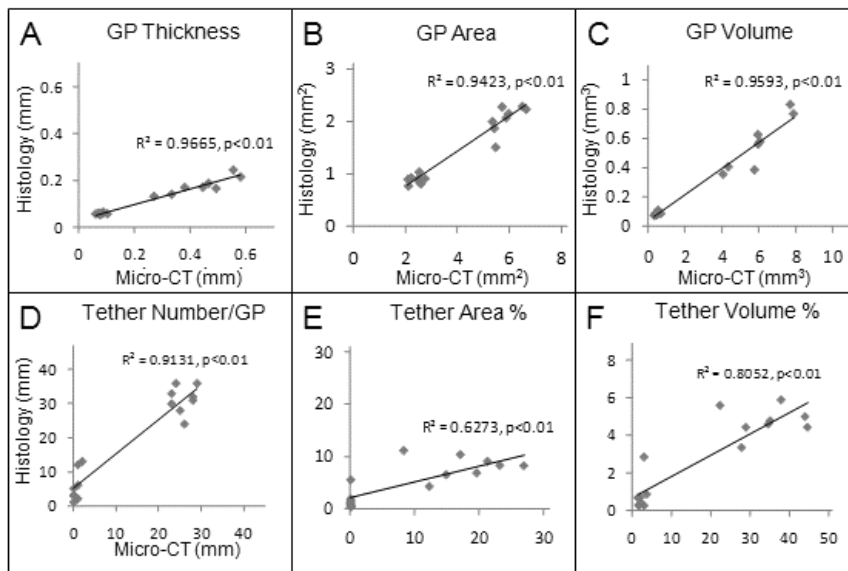
Figure 3.6: Comparison of Micro-CT and Histology Parameters
(A) Micro-CT measurement versus histological measurement for individual samples of growth plate thickness, (B) growth plate projected area, (C) growth plate volume, (D) number of tethers, (E) tether projected area percentage, and (F) tether volume percentage. Each comparison has n=16.

Shrinkage percentages due to decalcified histological processing of each sample were then compared to corresponding microCT measurements of tether parameters. Linear regression analysis showed that tether volume percentage was highly correlated with decreased shrinkage in both growth plate thickness and volume and the number of tethers also showed strong correlations to decreased shrinkage percentages for both thickness and volume (Table 3.2). Correlations between tether area percentage and decreased thickness and volume shrinkage were not as strong. Meanwhile, none of the tether parameters were correlated with projected growth plate area shrinkage.

Table 3.2: Correlation (R^2 values) Between Shrinkage Percentages and Tether Parameters (n=16)

	Tether Number	Tether Volume %	Tether Area%
Shrinkage % of thickness	0.816, p<0.01	0.872, p<0.01	0.643, p<0.01
Shrinkage % of area	0.143, p>0.1	0.089, p>0.1	0.059, p>0.1
Shrinkage % of volume	0.824, p<0.01	0.862, p<0.01	0.576, p<0.02

Rescue Diet

The rescue diet was effective in restoring VDR-/- growth plate volume at 10 weeks of age (Figure 3.7A) as growth plate volume was reduced by 88.6% compared to VDR-/- growth plates treated with a regular diet, and there was no statistical difference between wild type and knock out samples. Additionally, rescue diets had no effect on VDR+/+ growth plate volume. For mice fed a regular diet, 10 week old VDR+/+ growth plate volumes were 20% smaller than VDR+/+ growth plate volumes at 8 weeks, but 10 week old VDR-/- growth plates volumes were 11.7% larger than VDR growth plate volumes at 8 weeks (Figures 3.7A, 2C). 3D colored images showed extensive tether formation throughout the growth plate at 10 weeks compared to 8 week old samples (Figure 3.7B, 3.3H).

Rescue diet treatment did not restore normal tether formation in VDR-/- growth plates at 10 weeks of age. VDR null mice on a rescue diet had a 26 fold increase in tether volume percentage compared to VDR-/- mice on a regular diet but only restored 12.4% of the total volume percentage compared to VDR+/+ growth plates (Figure 3.7C). Also, rescue diets did not have a statistically significant effect on VDR+/+ tether volume percentage. For mice fed a regular diet, 10 week old VDR+/+ growth plates had a 78% larger tether volume percentage compared to 8 week old VDR+/+ growth plates but 8 week old VDR-/- growth plates had a 87% higher tether volume percentage compared to 10 week old VDR-/- growth plates (Figure 3.7B, 3.4E). Tether distribution in VDR-/- growth plates treated with a rescue diet also resembled growth plates of VDR-/- mice on a normal diet (Figure 3.7D, 3.3I).
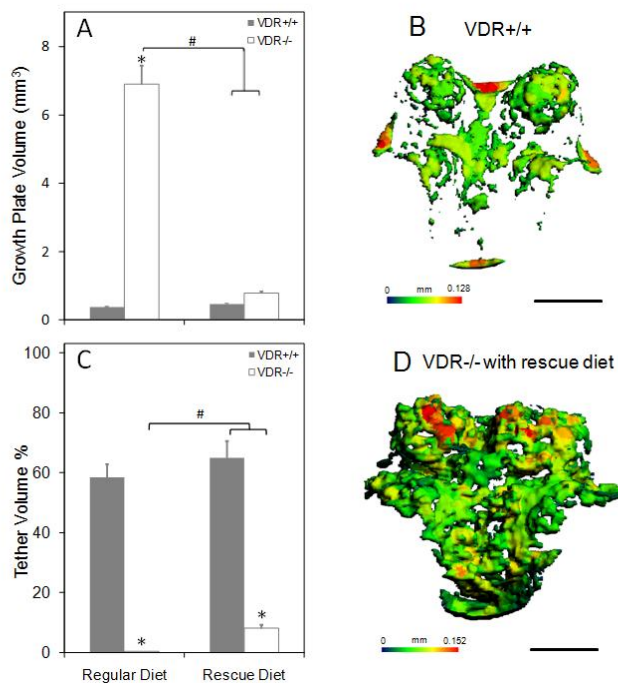
Figure 3.7: Morphology of Growth Plates and Tethers of VDR+/+ and VDR-/- Mice
(A) Growth plate volume (B) 3-D micro-CT color image of a VDR+/+ growth plate at 10 wks (C) Tether volume percentage (D) VDR-/- growth plate on a rescue diet. n=6 ±SE, (*) $p < 0.05$. For all images, white spots represent X-ray opaque tethers; bar represents 1mm.

DISCUSSION

This study is the first to show that mouse femoral growth plates, like rat tibial growth plates [262], contain X-ray opaque bone-like tethers visible by microCT. Moreover, it is the first to thoroughly show by direct morphometric analysis that X-ray opaque bone-like tethers evident in microCT images correspond to specific morphological entities in histological micrographs of the same tissues. In addition, this study shows for the first time that the lack of a functional VDR results in a marked reduction in tether formation, as well as alterations in tether morphology and anatomic distribution. This study also demonstrates that normal mouse growth plates at 8 and 10 weeks are different in both size and tether composition and that knocking out the VDR has increasing adverse effects with age. Finally, this study shows that the presence of tethers is not solely dependent on normal mineral homeostasis and that signaling via the VDR not associated with extracellular calcium ion content may be involved in tether formation.

The rachitic pathology in the distal femur of VDR-/- mice seen in this study was characterized by a broadening of the epiphysis and metaphysis as a consequence of loss of morphologic integrity of the VDR-/- growth plates. This was consistent with the previous reports of VDR-/- murine growth plates [270], including a significant increase in thickness due to the expansion of the hypertrophic cell zone, leading to bowing of the epiphyses. In addition to changes in the growth plate, the bones were also affected, exhibiting large marrow spaces and thin trabeculae, which previous investigators linked to increased mechanical fragility [259].

Our results demonstrated the utility of using microCT to assess growth plate structural elements in a volumetric manner. MicroCT images showed that many tethers were distributed throughout the growth plate in VDR+/+ mice but a fewer amount were limited to the central region in VDR-/- growth plates. Tethers in VDR+/+ growth plates were thin and appeared highly calcified whereas tethers present in VDR-/- were thicker with little calcification. These microCT observations were validated histologically. Non-decalcified sections were used to orient the growth plate to the microCT image and serial sections of decalcified paraffin embedded tissue provided a means to assess the effectiveness of using 3D reconstructions from microCT imaging to evaluate tether formation. Structures reminiscent of "multiple tide-lines and a sharp change in texture" observed during epiphyseal closure in mammals [263] connected the epiphysis and metaphysis in decalcified serial sections of the VDR+/+ femurs. In contrast, tether distribution and morphology were affected by the lack of a functional VDR in the VDR-/- mice.

Although the tether volume percentage and number of tethers in microCT images and decalcified histological micrographs of VDR-/- tissues were markedly reduced, tether volumes for both VDR+/+ and VDR-/- growth plates remained the same. This finding suggests that although tether formation is significantly decreased when the VDR is knocked out, the length of the tether increases significantly with growth plate thickness causing the tether volume within the growth plate to remain constant. The growth plate volume, however, is increased by the thickness cubed, which is why tether volume percentage is significantly less without a functional VDR.

The projected tether area percentage per growth plate decreased significantly for both microCT and histological measurements in VDR-/- tissues, but microCT measurements of projected tether area per growth plate decreased whereas histological measurements increased in VDR-/- femurs. This result suggests that projected tether area is a poor assessment of tether formation since it does not take into account the sinuous contours of the growth plate. The inability of projected tether area to predict tether formation is further confirmed as measurements by histology and microCT showed no correlation. The relatively wide range of tether volume per growth plate values measured by microCT compared to narrow distribution of values measured by decalcified histology may imply that microCT imaging is more sensitive in detecting the presence of tethers. Furthermore, strong correlations between microCT and histological measurements of growth plate geometry, tether number, and tether volume percentage emphasize that microCT imaging is an effective imaging and analytical modality for studying tether formation.

Thus, even though microCT and histological measurements were generally correlated with each other, differences did exist between the actual measurements. Several reasons may explain why there were similar trends but absolute differences for some of the measured parameters. First and foremost, tissue shrinkage accounts for most of the discrepancies between microCT and histological analyses, and histological processing may cause additional damage to the tissue structure. At the same time, since tethers are heterogeneously distributed throughout the growth plate tissue shrinkage may not be uniform within the tissue. In addition, due to the small size of the mouse femurs, it is possible that the very thin tethers visible in histological sections may have been

below the voxel size resolution of microCT imaging used in this study. Additionally, hematoxylin and eosin staining of decalcified sections may not be as effective in detecting the presence of calcified structures in the growth plate compared to microCT imaging.

It was surprising that thickness and volume shrinkage percentages were statistically different between VDR+/+ and VDR-/- growth plates but the projected area shrinkage percentage was about the same. Further analysis showed that decreased shrinkage in growth plate thickness and volume were strongly correlated to tether formation whereas projected area shrinkage had no dependence on tether formation. These results suggested that differences in horizontal and vertical shrinkage of VDR+/+ and VDR-/- growth plate might result from differences in mechanical properties; specifically, bone-like tethers may provide structural stability in growth plates along the axial direction.

While the mechanical properties of the growth plate have not been extensively characterized, the static compressive properties of newborn swine growth plate explants are non-uniform along its thickness with the reserve zone being twice as stiff as the proliferative and hypertrophic zones in the axial direction [267]. However, the strain patterns of loaded rat tibia growth plates reveal that at 5 weeks of age, the proliferative zone is the stiffest portion of the growth plate [268] suggesting that growth plates may exhibit different mechanical behavior due to changing tissue compositions at different stages of development. In comparing normal mice growth plates at 8 and 10 weeks in this study, noticeable differences were seen in tether volume formation. Whether or not tether formation plays a role in the temporal change of growth plate mechanical behavior

or provides mechanical stability of growth plates during bone growth and active loading, however, cannot be assessed without a more extensive measurement of tether formation throughout skeletal development and vigorous comparisons between growth plate mechanics and tether composition.

Normal mineral homeostasis imparted by a diet high in calcium, phosphorous, lactose, and vitamin D_3, was able to restore growth plate volume in mice lacking a functional VDR but was not enough to create normal levels of tether formation, suggesting that tether formation maybe dependent on signaling via the VDR not associated with extracellular calcium content. It is well known that cells in the growth plate respond to different metabolites of vitamin D_3 [83, 261], and although these metabolites can interact with a membrane receptor independent of VDR [273, 274], it seems reasonable for VDR mediated signaling to be partially responsible for tether formation. In mice with pseudo vitamin D deficiency rickets caused by mutations in the 25-hydroxyvitamin D-1α-hydroxylase gene, a high calcium diet was able to restore bone morphology and biomechanical properties but, unlike $1α,25(OH)_2D_3$ replacement therapy, was unable to restore bone growth [275]. The fact that both tether formation and bone growth are disrupted in the absence of $1α,25(OH)_2D_3$ signaling via the VDR, despite having normal bone structure and mechanics, should be further investigated and may provide beneficial insight into skeletal development. Additionally, it will be important to determine what other biological factors are required for tether development in order to truly understand their function. Knocking out extracellular matrix proteins like collagen type II has been linked to abnormal endochondral ossification [276] and may play a role in the beginning stages of tether development.

CONCLUSION

In summary, our results show that tethers are present in vitamin D replete C57BL/6 mouse growth plates with functional VDRs and that they occur in specific regions that can be mapped. MicroCT images indicate that the number of mineralized tethers and tether volume percentage is reduced significantly in the rachitic growth plates of VDR-/- mice in comparison with their VDR+/+ littermates, and those that occur appear to be less calcified and are localized to the central region. Additionally, a rescue diet that restores normal mineral homeostasis is able to restore growth plate size but not tether formation in VDR-/- growth plates, suggesting that VDR mediated signaling independent of calcium ion homeostasis plays a critical role in tether formation. Serial decalcified histological sections confirm the findings from microCT analysis as number and volume percentage measurements are strongly correlated between the two imaging and analytical techniques, suggesting that microCT imaging is an effective nondestructive tool for analyzing tether formation. Shrinkage in the axial direction was correlated with tether formation, suggesting that bone-like tethers may provide mechanical stability. Growth plate size and the extent of tether formation were also different between animals of different ages. Although extensive studies are still needed to determine the role of tethers in growth plate mechanics and bone development, it is now known that tether formation is regulated in part by the VDR, which may prove to be beneficial in developing treatments for diseased or damaged growth plates.

CHAPTER 4

CORDINATED TEHTER FORMATION IN ANATOMICALLY DISTINCT GROWTH CENTERS IS DEPENDENT ON A FUNCTIONAL VITAMIN D RECEPTOR AND IS TIGHTLY LINKED TO THREE-DIMENSIONAL TISSUE MORPHOLOGY

INTRODUCTION

In order for coordinated and proportional skeletal growth to occur, endochondral ossification at growth centers throughout the body, such as growth plates of the long bones and synchondroses of the cranial base, need to be tightly regulated. Disruptions to normal growth in these tissues can lead to limb, body, and craniofacial deformities. Although the mechanisms regulating endochondral bone growth of long bones have been characterized extensively, less is known about differential modulation of endochondral ossification and growth center fusion in other cartilaginous tissues throughout the body. Growth plates and synchondroses can be divided into a series of anatomic zones with distinct morphological and biochemical properties that are tightly controlled by growth factor signaling pathways [48, 50, 277, 278]. In addition, cells in the growth plate are modulated by systemic hormones, including estrogen and vitamin D. Specifically, the vitamin D metabolites $1\alpha,25$-dihydroxy vitamin D_3 [$1\alpha,25(OH)_2D_3$] and 24R,25-dihydroxy vitamin D_3 [$24R,25(OH)_2D_3$] act on different cells in growth centers to regulate chondrocyte differentiation and bone lengthening [83, 88, 279].

Deficiency in $1\alpha,25(OH)_2D_3$ during long bone growth results in rickets, a condition where the growth plate enlarges because hypertrophic chondrocytes are unable to calcify their extracellular matrix [255], partially due to abnormal mineral homeostasis. As hypertrophic chondrocytes continue to pile onto each other, structural deformities in the bone ensue. Abnormal mineral homeostasis and resulting rachitic growth plates are also seen in mouse models with an ablated vitamin-D receptor (VDR-/-) [256, 269]. The gross morphology of the growth plate can be restored by returning serum calcium concentration to normal levels [258, 259, 280], either via systemic injection or by feeding the mice a high lactose, high calcium "rescue" diet, supporting the hypothesis that rickets is due to defective Ca^{2+} ion homeostasis [260]. The $1\alpha,25(OH)_2D_3$-dependent membrane associated protein disulfide isomerase family A, member 3 (PDIA3) signaling pathway is still functional in growth plate chondrocytes from these mice [271], suggesting that it may provide sufficient response to $1\alpha,25(OH)_2D_3$ to support matrix calcification with adequate restoration of extracellular Ca^{2+}. However, it is clear that simply raising Ca^{2+} is not the only function of $1\alpha,25(OH)_2D_3$ in regulating the biology of growth centers. Studies using growth plate chondrocyte cultures show that $1\alpha,25(OH)_2D_3$ mediates a broad range of responses including synthesis and maturation of extracellular matrix [261, 281]. Recently, we observed that the failure of VDR-/- mice to form growth plate tethers could not be rescued using the rescue diet, indicating that their development may be VDR-dependent [280].

Tethers are mineralized struts present in the growth plates of long bones of mice, rats, dogs, pigs, and human [262, 263, 280, 282]. They form perpendicular to the plane of the growth plate and eventually connect the epiphyseal and metaphyseal bone surfaces.

Although rat and murine growth plates never fully fuse, they become thinner as tether formation increases with time [262]. We have previously shown that μCT is an accurate modality for studying tethers by correlating computed measurements with histological observations [280]. In VDR-/- mice, tether formation is markedly reduced and those tethers that are present are localized to the center of the growth plate. Although VDR-/- mice that were raised on the high lactose, high calcium rescue diet had growth plates with normal volumes, tether formation was only partially restored.

Little is known about the functional role tethers play in bone growth and maintenance. They have been linked to changing growth plate morphology and fusion [262] and to providing tissue stability [280], suggesting that they play a mechanical role – potentially limiting fractures through the growth plate during post fetal development. Whether tethers are present in other growth centers is not known, nor is it known if growth centers that experience different kinds of loads will have tethers that are regulated in a similar fashion.

Synchondroses in the skull are believed to be regulated similarly to the growth plates of long bones [283], but because of their anatomic location, they serve other functions in addition to longitudinal growth. The cranial base has been considered as a guide for maxillary-mandibular complex, midface, and lower facial development, linking the development of the cranial vault with that of the facial skeleton [283-285]. The spheno-occipital synchondrosis (SOS) is the main remnant of a cartilaginous basicranium from embryonic development and has a cellular organization resembling two adjacent growth plates with the reserve zones back to back [283]. After birth, a mineralized bipolar column eventually develops within the reserve zones, separating the

synchondrosis into two regions. Endochondral ossification of the SOS has a direct contribution to basicranial growth and subsequent craniofacial development [286, 287] and disruptions to SOS growth can lead to cranial malformations that are characteristic of achondroplasia [288], Apert's syndrome [289, 290], anterior transverse crossbite [291], and cleidocranial dysplasia [292, 293]. The SOS is still visible on lateral radiographs through adolescence and has been shown to widen in response to maxillary and midpalatal suture expansion [294]. Additionally, clinical and laboratory investigations have suggested that premature closure of the cranial vault sutures in nonsyndromic craniosynostosis is associated with characteristic alterations in SOS morphology [31].

The purpose of this study was to determine if tether formation is a conserved feature of growth centers other than the growth plates and if so, whether tethers are regulated in a similar manner and have similar phenotype and function at different anatomic locations. To do this, we used μCT to compare the growth plate in the distal femoral condyle to the SOS in normal C57Bl/6 mice of various ages. We took advantage of our VDR-/- mouse model to assess the regulation of tether formation in these two anatomical sites. VDR+/+ and VDR-/- mice were fed a regular diet or a rescue diet with and without vitamin D_3. Finally, to gain insight into what role tethers may have in affecting tissue morphology or stability, correlations were analyzed among animal weight, growth center thickness, and tether phenotype. We hypothesized that the three-dimensional morphology of both the femoral growth plate and SOS would be similar with respect to temporal development. We also hypothesized that lack of a functional VDR would increase the size of both the growth plate and SOS while greatly reducing

the presence of tethers. Additionally, we hypothesized that restoring normal mineral homeostasis would restore the morphology of the growth centers but not the presence of tethers. Finally, we hypothesized that tether phenotype would be correlated to animal weight and growth center morphology.

MATERIALS AND METHODS

Animal Maintenance

All animal procedures were conducted under an Institutional Animal Care and Use Committee approved protocol in the vivarium in the Institute for Bioengineering and Bioscience at the Georgia Institute of Technology. To investigate tether formation with age in normal murine growth plates and synchondroses, male C57Bl/6 murine pups were obtained from Jackson Laboratory (Bar Harbor, ME). Animals were weaned, then fed Purina rodent chow (5010, Ralston Purina Co., St. Louis, MO) containing 1% calcium, 0.67% phosphorus, 0% lactose, and 4.4 IU vitamin D/g (regular diet) with water, and euthanized at ages 2, 4, 6, 7, 8, 10, and 15 weeks. This age range was chosen since the epiphysis was not visible in microCT scans at 10 days and animals exhibited no statistical change in weight between 12 and 15 weeks.

To investigate the role VDR-mediated signaling may have in tether formation, VDR-/- mice were used, in which structural stability of the growth plate is compromised due to rickets [269] and abnormal mineral homeostasis is exhibited [256]. A heterozygous (VDR+/-) breeding pair, which was generated in a C57Bl/6 background [269], was obtained as a gift from Dr. Marie Demay (Harvard Medical School, Massachusetts General Hospital, Boston, MA), and a mouse colony was established.

Offspring were genotyped two weeks after birth and VDR+/- mice were allowed to breed. To normalize blood mineral ion levels [258], male and female homozygous VDR+/+ and VDR-/- mice were fed a rescue diet containing 20% lactose, 2% calcium, 1.25% phosphorus, and 2200IU vitamin D_3/kg (TD96348, Teklad, Madison, WI) from day 22. This diet has previously been shown to restore serum ionized calcium levels, phosphorus levels, and immunoreactive PTH levels in the VDR null mice compared to wild type mice at 70 days of age [258]. To gain better insight into the role metabolites of vitamin D_3 may have in tether formation, mice were also fed a rescue diet without the added vitamin D_3 (TD87095, Teklad). Therefore, six groups of animals were investigated: VDR+/+ mice on regular diet, rescue diet, and rescue diet with vitamin D_3 and VDR-/- mice on regular diet, rescue diet, and rescue diet with vitamin D_3. All mice were euthanized when 10 weeks old. This age was chosen to accurately assess the rescue diet's effect on mineralization since over 85% of the bone surface is covered with osteoid in VDR-/- mice fed a regular diet at this time [259]. In addition to genotyping, homozygotes were assessed for evidence of rickets by histologic analysis of the costochondral cartilages. VDR-/- mice exhibited phenotypic markers of vitamin D deficiency, including rachitic growth plates with expanded hypertrophic cell zones.

Sample Preparation and MicroCT Processing

Once animals were euthanized, both the right femur and cranial base were excised from all mice (n=6 for each age and n=6 for each genotype and diet) and cleaned of soft tissues by sharp dissection. Bone samples were then fixed in 10% buffered formalin for 24 hours and post fixed in 70% ethanol. The distal portion of the right femur was scanned by μCT (μCT 40, Scanco Medical, Switzerland) with a voxel size of 12μm [280]

while the cranial base was scanned at a voxel size of 8μm because of the smaller growth center size. Both the distal femoral growth plate (GP) and the anterior region of the SOS were isolated with user-guided contours and evaluated at a threshold corresponding to 250mg hydroxyapatite/cm^3. This threshold was previously confirmed to be accurate for tether evaluation by comparing histomorphometric results to μCT [280]. To qualitatively assess tissue morphology and tether distribution, 3D reconstructions of the GP (Figure 4.1A) and the SOS (Figure 4.1B) were used to create 3D color images to visualize growth plate morphology and 3D tether maps to visualize formation within the growth center and along the surface. For quantitative measurements, Scanco software using a direct distance transformation method was implemented to determine microarchitecture morphology of both the GP and SOS and the tethers within each as previously discussed [295, 296]. Specifically, this method results in global volumetric measurements that represent averages along all relevant axes. Parameters derived in both the growth plate and SOS include tissue volume (mm^3), tether volume/growth center (GC) volume, tether number (#/mm), tether thickness (mm), and tether spacing (mm). Additionally, average tissue thickness (mm) along the axial direction between the epiphysis and metaphysis was also measured.

<u>Statistical Analysis</u>

One way ANOVA comparing VDR+/+ mice from 2 to 15 weeks of age and two-way ANOVA comparing VDR+/+ to VDR-/- on regular and rescue diets were performed with Statistix (Analytical Software, FL, USA) using a post-hoc Bonferroni correction test for pairwise comparison (p<0.05) to determine statistical differences. A power analysis on a preliminary study determined that a sample size of 6 (n=6) was sufficient to detect

significant statistical differences between groups. Additionally, the preliminary study showed no statistically significant difference between male and female VDR+/+ mice and between male and female VDR-/- mice in terms of growth center thickness and tether volume. Because it was unfeasible to get only 10 week old males for all six groups (VDR+/+ and VDR-/- mice on regular diet, rescue diet, and rescue diet with vitamin D_3) measurements were expressed as overall means ± standard errors of both male and female mice. The correlations between tether parameters and other measurements were investigated in Minitab 15 (Minitab Inc., State College, PA, USA). The correlation coefficient for each parameter was compared with a critical value for the number of corresponding measurements in the study to determine statistical significance (2-tail analysis, $p<0.05$) [272].

RESULTS

Normal Morphological Development of the GP and SOS

Both the murine GP and SOS decreased rapidly in size over the course of 15 weeks after birth (Figure 4.1C, D). Specifically, X-ray cross-sections showed the GP becoming thinner in the axial direction with increasing curvature while the bipolar column of the SOS started to develop and thicken. 3D color maps of growth center morphologies (Figure 4.1E, F) confirmed the decrease in tissue thickness. The overall GP and SOS morphologies experienced the most change between weeks 2 and 7, with little to no change in shape between weeks 7 and 15. At week 15, an accumulation of X-ray opaque regions seen in the 3D color maps signified tethers that traversed the entire length of the growth plate. Quantitative analysis revealed that both the GP and SOS

decreased in thickness by approximately 85% between weeks 2 and 8 (Figure 4.1G, I) with little to no decrease afterwards. GP and SOS volumes experienced a similar trend with an approximately 50% decrease in size between weeks 4 and 8 (Figure 4.1H, J). Although growth center thickness experienced a rapid decrease between weeks 2 and 4, GP and SOS volumes did not decrease because of corresponding tissue expansions in the sagital and axial directions respectively.
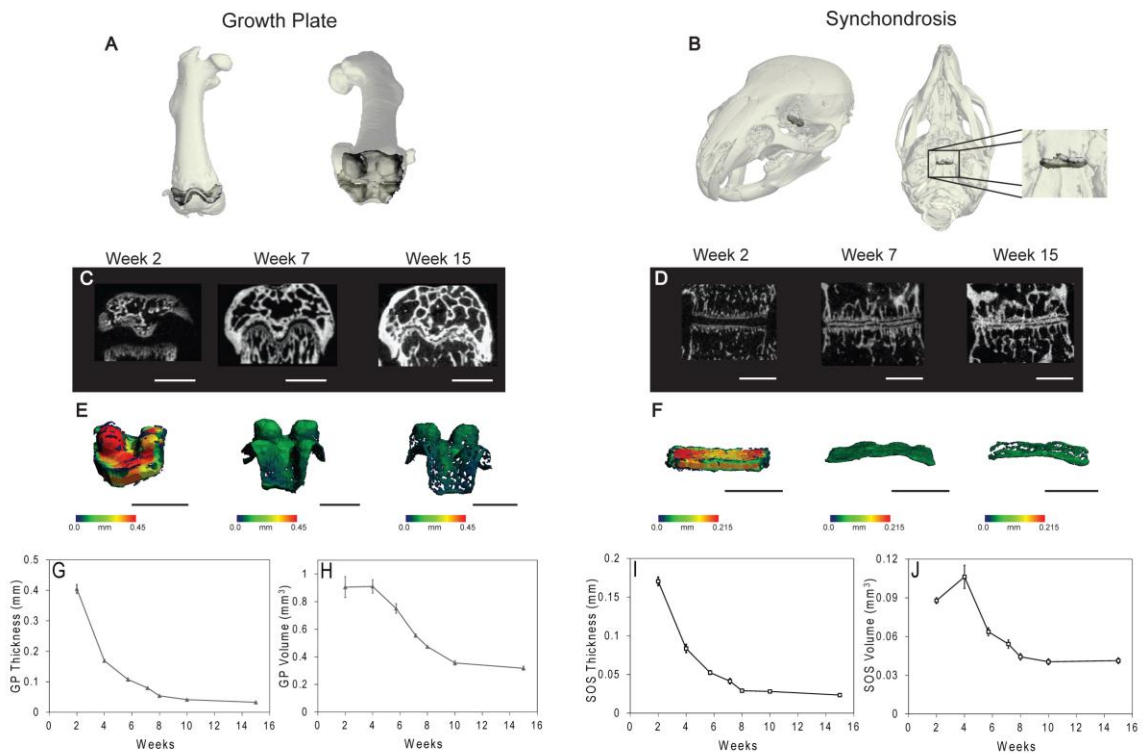
Figure 4.1: Normal Morphological Development of the GP and SOS
μCT imaging and 3D evaluation of the (A) growth plate (GP) and (B) spheno-occipital synchondrosis (SOS). X-ray cross-sections from 2 to 15 weeks show a decrease in (C) GP and (D) SOS size. 3D color maps of the (E) growth plate and (F) synchondrosis show changing morphology with age (bar represents 1mm for all images). Quantified (G) average GP thickness, (H) GP volume, (I) SOS thickness, and (J) SOS volume decrease with age from 2 to 15 weeks (n=6, mean±SE for each time and tissue).

The Role of Mineral Homeostasis and VDR in Growth Center Morphology

The size of the GP was greatly expanded in VDR-/- mice, leading to a disorganized morphology (Figure 4.2A). The SOS also expanded in VDR-/- mice,

resulting in a distorted morphology with minimal calcification of the bipolar column (Figure 4.2B). Rescue diets with and without vitamin D_3 had similar effects on the GP and SOS as tissue size was almost restored, but morphology was visibly different from VDR+/+ mice in both x-ray cross-sections and 3D color images of each tissue (Figure 4.2C-D). Specifically, VDR-null GPs with normal mineral homeostasis had rougher surfaces and less curvature compared to VDR+/+ GPs. Meanwhile, VDR-/- SOSs with normal mineral homeostasis had more curvature than VDR+/+ SOSs with slight bowing of the tissue.

Average GP and SOS thicknesses increased by 7.8-10 fold in the VDR-/- mice (Figure 4.2E, G). Rescue diets with and without vitamin D_3 were able to decrease tissue thicknesses by 75% but did not restore GP or SOS thicknesses as seen in VDR+/+ mice. GP and SOS volumes experienced a similar trend by increasing 5-10 fold in the absence of VDR and rescue diets significantly reducing tissue volume (Figure 4.2F, H). Rescue diets with vitamin D_3 were effective in restoring VDR-/- GPs and SOSs to wild-type volumes.

Normal Tether Development in the GP and SOS

Tethers that traversed the entire GP and SOS were apparent in x-ray cross-sections of both 7 and 15 week old tissues (Figure 4.3A, B). For both the GP and SOS at week 15, there appeared to be a higher density of thicker tethers present. 3D tether maps further confirmed these findings as a large accumulation of underlying tethers budding along the surface and within the growth centers were observed at both weeks 7 and 15 (Figure 4.3C, D). Tether volume/GC volume increased rapidly from week 8 to 15 in both the GP and SOS with nearly identical trends over 15 weeks (Figure 4.3E). Tether

number/mm for both the GP and SOS increased by 4-5 fold from week 6 to 15 (Figure 4.3F) as tether width increased by 3-3.5 fold over the first 8 to 10 weeks of age with little increase afterwards (Figure 4.3G).   Tether spacing decreased rapidly over the first 8 weeks in both the GP and SOS (Figure 4.3H). At all ages, tether number/mm was greater in the SOS, but tether width and spacing were greater in the GP.
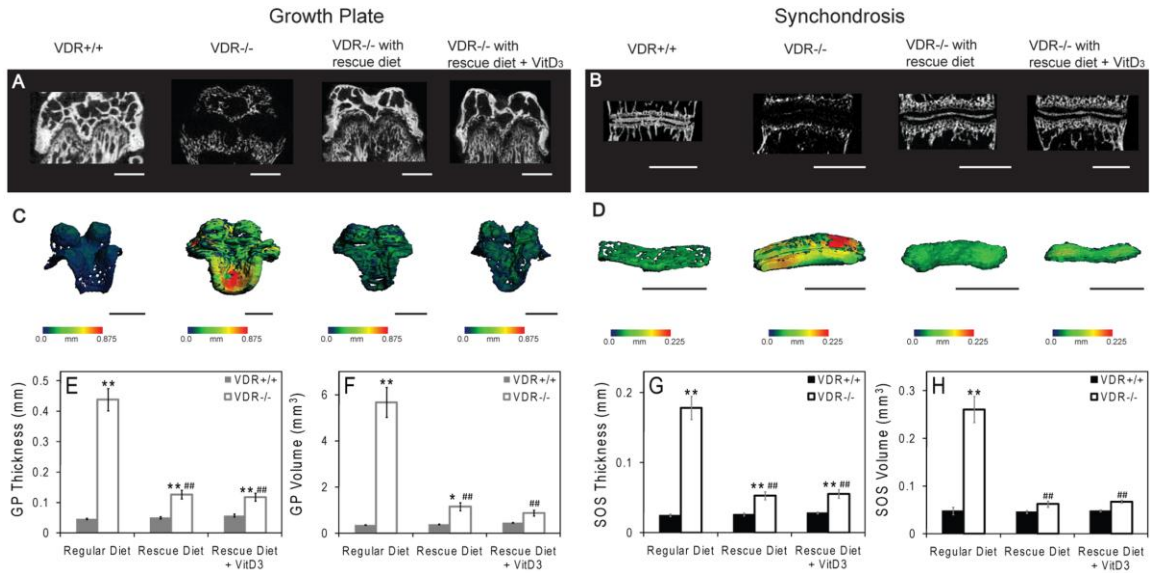
Figure 4.2: Effect of Mineral Homeostasis and VDR on GP and SOS Morphology
X-ray cross sections of (A) GPs and (B) SOSs of 10 week old VDR+/+ and VDR-/- mice on regular and rescue diets with and without vitamin D_3 show that growth center morphology is largely influenced by normal mineral homeostasis.   3D color maps of (C) GPs and (D) SOSs show restored size but altered morphologies of 10 week old VDR-/- mice on regular and rescue diets with and without vitamin D_3 (bar represents 1mm for all images).   (E) GP thickness is partially restored by rescues diets whereas (F) GP volume is statistically restored with rescue diet and vitamin D_3.   (G) SOS thickness is partially restored by rescue diets whereas (H) SOS volume is restored with rescue diets (n=6, mean±SE for each tissue and treatment, *$p<0.05$ vs. corresponding VDR+/+, **$p<0.001$ vs. corresponding VDR+/+, #$p<0.05$ vs. VDR-/- on regular diet, ##$p<0.001$ vs. VDR-/- on regular diet).
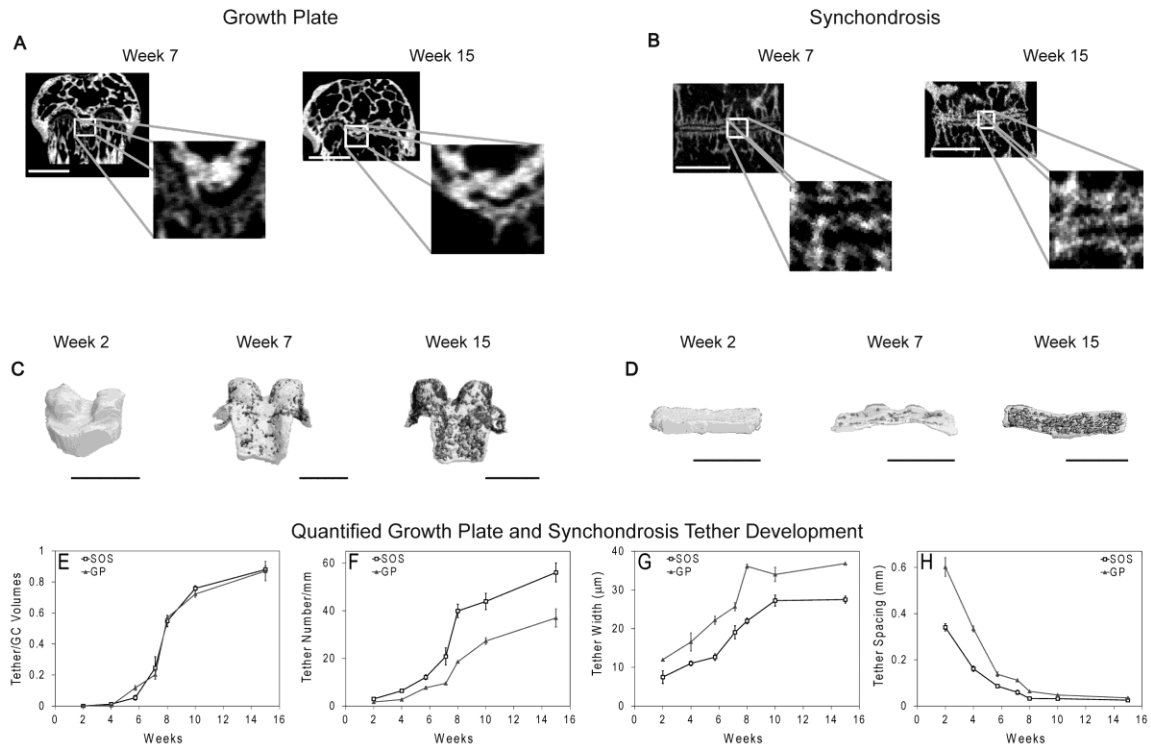
Figure 4.3: Normal Tether Development in the GP and SOS
X-ray cross sections in the (A) GP and (B) SOS show increased tether width and accumulation between weeks 7 and 15. 3D tether maps of the (C) GP and (D) SOS show tether accumulation between weeks 7 and 15 within each tissue (bar represents 1mm for all images). (E) Tether volume/growth center volumes in each growth center have similar increases with age. (F) Tether number/mm and (G) tether width in both tissues increase as (H) tether spacing decreases with age (n=6, mean±SE).

The Role of VDR-mediated Signaling in Tether Formation

Tether formation was nearly abolished in VDR-/- mice and although rescue diets were effective in restoring growth center volume, few to no tethers that traversed the entire tissue were present in either the GP (Figure 4.4A) or SOS (Figure 4.4B). 3D tether maps confirmed these results as little tether formation was observed in VDR-/- tissues with normal mineral homeostasis (Figure 4.4C, D). A more thorough quantitative assessment showed tether volume/GP volume and tether volume/SOS volume in VDR-/- mice on a regular diet was 0.2-0.4% of those in VDR+/+ mice (Figure 4.4 E, I). Rescue diets were partially effective in restoring the tether phenotype, increasing tether

67

volume/tissue volume by 35 and 150 fold in the GP and SOS, respectively, but only restored 20-25% of the tether formation found in their wild-type littermates. Tether number/mm in both tissues was similar to tether volume/tissue volume, as rescue diets were only able to partially restore tether accumulation (Figure 4.4F, J). The effect of knocking out VDR on tether width was not as pronounced as a statistically insignificant decrease was observed in the GP and a 33% decrease was seen in the SOS (Figure 4.4G, K). Rescue diets had no influence on tether width. Tether spacing in the GP and SOS was significantly higher in VDR-/- mice as rescue diets partially reduced tether spacing in the GP but not the SOS (Figure 4.4H, L).

Relationships among Animal Weight, Growth Center Morphologies, and Tethers

In VDR+/+ mice 2 to 15 weeks of age, normalized GP and SOS average thicknesses with respect to the thickness at 2 weeks of age were inversely correlated with animal weight (Fig. 5A) as the two correlations were nearly indistinguishable from each other. Animal weight in these VDR+/+ mice was correlated to animal length ($R^2=0.8761$, $p<1\times10^{-5}$), femur length ($R^2=0.926$, $p<1\times10^{-5}$), and basicranial length ($R^2=0.8415$, $p<1\times10^{-5}$). Tether volume/growth center volume was exponentially related to animal weight as GP and SOS correlations were nearly identical (Fig. 5B). Tether number/mm versus animal weight was also exponentially related for both the SOS and GP (Fig. 5C). Tether width was linearly correlated with animal weight in both the GP and SOS (Fig. 5D) as tether spacing was inversely correlated with weight in both tissues (Fig. 5E). These tether parameters for the GP and SOS had similar relationships to femur length and basicranial length respectively.

Tether number/mm had an inverse exponential relationship with normalized tissue thickness in the GPs and SOSs of VDR+/+ mice 2 to 15 weeks of age (Fig. 5F). In 10 week old VDR+/+ and VDR-/- mice on regular and rescue diets, tether number/mm also had a similar inverse exponential relationship with normalized growth center thickness for both the GP and SOS (Fig. 5G). GP and SOS tether spacing in VDR+/+ mice 2 to 15 weeks in age were linearly correlated with corresponding tissue thicknesses (Fig. 5H), and these correlations between tether spacing and GP and SOS thicknesses were nearly identical in 10 week old VDR+/+ and VDR-/- mice on regular and rescue diets.
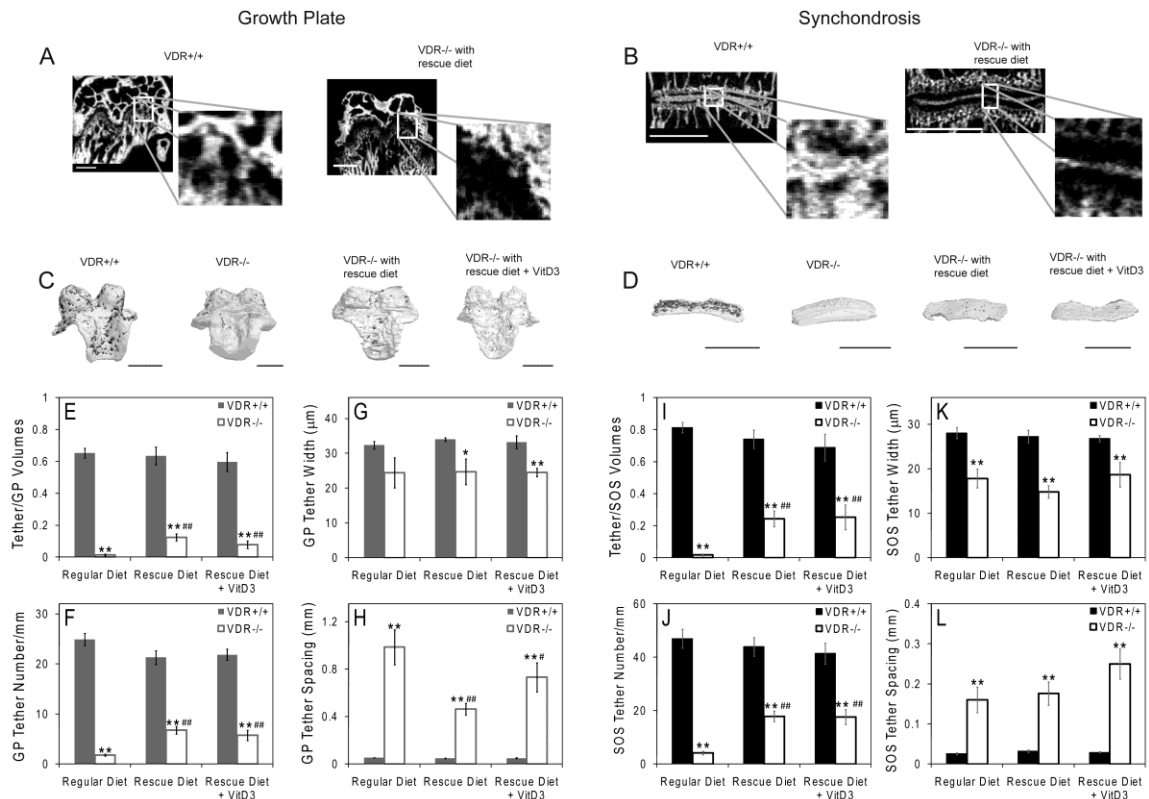
Figure 4.4: The Role of VDR-mediate Signaling in Tether Formation
X-ray cross sections of 10 week old VDR+/+ and VDR-/- (A) GP and (B) SOS treated with rescue diets. 3D tether maps of (C) GPs and (D) SOSs (bar represents 1mm for all images). (E) Tether volume/GP volume, (F) GP tether number/mm, (G) GP tether width and (H) GP tether spacing. (I) Tether volume/SOS volume, (J) SOS tether number/mm, (K) SOS tether width, and (L) SOS tether spacing (n=6, mean±SE,*$p<0.05$ vs. corresponding VDR+/+, **$p<0.001$ vs. corresponding VDR+/+, #$p<0.05$ vs. VDR-/- on regular diet, ##$p<0.001$ vs. VDR-/- on regular diet).
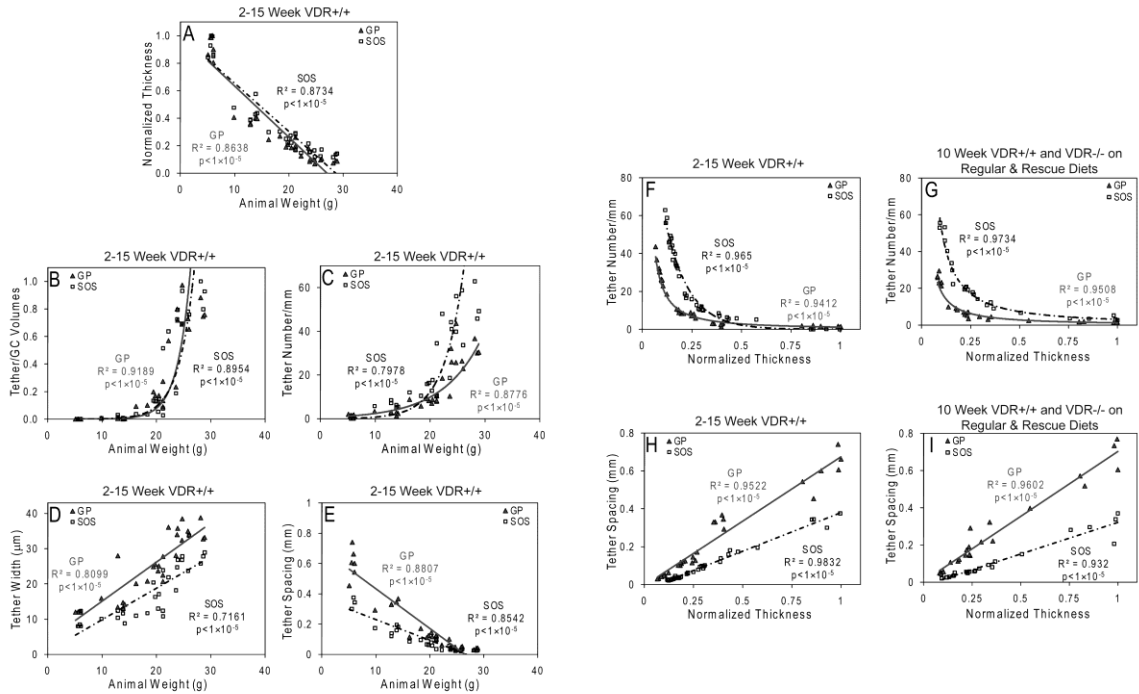
Figure 4.5: Relationships among Animal Weight, Growth Center Morphologies, and Tethers
(A) Normalized growth center thickness with respect to the thickness at 2 weeks of age is inversely correlated to animal weight. (B) Tether volume/growth center volume and (C) tether number/mm are exponentially related to animal weight. Growth center (D) tether width is correlated to animal weight whereas (E) tether spacing is inversely correlated. Growth center tether number/mm in (F) 2 to 15 week old VDR+/+ mice and (G) 10 week old VDR+/+ and VDR-/- mice on regular and rescue diets have an inverse exponential relationship with corresponding normalized tissue thickness. Tether spacing in (H) 2 to 15 week old VDR+/+ mice and (I) 10 week old VDR+/+ and VDR-/- mice on regular and rescue diets are correlated to their respective normalized growth center thickness (GP [——], SOS [-------]).

DISCUSSION

Tether formation in the tibia and femur occurs naturally [280, 297], but little is known about its functional role, its presence in other growth centers during endochondral ossification, or the mechanism that regulates its formation. This study is the first to demonstrate that in addition to growth plates found in long bones, tethers are also present in the spheno-occipital synchondrosis, a growth center located at the base of the skull that serves other functions in addition to longitudinal growth. Specifically, this study

70

demonstrated that tether morphology in both the growth plate and synchondrosis have strikingly similar patterns of post-fetal development; the VDR and mineral homeostasis have analogous effects on growth center tissue and tether formation in long bones and the cranial base; tether formation in both the growth plate and synchondrosis is significantly associated with animal weight and respective bone length; and tether phenotype appears strongly linked to growth center thicknesses in normal development and diseased animals with rescued phenotypes.

In both the growth plate and synchondrosis, there appears to be two stages of tether development: an initial phase of tether thickening that is followed with rapid accumulation in number. Tether thickening appears to be most dominant in post-fetal development between weeks 2 and 8 while tether density and overall accumulation has their most rapid increase starting at week 6. These trends in tether phenotype appear to have an inverse relationship with growth center morphology in normal post-fetal development, which steadily decreases in thickness and size after week 2. Additionally, these trends between tether phenotype and growth center morphology are seen in rachitic growth centers as tethers are less dense and thinner while growth center volumes and thicknesses of these diseased tissues are larger.

To thoroughly investigate the relationship between growth center morphology and tether formation, correlations between tether phenotype and tissue thickness were investigated in the growth plates and synchondroses of both normal mice at different ages and of 10 week old VDR ablated mice with and without normal mineral homeostasis. Tether density – which appears most dominant in later stages of tether formation – had an overall inverse exponential relationship with tissue thickness, but was linearly correlated

once the growth centers reached a quarter of their original size. Meanwhile, tether spacing – a parameter that takes into account both initial tether thickening and later tether accumulation – appeared to be directly correlated with tissue thickness throughout growth center development in all groups. These findings suggest that tether formation and tissue morphology are somehow linked in normal and diseased tissues. Specifically, it appears that overall tether spacing is connected to tissue thickness throughout development whereas tether density has a role once the growth center tissue starts to decrease in size.

Despite this very strong link between tether formation and thinning growth centers in different anatomical locations, it is unclear if there is a definitive mechanism that links the two. Although it is possible that tether formation can be partially attributed to endochondral ossification, it is not the main mechanism for tether development. Specifically, this study showed that restoring mineral homeostasis in VDR-/- mice with rescue diets containing vitamin D_3 was able to restore growth plate and synchondrosis volume but unable to restore their respective tether phenotype – specifically tether density and spacing. This finding suggests that $1\alpha,25$-dihydroxy vitamin-D_3 acting through its receptor regulates tether accumulation in growth centers throughout the body, not endochondral ossification. It may also be hypothesized that tethers facilitate the changing morphology of growth centers during the pubertal growth spurt and their eventual closure during sexual maturity, which has been reported to be between five to six weeks of age [298]. Although the largest changes in growth center volumes and tether numbers occur immediately after this time frame, it may be difficult to prove that tethers lead to growth center closure during sexual maturity since the wide array of

variables that influence growth plate closure is not completely understood. Specifically, weight loading [266], injuries [264, 299], abnormal hormone levels [300, 301], and genetic mutations [302, 303] all have an influence on growth plate morphology and subsequent closure, but how they influence tethers is unknown. Finally, it is not clear how to decouple tether formation from temporal changes in growth plate morphology.

We have previously suggested that tethers may contribute to overall tissue stability in the axial direction [280], and to gain insight into this possible role for tethers, the relationship between tether phenotype and animal weight was investigated. Tether density, width, and spacing appeared to be linked with animal weight. Tether width was linearly correlated and tether spacing was inversely correlated with weight up to 30 grams. Although the differences in mechanical properties and experienced mechanical loads of long bone growth plates and the spheno-occipital synchondrosis in mice are unknown, it is interesting to note the differences in tether phenotype at these distinctly different anatomical locations. Specifically, at all ages, tethers in the growth plate are thicker and spaced farther apart whereas thinner tethers in the synchondrosis occur at a higher density. Investigating tether formation in heavier mouse strains and in bipedal species in which body weight is distributed differently would provide further insight into the role of tethers in tissue stability. However, it is also possible that the increase in tether size and number and decrease in tether spacing can be the result of animal growth and not a response to tissue stability due to increased weight; specifically, tether size, number, and spacing had the same correlations to length as weight. Additionally, the correlations between weight and tether formation will most likely be different for males and females. Regardless, more extensive comparisons between growth plate mechanics

and tether composition need to be performed to arrive at a definitive conclusion about tethers' role in tissue stability.

Disruptive skeletal growth and corresponding growth center organization may provide insight into the role of tethers. In a rat defect model of growth plate injury, length reduction was correlated with percentage difference in growth plate thickness [297], suggesting that growth plate morphology may play a role in bone growth. Although the change in bone tether volume was not correlated to length reduction, tethers in these animals were associated with bone bridges that form during trauma [264, 265] and may not be comparable to tethers seen in healthy tissue. In homozygous brachymorphic (bm/bm) mice, which are characterized by a disproportionately short stature, the SOS was significantly larger than wild-type, lacked a calcified biopolar column or tethers, and had a disturbed morphology that resembled that seen in VDR-/- mice with no rescue diet [291]. Additionally, the anteroposterior length of the posterior cranial base in the bm/bm mice was significantly shorter, suggesting that synchondrosis morphology is important for normal bone growth. In mice with pseudo vitamin D deficiency rickets caused by mutations in the 25-hydroxyvitamin D-1α-hydroxylase gene, a high calcium diet was able to restore bone morphology and biomechanical properties but, unlike $1\alpha25(OH)_2D_3$ replacement therapy, was unable to restore bone growth [275]. The elimination of bone growth and tether accumulation in the absence of $1\alpha,25(OH)_2D_3$ signaling via its receptor – along with the previously reported relationships between tethers, growth center morphology, and subsequent bone growth – suggests that tethers may play a role in bone lengthening. Although our study showed that tether accumulation in two different growth centers was strongly linked to animal

weight and respective bone length during normal post-fetal development, the relationship between tether formation and bone growth rates should be further investigated.

CONCLUSION

In summary, tethers are present in both the growth plates of long bones and synchondroses of the cranial base. Tethers in both growth centers thicken and accumulate in number with age as the tissue decreases in size. When the VDR is ablated, tether formation is nearly eliminated in both rachitic growth plates and synchondroses. Restoring mineral homeostasis with rescue diets restored the overall size of both growth centers but only partially restored growth center morphology and tether formation, suggesting that tether formation in both growth centers is partially regulated by VDR signaling via 1α,25-dihydroxy vitamin-D_3. During post-fetal development from 2 to 15 weeks of age, tether phenotype had significant relationships to animal weight. Synchondrosis and growth plate thicknesses were inversely correlated to weight in wild-type mice, whereas in both 2-15 week old normal mice and 10 week old VDR-/- mice with normal and abnormal mineral homeostasis, tether phenotype was tightly linked to growth center thickness. The strong association between tether formation and growth center morphology may have implications on normal skeletal development and homeostasis, and further investigation may provide insight into strategies to regulate bone growth.

CHAPTER 5

TAILORING ADIPOSE STEM CELL TROPHIC FACTOR PRODUCTION WITH DIFFERENTIATION MEDIUM COMPONENTS TO REGENREATE CARTILAGE

INTRODUCTION

Adipose stem cells (ASCs) have been considered a promising candidate for cartilage repair because of their easy accessibility and chondrogenic potential [304, 305]. More recently, ASCs have demonstrated the ability to secrete trophic factors that can potentially stimulate endogenous cartilage regeneration [306], eliminating the need for ASCs to directly replace damaged chondrocytes or synthesize new cartilaginous tissue. However, ASCs secrete other factors that can delay or even inhibit cartilage repair. Specifically, VEGF-A, an angiogenic growth factor that is secreted in large quantities by ASCs [155, 307], has been shown to increase matrix metalloproteinase expression in chondrocytes [68] and is highly expressed in osteoarthritic cartilage [71]. Additionally, prolonged exposure to hypertrophic growth factors like FGF-18 and BMP-2 and can lead to hypertrophic differentiation, calcification, skeletal vascularization, and subsequent bone formation [53, 63, 308]. Growth factors such as FGF-2, IGF-I, and PTHrP can increase chondrocyte proliferation and regulate hypertrophy [309-312], while growth factors such as TGF-β1 and TGF-β2, can stimulate proteoglycan synthesis [313, 314]. Furthermore, BMP inhibitors like noggin have an important role in regulating cartilage differentiation and endochondral ossification [315]. Therefore, well defined methods that

76

increase ASC secretion of factors that promote chondrocyte proliferation and cartilaginous tissue synthesis, decrease secretion of angiogenic factors, and limit secretion of hypertrophic factors from ASCs are needed to treat chondral defects effectively.

Although viral and non-viral genetic manipulations of ASCs can be used to increase or decrease secretion of specific trophic factors, their ability to target only one gene at a time limits their therapeutic potential since cartilage formation is orchestrated by numerous growth factors and other signaling molecules [32, 53]. Furthermore, the potentially harmful side effects of genetic manipulations have hindered the clinical potential of these techniques [32, 316]. Therefore, preconditioning stem cells *in vitro* to obtain a desired secretory profile has also been suggested. While hypoxic exposure, heat induction, and biophysical stimulation have previously been used to augment the paracrine actions of stem cells [32, 159, 317], pharmacological treatments (chemical compounds) and biological treatments (growth factors and hormones) may provide the most precision in controlling the intensity and time of preconditioning. Additionally, providing different structural microenvironments (3-D scaffolds, cell-cell interactions) such as microencapsulation may further control the secretome of stem cell therapies *in vitro* and *in vivo*. Microencapsulation of ASCs may also provide a delivery method to localize these therapies.

The effects of differentiation media, such as chondrogenic medium, on multiple stem cell sources under varying structural environments are well defined [243, 304, 318]. However, the effects that short-term exposure to these media has on trophic factor production from ASCs are unknown. To decide if chondrogenic medium and its

individual components could be used to effectively precondition ASCs to secrete factors for regenerating cartilage, the objectives of this study were to determine the effect chondrogenic medium has on ASC growth factor secretion in different structural environments and to determine the effect different chondrogenic medium components have on ASC growth factor production.

MATERIALS AND METHODS

Cell Isolation

ASCs were isolated from the inguinal fat pads of 125 g male Sprague-Dawley rats (Harlan Laboratories, Indianapolis, IN, USA) as previously described in detail [319, 320] and cultured in Lonza Mesenchymal Stem Cell Growth Medium (MSCGM, Lonza, Walkersville, MD, USA). After one passage, these cells were negative for CD 45 and positive for CD73 and CD271 [320]. Costochondral chondrocytes from the ribs of 125 g male Sprague Dawley rats were isolate as described previously [82, 321]. Primary cells were cultured in Dulbecco's Modified Eagle Medium (DMEM) containing 10% fetal bovine serum (FBS) and 50 μg/ml ascorbic acid (Invitrogen, Carlsbad, CA, USA) until fourth passage prior to experimental analysis. These cells continue to express type II collagen, aggrecan, and cartilage oligomeric matrix protein [321].

Microencapsulation

When primary ASCs reached 90% confluence, they were harvested by trypsinization and microencapsulated in low molecular weight (~150 kDa) alginate with a high mannuronate to guluronate ratio (40% guluronate, FMC BioPolymer, Sandvika, Norway) as previously described [322]. The alginate (20 mg/mL) was dissolved in

sterile-filtered saline (Ricca Chemical, Arlington, TX, USA). Cells were suspended in the alginate solution at a concentration of 25×10^6 cells/mL. Microbeads were formed using a Nisco Encapsulator VAR V1 LIN-0043 (Nisco Engineering AG, Zurich, Switzerland) and a crosslinking solution of 50 mM $CaCl_2$, 150 mM glucose, and 15 mM 4-(2-hydroxyethyl)-1-piperazineethanesulfonic acid (HEPES buffer, pH=7.3, Sigma, St. Louis, MO, USA). Microbeads were washed three times in GM prior to cell culture studies. First passage ASCs were also plated in 6-well plates.

Cell Culture

Once first passage ASCs reached 90% confluence, ASC monolayers and microbeads were then treated for 5 days with either GM or chondrogenic medium (CM) consisting of DMEM containing 4.5g/L glucose with 1 mM sodium pyruvate (Mediatech, Manassas, VA, USA), 40 µg/ml proline (Sigma), 50 µg/ml ascorbic acid 2-phosphate (AA2P, Sigma), 1% ITS+ (Sigma), 100 nM dexamethasone (Dex, Sigma), 10 ng/ml recombinant human transforming growth factor beta-1 (TGF-β1, R&D Systems, Minneapolis, MN, USA) and 100 ng/ml recombinant human bone morphogenic protein 6 (BMP-6, PeproTech, Rocky Hill, NJ, USA). In subsequent studies, ASC monolayers were treated for five days with either GM that was supplemented with different combinations of 50µg/mL AA2P, 100nM Dex, 10ng/mL TGF-β1, and 100ng/mL BMP-6 or with CM that lacked different combinations of 50µg/mL AA2P, 100nM Dex, 10ng/mL TGF- β1, and 100ng/mL BMP-6. Once media were changed on the fifth day, RNA was collected after 8 hours as described below. Conditioned media and ASCs were collected after 24 hours, and ASCs were lysed in 0.05% Triton X-100. Monolayer fourth passage chondrocytes cultured in DMEM, 10% FBS, and 50 µg/mL ascorbic acid and Sprague

Dawley-derived clone 9 liver cells (ATCC, Manassas, VA, USA) cultured in F12K medium and 10% FBS served as a reference. All media contained 1% penicillin and streptomycin.

RNA Isolation and Reverse Transcription

Alginate microbeads were uncrosslinked in 82.5 mM sodium citrate (Sigma), pelleted at 500×g for 10 minutes and washed two more times in sodium citrate to remove any residual alginate. TRIzol reagent (Invitrogen) was added to the resulting cell pellet, homogenized using a QIAshredder (QIAGEN, Valencia, CA, USA), and RNA was isolated using chloroform and an RNeasy Kit (QIAGEN) as previously described [323]. 1 μg RNA was then reverse transcribed to cDNA using a High Capacity Reverse Transcription cDNA kit (Applied Biosystems, Carlsbad, CA, USA).

Microarray Analysis

cDNA was converted into cRNA using a RNA transcript labeling kit (Enzo Diagnostics, Farmingdale, NY, USA). Biotin labeled cRNA was cleaned up using a GeneChip Sample Cleanup Module (Affymetrix Inc., Santa Clara, CA, USA) and fragmented at 94°C in Fragmentation Buffer for 35 minutes. Following fragmentation, 15 μg biotinylated cRNA was hybridized to an Affymetrix Rat Genome GeneChip (Rat 230_2.0) at 45°C for 16 hours, washed, stained with streptavidin phycoerythrin (Fluidics Station 400, Affymetrix), and scanned according to manufacturer's guidelines. The GeneChips were then assessed for data quality using Affymetrix-developed quality controls. Data analysis was performed using GeneSifter (Geospiza, Seattle, WA) with significant differences in expression of a single gene being defined as a 3-fold change in mRNA levels. Significant differences in mRNAs of Kyoto Encyclopedia of Genes and

Genomes (KEGG) pathways were defined as z-scores greater than 2.0. RNA isolated from rat liver tissue served as a reference control.

Growth Factor mRNA Levels and Production

Because chondrogenesis is a complex process orchestrated by a wide array of growth factors, mRNA levels and production of paracrine factors involved in chondrocyte proliferation, proteoglycan synthesis, hypertrophic differentiation, and vascular invasion were quantified. Along with these paracrine factors, mRNAs for chondrocytic markers were also quantified as previously described using real-time PCR with gene-specific primers using the Step One Plus Real-time PCR System and Power Sybr® Green Master Mix (Applied Biosystems) [166]. All primers were designed using Beacon Designer software (Premier Biosoft, Palo Alto, CA, USA) and synthesized by Eurofins MWG Operon (Huntsville, AL, USA), unless otherwise noted (Table 1). Growth factor production over the last 24 hours of culture was quantified using ELISA (R&D Systems) and normalized to DNA content measured with a Quant-iT PicoGreen kit (Invitrogen). To measure growth factor retention within the microbeads, cultures were uncrosslinked in 82.5mM sodium citrate and both supernatants and cells were frozen at -80°C. Samples were then lyophilized for 24 hours and the resulting dried constructs were digested in 1 unit/mL alginate lyase (Sigma) for 1 hour and measured with ELISA. TGF-β1 production and secretion was not measured because of the large concentration of recombinant human TGF-β1 in chondrogenic medium. Quantified mRNA levels were referred to by the name of the gene whereas quantified protein levels were referred to by the name of the growth factor.

Table 5.1: Primer Sequences for Rat ASCs

Gene	Direction	Sequence
Acan	Sense	GCTTCGCTGTCCTCAATGC
	Antisense	AGGTGTCACTTCCCAACTATCC
Bmp2	Sense	TGTGAGGATTAGCAGGTCTTTG
	Antisense	CTTCCGCTGTTTGTGTTTGG
Bmp6	Sense	CCGCAGCAGCAACAATCG
	Antisense	ATCCTCTTCGTCGTCCTTGG
Col2	Sense	CGAGTATGGAAGCGAAGG
	Antisense	GCTTCTTCTCCTTGCTCTTGC
Comp	Sense	AGTGACAGCGATGG GATGG
	Antisense	TCCCCGTCCTGGTCTTGG
Fgf2	Sense	Global Gene Sequence (Qiagen)
	Antisense	
Fgf18	Sense	CTTCCAGGTTCAGGTGTTG
	Antisense	GCTTCCGACTCACATCATC
Igf1	Sense	GGTTCCTTATCTCCATTTCTTCC
	Antisense	CCCAGTTGCTATTGCTTTCG
Nog	Sense	TAAGCCATCCAAGTCTGTG
	Antisense	AGCAGGAACACTTACACTC
Pdgfa	Sense	GAGGAGACGGATGTGAGG
	Antisense	ACGGAGGAGAACAAAGACC
Pthlh	Sense	TGGTCGCAGGCTAAAACG
	Antisense	TGTGGATCTCCGCAATCAG
Rps18	Sense	TCGCTATCACTGCCATTAAGG
	Antisense	TGTATTGTCGTGGGTTCTGC
Sox9	Sense	GTGGGAGCGACAACTTTACC
	Antisense	ATCGGAGCGGAGGAG GAG
Tgfb1	Sense	AGCCTGCTTCTTGAGTCC
	Antisense	AAGTGGGGTGTTCTTAAATAGG
Tgfb2	Sense	AGCCTGCTTCTTGAGTCC
	Antisense	CTCAGAGGAAGGGATGGG
Tgfb3	Sense	AAGGAGTGGACAACGAAG
	Antisense	CGGTGTGGAGGAATCATC
Vegfa	Sense	GGACATCTTCCAGGAGTACC
	Antisense	CGTCTTGCTGAGGTAACC

Statistical Analysis

Statistical differences among all experimental groups were determined via ANOVA with a post hoc Tukey test (GraphPad Prism, La Jolla, CA, USA). Statistical differences between control and experimental groups were determined via Student's t-test. Differences in means were considered to be statistically significant if the p-value was less than 0.05. All *in vitro* experiments had six independent cultures per treatment group to ensure sufficient power to detect statistically significant differences and were conducted multiple times to validate the observations. However, only data from a single representative experiment are shown and are expressed as means ± standard errors.

RESULTS

Growth Factor Signaling Pathways with High and Low Expressions in ASC Cultures

mRNAs for 21 out of 52 proteins associated with the TGF-β signaling pathway were higher in ASC monolayers compared to liver RNA (Table 5.2). These higher mRNAs included paracrine factor genes bmp2, nog, tgfb1, tgfb2, and tgfb3; receptor genes tgfbr2, tgfbr3, and bmpr2; and secondary messengers genes smad2, smad3, smad4, and p300 (data not shown). mRNAs for proteins associated with the mitogen activated protein kinase (MAPK) signaling pathway were also higher in ASC monolayers and microbeads compared to liver RNA with z-scores of 3.27 and 2.26 respectively (Table 5.2). Higher mRNAs included numerous fgfs and pdgfa, pdgfra, pdgfrb, fgfr, mapk3, rras, prkcc, and rac1 (data not shown). mRNAs for proteins associated with the Wnt signaling pathway were higher in both ASC monolayers and microbeads (Table 2) compared to liver. However, higher mRNA levels were mainly due to secondary messengers of the Wnt canonical pathway; Wnt2 and 4 were the only Wnt proteins with higher mRNA levels. mRNAs for proteins associated with PPAR signaling pathway were significantly lower in both ASC monolayers and microbeads with z-scores of 3.22 and 4.63 respectively. Based on these results, paracrine factors associated with TGF-β were MAPK were further investigated.

Table 5.2: Gene Array of Signaling Pathways

Signaling Pathways Different Than Control (liver)		Treatment	# Different Genes/# Total Genes	# Higher Genes	#Lower Genes	z-score (Higher)	z-score (Lower)
TGF-β	signaling	monolayer	27/52	21	6	3.5	-2.08
pathway		microbeads	18/52	14	4	1.65	-1.99
MAPK	signaling	monolayer	90/185	56	34	3.27	-1.75
pathway		microbeads	71/185	45	26	2.26	-1.53
Wnt signaling pathway		monolayer	40/87	30	10	3.18	-2.71
		microbeads	32/87	23	9	2.04	-1.94
PPAR	signaling	monolayer	31/58	7	24	-1.67	3.22
pathway		microbeads	32/58	8	24	-0.88	4.63
Jak-STAT	signaling	monolayer	38/84	14	24	-0.97	1.08
pathway		microbeads	26/84	18	8	0.79	-2.1

Effect of Chondrogenic Medium on ASC Cultures

CM increased igf1, pthlh, tgfb2, and bmp2 by 1.8 to 46 fold (Figure 5.1A) and nog by 110 fold (Table 5.3) in ASC monolayers. ASC microbeads experienced a similar increase in igf1 and tgfb2 when treated with CM (Figure 5.1A). CM decreased fgf2 and vegfa in both ASC monolayers and microbeads by 3 to 4 fold while microencapsulation alone increased igf1, pthlh, tgfb2, and bmp2 (Figure 5.1A). CM also increased acan, sox9, and comp in both ASC monolayers and microbeads (Table 5.3). Compared to chondrocytes, ASC cultures treated with CM had similar amounts of tgfb2 and vegfa and higher amounts of igf1, pthlh, and tgfb2 when compared to liver cells.

CM had similar effects on protein secretion as it increased ASC monolayer IGF-I, TGF-β2, and TGF-β3 secretion by 6.3 to 30 fold (Figure 5.1B, Table 5.3). CM also increased secretion of IGF-I, TGF-β2, and TGF-β3 from ASC microbeads by 2 to 37 fold. Microencapsulation alone increased IGF-I, TGF-β2, VEGF-A, and FGF-2 secretions by 3 to 40 fold (Figure 5.1B, Table 5.3). CM decreased VEGF-A secretion from ASC monolayers and microbeads by 15 to 20 fold and decreased FGF-2 secretion from ASC microbeads by 2.4 fold. ASC monolayers treated with CM had higher

secretion levels of TGF-β2 and TGF-β3, similar secretion levels of VEGF-A and FGF-2, and lower secretion levels of IGF-I compared to chondrocytes (Figure 5.1, Table 5.3). Detectable amounts of FGF-2, IGF-I, TGF-β2, and VEGF-A were maintained within the microbeads as CM decreased the amounts of FGF-2, IGF-I, and VEGF-A and increased the amount of TGF-β2 inside the microbeads.

Table 5.3: Effect of Chondrogenic Medium on ASC Monolayers and Microbeads

	Chond	ASCs	+CM	+Microbead	+CM +Microbead	Liv
mRNA Levels						
Bmp6/Rps18	11.8± 4.0	14.9±2.0	9.5± 1.7	*26.7± 5.1	*1.6± 0.4	*35.7± 5.0
Fgf18/Rps18	21.8± 6.7	*49.0±8.1	19.8± 4.6	*125.3±21.8	8.7± 0.7	*366.6±70.9
Nog/Rps18	55.8±19.6	17.5±2.3	*1995.3± 442.4	100.3±16.0	*589.3±156.0	69.7± 6.1
Pdgfa/Rps18	1.7± 0.1	1.2±0.2	1.5± 0.2	0.7± 0.1	*0.5± 0.1	1.2± 0.2
Tgfb1/Rps18	6.0± 1.8	3.5±0.5	7.7± 0.8	4.7± 0.8	11.0± 2.9	3.1± 0.3
Tgfb3/Rps18	207.9±57.5	*17.4±1.8	265.3± 29.4	*9.5± 1.3	106.1± 21.9	17.2± 1.6
Acan/Rps18	7.5± 2.2	*[1]0.0±0.0	*46.0± 6.3	*0.4± 0.1	*54.7± 8.9	*[1]0.0±0.0
Col2/Rps18	13.5± 1.6	*0.2±0.0	*0.2± 0.0	*[1]0.0± 0.0	*0.1± 0.0	*[1]0.0± 0.0
Comp/Rps18	14.0± 4.4	*0.2±0.0	*31.5± 5.3	*0.8± 0.2	*164.2± 70.4	*0.3± 0.1
Sox9/Rps18	8.4± 2.4	14.0±1.4	*35.4± 7.1	9.6± 1.7	*44.1± 6.8	*4.7± 0.6
Growth Factor Production						
FGF-2/DNA[2]	0.4± 0.0	0.4±0.0	0.4± 0.0	*1.2± 0.1	0.5± 0.0	n.m.
TGF-β3/DNA[2]	8.3± 4.6	11.9±6.5	*75.4± 18.2	13.3± 6.9	*23.8± 6.4	n.m.
FGF-2/DNA[2] (in microbeads)	n.m.	n.m.	n.m.	2.1± 0.4	0.9± 0.1	n.m.
IGF-I/DNA[2] (in microbeads)	n.m.	n.m.	n.m.	1.3± 0.2	0.3± 0.1	n.m.
TGF-β2/DNA[2] (in microbeads)	n.m.	n.m.	n.m.	[1]0.0± 0.0	[1]0.0± 0.0	n.m.
TGF-β3/DNA[2] (in microbeads)	n.m.	n.m.	n.m.	34.2± 2.6	63.4± 7.9	n.m.
VEGF-A/DNA[2] (in microbeads)	n.m.	n.m.	n.m.	12.0± 0.7	4.0± 0.7	n.m.

*p<0.05 vs. Chond, n = 6, mean±SE
[1]Value less than 0.05.
[2] Units of ng/μg.
n.m. Not Measured

85
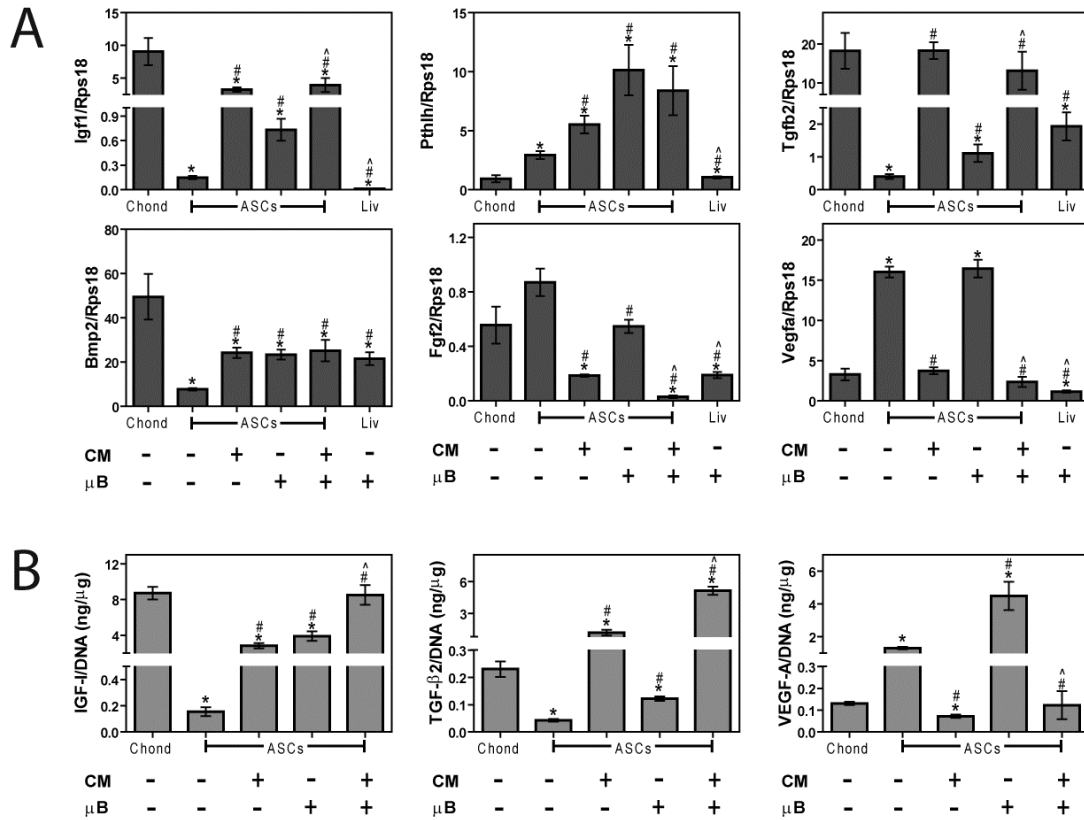
Figure 5.1: Effect of Chondrogenic Medium on ASC Monolayers and Microbeads
(A) Trophic factor mRNA levels of ASCs in chondrogenic medium (CM) or microbeads (μB) with chondrocytes (Chond) and liver cells (Liv) serving as controls. (B) Growth factor secretion from ASCs in chondrogenic medium (CM) or microbeads (μB) with chondrocytes (Chond) serving as controls (n = 6, mean±SE, *p<0.05 vs. Chond, #p<0.05 vs. ASCs, ^p<0.05 vs. ASC μB).

<u>Effect of Ascorbic Acid-2-Phodphate, Dexamethasone, and Growth Factors in MSC Growth Medium</u>

Adding AA2P to GM decreased bmp6, fgf18, nog, and pdgfa by 2.9 to 10.9 fold (Table 5.4) while adding Dex to GM increased igf1, tgfb2, bmp2, fgf18, nog, pdgfa, and tgfb3 by 1.5 to 10.2 fold (Figure 5.2A, Table 5.4). AA2P also increased IGF-I, FGF-2, and TGF-β3 secretion by 2.7 to 8.9 fold (Figure 5.2B, Table 5.4). Adding Dex decreased pthlh, fgf2, and vegfa by 1.3 to 5.2 and VEGF-A secretion by 87 fold (Figure 5.2A, B). Adding both AA2P and Dex to GM was not as effective in increasing igf1, bmp2, fgf18, and nog as adding only Dex to GM. The combination of adding both AA2P and Dex in GM effectively increased acan but not col2 or comp.

Adding TGF-β1 and BMP-6 to GM had the opposite effect of AA2P and Dex on igf1, fgf2, and vegfa (Figure 5.2A). Exogenous TGF-β1 decreased igf1 by 48 fold and increased fgf2 and vegfa by 11 and 3.8 fold respectively (Figure 5.3A). TGF-β1 also decreased pthlh by 4 fold and increased tgfb2, bmp2, fgf18, and pdgfa by 1.6 to 6.3 fold (Figure 5.3A, Table 5.4). BMP-6 decreased pthlh and increased tgfb2, fgf2, fgf18, and nog. Growth factor secretion by ASCs in GM was also influenced as exogenous TGF-β1 increased TGF-β2, VEGF-A, and FGF-2 secretion by 2.5 to13.6 fold (Figure 5.3B, Table 5.4). BMP-6 increased TGF-β2 secretion by 3.5 fold.

Table 5.4: Effect of Components in MSC Growth Medium

The Effect of Ascorbic Acid 2-Phosphate, Dexamethasone, and Growth Factors on ASC Monolayers

	MSCGM	+AA2P	+DEX	+AA2P +DEX	+TGF-β1 +BMP-6
mRNA Levels					
Bmp6/Rps18	97.9±12.0	*33.3± 18.1	*51.7± 3.9	*49.6± 11.9	*37.4± 9.7
Fgf18/Rps18	487.5±61.4	*44.9± 6.1	*1974.8±499.9	895.3± 186.2	*2385.3±422.9
Nog/Rps18	32.3± 7.0	*8.8± 2.0	*52.9± 7.1	29.7± 5.3	*414.6± 29.0
Pdgfa/Rps18	10.9± 1.2	*4.4± 1.3	*16.8± 2.0	*25.7± 3.6	*44.8± 3.8
Tgfb1/Rps18	28.2± 4.7	*13.2± 3.2	*5.2± 0.4	*5.2± 1.0	*60.7± 16.0
Tgfb3/Rps18	51.6± 8.0	58.4± 8.8	*158.2± 10.9	*237.2± 53.2	47.3± 9.6
Acan/Rps18	0.2± 0.0	0.2± 0.1	0.2± 0.0	*0.5± 0.1	*2.8± 0.3
Col2/Rps18	[1]0.0± 0.0	[1]0.0± 0.0	[1]0.0± 0.0	0.0± 0.0	0.5± 0.2
Comp/Rps18	0.1± 0.0	0.0± 0.0	[1]0.0± 0.0	0.0± 0.0	0.2± 0.1
Sox9/Rps18	0.3± 0.1	*0.1± 0.0	*0.1± 0.0	0.1± 0.0	*0.3± 0.1
Growth Factor Production					
FGF-2/DNA[2]	4.8± 1.3	*42.7± 7.6	3.5± 0.7	3.0± 0.7	*11.6± 1.1
TGF-β3/DNA[2]	9.4± 1.0	*26.8± 4.3	5.5± 1.5	30.3± 1.5	*14.7± 1.4

The Effect of TGF-β1 and BMP-6 on ASC Monolayers

	MSCGM	+TGF-β1	+BMP-6	+TGF-β1 +BMP-6
mRNA Levels				
Bmp6/Rps18	43.7± 5.0	30.9± 6.9	45.8± 4.3	27.7± 9.2
Fgf18/Rps18	385.8±115.8	*619.2± 109.0	*1141.1±246.0	*1203.3±212.4
Nog/Rps18	2.6± 0.8	3.5± 0.9	*30.3± 6.8	*13.8± 4.8
Pdgfa/Rps18	6.9± 1.4	*43.5± 7.0	7.8± 0.9	*51.2± 1.6
Tgfb1/Rps18	4.7± 0.8	9.9± 2.2	5.9± 0.8	*9.7± 1.6
Tgfb3/Rps18	0.1± 0.0	0.3± 0.1	*0.3± 0.0	0.6± 0.2
Acan/Rps18	0.1± 0.0	0.1± 0.0	0.1± 0.0	0.1± 0.0
Col2/Rps18	[1]0.0± 0.0	[1]0.0± 0.0	[1]0.0± 0.0	0.0± 0.0
Comp/Rps18	0.1± 0.0	0.1± 0.0	0.1± 0.0	0.1± 0.0
Sox9/Rps18	0.2± 0.0	0.1± 0.0	*1.2± 0.6	0.1± 0.0
Growth Fctor Production				
FGF-2/DNA[2]	14.7± 1.0	*201.8± 21.2	18.1± 3.8	*175.5± 7.2
TGF-β3/DNA[2]	8.0± 0.6	9.5± 0.7	6.8± 0.5	12.6± 2.2

*p<0.05, vs. MSCGM, n = 6, mean±SE
[1]Value less than 0.05.
[2] Units of ng/μg.
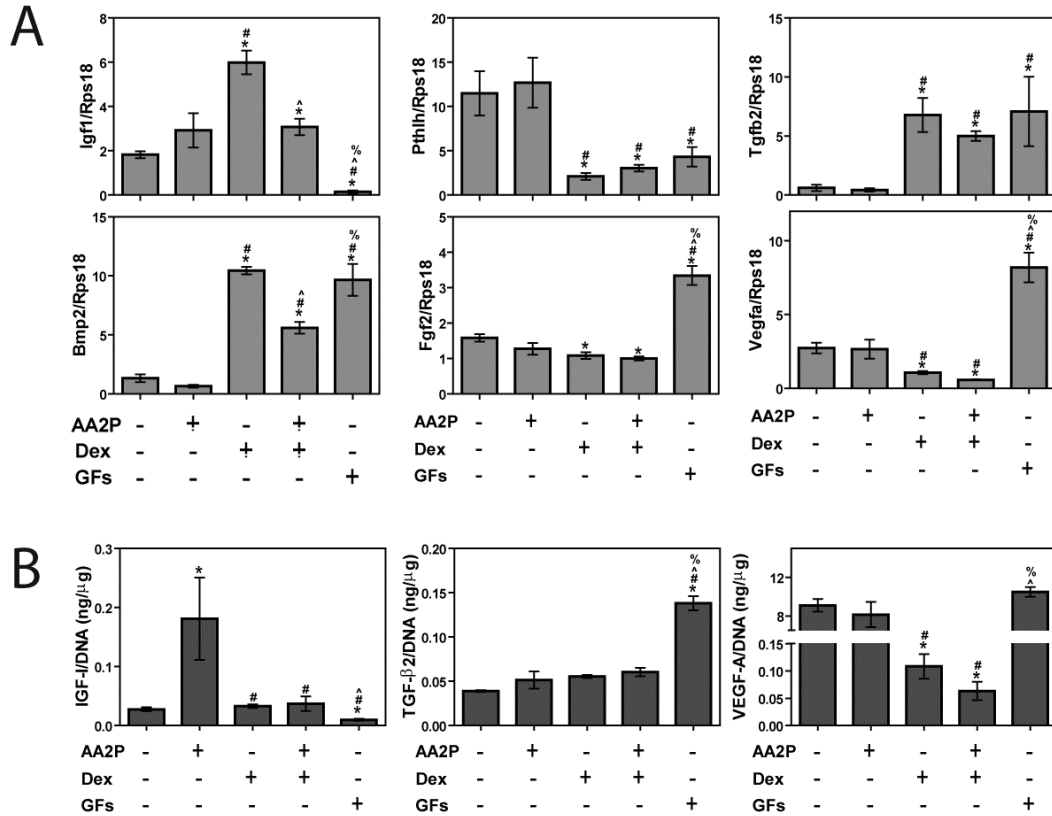
Figure 5.2: Effect of AA2P, Dex, and Growth Factors in Growth Medium
(A) Trophic factor mRNA levels of ASCs in growth medium with ascorbic acid 2-phosphate (AA2P), dexamethasone (Dex), or TGF-β1 and BMP-6 (GFs). (B) Growth factor secretion from ASCs in growth medium with ascorbic acid 2-phosphate (AA2P), dexamethasone (Dex), or TGF-β1 and BMP-6 (GFs) (n = 6, mean±SE, *p<0.05 vs. growth medium, #p<0.05 vs. +AA2P, ^p<0.05 vs. +Dex, %p<0.05 vs. +AA2P + Dex).

Figure 5.3: The Effect of TGF-β1 and BMP-6 in Growth Medium
(A) Trophic factor mRNA levels of ASCs in growth medium with TGF-β1 and BMP-6.
(B) Growth factor secretion from ASCs in growth medium with TGF-β1 and BMP-6. (n = 6, mean±SE, *p<0.05 vs. growth medium, #p<0.05 vs. + TGF-β1, ^p<0.05 vs. + BMP-6.

Effect of Effect of Ascorbic Acid-2-Phodphate, Dexamethasone, and Growth Factors in Chondrogenic Medium

Removing AA2P from CM decreased igf1, tgfb2, and fgf2 mRNAs by 1.2 to 6.3 fold (Figure 5.4A). The absence of AA2P also increased vegfa and fgf18 2.5 to 2.8 fold (Figure 5.4A, Table 5.5). Taking out Dex from CM decreased igf1, pthlh, bmp2, bmp6, fgf18, and nog 2.1 to 9.2 fold (Figure 5.4A, Table 5.5). The lack of Dex from CM also increased tgfb2, fgf2, vegfa, pdgfa, and tgfb1 1.2 to 3 fold. Removing both AA2P and Dex further decreased igf1 mRNA while increasing vegfa and pdgfa (Figure 5.4A, Table 5.5). Individually removing AA2P and Dex from CM decreased IGF-I secretion 10.5 to 22 fold and increased VEGF-A secretion 5.3 to 58 fold (Figure 5.4B). Removing AA2P also decreased TGF-β2 secretion 2.5 fold while removing Dex increased TGF-β2 secretion 2.4 fold. Removing AA2P decreased acan, comp, and sox9 1.8 to 3.1 fold while leaving out Dex increased mRNAs for these same genes 1.5 to 23 fold (Table 5.5).

Removing both exogenous TGF-β1 and BMP-6 from CM significantly decreased igf1, pthlh, and vegfa by 1.4 to 10.1 fold (Figure 4A); nog 1000 fold; and tgfb3 16 fold (Table 5.5). Specifically, the lack of TGF-β1 reduced igf1, pthlh, tgfb2, fgf18, tgfb1, and tgfb3 2.7 to 25 fold while the lack of BMP-6 reduced pthlh, tgfb2, bmp2, vegfa, fgf18, and nog 2.2 to 220 fold (Figure 5.5A, Table 5.5). Taking out TGF-β1 also increased bmp2, fgf2, bmp6, and nog 1.8 to 4.3 fold while the lack of BMP-6 increased bmp6 8.6 fold. Individually removing exogenous TGF-β1 and BMP-6 from CM decreased IGF-I secretion 1.7 to 2.4, TGF-β2 secretion 8.3 to 25 fold, and VEGF-A secretion 1.3 to 1.6 fold. The absence of TGF-β1 and BMP-6 had similar effect on acan and comp, reducing their mRNA levels 1.7 to 31 fold.

Table 5.5: Effect of Components in Chondrogenic Medium

The Effect of Ascorbic Acid 2-Phosphate, Dexamethasone, and Growth Factors on ASC Monolayers

	CM	-AA2P	-DEX	-AA2P -DEX	-TGF-β1 -BMP-6
mRNA Levels					
Bmp6/Rps18	67.0± 6.6	114.9± 24.9	27.3± 3.2	53.6± 5.1	62.2± 9.8
Fgf18/Rps18	887.6± 73.3	*2497.2±634.0	*96.9±13.3	*570.7±45.1	*132.1±29.7
Nog/Rps18	1746.1±171.4	1382.8±205.8	*310.3±33.7	*826.7±70.7	*1.7± 0.4
Pdgfa/Rps18	12.2± 1.2	12.3± 2.6	*22.2± 2.9	*27.7± 2.5	*2.1± 0.7
Tgfb1/Rps18	15.8± 2.6	15.6± 1.9	*47.9±11.5	*47.3± 2.8	*1.7± 0.3
Tgfb3/Rps18	748.9± 50.2	656.0± 85.4	656.4±82.4	*604.2±30.0	*47.4± 8.5
Acan/Rps18	6.7± 0.4	*3.6± 0.3	*153.8±19.7	*95.0± 5.3	*0.7± 0.2
Col2/Rps18	0.4± 0.2	0.1± 0.0	0.6± 0.1	[1]0.1± 0.0	0.2± 0.1
Comp/Rps18	17.5± 2.2	*5.7± 0.7	*95.1±26.5	*146.6±45.7	*0.2± 0.1
Sox9/Rps18	5.2± 0.2	*3.0± 0.4	*7.8± 0.7	*3.6± 0.2	*[1]0.0± 0.0
Growth Factor Production					
FGF-2/DNA[2]	7.2± 2.2	2.4± 0.6	3.2± 1.1	6.1± 2.7	4.6± 1.4
TGF-β3/DNA[2]	46.5± 3.2	61.7± 7.3	*183.1±30.0	*97.6±10.7	*19.2± 1.7

The Effect of TGF-β1 and BMP-6 on ASC Monolayers

	CM	-TGF-β1	-BMP-6	-TGF-β1 -BMP-6
mRNA Levels				
Bmp6/Rps18	12.2± 1.4	*21.5± 3.4	*103.9±22.6	*37.8±5.7
Fgf18/Rps18	59.6±17.0	13.9± 2.9	*13.0± 4.7	36.6±7.1
Nog/Rps18	18.5± 3.4	*80.4±17.7	0.1± 0.0	*0.3±0.1
Pdgfa/Rps18	18.9± 3.9	13.7± 2.1	26.1± 7.6	6.9±0.8
Tgfb1/Rps18	4.8± 1.0	*1.7± 0.3	4.0± 0.8	*1.6±0.4
Tgfb3/Rps18	7.0± 1.1	*2.6± 0.6	4.5± 1.3	*0.6±0.1
Acan/Rps18	3.0± 0.8	*0.6± 0.2	*0.1± 0.1	0.1±0.0
Col2/Rps18	0.1± 0.0	0.1± 0.0	0.1± 0.0	0.1±0.0
Comp/Rps18	0.4± 0.1	*0.1± 0.0	0.1± 0.0	0.1±0.0
Sox9/Rps18	0.8± 0.2	1.0± 0.2	0.5± 0.1	0.0±0.0
Growth Factor Production				
FGF-2/DNA[2]	22.4± 1.0	*15.5± 2.1	22.7± 0.8	16.7±2.3
TGF-β3/DNA[2]	33.7± 2.3	*19.5± 0.9	42.7± 4.4	*17.6±0.6

*p<0.05 vs. CM, n = 6, mean±SE
[1]Value less than 0.05.
[2] Units of ng/µg.
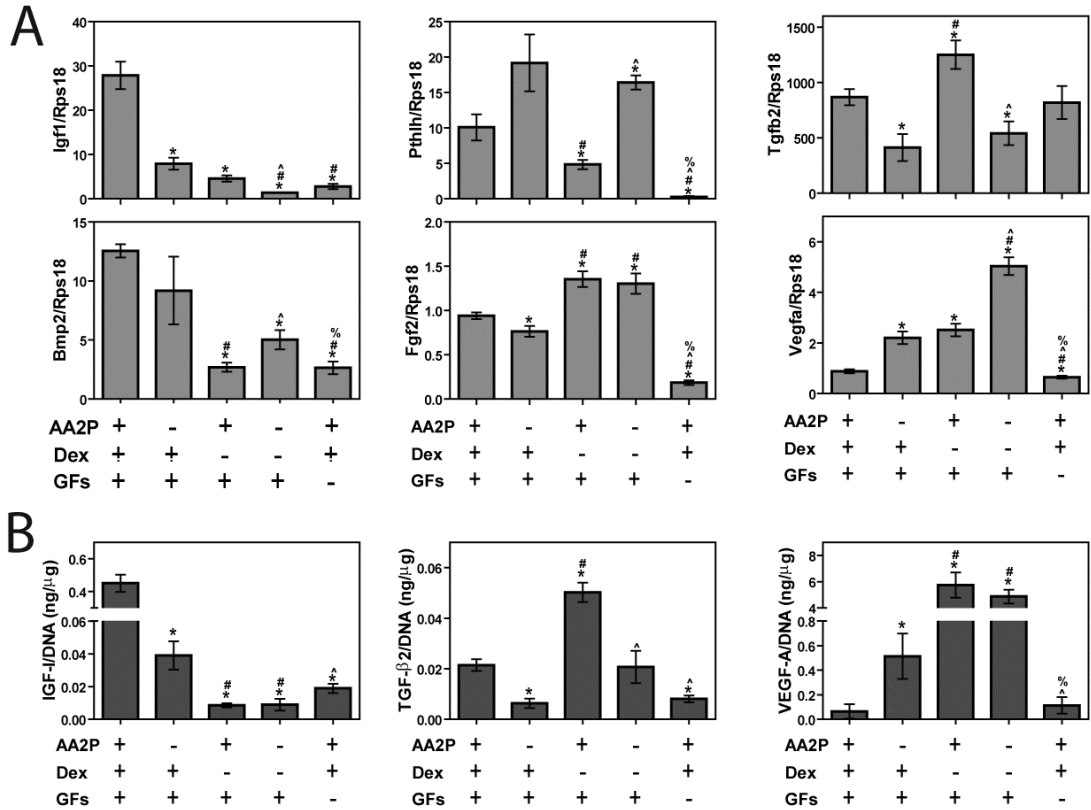
Figure 5.4: Effect of AA2P, Dex, and Growth Factors in Chondrogenic Medium
(A) Trophic factor mRNA levels of ASCs in chondrogenic medium without ascorbic acid 2-phosphate (AA2P), dexamethasone (Dex), or TGF-β1 and BMP-6 (GFs). (B) Growth factor secretion from ASCs in chondrogenic medium without ascorbic acid 2-phosphate (AA2P), dexamethasone (Dex), or TGF-β1 and BMP-6 (GFs) (n = 6, mean±SE, *p<0.05 vs. chondrogenic medium, #p<0.05 vs. +AA2P, ^p<0.05 vs. +Dex, %p<0.05 vs. +AA2P + Dex).
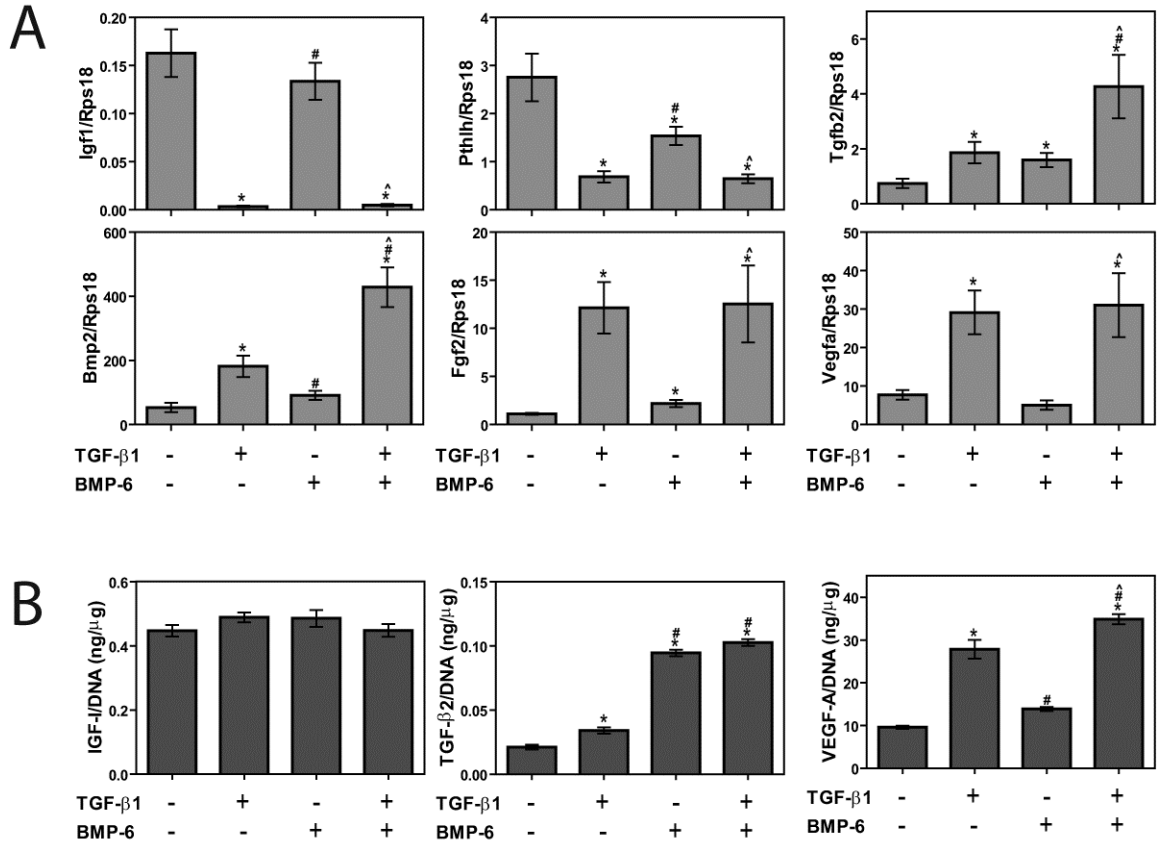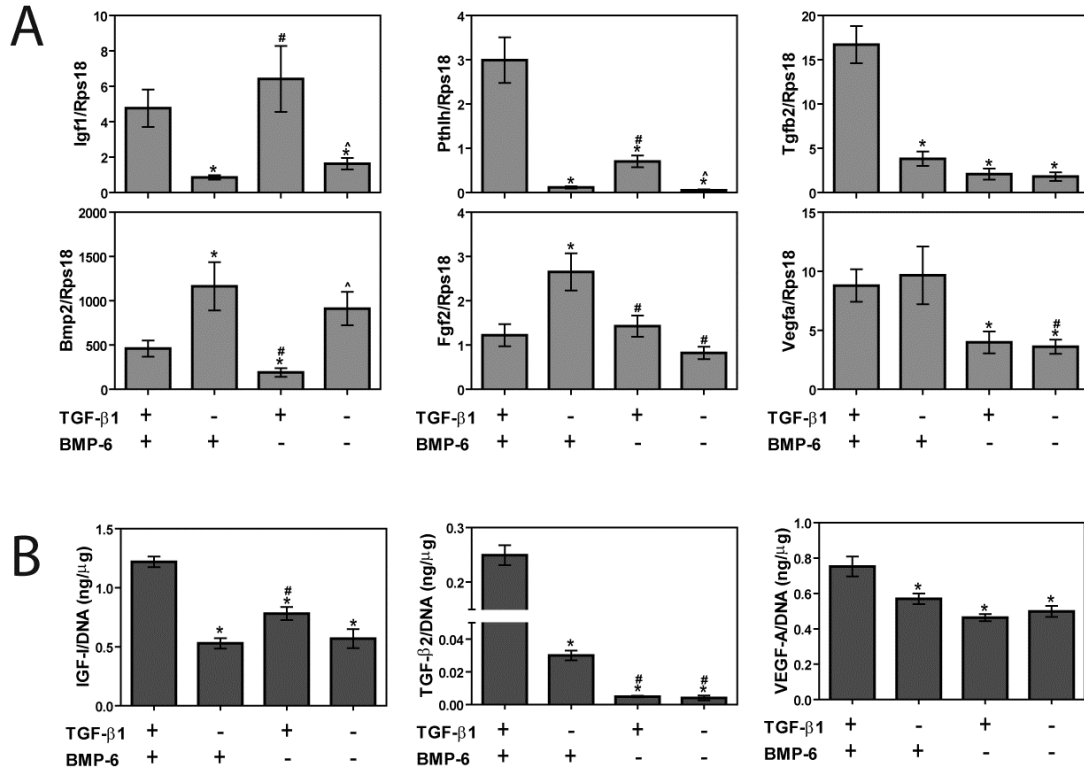
Figure 5.5: The Effect of TGF-β1 and BMP-6 in Chondrogenic Medium.
(A) Trophic factor mRNA levels of ASCs in chondrogenic medium without TGF-β1 and BMP-6. (B) Growth factor secretion from ASCs in chondrogenic medium without TGF-β1 and BMP-6. (n = 6, mean±SE, *p<0.05 vs. growth medium, #p<0.05 vs. + TGF-β1, ^p<0.05 vs. + BMP-6.

DISCUSSION

This is the first comprehensive study to show that microencapsulation and different components in chondrogenic medium have distinct effects on growth factor production from ASCs and that ASC microbeads can promote cartilage regeneration in a focal cartilage defect.

In this study, ascorbic acid 2-phosphate regulated secretion of IGF-I and FGF-2, both potent stimulators of chondrocyte proliferation [309], and decreased mRNA for FGF-18, a growth factor associated with hypertrophic differentiation [63]. These results are consistent with previous findings where ascorbic acid 2-phosphate and other vitamin C derivatives stimulated cell proliferation in a variety of different cell types [324-326] and stimulated IGF-I production from dermal papilla cells [327]. Meanwhile, dexamethasone, an anti-inflammatory and immunosuppressant corticosteroid, decreased mRNA for FGF-2 and secretion of VEGF-A and increased mRNAs for BMP-2 and FGF-18 in ASCs. These results are supported by the observation that dexamethasone decreased VEGF-A production from hemangioma-derived stem cells, inhibiting tumor vasculogenesis in a murine model [177], and upregulated FGF-18 during osteogenesis in MSCs [178]. Also in this study, TGF-β1 and BMP-6 increased mRNA levels and secretion of factors associated with chondrogenesis and hypertrophic differentiation while TGF-β1 also increased secretion of factors associated with angiogenesis. Others have shown that TGF-β1 stimulated production of cartilaginous tissue from chondrocytes and progenitor cells [308, 314, 328] but also controlled endothelial cell proliferation, invasion, and extracellular matrix turnover [329, 330]. Likewise, BMP-6 has previously been shown to stimulate chondrocyte maturation [331] and bone nodule formation [332].

Interestingly, microencapsulation alone increased mRNA levels for PTHrP and production of IGF-I and TGF-β2 after 5 days in growth medium but not in chondrogenic medium. This observation may be due to the high density and round morphology that ASCs have in alginate microbeads, both of which have been shown to support chondrogenesis [333, 334], and may explain why ASC microbeads just preconditioned in growth medium promoted tissue ingrowth in focal cartilage defects. However, high cell density and round cell morphology may have less of an effect in chondrogenic medium because of the overwhelmingly high concentrations of TGF-β1, BMP-6, and dexamethasone. Microencapsulation also increased VEGF-A production, possibly due to hypoxia caused by the high cell density. Although hypoxic conditions inside the microbead were not assayed, increasing cell densities in hydrogel cultures has been shown to increase oxygen tension and gradients [335] and, hypoxic conditions can increase VEGF-A and FGF-2 secretion from ASCs [336]. The microenvironment can also influence the response of ASCs to dexamethasone and TGF-β1 since they exert different chondrogenic effects on synovial MSC aggregates and synovial explants [337].

Along with the structural environment imparted by microencapsulation, exposure time to chondrogenic medium and its individual components may have significant effects on growth factor production from ASCs. Chondrogenic medium treatment lengths needed to induce optimal chondrogenesis of MSCs and ASCs in 3-D cultures have varied between 3 and 12 weeks [243, 304, 338], significantly longer than the treatment times used in this study. This difference in treatment times may explain the minimal effect chondrogenic medium components had on type II collagen expression and may suggest that longer treatment times are needed to optimize the effects different medium

96

components have on growth factor production. However the differences in treatment times and subsequent effects on cell behavior between previous studies and this current work do not take into account the mass-transfer properties of larger 3-D hydrogels.

The specific concentration of different components may also have a significant effect on growth factor production from ASCs. It is well known that TGF-β1 has a biphasic effect: at concentrations ranging from 100 pg/mL to 1 ng/mL, TGF-β1 increases endothelial cell proliferation [329] and the effect of FGF-2 and VEGF-induced invasion [330] whereas at concentrations ranging from 5 to 10 ng/mL, TGF-β1 inhibits endothelial cell invasion and capillary formation [330] and induced ASC chondrogenesis [304, 339]. Although ascorbic acid 2-phosphate and dexamethasone are also at their optimal concentrations for inducing chondrogenesis [243, 304], the concentration of BMP-6 was only at 20% of its optimal chondrogenic dose for ASCs [339]. It is possible that higher BMP-6 concentrations would significantly affect its actions on ASC growth factor production.

The effects of ascorbic acid 2-phosphate, dexamethasone, TGF-β1, and BMP-6 on certain growth factor production in this study were dependent on the presence and concentration of each other and other chondrogenic medium components. For instance, TGF-β1 decreased mRNAs for IGF-I and PTHrP in growth medium but increased these mRNAs in chondrogenic medium. Additionally, TGF-β1 was responsible for the increased VEGF-A secretion in growth medium, but BMP-6 was also responsible for increased VEGF-A secretion in chondrogenic medium. These different responses in these distinct media may be due to the differences in glucose concentrations and the presence or absence of ascorbic acid 2-phosphate, dexamethasone, proline, ITS+ culture

supplement, and serum. Although the effects of glucose, proline, ITS+ culture supplement, and serum were not directly investigated in this study, these components may also have significant effects on ASC growth factor production.

It is important to note that this study only disclosed methods to use chondrogenic medium components to affect the production of factors associated with angiogenesis, chondrogenesis, and hypertrophic differentiation. Determining the ideal ASC secretory profile for cartilage regeneration is a more complex problem due to the differential effects individual growth factors have. For instance, although VEGF-A is an angiogenic growth factor that is detrimental to chondrocytes and cartilage [68, 71], FGF-2, another important facilitator for blood vessel formation [340], is known to improve cartilage regeneration [341]. Additionally, factors associated with hypertrophic differentiation, like BMP-2 are important for progenitor cell proliferation and differentiation during early stage cartilage development [53] and may be needed to initiate cartilage regeneration. Meanwhile, factors like IGF-I and TGF-β1 are essential for chondrogenesis, cartilage formation, and homeostasis, but it is unknown whether long-term secretion of these factors from ASCs will lead to hypertrophic differentiation or other unforeseen side effects. In this study, it is unknown which factors will be most involved in tissue repair, whether different preconditioning treatments will accelerated cell infiltration and extracellular matrix deposition, or how long ASC microbeads will be needed more to enhance cartilage regeneration.

CONCLUSION

ASC cultures had high mRNA levels of proteins associated with the TGF-β and MAPK signaling pathways, and preconditioning ASC cultures with chondrogenic medium and its individual components had distinct effects on trophic factor production. For ASC cultures in 2-D monolayer and 3-D alginate microbeads, chondrogenic medium increased the mRNA levels and secretion of IGF-I, TGF-β2, and TGF-β3 and decreased the mRNA levels and secretion of VEGF-A and FGF-2. Microencapsulation alone increased mRNA levels for PTHrP and secretion of IGF-I, TGF-β2, and VEGF-A in growth medium, but not necessarily in chondrogenic medium. In subsequent studies with ASC monolayers cultured in growth and chondrogenic media, ascorbic acid 2-phosphate decreased mRNA levels for FGF-18 and secretion of VEGF-A but increased IGF-I and TGF-β2 secretion. Meanwhile, dexamethasone increased mRNA levels for BMP-2 and FGF-18, decreased mRNA levels for FGF-2, and decreased secretion of VEGF-A in growth and chondrogenic media. TGF-β1 and BMP-6 increased secretion of TGF-β2 and mRNA levels for FGF-18 while TGF-β1 also increased secretion of FGF-2 and VEGF-A. This study demonstrated that different components of differentiation media can be used to tailor the secretome of stem cell therapies to regenerate musculoskeletal tissues.

CHAPTER 6

HUMAN ADIPOSE STEM CELL MICROBEADS AS GROWTH FACTOR PRODUCTION SOURCES FOR CARTILAGE REGNERATION

INTRODUCTION

Adult stem cell therapies such as adipose stem cells (ASCs) are an attractive option for various clinical applications because of their accessibility and ability to differentiate into multiple cell types [305]. However, challenges related to their delivery, such as high injection pressures [223], low retention in the desired site [342, 343], and low viability *in vivo* when injected or delivered on scaffolds [17, 18], may limit their effectiveness in clinical studies [344]. To address these problems, we have recently developed a microencapsulation technology where ASC microbeads under 200 microns can be injected under low injection pressures without any changes in shape, can maintain greater than 80% cell viability for at least 3 weeks post-injection, and can be localized in the desired site *in vivo* for at least 3 months [223].

Although ASCs can be used for a variety of clinical applications, repairing cartilage focal lesions is an attractive option because of the tissue's limited regenerative capacity and the lack of an effective treatment [6, 345]. Current cell therapies, such as autologous chondrocyte implantation aim to directly regenerate cartilage by providing a source of cells that can then synthesize new tissue. However, this strategy has had limited clinical adoption mainly due to high variability in cartilage quality and functional

100

outcomes [11, 12]. Therefore, a new paradigm has emerged in using stem cells as growth factor production sources to stimulate diseased or damaged musculoskeletal tissues like cartilage to regenerate themselves [32, 306]. ASC microbeads are highly favorable for this new strategy, not only because of their distinct advantages in delivery, but also because of the microbeads' potential ability to control the production and secretion of different growth factors.

Before ASC microbeads consisting of alginate can be used as growth factor production sources for regenerating cartilage and other tissues, a few unanswered issues need to be addressed. First, even though the mass transfer properties of soluble compounds and growth factors in alginate have been characterized [152, 195, 346], it is unknown how microencapsulation affects growth factor production and secretion from ASCs. Additionally, although chondrogenic medium can be used to differentiate ASCs in alginate hydrogels into chondrocytes [211], it is unknown if chondrogenic medium can also affect growth factor production and secretion from ASC microbeads. Furthermore, it is unknown if chondrogenic treatment and microencapsulation have consistent effects on ASCs derived from different donors in terms of growth factor expression and secretion. Finally, although the mass transfer properties of alginate hydrogels are dependent on the divalent crosslink [347, 348] and the type of alginate polymer used [195], the effects these parameters have on growth factor expression and production from ASCs is unknown. Therefore, the objectives of this study were to determine the time course of growth factor production and secretion from microencapsulated commercially human ASC microbeads cultured in growth and chondrogenic media, to determine if microencapsulation and chondrogenic medium treatments have consistent effects on

human ASCs from different donors, and to determine the effect microbead composition has on growth factor expression and production.

MATERIALS AND METHODS

<u>Cell Isolation and Passaging</u>

To determine the extent of growth factor production and secretion from ASC microbeads over time, first passage human ASCs from a 28 year old male donor were commercially obtained (Lonza, Basel, Switzerland) and cultured up to third passage in Lonza Mesenchymal Stem Cell Growth Medium (GM, Lonza) prior to microencapsulation. To test whether chondrogenic medium and microencapsulation had consistent effects on ASCs from different donors, adipose tissue was collected from 6 female patients ranging from 18 to 49 years of age (mean age ± standard error = 32.7±4.1) under an approved IRB protocol at Georgia Institute of Technology, Northside Hospital, and Children's Healthcare of Atlanta. Fat was obtained by breast reduction from 5 donors and abdominoplasty from 1 donor. All patients gave written consent to both the procedure and handling of fat thereafter. ASCs were isolated using a collagenase and dispase digestion cocktail as previously described [320]. Cells were then seeded at 5,000 cells/cm^2 and cultured in GM. When primary ASCs from 3 of the donors were at 90% confluence (P1 ASCs), they were trypsinized and were microencapsulated immediately. Cells from the other 3 donors were pelleted at 500 g for 10 minutes, resuspended in GM with 5% DMSO at 3×10^6cells/ml, cooled from room temperature to -80°C at 1°C/min, stored at -80°C overnight, and transferred to liquid nitrogen for later use. After 2 to 8 months, these cryopreserved cells were then cultured up to third passage

and microencapsulated (P3 ASCs). To determine the effects microbead composition had on growth factor production, cryopreserved ASCs from a 33 year old donor's breast tissue were cultured up to third passage and microencapsulated.   Prior to microencapsulation, all ASCs were positive for CD73 and CD271 and negative for CD45.

<u>Microencapsulation</u>

For all studies, alginate powders (FMC BioPolymer, Sandvika, Norway) were UV light sterilized overnight and dissolved in 0.22μm sterile filtered (Thermos Fisher Scientific, Rochester, NY, USA) saline (Ricca Chemical, Arlington, TX, USA) at 20 mg/mL. ASCs were then suspended in the alginate solution at 10^7 cells/mL. Microbeads containing the commercial ASCs were created using a Nisco Encapsulator VAR V1 LIN-0043 (Nisco Engineering AG, Zurich, Switzerland) at a 10 mL/hr flow rate, 0.12 mm inner diameter nozzle, and 6kV/cm electrostatic potential [223, 322]. Microbeads were imaged with an inverted microscope (Motic, Richmond, British Columbia, Canada) and had a mean diameter ± standard deviation of 122±15 microns (Motic Images Plus 2.0).

In studies determining growth factor production and secretion from ASC microbeads over time and in studies determining the effect of chondrogenic medium and microencapsulation on ASCs from multiple donors, microbeads with 130 kDa, 44% guluronate alginate (LVM, low viscosity high mannuronate) were crosslinked in a solution of 50 mM $CaCl_2$ (Sigma, St. Louis, MO, USA), 150 mM glucose (Sigma), and 15 mM 4-(2-hydroxyethyl)-1-piperazineethanesulfonic acid (HEPES, Sigma) at pH 7.3 for at least 15 minutes. To determine the effect Ca^{++} crosslinks had on growth factor production and secretion, ASC microbeads consisting of LVM were also crosslinked in a

solution of 20 mM BaCl$_2$ (Sigma, St. Louis, MO, USA), 150 mM glucose, and 15 mM HEPES at pH 7.3. To determine the effect alginate molecular weight and chemistry had on growth factor production and secretion, ASC microbeads were also made with the following alginates: 170 kDa, 66% guluronate (LVG, low viscosity high guluronate); <50 kDa, 44% guluronate (VLVM, very low viscosity high mannuronate); and 220kDa, 43% guluronate (MVM, medium viscosity high mannuronate). These ASC microbeads were crosslinked in the CaCl$_2$ solution as described above. For all studies, microbeads were washed three times in GM to remove any excess crosslinking solution. ASCs were also plated in 6-well tissue culture polystyrene (TCPS) plates (BD Biosciences, San Jose, CA, USA) for comparison.

Chondrogenic Treatment

Once ASCs in the 6-well plates reached 90% confluence, TCPS and microbead cultures were treated with either GM or chondrogenic medium (CM) consisting of Dulbecco's modified Eagle medium (DMEM) with 4.5g/L glucose and 1 mM sodium pyruvate (Mediatech, Manassas, VA, USA), 40 μg/ml proline (Sigma), 50 μg/ml ascorbate-2-phosphate (Sigma), 1% ITS+ (Sigma), 100 nM dexamethasone (Sigma), 10 ng/ml recombinant human transforming growth factor beta-1 (TGF-β1, R&D Systems, Minneapolis, MN, USA) and 100 ng/ml recombinant human bone morphogenic protein 6 (BMP-6, PeproTech, Rocky Hill, NJ, USA). For studies determining cumulative growth factor production and secretion from ASC microbeads over time, media were collected with each media change at 3, 5, 7, 10, 12, 14, and 15 days. For all subsequent studies, treatments lasted 7 and 14 days, RNA was collected 6 hours after the last media change

as described below, and media and ASC and lysates in 0.05% Triton X-100 (Sigma) were collected 24 hours after the last media change.

<u>RNA Isolation</u>

Alginate microbeads crosslinked in $CaCl_2$ (Ca microbeads) were uncrosslinked in 82.5 mM sodium citrate (Sigma) whereas alginate microbeads crosslinked in $BaCl_2$ (Ba microbeads) were uncrosslinked in 30 mM ethylenediaminetetraacetic acid (EDTA, Sigma) and 135 mM NaCl (Sigma). Released cells were then pelleted and washed two more times in their respective uncrosslinking solution to remove any residual alginate. TRIzol reagent (Invitrogen, Carlsbad, CA, USA) was added to the cell pellet, which was fed through a QIAshredder (QIAGEN, Valencia, CA, USA), and RNA was isolated using chloroform and an RNeasy Kit (QIAGEN) as previously described [323]. A high capacity reverse transcription cDNA kit (Applied Biosystems, Carlsbad, CA, USA) was used to reverse transcribe 1 μg RNA to cDNA.

<u>Quantifying mRNA Levels and Growth Factor Production</u>

Chondrogenesis is a multi-step process that is regulated by numerous paracrine factors. Therefore, mRNA levels and secretion of multiple signaling molecules were measured to assess the therapeutic potential of ASC microbeads. FGF-2, IGF-I, and PTHrP were investigated because of their ability to increase chondrocyte proliferation and regulate hypertrophy [309-312]. TGF-β3 secretion was investigated since TGFs are potent stimulators of proteoglycan synthesis [313, 314]. However, TGF-β1 secretion was not investigated due to its large concentration in chondrogenic medium. Noggin was investigated because of its role in cartilage differentiation [315]. VEGF-A was investigated because of its detrimental effects on cartilage regeneration: this growth

factor has been shown to increase matrix metalloproteinase expression in chondrocytes [68] and may have a potential role in osteoarthritis progression [71].

Messenger RNA levels for the genes listed in Table 6.1 were quantified using real-time PCR with gene-specific primers using the Step One Plus Real-time PCR System and Power Sybr® Green Master Mix (Applied Biosystems) as previously described [166]. All primers were designed with Beacon Designer software (Premier Biosoft, Palo Alto, CA, USA) and synthesized by Eurofins MWG Operon (Huntsville, AL, USA) unless otherwise noted (Table 1). Growth factor production was quantified using ELISA (R&D Systems) and normalized to DNA content measured by a Quant-iT PicoGreen kit (Invitrogen). To measure growth factor retention within the microbead, microbeads were uncrosslinked in 82.5 mM sodium citrate and frozen at -80°C overnight. Samples were then lyophilized at -50°C and 10 Pa for 24 hours. The resulting dried constructs were then digested in 1 unit/mL alginate lyase (Sigma) for at least 1 hour at 37°C and growth factors measured with ELISA. Quantified mRNA levels were referred to by the name of the gene whereas quantified protein levels were referred to by the name of the growth factor.

Table 6.1: Primer Sequences for Human ASCs

Gene	Direction	Sequence
Acan	Sense	TCAGCGGTTCCTTCTCCA G
	Antisense	GCAGTTGTCTCCTCTTCTACG
Col2	Sense	CTGCTCGTCGCCGCTGTCCTT
	Antisense	AAGGGTCCCAGGTTCTCCATC
Col10	Sense	TTACGCTGAACGATACCAAATG
	Antisense	GCTCTCCTCTTACTGCTATACC
Comp	Sense	CCTGCGTTCTTCTGCTCAC
	Antisense	GCGTCACACTCCATCACC
Fgf2	Sense	GCGACCCTCACATCAAGC
	Antisense	AGCCAGTAATCTTCCATCTTCC
Igf1	Sense	GGAGGCTGGAGATGTATTG
	Antisense	GACTTCGTGTTCTTGTTGG
Nog	Sense	Global Gene Sequence (Qiagen)
	Antisense	
Pthlh	Sense	CTCGCTCTGCCTGGTTAG
	Antisense	CAATGCCTCCGTGAATCG
Rps18	Sense	CGTCTGCCCTATCAACTTTCG
	Antisense	CTTGGATGTGGTAGCCGTTTC
Sox9	Sense	GAGCAGCGAAATCAACGAGAAAC
	Antisense	ACAAAGTCCAAACAGGCAGAGAG
Tgfb1	Sense	CAACAATTCCTGGCGATACCTC
	Antisense	CCACGGCTCAACCACTGC
Tgfb2	Sense	CGAGAGGAGCGACGAAGAG
	Antisense	TAGAAAGTGGGCGGGATGG
Tgfb3	Sense	CAACGAACTGGCTGTCTG
	Antisense	CTCTGCTCATTCCGCTTAG
Vegfa	Sense	CTTGCCTTGCTGCTCTACC
	Antisense	TTCTGCCCTCCTCCTTCTG

Statistical Analysis

All experiments had six independent cultures per treatment group and were conducted multiple times to confirm the findings. For studies involving six donors, all data are presented in the form of treatment (i.e. CM or microencapsulation [µB]) over control (i.e. GM or TCPS). For these studies, the sample sizes were the mean of six samples from each of the six donors and statistical differences between the treatment and control groups and among the different groups at 1 and 2 weeks were determined via a Mann-Whitney-Wilcoxon test (GraphPad Prism, La Jolla, CA, USA). The significance of medium, microencapsulation, culture time, passage number, and their interactions on ASC growth factor mRNA levels and production were determined via a 4-way ANOVA

(MATLAB, MathWorks, Natick, MA, USA). For studies that did not investigate ASCs from six donors, only data from a single representative experiment are shown and are expressed as means ± standard errors. Statistical differences among these experimental groups were determined via ANOVA with a post hoc Tukey test (GraphPad Prism). Linear regression was used to assess cumulative growth factor secretion profiles from ASC microbeads and monolayers (GraphPad Prism). All differences and effects were considered to be statistically significant if the p-value was less than 0.05.

RESULTS

Effect of Chondrogenic Medium and Microencapsulation on Multiple Donors

For 6 different donors, CM decreased fgf2 in TCPS cultures by 8.8 to 9.6 fold and microbeads by 3.7 to 4.2 fold at day 7 and 14 (Figure 6.1A). CM treatment for 7 and 14 days also decreased vegfa in the TCPS cultures and microbeads by 4.3 to 6.5 fold. 7 and 14 days of CM treatment increased nog in TCPS cultures by 66 and 146 fold respectively, but nog in microbeads only increased by 7.2 and 12.8 fold.

CM did not decrease FGF-2 secretion on day 7 or 14 (Figure 6.1B) as FGF-2 production from TCPS cultures in CM was 2 fold higher than TCPS cultures in GM on day 7. VEGF-A secretion from microbeads in CM was 4.9 fold lower than microbeads in GM on day 14. CM also increased acan, col2, col10, comp, igf1, sox9, and tgfb3 and decreased pthlh in ASC cultures (Table 6.2).
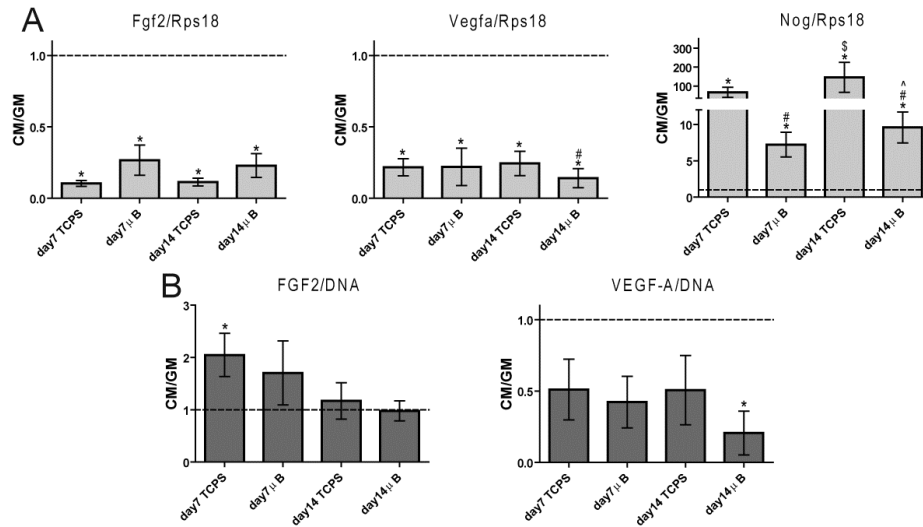
Figure 6.1: Effect of Chondrogenic Medium on Growth Factor mRNA Levels and Secretion from ASCs Isolated from Different Donors

(A) mRNA levels and (B) growth factor secretion/DNA content on day 7 and day 14 from ASCs cultured in chondrogenic medium (CM) on tissue culture polystyrene (TCPS) and within alginate microbeads (µB) normalized to matching 2-D and 3-D cultures in growth medium (GM) (n = 6 donors, mean±SE, *p<0.05 CM vs. GM, #p<0.05 vs. wk1 TCPS, $p<0.05 vs. wk1 µB, ^p<0.05 vs. wk2 TCPS).

Microencapsulation had differential effects on chondrocyte phenotypic mRNA levels of ASCs. After 7 days in CM, microencapsulation decreased acan and comp by 3.3 and 5.3 fold respectively but increased col2 by 6.2 fold (Figure 6.2). After 14 days in CM, microencapsulation increased col10 by 8.6 fold. Meanwhile, microencapsulation had no effect on sox9 in either GM or CM. For growth factor mRNA levels, microencapsulation consistently decreased igf1 for 6 different donors with a 4.2 fold decrease in CM after 7 days (Figure 6.3A). The effects of microencapsulation on pthlh and tgfb3 were media dependent. Microencapsulation only increased pthlh in GM by 5.3 and 3.7 fold after 7 and 14 days respectively. Microencapsulation increased tgfb3 in GM by 8.2 and 4.8 fold after 7 and 14 days respectively but decreased tgfb3 in CM by 2.3 fold at day 7.

Microencapsulation increased IGF-I secretion at day 7 in GM and CM by 11.9 and 7.6 fold respectively (Figure 6.3B). Microencapsulation also increased TGF-β3 secretion by 2.3 fold at day 7 in CM and by 4.6 fold on day 14 in GM. VEGF-A secretion from ASCs was not affected by microencapsulation, but microencapsulation did increase FGF-2 secretion at day 14 in GM and decreased nog expression after 7 and 14 days in CM (Table 6.2).
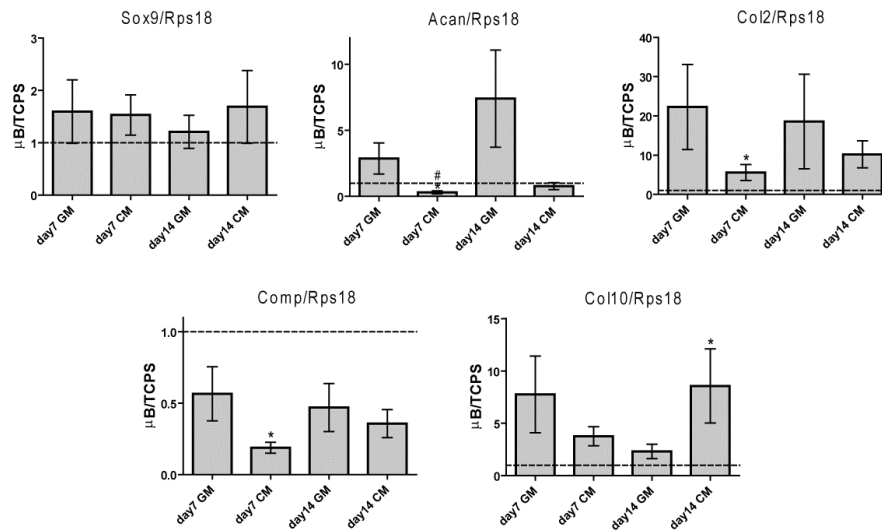
Figure 6.2: Effect of Microencapsulation on Phenotypic mRNA Levels of ASCs Isolated from Different Donors
(A) mRNA levels on day 7 and day 14 of ASC microbeads cultured in growth medium or chondrogenic medium (CM) normalized to ASCs on tissue culture polystyrene (TCPS) cultured in matching media. (n = 6 donors, mean±SE, *p<0.05 μB vs. TCPS, #p<0.05 vs. wk1 GM, $p<0.05 vs. wk1 CM, ^p<0.05 vs. wk2 GM).
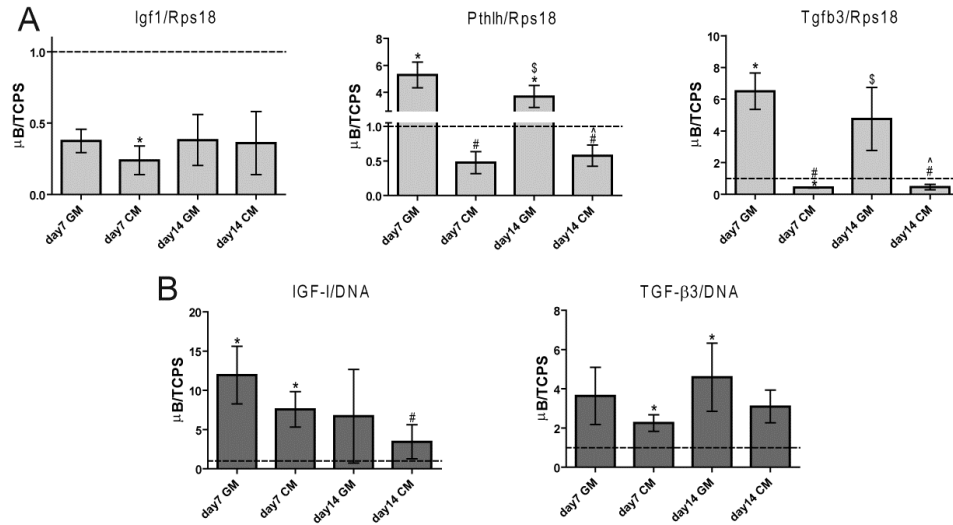
Figure 6.3: Effect of Microencapsulation on Growth Factor mRNA Levels and Secretion from ASCs Isolated from Different Donors

(A) mRNA levels and (B) growth factor secretion/ DNA content on day 7 and day 14 from ASC microbeads cultured in growth medium or chondrogenic medium (CM) normalized to ASCs on tissue culture polystyrene (TCPS) cultured in matching media (n = 6 donors, mean±SE, *p<0.05 µB vs. TCPS, #p<0.05 vs. wk1 GM, $p<0.05 vs. wk1 CM, ^p<0.05 vs. wk2 GM).

Table 6.2: Effect of Chondrogenic Medium and Microencapsulation on ASCs from Multiple Donors

	CM/GM			
	wk1 TCPS	wk1 µB	wk2 TCPS	wk2 µB
mRNA Levels				
Acan/Rps18	*94.5±41.3	*9.9±4.0	*184.7±95.6	*18.3± 5.6
Col2/Rps18	3.6± 1.4	2.4±1.5	2.5± 0.8	10.0± 4.5
Col10/Rps18	*48.8±33.8	*14.9±4.2	*11.7± 7.9	*23.4±11.2
Comp/Rps18	*8.7± 2.1	*4.1±1.0	*8.0± 1.9	*8.2± 2.4
Igf1/Rps18	*2.8± 0.8	1.6±0.6	4.6± 1.3	*3.3± 0.6
Pthlh/Rps18	*0.6± 0.2	*0.1±0.0	0.5± 0.1	*0.1± 0.0
Sox9/Rps18	1.8± 0.3	*1.9±0.3	*2.2± 0.6	*2.4± 0.2
Tgfb1/Rps18	*2.0± 0.2	1.5±0.4	*1.6± 0.2	1.0± 0.2
Tgfb2/Rps18	1.4± 0.3	1.0±0.5	1.5± 0.3	1.1± 0.3
Tgfb3/Rps18	*8.4± 1.8	0.6±0.2	*5.0± 1.2	0.6± 0.2
Growth Factor Secretion				
IGF-I/DNA	*4.7± 2.4	1.9±0.3	6.0± 2.9	2.0± 0.7
TGF-β3/DNA	1.2± 0.1	1.0±0.1	1.1± 0.2	1.0± 0.3

	µB/TCPS			
	wk1 GM	wk1 CM	wk2 GM	wk2 CM
mRNA Levels				
Fgf2/Rps18	*0.3±0.1	*0.5±0.1	0.6±0.3	0.7±0.3
Nog/Rps18	1.1±0.6	*0.1±0.0	1.4±0.7	*0.2±0.1
Tgfb1/Rps18	1.9±0.3	1.5±0.4	1.8±0.3	1.0±0.2
Tgfb2/Rps18	6.1±1.7	2.0±0.5	2.4±0.6	1.6±0.3
Vegfa/Rps18	2.2±0.7	0.9±0.3	2.0±0.7	1.3±0.5
Growth Factor Secretion				
FGF-2/DNA	0.8±0.4	1.6±1.4	*6.1±2.3	5.0±2.4
VEGF-A/DNA	0.5±0.2	1.1±0.7	1.3±0.5	2.1±1.1

*p<0.05 CM vs. GM for CM/GM values and µB vs.TCPS for µB/TCPS values

4-way ANOVA showed that media treatment significantly influenced acan, col10, comp, fgf2, igf1, nog pthlh, and sox9 as well as IGF-I and VEGF-A secretion (Table 6.3). Microencapsulation significantly affected col2, col10, comp, fgf2, igf1, nog, and tgfb2 as well as IGF-I and TGF-β3 secretion. 7 days versus 14 days in culture did not influence baseline gene expression but did influence FGF-2 and TGF-β3 secretion. The interaction between medium and microencapsulation had significant effects on nog, pthlh, and tgfb3 but not on growth factor secretion. Although there were significant differences in baseline growth factor expression and secretion between freshly isolated P1 ASCs and cryopreserved P3 ASCs, the interaction between microencapsulation and cell passage did not affect mRNA levels but did affect FGF-2 and IGF-I secretion.

Table 6.3: P-values of 4-Way ANOVA of Media, Microencapsulation (μB), Culture Time (Time), and Passage Number (Passage)

	Media	μB	Time	Passage	Media × μB	μB × Time	μB × Passage
mRNA Levels							
Acan/Rps18	*<0.001	0.822	0.328	0.128	0.058	0.453	0.217
Col2/Rps18	0.180	*0.001	0.853	*0.006	0.638	0.962	0.101
Col10/Rps18	*<0.001	*<0.001	0.172	*0.003	0.524	0.546	0.673
Comp/Rps18	*<0.001	*0.001	0.339	0.198	0.580	0.720	0.299
Fgf2/Rps18	*<0.001	*<0.001	0.931	*0.070	0.074	0.544	0.831
Igf1/Rps18	*0.022	*<0.001	0.546	0.612	0.537	0.893	0.978
Nog/Rps18	*<0.001	*<0.001	0.795	*0.003	*0.019	0.588	0.232
Pthlh/Rps18	*<0.001	0.428	0.335	*<0.001	*<0.001	0.972	0.386
Sox9/Rps18	*0.002	0.352	0.818	0.654	0.707	0.787	0.151
Tgfb1/Rps18	0.465	0.456	0.590	*0.001	0.596	0.827	0.991
Tgfb2/Rps18	0.968	*0.001	0.328	*<0.001	0.496	0.130	0.703
Tgfb3/Rps18	0.141	0.393	0.814	*0.045	*<0.001	0.452	0.943
Vegfa/Rps18	*0.001	0.895	0.881	*0.017	0.626	0.931	0.463
Protein Secretion							
FGF-2/DNA	0.799	0.132	*0.007	0.250	0.730	0.931	*0.031
IGF-I/DNA	*0.026	*<0.001	0.184	*<0.001	0.379	*0.028	*0.023
TGF-β3/DNA	0.965	*<0.001	*0.001	*0.001	0.825	0.108	0.181
VEGF-A/DNA	*<0.001	*0.029	0.512	0.947	0.981	0.556	0.229

*p<0.05 CM vs GM for media, μB vs.TCPS for μB, 1 week vs. 2 weeks for time, 1 passage vs. 3 passages for passage.

Igf1 in Ba microbeads was less than that of Ca microbeads (Figure 6.4A). Ba microbeads also secreted less IGF-I than Ca microbeads on day 7 (Figure 6.4B) and Ba microbeads maintained 10 fold less IGF-I within than Ca microbeads over 7 days (Figure

6.4C). However, both Ca microbeads and Ba microbeads secreted 10.9 and 4.4 fold greater IGF-I than TCPS cultures on day 7 (Figure 6.4B). Pthlh and tgfb3 in Ba microbeads were not statistically different from Ca microbeads and was 28 to 29 fold greater than TCPS cultures (Figure 6.4A). Ca and Ba microbeads secreted similar amounts of TGF-β3 on day 7 (Figure 6.4B), and although Ca microbeads maintained more TGF-β3 than Ba microbeads (Figure 6.4C), this difference was not significant.
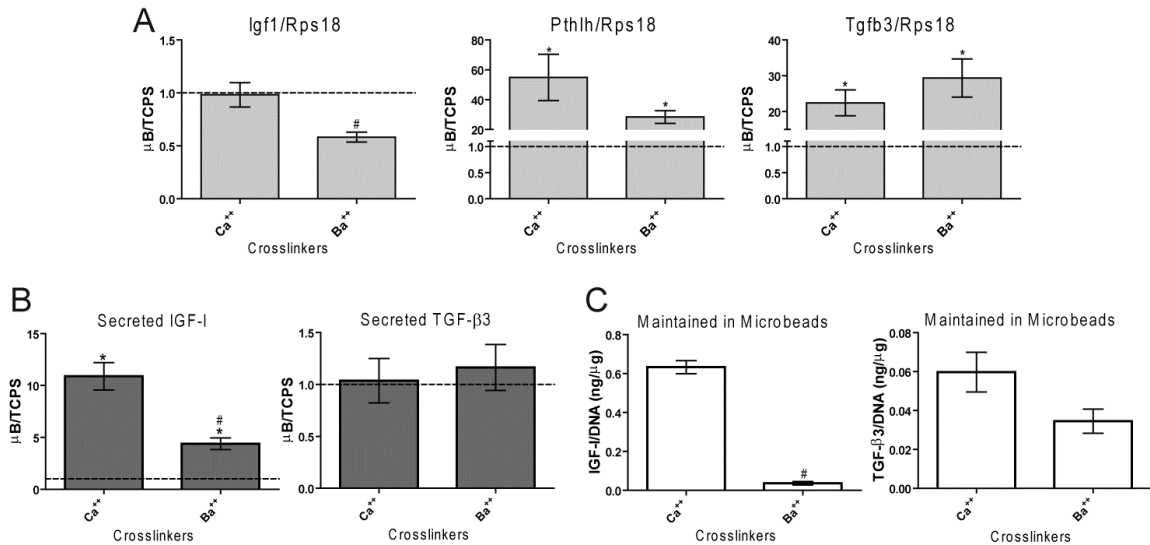
Figure 6.4: Effect of Divalent Crosslinks in ASC Microbead on Growth Factor mRNA Levels and Production
(A) mRNA levels and (B) growth factor secretion/DNA content on day 7 from ASC microbeads crosslinked in $CaCl_2$ (Ca^{++}) or $BaCl_2$ (Ba^{++}), cultured in growth medium, and normalized to ASCs on tissue culture polystyrene (TCPS). (C) Growth factor retained within microbeads normalized to DNA content (n = 6 samples, mean±SE, *$p<0.05$ μB vs. TCPS, #$p<0.05$ vs. Ca^{++}).

MVM microbeads had 2.3 fold lower pthlh than LVM microbeads, but all microbeads had at least 24 fold higher pthlh than TCPS cultures (Figure 6.5A). LVG microbeads had 2.9 fold higher tgfb3 than LVM, but all microbeads still had at least 22 fold higher tgfb3 than TCPS cultures. Although the different alginate polymers did not have a significant effect on igf1 (Figure 6.5A), VLVM microbeads secreted 2.8 fold less IGF-I than LVM microbeads on day 7 (Figure 6.5B). Additionally, LVM, LVG, and

MVM microbeads secreted 2.9 to 4.3 fold more IGF-I than TCPS cultures, but VLVM microbeads secreted similar levels of IGF-I to TCPS cultures on day 7. LVG microbeads retained 2.4 fold more IGF-I than LVM microbeads over 7 days (Figure 6.5C). The molecular weight and guluronate content of the alginate polymer had no effect on TGF-$\beta 3$ secreted or retained in the microbeads (Figure 6.5B, C).
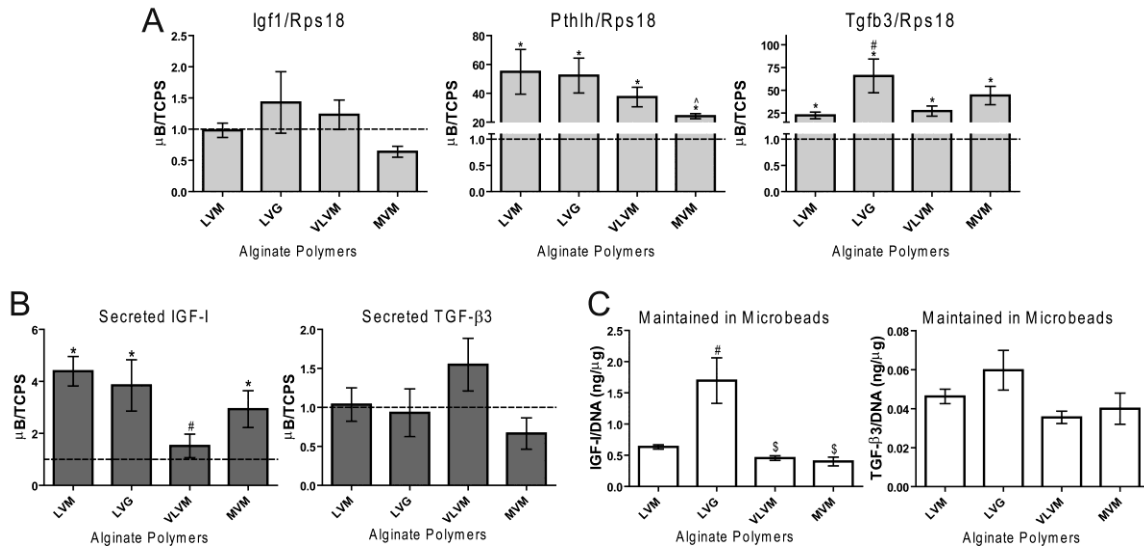
Figure 6.5: Effect of Alginate Molecular Weight and Chemistry in ASC Microbead on Growth Factor mRNA Levels and Production
(A) mRNA levels and (B) growth factor secretion/DNA content on day 7 from ASC microbeads consistent of LVM, LVG, VLVM, and MVM alginates; cultured in growth medium; and normalized to ASCs on tissue culture polystyrene (TCPS). (C) Growth factor retained in microbeads normalized to DNA content (n = 6 samples, mean±SE, *p<0.05 µB vs. TCPS, #p<0.05 vs. LVM, $p<0.05 vs. LVG).

DISCUSSION

This study demonstrated that ASC microbeads have the potential to be growth factor production sources for regenerating cartilage. Specifically, ASC microbeads can secrete growth factors at a consistent rate over a two week period, microencapsulation and chondrogenic medium have consistent effects on growth factor expression and secretion from ASCs derived from multiple donors, and microbead composition can influence the production and secretion of certain growth factors. These findings are

consistent with previous studies delivering progenitor cells within alginate. These studies showed that alginate microcapsules could maintain growth factor gene expression and sustain growth factor release for at least 22 days while promoting bone and myocardial muscle regeneration [169, 349]. Additionally, barium crosslinks have previously been shown to reduce secretion of protein from alginate beads [348] and that low guluronate content alginate hydrogels with a more flexible polymer backbone have greater solute diffusivity [195].

It is important to note that other parameters, such as alginate degradation and electrostatic interaction between the alginate and growth factor, can influence growth factor diffusive properties and subsequent secretion from alginate microbeads [152, 350]. Additionally, including biomimetic peptides within the microbeads, such as RGD, can manipulate the expression of certain growth factors [169]. In this study, the alginate backbone of the microbeads was not chemically modified and microbead degradation was not apparent, but growth factor retention within the microbead was observed. Although manipulating the ASCs with chondrogenic medium and alginate chemistry were the main drivers for controlling growth factor secretion from microbeads, methods for controlling alginate degradation may release growth factors stuck within the alginate hydrogel, providing another mechanism to tailor the secretory profile from ASC microbeads.

Interestingly, microencapsulation increased mRNA levels for both PTHrP and TGF-β3 in ASCs in growth medium but decreased mRNA and the secretion profile of TGF-β3 in chondrogenic medium. Calcium has been shown to increase secretion of PTHrP from human cells [183], but this current study showed that increases in PTHrP

and TGF-β3 mRNA levels were independent of the calcium crosslinks. Previous studies have shown that soluble components of serum can hinder chondrogenesis [351] whereas TGF-β1 and BMP-6 in chondrogenic medium can increase chondrocytic phenotype in ASCs [211, 305, 352]. Although the effects of individual serum components on growth factor production were not directly measured in this study, microencapsulation may have hindered the mass transport of these inhibitory soluble factors in growth medium and stimulatory soluble factors in chondrogenic medium.

Encapsulation in alginate is well known to restore the chondrocytic phenotype of dedifferentiated chondrocytes and to enhance the differentiation of mesenchymal stem cells [243, 353]. These chondrogenic effects have been attributed to the round cell morphology and cell-cell interactions imparted by high density encapsulation [333, 354]. This study also showed that alginate microbeads can retain endogenously produced IGF-I and TGF-β3. The retention of these chondrogenic factors may have also been responsible for the increased PTHrP and TGF-β3 mRNA levels in ASC microbeads cultured in growth medium. These attributes suggest that the microenvironment within ASC microbeads may mimic that of native cartilage, making them ideal candidates as trophic factor production sources for cartilage regeneration.

Several studies have investigated whether donor age or body mass index affect ASC density in tissue and their chondrogenic potential, but the results have been conflicting [355-357]. These discrepancies may be due to differences in tissue harvesting techniques, anatomical location, and donor sex, all of which have been shown to affect ASC yield and differentiation potential [355, 358, 359]. Furthermore, extended passaging has been shown to increase the chondrogenic potential of these cells [354].

The variability in these parameters in this current study may have caused the inconsistencies among the different cell culture experiments, specifically in the effect of microencapsulation on growth factor secretion between different studies. Additionally, the effects of microencapsulation on growth factor mRNA levels were often not consistent with the effects of microencapsulation on growth factor secretion. These discrepencies may be due to post-transcriptional regulation, post-translational modifications, or parameters that affect growth factor diffusion and secretion but not production as already discussed.

CONCLUSION

Microencapsulation consistently increased the gene expression of PTHrP and secretion of IGF-I and TGF-β3 from ASCs from multiple donors. Meanwhile, chondrogenic medium consistently decreased the expression of FGF-2 and secretion of VEGF-A from ASC microbeads derived from the same donor population. Crosslinking microbeads in $BaCl_2$ instead of $CaCl_2$ did not eliminate the beneficial effects of microencapsulation, but did decrease IGF-I gene expression and production. Increasing the guluronate content of the alginate microbead increased TGF-β3 expression and IGF-I maintained within. Decreasing the molecular weight of the alginate used eliminated the beneficial effects microencapsulation had on IGF-I secretion while increasing the molecular weight of alginate used decrease PTHrP gene expression. This study demonstrated that ASC microbeads may be a reliable source for delivering multiple growth factors to facilitate cartilage regeneration.

CHAPTER 7

ADIPOSE STEM CELLS CAN SECRETE ANGIOGENIC FACTORS THAT CAN INHIBIT HYALINE CARTILAGE REGENERATION

INTRODUCTION

Adult stem cells, such as adipose stem cells (ASCs) are an emerging clinical option for treating tissue damage and diseases because of their accessibility and ability to differentiate into multiple cell lineages [305, 360]. More recently, ASCs and other adult stem cells have been shown to secrete a wide range of trophic factors that can stimulate regeneration of tissues from multiple lineages [32]. As these cell therapies become more prevalent in different clinical procedures, their secretory profiles need to be more thoroughly investigated in terms of the role stem cell-secreted factors have in tissue regeneration and in possible side effects.

Hyaline cartilage is the most prevalent cartilaginous tissue found in the body, with adult stem cell therapies used to regenerate hyaline cartilage in the knee and trachea of humans [361, 362] and to repair cartilage in the larynx, bronchial stump, and growth plate of animals in preclinical studies [363-365]. Unlike most other tissues, hyaline cartilage is an avascular and aneural tissue that has complex spatial variation in its mechanical properties and composition despite a relatively homogeneous cell population. Therefore, adult stem cell therapies used for chondral defect repair must secrete factors that stimulate synthesis of specific proteoglycans and collagens without facilitating the

infiltration of other tissues – especially blood vessel formation – or enabling hypertrophic differentiation of chondrocytes typical of endochondral ossification.

Although the secretory profile of ASCs for cartilage regeneration have been investigated [306], an in-depth study determining the role ASC-secreted factors have on chondrocyte proliferation, phenotype, and cartilage regeneration has yet to be conducted. Additionally, techniques such as microencapsulation and differentiation medium treatments have been used to improve the regenerative capacity for mesenchymal stem cells [223, 349, 366], but no study has investigated the effects these two parameters have on the secretion of trophic factors from ASCs. Therefore, the overall objective of this study was to determine the role ASC-secreted trophic factors have in cartilage regeneration. The effect of microencapsulation and chondrogenic medium treatment on angiogenic factor production was determined. Then co-culture and conditioned media studies were conducted to determine how ASC-paracrine signaling and ASC-secreted factors affect chondrocytes. Finally, ASCs were implanted into a chondral defect in the xiphoid to determine the effect ASCs have on hyaline cartilage regeneration.

METHODS

Cell Isolation

ASCs were isolated from inguinal fat pads of 125 g male Sprague Dawley rats (Harlan Laboratories, Indianapolis, IN, USA) as described in detail previously [320] and cultured in Lonza Mesenchymal Stem Cell Growth Medium (GM, Lonza, Walkersville, MD, USA). After one passage, these cells were positive for CD73 and CD271 and negative for CD45 [320]. Costochondral chondrocytes from the ribs of 125 g male

Sprague Dawley rats were isolate as described previously [321]. Primary cells were cultured in DMEM containing 10% fetal bovine serum (FBS) and 50 μg/ml ascorbic acid (Invitrogen) until fourth passage prior to experimental analysis. These cells continue to express type II collagen, aggrecan, and cartilage oligomeric matrix protein [321].

Microencapsulation

Once primary ASCs reached 90% confluence, cells were trypsinized and microencapsulated in 20 mg/mL low molecular weight (~150 kDa) alginate (FMC BioPolymer, Sandvika, Norway) with a high mannuronate to guluronate ratio (40% guluronate) at a concentration of 25×10^6 cells/mL using a Nisco Encapsulator VAR V1 LIN-0043 (Nisco Engineering AG, Zurich, Switzerland) as previously described [322]. The microbeads were washed three times in GM prior to cell culture studies. First passage ASCs were also plated in 6-well plates (Figure 7.1A).

ASC Cell Culture

Once first passage ASCs reached 90% confluence (Figure 1A), ASC monolayers and microbeads were then treated for 5 days with either GM or chondrogenic medium (CM) consistent of high glucose DMEM with 1 mM sodium pyruvate (Mediatech, Manassas, VA, USA), 40 μg/ml proline (Sigma), 50 μg/ml ascorbate-2-phosphate (Sigma), 1% ITS+ (Sigma), 100 nM dexamethasone (Sigma), 10 ng/ml recombinant human transforming growth factor beta-1 (TGF-β1, R&D Systems, Minneapolis, MN, USA) and 100 ng/ml recombinant human bone morphogenic protein 6 (BMP-6, PeproTech, Rocky Hill, NJ, USA). Once media were changed on the fifth day, RNA was collected after 8 hours as described below while media and ASCs lysed in 0.05% Triton X-100 were collected after 24 hours. Fourth passage chondrocytes cultured in DMEM,

10% FBS, and 50 μg/mL ascorbic acid and Sprague Dawley-derived clone 9 liver cells (ATCC, Manassas, VA, USA) cultured in F12K medium and 10% FBS served as controls. All media contained 1% penicillin and streptomycin.

Growth Factor Expression and Production

Microbeads were uncross-linked in 82.5 mM sodium citrate (Sigma), pelleted at 500 g for 10 minutes and washed two more times in sodium citrate to remove any residual alginate. TRIzol reagent (Invitrogen) was added to the resulting cell pellet, homogenized using a QIAshredder (QIAGEN, Valencia, CA, USA), and RNA was isolated using chloroform and an RNeasy Kit (Qiagen) as previously described [323]. 1 μg RNA was then reverse transcribed to cDNA using a High Capacity Reverse Transcription cDNA kit (Applied Biosystems, Carlsbad, CA, USA). Gene expressions were quantified as previously described [166]. Primers were designed using Beacon Designer software (Premier Biosoft, Palo Alto, CA, USA) and synthesized by Eurofins MWG Operon (Huntsville, AL, USA) unless otherwise noted (Table 7.1). VEGF-A and FGF-2 production over the last 24 hours of culture was quantified using ELISA (R&D Systems) and normalized to DNA content measured with a Quant-iT PicoGreen kit (Invitrogen).

Paracrine Signaling

ASC-Chondrocyte Co-culture

To assess the effects paracrine signaling between ASCs and chondrocytes have on chondrocyte phenotype, the two cell types were co-cultured in a trans-well system (Figure 7.2A). Initial studies determined the number of microbeads per insert needed to have the same cell number as ASC confluent trans-well inserts. ASC monolayers and

microbeads were treated with GM or with CM for 5 days in 0.2μm high density cell culture inserts (BD Biosciences, Franklin Lakes, NJ, USA). ASC cultures and inserts were then washed in DMEM three times and added to wells with confluent chondrocytes. The two cell groups were then cultured in 4.5 mL DMEM + 10% FBS. After 7 days, RNA was isolated from the chondrocytes to quantify chondrogenic gene expression. Microencapsulated clone 9 liver cells served as a control.

Chondrocyte Cultures Treated with ASC-Conditioned Media

To assess the effects ASC-secreted factors have on chondrocytes, chondrocytes were cultured in different ASC-conditioned media (Figure 7.2C) obtained from T-75 flasks. Initial studies determined the number of microbeads per T-75 needed to have the same cell number as ASC confluent T-75 flasks. To obtain ASC-conditioned media, ASC monolayers and microbeads were treated with GM or CM for 5 days in T-75s. After the fifth day of treatment, ASC monolayers and microbeads were washed in DMEM three times and 10 mL DMEM +10% FBS was added to each culture. After 24 hours, media containing the ASC-secreted factors were collected then immediately added to confluent chondrocyte cultures. After 12 hours in ASC-conditioned medium, RNA was isolated from chondrocytes to quantify chondrogenic gene expression. To assess chondrocyte phenotype, apoptosis, and angiogenic response, the following assays were performed after 24 hours of ASC-conditioned medium treatments. Conditioned medium from microencapsulated clone 9 liver cells served as a control.

Chondrocyte Responses

[3H]-Thymidine Incorporation

DNA synthesis was assayed by measuring [3H]-thymidine incorporation as described previously [90]. 40% confluent chondrocytes were treated with DMEM + 1% FBS to induce quiescence. Four hours before harvest, [3H]-thymidine was added to a final concentration of $0.25\mu Ci/mL$. Radioactivity in trichloroacetic acid-insoluble cell precipitates was measured by liquid scintillation spectroscopy.

[35S]-Sulfate Incorporation

Proteoglycan synthesis was assayed by measuring [35S]-sulfate incorporation as previously described [328]. [35S]-sulfate was added to a final concentration of $18\mu Ci/mL$ for the final 4 hours of culture. Only [35S]-sulfate incorporation in the monolayer was measured since less than 15% of total radiolabeled proteoglycan production is secreted into the medium [367]. [35S]-sulfate incorporation was normalized to protein content measured with a Pierce Macro BCA protein kit (ThermoScientific, Rockford, IL, USA).

Alkaline Phosphatase Activity

Alkaline phosphatase specific activity in chondrocyte lysates was measured as a function of release of p-nitrophenol from p-nitrophenylphosphate as previously described [89] and normalized to protein content measured with a Pierce Macro BCA protein kit (ThermoScientific).

Effects of ASCs on Chondrocyte Apoptosis

DNA Fragmentation

To assess effects of ASC-secreted factors on DNA fragmentation, confluent chondrocytes were pulsed with [3H]-thymidine for 4 hours prior to ASC-conditioned

medium treatment. Chondrocytes were lysed and centrifuged at 13,000 g for 15 minutes to separate intact DNA from fragmented DNA as previously described [82]. The amount of incorporated [^{3}H]-thymidine was determined in each fraction to establish the total amount of fragmented DNA.

Caspase-3 Activity

Caspase-3 activity was determined using a colorimetric CaspACE™ Assay System from Promega (Madison, WI, USA) following the manufacturer's protocol 24 hours after ASC conditioned media were added to confluent chondrocytes. Caspase-3 activity was normalized to total protein content measured with a Pierce 660nm protein assay (ThermoScientific).

Effect of Secreted Factors on Angiogenic Response

Angiogenic responses to different ASC-conditioned media were assessed with endothelial cells cultured in a fibrin gel assay as previously described [368]. Human aortic endothelial cells (HAECs, Lonza) were plated in endothelial cell basal medium (EGM-2, Lonza) at 5×10^3 cells/well on fibrin gel and cultured at 37°C for 24 hours. At 24 hours, medium was removed, a second layer of fibrin was added on top, and ASC conditioned media were added. After 12 hours, images were taken for morphometric analysis and total endothelial tube length was determined using Image Pro Plus.

Role of VEGF-A and FGF-2

To determine the effect exogenous vascular endothelial growth factor A (VEGF-A) and fibroblastic growth factor 2 (FGF-2) have on chondrocytes, 1 ng/mL and 20 ng/mL of recombinant human VEGF-A$_{165}$ and recombinant human FGF-2 (R&D Systems) were added to monolayer cultures of fourth passage chondrocytes. To

determine the effect VEGF-A and FGF-2 secreted by ASCs have on chondrocytes, conditioned medium from GM-treated ASC monolayers was supplemented with 1 μg/mL goat anti rat IgG, 1 μg/mL goat anti-rat VEGF-A neutralizing antibody, or 1 μg/mL goat anti-rat FGF-2 neutralizing antibody (R&D Systems) and added to fourth passage chondrocyte monolayers as determined by the manufacturer's protocol. After 24 hours, [^{35}S]-sulfate incorporation, caspase-3 activity, and [^{3}H]-thymidine incorporation were measured as described above. DMEM + 10% FBS and conditioned medium from ASC monolayers treated with CM served as controls.

<u>Xiphoid Defect in Vivo</u>

To assess if ASCs would inhibit cartilage regeneration, non-critically sized chondral defects were made in the xiphoids of 125g male Sprague-Dawley rats as previously described [369]. The protocol was approved by the Institutional Animal Care and Use Committee of the Georgia Institute of Technology and each group was tested in seven rats. A full-thickness 1 mm cylindrical defect was made in the center of the xiphoid using a dermal biopsy punch (Mitex, Plainsboro, NJ, USA). This defect size was chosen because cartilage regeneration was previously observed after 35 days and the defect is large enough to contain cell pellets 1×10^6 ASCs in size [369]. ASC monolayers cultured in GM or CM were pelleted at 1×10^6 ASCs/pellet and implanted into the defect. Empty defects and autografts (excised cartilage is re-implanted) served as controls. To maintain groups in the defect and to serve as an adhesion barrier, SepraFilm® (Genzyme, Cambridge, MA, USA) was then placed on the dorsal and ventral sides of the defect. Xiphoids were excised 35-days post-surgery and examined as described below.

Radiographic imaging (Faxitron Bioptics, Lincolnshire, IL, USA) was performed in the coronal plane at a voltage of 22 mV and exposure time of 16 s to visualize soft tissue penetration as previous described [369]. A blind observer then scored the presence of soft tissue penetration with a score of 0 representing no healing, a score of 0.5 representing partial healing, and a score of 1 representing full healing.

Equilibrium partitioning of an ionic contrast agent via micro-computed tomography (EPIC-µCT) was used to visualize the distribution of proteoglycans within the xiphoid defects as previously described [369, 370]. Xiphoids were incubated in 40% Hexabrix (Mallinckrodt, St. Louis, MO, USA) in phosphate buffered saline (PBS) containing 1% proteinase inhibitor cocktail (CalBiochem, Darmstadt, Germany) overnight and scanned using pre-determined settings [369]. Low X-ray attenuation (green/yellow) of three-dimensional color images corresponded to regions of high proteoglycan concentration and no or high X-ray attenuation (black and red/orange) indicated regions of low proteoglycan concentration. To determine cartilage volume, the 1 mm defect was isolated with user-guided contours and evaluated at a 100 – 250 threshold range.

After scanning, samples were washed in PBS for four hours, fixed in 10% phosphate-buffered formalin for 48 hours, and embedded in paraffin. Seven-micrometer thick serial sections were stained with haematoxylin and eosin stain (H&E) to highlight cells and extracellular matrix on microscope images (DMLB; Leica, Nussloch, Germany).

Statistical Analysis

All *in vitro* experiments had six independent cultures per treatment group to ensure sufficient power to detect statistically significant differences. All *in vitro* experiments were conducted multiple times to validate the observations, but only data from a single representative experiment are shown and are expressed as means ± standard errors. A power analysis determined that seven samples per group were needed for the *in vivo* study based on results from a previous study [369]. Statistical analysis was conducted using ANOVA analysis with a post hoc Tukey test (GraphPad Prism, La Jolla, CA, USA). Differences in means were considered to be statistically significant if the p-value was less than 0.05.

Table 7.1: Phenotypic and GF Primer Sequences for Rat ASCs

Gene	Direction	Sequence
Acan	Sense	GCT TCG CTG TCC TCA ATG C
	Antisense	AGG TGT CAC TTC CCA ACT ATC C
Col2	Sense	CGAGTATGGAAGCGAAGG
	Antisense	GCTTCTTCTCCTTGCTCTTGC
Comp	Sense	AGT GAC AGC GAT GGT GAT GG
	Antisense	TCC CCG TCC TGG TCT TGG
Fgf2	Sense	Global Gene Sequence (Qiagen)
	Antisense	
Pdgfa	Sense	GAGGAGACGGATGTGAGG
	Antisense	ACGGAGGAGAACAAAGACC
Runx2	Sense	TTGGACACCTTGGACGCTAATT
	Antisense	AGA GGC AGA AGT CAG AGG
Sox9	Sense	GTG GGA GCG ACA ACT TTA CC
	Antisense	ATC GGA GCG GAG GAG GAG
Vegfa	Sense	GGACATCTTCCAGGAGTACC
	Antisense	CGTCTTGCTGAGGTAACC

RESULTS

Angiogenic Growth Factor Production from ASCs

ASC monolayers and microbeads cultured in GM had 1.5-3 times higher levels of mRNAs for fgf2 and vegfa compared to chondrocytes while CM reduced mRNAs for both vegfa and fgf2 to levels similar to that of chondrocytes (Figure 7.1B). CM did not influence pdgfa expression in ASCs, which was half the expression seen in chondrocytes. ASC monolayers and microbeads secreted 10-30 times more VEGF-A than chondrocytes while CM reduced secretion by 3-3.5 fold (Figure 7.1C). FGF-2 secretion from ASC cultures and chondrocytes was very low compared to VEGF-A production.
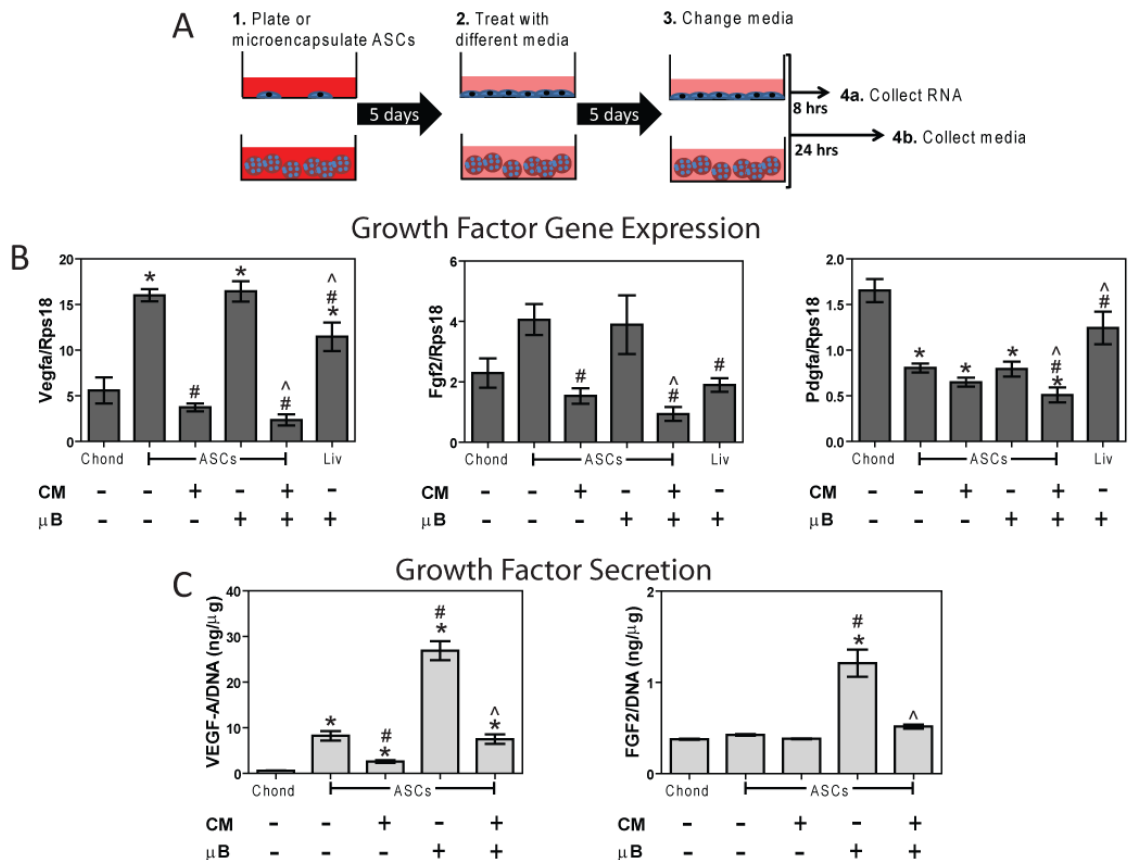
Figure 7.1: Effects of Microencapsulation and CM on Angiogenic Factors
(A) Diagram of ASC monolayer and microbead (μB) treatments with CM. (B) Gene expression and (C) growth factor production of ASCs, chondrocytes (chond), and liver cells (liv) (n=6±SE. *p<0.05 vs. chond, #p<0.05 vs. ASCs, ^p<0.05 vs. ASC microbeads (ASC + μB)).

Effect of ASC Paracrine Signaling and Secreted Factors on Chondrocyte Gene Expression

Chondrocytes co-cultured with ASC monolayers cultured in GM experienced 3.5-4 fold reductions in col2, comp, and runx2 mRNAs compared to chondrocytes with no co-culture (Figure 7.2B). However, CM-treated ASC monolayers increased acan expression in chondrocytes and had no effect on col2, comp, and runx2 expression in chondrocytes compared to control. GM-cultured ASC microbeads reduced col2 expression in chondrocytes but CM-treated ASC microbeads reduced col2, comp, and runx2 expression in chondrocytes compared to control. ASC co-cultures did not affect sox-9 expression and co-culture with clone 9 liver cell microbeads did not influence chondrocyte gene expression compared to control.

Conditioned medium from GM-cultured ASC monolayers decreased chondrocyte mRNAs for sox9 by 50%, acan by 78%, and col2 by 35% compared to chondrocytes treated with control medium (Figure 7.2D). However, conditioned medium from CM-treated ASC monolayers had no effect on chondrogenic gene expression compared to control medium. Conditioned medium from GM-cultured ASC microbeads decreased acan expression, but conditioned medium from CM-treated ASC microbeads had no effect on chondrocyte gene expression. Clone 9 liver cell microbeads decreased mRNAs for acan in chondrocytes but had no effect on sox9, col2, comp, or runx2.
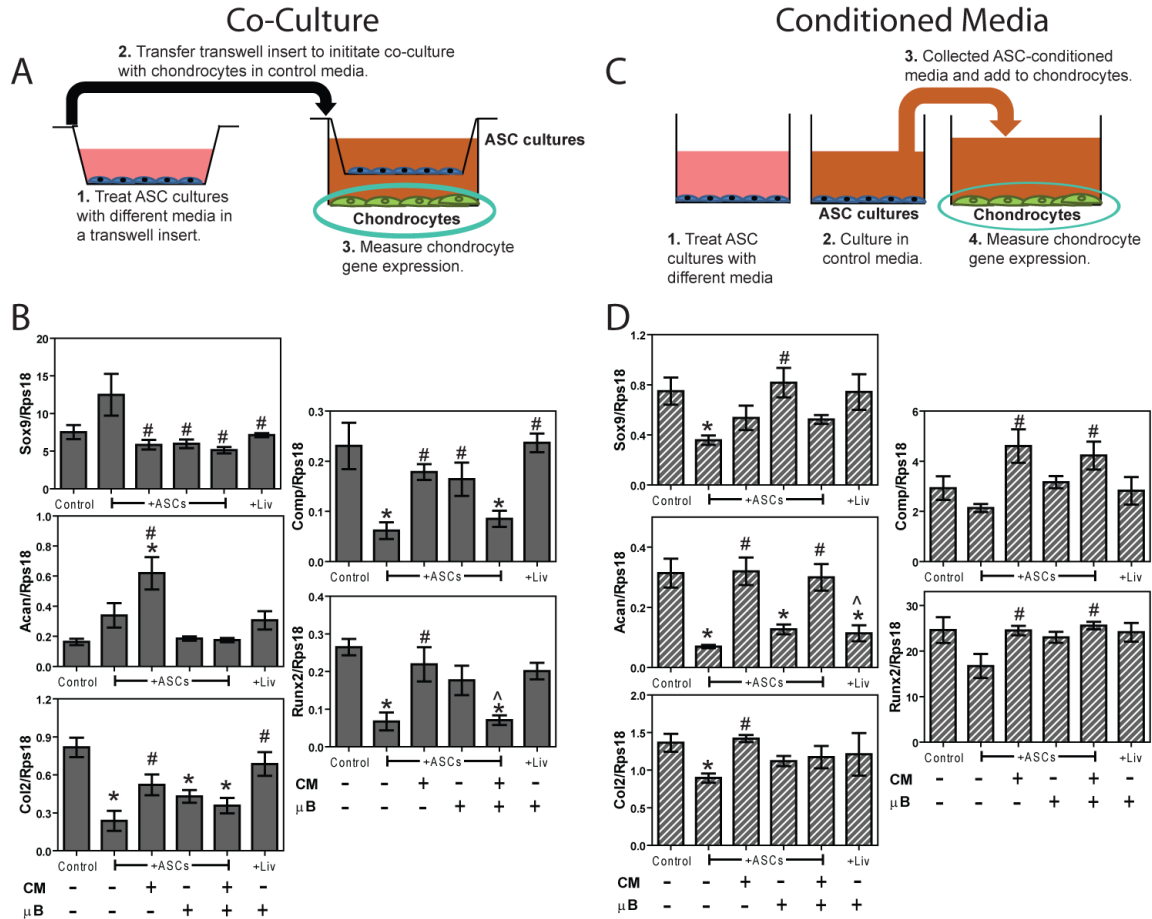
Figure 7.2: Effects of ASC co-culture and ASC-conditioned media on Chondrocyte Phenotypic Expression

(A) Diagram of ASC co-culture and (B) gene expression of chondrocytes after 7 days. (C) Diagram of ASC-conditioned media treatment and (D) gene expression of chondrocytes after 12 hours (n=6±SE. *p<0.05 vs. control, #p<0.05 vs. ASCs, ^p<0.05 vs. ASC microbeads (ASC + μB)).

Effect of ASC-secreted Factors on Proliferation, Phenotype, and Apoptosis

Conditioned media from GM-cultured ASC monolayer and microbeads decreased [^{35}S]-sulfate incorporation by 75% and 60% respectively (Figure 7.3B), had no effect on alkaline phosphatase activity (Figure 7.3C), and decreased [^{3}H]-thymidine incorporation by approximately 76% (Figure 7.3D) compared to chondrocytes treated with control medium. Treating ASC monolayers and microbeads with CM prior to conditioned media collection eliminated the deleterious effects ASC-secreted factors had on chondrocytes (Figure 7.3B, D). Liver microbead conditioned medium did not affect [^{3}H]-thymidine incorporation, [^{35}S]-sulfate incorporation, or alkaline phosphatase activity (Figure 7.3B-D).

Conditioned medium from GM-cultured ASC monolayers increased caspase-3 activity 120%, bax/bcl expression 79%, and DNA fragmentation 114% compared to control medium (Figure 7.3E-G). Treating ASC monolayers with CM prior to collecting conditioned medium eliminated the apoptotic effects ASC-secreted factors had on chondrocytes. Conditioned medium from ASC microbeads cultured in GM did not increase apoptosis compared to control medium. Conditioned medium from liver microbeads had no effect on caspase-3 activity and bax/bcl, but did increase DNA fragmentation compared to control (Figure 7.3E-G).

ASC monolayer and microbead conditioned media increased endothelial tube length by 2.6 fold and 2 fold respectively (Figure 7.3G). Treating ASC monolayers and microbeads with CM prior to conditioned media collection eliminated this angiogenic response. Conditioned medium from liver microbeads had no effect on endothelial tube length.
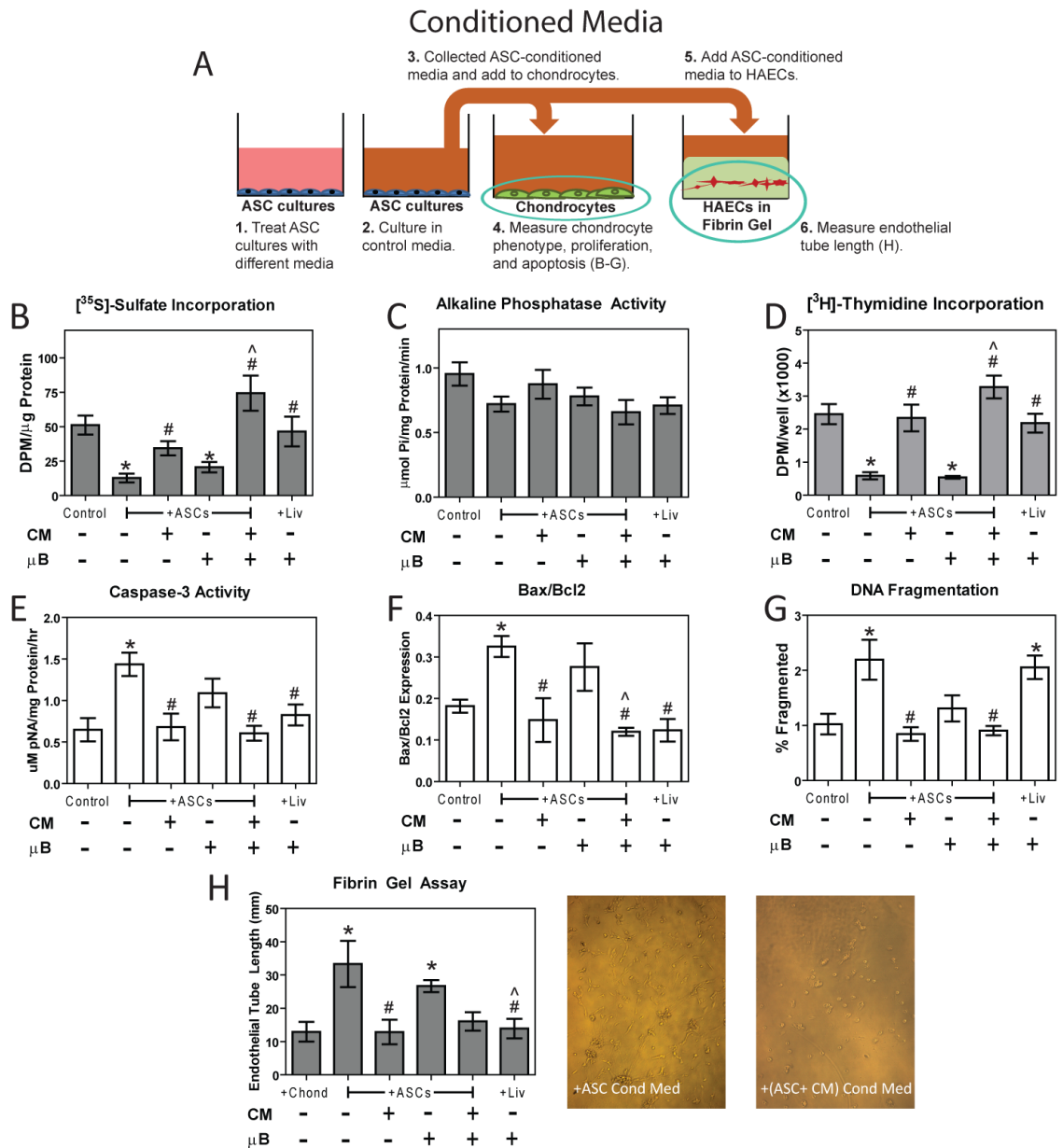
Figure 7.3: Effects of ASC-conditioned Medium on Chondrocyte Phenotype, Proliferation, Apoptosis, and Angiogensis

(A) Diagram of ASC-conditioned media experiments, (B) [^{35}S]-sulfate incorporation, (C) alkaline phosphatase activity, (D) [^{3}H]-thymidine incorporation, (E) caspase-3 activity, (F) bax/bcl2 expression, (G) DNA fragmentation, and (H) endothelial tube length (n=6±SE. *p<0.05 vs. control, #p<0.05 vs. ASCs, ^p<0.05 vs. ASC microbeads (ASC + μB)).

Effect of Exogenous VEGF-A and FGF-2 on Chondrocytes

1 ng/mL and 20 ng/mL of VEGF-A reduced [^{35}S]-sulfate incorporation by approximately 30% and 50% respectively (Figure 7.4A). Adding FGF-2 at both 1 and 20 ng/mL alone had no effect on [^{35}S]-sulfate incorporation but did eliminated the inhibitory effect rhVEGF-A had on [^{35}S]-sulfate incorporation at both concentrations. Meanwhile both 1 ng/mL and 20 ng/mL VEGF-A significantly increased caspase-3 activity by 32% and 84% respectively (Figure 7.4B). Adding 1 ng/mL of FGF-2 had no effect on caspase-3 activity and did not reduce the apoptotic effect of VEGF-A compared to control. However, 20 ng/mL FGF-2 eliminated the apoptotic effect of VEGF-A. VEGF-A and FGF-2 had a more limited effect on chondrocyte proliferation, as only the 20 ng/mL FGF-2 dosage increased [^{3}H]-thymidine incorporation (Figure 7.4C).
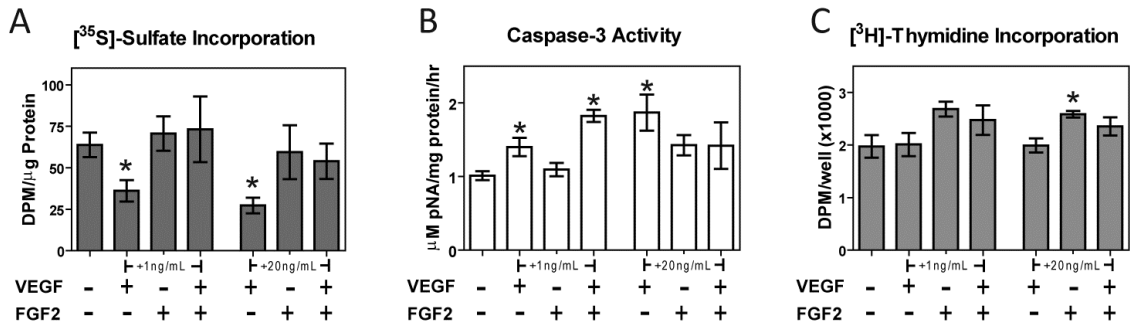
Figure 7.4: Effects of Exogenous VEGF-A and FGF-2 on Chondrocytes
(A) [^{35}S]-sulfate incorporation of chondrocytes treated with recombinant human VEGF-A and FGF-2, (B) caspase-3 activity of chondrocytes treated with recombinant human VEGF-A and FGF-2, and (C) [^{3}H]-thymidine incorporation of chondrocytes treated with recombinant human VEGF-A and FGF-2 (n=6±SE. *$p < 0.05$ vs. control, #$p < 0.05$ vs. ASCs).

Effect of ASC-secreted VEGF-A and FGF-2 on Chondrocytes

ASC-conditioned medium with a goat-anti-rat IgG and FGF-2 neutralizing antibody decreased [^{35}S]-sulfate incorporation by approximately 50% (Figure 7.5B) and increased caspase-3 activity by approximately 94% (Figure 7.5C) compared to control medium.   Adding VEGF-A neutralizing antibody to ASC-conditioned medium eliminated both its deleterious effect on chondrocyte phenotype and apoptotic effect. ASC conditioned media with or without VEGF-A or FGF-2 neutralizing antibodies all decreased [^{3}H]-thymidine incorporation compared to control medium (Figure 7.5D). As previously observed, conditioned medium from ASC monolayers treated with CM had no effect on chondrocyte caspase-3 activity, [^{35}S]-sulfate, and [^{3}H]-thymidine incorporation compared to control medium (data not shown).
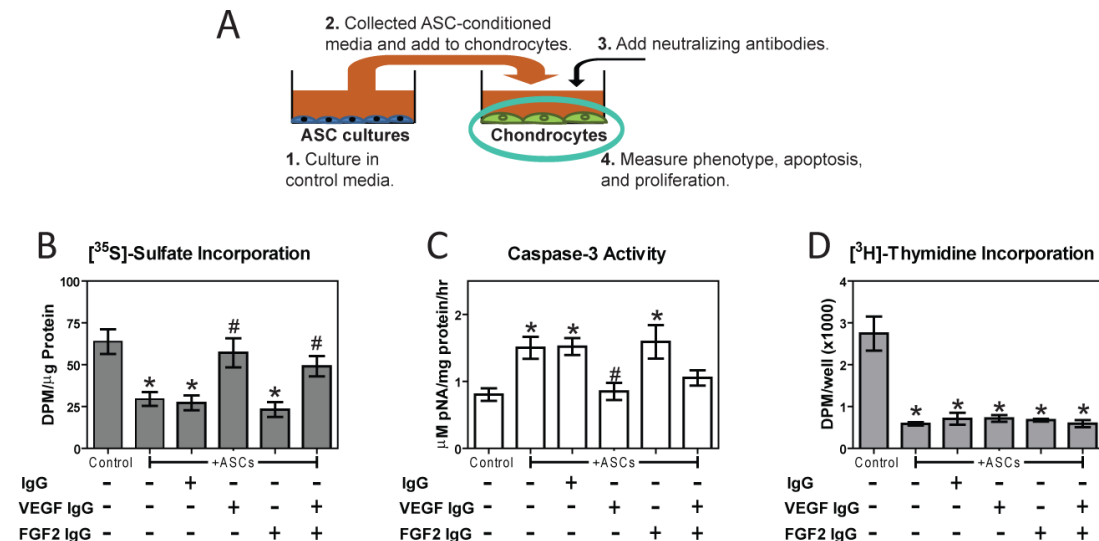
Figure 7.5: Effects of ASC-secreted VEGF-A and FGF-2 on Chondrocytes
(A) Schematic outlining chondrocytes treated with ASC-conditioned medium with VEGF-A and FGF-2 neutralizing antibodies and assayed for (B) [^{35}S]-sulfate incorporation, (C) caspase-3 activity, and (D) [^{3}H]-thymidine incorporation (n=6±SE. *p<0.05 vs. control, #p<0.05 vs. ASCs).

<u>Effect of ASCs in Cartilage Defect</u>

Radiograph images showed that 7 of 7 defects with autografts had partial or full healing and empty defects had 3 of 7 defects with partial or full healing; however, only 1 of 7 defects with ASC pellets had partial healing whereas 4 of 7 defects with pellets of ASCs treated with chondrogenic media had partial or full healing (Figure 7.6A). Proteoglycan was visible in EPIC-μCT images of empty defects and defects with pellets of CM-treated ASCs but absent from defects with pellets of GM-cultured ASCs (Figure 7.6B). EPIC-μCT calculated cartilage volume for defects with ASC pellets was significantly smaller than cartilage volume in both autografts and empty defects. Defects with CM-treated ASCs had more cartilage than defects with GM-cultured ASCs, but were not different from empty defects (Figure 7.6B).

In histological sections of defects with autografts, early-stage cartilage and infiltrating cells were starting to integrate the graft with the surrounding xiphoid (Figure 7.6C). Similar tissue deposition and cell infiltration was observed for empty defects and defects with ASCs treated with chondrogenic media. However, defects with ASCs were infiltrated with surrounding epithelial tissue instead and lacked the connective tissue that was observed in empty defects.
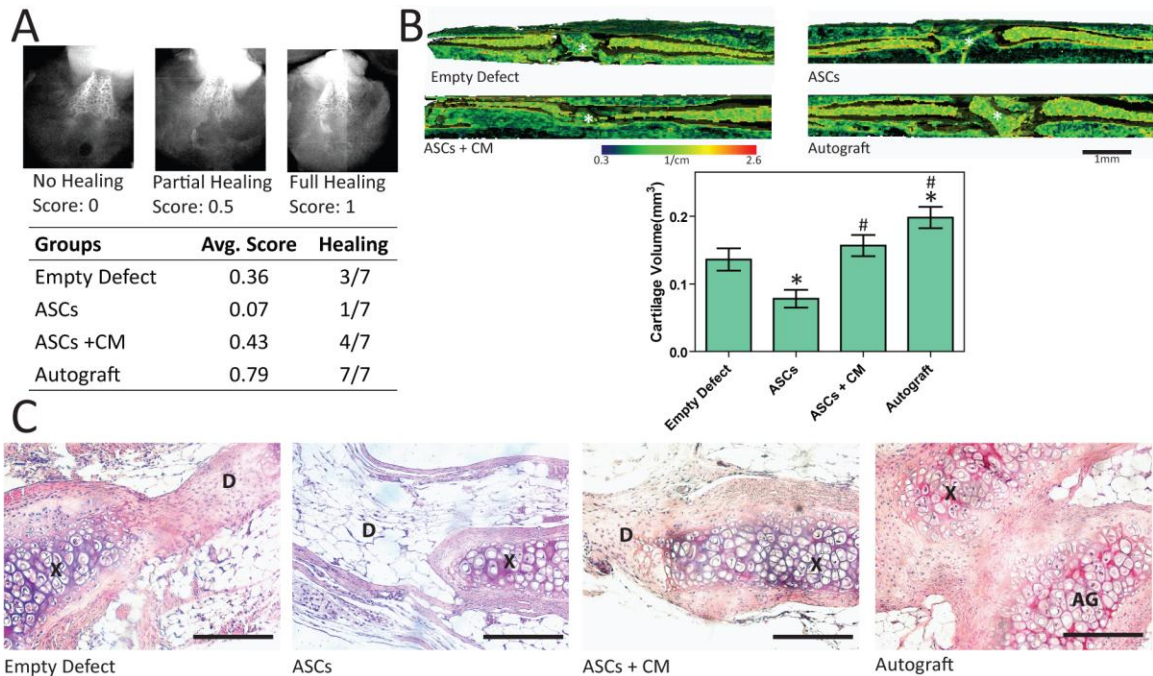
Figure 7.6: Effects of ASCs on Cartilage Regeneration
(A) Radiographic scoring. (B) 3-D EPIC-μCT images of xiphoids and calculated cartilage volume within defects (n=7±SE. *p<0.05 vs. empty defect, #p<0.05 vs. ASCs). (C) Representative H&E staining. Bar represents 100 μm at 20x magnification (D = defect, X = xiphoid, AG = autograft).

DISCUSSION

This study is the first to definitively show that adipose stem cells secrete angiogenic factors that are detrimental for chondrocytes and can prevent cartilage regeneration. Specifically, ASCs secrete a relatively large amount of VEGF-A, which can inhibit chondrocyte phenotype and lead to chondrocyte apoptosis. Additionally, ASCs secrete factors that negatively influence chondrocyte proliferation. Finally, ASCs prevent cartilage regeneration in a non-critical, hyaline cartilage defect *in vivo*. Despite these deleterious effects, treating ASCs with chondrogenic medium can reduce the expression and production of VEGF-A, eliminate the damaging effects ASC-secreted factors have on chondrocytes, and prevent the adverse effects ASCs have on regenerating cartilage *in vivo*.

Previous studies have extensively studied the secretory profiles of bone marrow-derived mesenchymal stem cells (MSCs) and ASCs, showing that they not only secrete several factors that can facilitate cartilage regeneration [52, 306], but that they also secrete a large amount of angiogenic factors [155, 307]. VEGF-A, an important initiator and mediator of angiogenesis [64, 65], was secreted in large quantities by ASC monolayers and microbeads, decreased chondrocyte proteoglycan production, and induced chondrocyte apoptosis in the current study. Although VEGF-A typically elicits anabolic responses from most cell types, this growth factor has catabolic effects on chondrocytes and has been shown to induce matrix metalloproteinase expression in these cells [68]. Although VEGF-A was not responsible for reduced chondrocyte proliferation due to ASC-secreted factors, ASCs also express pro-inflammatory factors [111], which may have inhibited chondrocyte proliferation.

Although VEGF-A alone did not prevent chondrocyte proliferation, it mitigated the ability of FGF-2 to stimulate chondrocyte proliferation at a high concentration. Additionally, FGF-2 restored proteoglycan production in chondrocytes treated with VEGF-A, and high concentrations of FGF-2 eliminated the apoptotic effect VEGF-A had on chondrocytes. Although both FGF-2 and VEGF-A are important mitogens and facilitators for angiogenesis [340, 371], had similar gene expression responses to chondrogenic medium treatment in this current study, and appear to be linked in terms of production in MG63 cells [368], ASCs secreted an order of magnitude lower amount of FGF-2 than VEGF-A. And unlike VEGF-A, FGF-2 has previously been shown to enhance the chondrogenic potential of different stem cell sources [372, 373], as well as improve cartilage regeneration [341, 374]. The combination of high VEGF-A secretion

and low FGF-2 secretion may be the main reason why ASC-secreted factors have deleterious effects on chondrocytes and subsequent cartilage regeneration.

In addition to enhancing catabolic pathways in chondrocytes, VEGF-signaling has been associated with osteophyte formation and osteoarthritis progression in articular cartilage [69-71] and blocking VEGF-signaling improves the chondrogenic potential and regenerative capacity of muscle-derived stem cells [375, 376]. Additionally, VEGF-A directs cartilage vascularization in hyaline cartilage and hypertrophic chondrocyte absorption that leads to subsequent ossification [66, 377]. Although chondrocytes exposed to ASC-secreted factors did not have increased mRNA levels of RUNX2 or increased alkaline phosphatase activity and cartilage defects with ASC pellets did not have signs of vascularization, hypertrophic differentiation, or bone formation, longer *in vitro* or *in vivo* studies may have revealed these effects. Additionally, ASCs may secrete trophic factors that prevent hypertrophic differentiation.

Several studies have investigated the effects chondrocyte-stem cell co-cultures and chondrocyte secreted factors have on stem cell differentiation [310, 375, 378], but few have provided insight into the effects stem cell-mediated paracrine signaling has on chondrocytes. Bian et al. showed that co-culturing chondrocytes with MSCs within the same gel reduced hypertrophy and increased compressive moduli, but it appeared that these improvements were independent of long-range MSC-paracrine signaling [379]. Additionally, results from Hildner et al. suggested that co-culturing ASCs and chondrocytes in the same matrix moderately increased SOX9, aggrecan, and cartilage oligomeric protein mRNA expression when normalized to the initial percentage of chondrocytes, but the findings provided little insight into the role of ASC-secreted factors

[380]. From the current study, the length of exposure to ASC-secreted factors and the ability for trophic factor interchange between ASCs and chondrocytes appear to be important variables in regulating chondrocyte phenotype. Twelve hour exposure to ASC-conditioned medium appeared to have the most significant effects on SOX9 and aggrecan, which are earlier stage markers of chondrogenesis, whereas seven days of ASC co-culture exerted the greatest effects on RUNX2, a later stage chondrogenic marker [53]. Additionally, 7 day co-culture with ASCs treated with chondrogenic medium increased aggrecan expression, possibly due to the interplay of chondrocyte and ASC signaling.

Although chondrogenic treatment that included both TGF-β1 and BMP-6 eliminated the deleterious effects ASCs secreted factors and ASCs had on chondrocytes and cartilage regeneration respectively, ASCs treated with chondrogenic medium did not secrete factors that improved chondrocytes' ability to produce cartilaginous extracellular matrix *in vitro*. This absence of improvement over baseline may be due to the short 5 day chondrogenic medium treatment time as several studies have shown optimal ASC and stem cell chondrogenesis to require at least 2 to 6 weeks of chondrogenic treatment [243, 352]. However, these studies did not investigate the effects varying the temporal application of chondrogenic medium had on trophic factor production.

CONCLUSION

This study showed that ASCs can inhibit cartilage regeneration in a focal hyaline cartilage defect *in vivo*. *In vitro*, ASCs monolayers or microbeads cultured in growth medium secrete a large amount of VEGF-A which causes chondrocyte apoptosis and

reduced proteoglycan synthesis. Additionally, these ASCs secrete factors that reduce chondrogenic gene expression and proliferation. Treating ASCs with chondrogenic medium reduces the secretion of VEGF-A, significantly reduces the deleterious effects ASC-secreted factors have on chondrocytes, and eliminates the inhibitory effect ASCs have on cartilage regeneration. Blocking VEGF-A in ASC-conditioned medium eliminates the deleterious effects ASC-secreted factors have on chondrocyte phenotype and apoptosis. Adding a high concentration of FGF-2 eliminates the apoptotic effect VEGF-A has on chondrocytes and adding both low and high concentrations of FGF-2 eliminates the detrimental effects VEGF-A has on chondrocyte phenotype. These results have significant implications on how ASCs and possibly other stem cell therapies are used for repairing cartilage. Specifically, these therapies must be pre-treated or modified to reduce the inhibitory effects of VEGF-A and other secreted factors on cartilage regeneration.

CHAPTER 8

REGULATING INVIVO CALCIFICATION OF ALGINATE MICROBEADS

INTRODUCTION

Alginate hydrogels have been used for a wide variety of tissue engineering and regenerative medicine applications because they have favorable mass transfer properties [197], can be molded into specific shapes [198, 199], have adjustable degradation kinetics [200-202], support a range of different cell phenotypes [203-205], can be mechanically and biochemically modified [196, 206, 207], support cell differentiation in large animal models [208], and are biocompatible for delivery of cells in human trials [209]. The most common method of incorporating bioactive molecules or cells into alginate matrices is via extrusion, in which an alginate suspension is extruded through a needle to form droplets that fall into a solution that contains divalent cations causing alginate crosslinking [204, 381-383]. Alginate microspheres can also be created by using air flow [210] or high electrostatic potentials [384] to overcome surface tension, and have been used to encapsulate and deliver pancreatic islets [204]. In addition to cell delivery, hydrogel microspheres have generally been used for spheroid cell culture, drug delivery, and as injectable tissue fillers. The ability of alginate microspheres as an injectable filler to deliver encapsulated cells has not been fully characterized, and, to further develop this technology, the mass transfer properties and reabsorption kinetics of alginate microspheres must be controllable *in vivo*.

Various pre-clinical and clinical studies have reported alginate calcification [31, 385, 386], which presents a critical challenge in developing large scale applications using this hydrogel. Our preliminary studies have shown that alginate microbeads calcify *in vivo*, which affects mass transfer in and out of the hydrogel while preventing reabsorption and creating unwanted mineralization foci within the tissue. Therefore, it would be advantageous to develop methods to prevent alginate calcification. However, if alginate calcification can be regulated temporally and spatially *in vivo*, this hydrogel could also be used as a stimulus for *in situ* bone repair and formation. To achieve this type of application, a thorough understanding of the mechanism of alginate calcification and methods to control it need to be developed. No study, however, has yet extensively characterized alginate calcification nor has any study thoroughly investigated methods to control this process.

The objective of this study was to investigate how alginate beads calcify and to develop different methods to control alginate calcification while characterizing the mineral formed. We first hypothesized that calcium-crosslinked alginate calcifies by sequestering the surrounding phosphate to form calcium phosphate. Alginate beads were cultured in a phosphate solution, and phosphate content and subsequent mineralization were analyzed. We then hypothesized that calcium-crosslinked alginate has the ability to calcify *in vivo* regardless of the presence of encapsulated cells, delivery method, site of delivery, or sex of the animal. Alginate microbeads seeded with or without human adipose stem cells were implanted intramuscularly or injected subcutaneously in male and female nude mice and the retrieved implants analyzed for mineral content and properties. Finally, we hypothesized that the type of mineral would be similar to

hydroxyapatite found in bone and that this calcification could be eliminated by varying divalent cations used to crosslink alginate or by buffering the pH in the beads before implantation. Barium was used as a crosslinking ion since it does not readily interact with phosphate ions [348] whereas aledronate was added since it is a bisphosphonate that chelates calcium and attaches strongly to hydroxyapatite to prevent crystal growth [387]. HEPES, an organic zwitterion buffering agent that does not contain phosphate, was used to buffer the crosslinking bath below physiological levels since hydroxyapatite crystals are stable to neutral to alkaline environments [388]. Implanted alginate microbeads created in different cross-linking solutions were retrieved and extensively characterized.

MATERIALS AND METHODS

<u>In Vitro Phosphorus Content</u>

To test our first hypothesis that calcium-crosslinked alginate calcifies by sequestering surrounding phosphate, an *in vitro* study was designed to assess the ability of calcium-crosslinked alginate to sequester phosphate. Low viscosity sodium alginate [Kelco Corp., Chicago, IL, USA] dissolved in 155 mM sodium chloride at a concentration of 12 mg/ml was dropped gently through a 25 gauge needle at a rate of 2-3 drops per second into a 102 mM calcium chloride bath. After 10 minutes, the beads (15-20 beads/10ml alginate) were washed four times with 155 mM NaCl. The beads were suspended in 25 ml 4 mM $(NH_4)_2HPO_4$ in 0.05 M Tris buffer at pH 7.4, and removed at different time points over a 4 hour period (0, 0.5, 1, 2, and 4hrs). After incubation at room temperature, the beads were collected by centrifugation, and the supernatants were assayed for phosphorus content using a commercially available kit [Sigma, St. Louis,

MO, USA] (n=3 for each experimental group and time). Beads were then lyophilized, mixed with KBr (~1 wt %), and made into KBr pellets for Fourier transform infrared spectroscopy (FTIR) analysis as outlined below. In some cases, the cloudy supernatant of the incubation buffer was centrifuged to a pellet, washed with acetone, air dried, and analyzed as a KBr pellet via FTIR.

Cell Isolation and Culture

To test our second hypothesis that calcium-crosslinked alginate microbeads with and without cells would calcify *in vivo*, adipose stem cells (ASCs) were isolated. Fat was excised from male and female patients less than 18 years of age undergoing cosmetic and reconstructive procedures at Children's Healthcare of Atlanta under an approved IRB protocol at Georgia Institute of Technology and Children's Healthcare of Atlanta. All patients and parents gave written consent to both the procedure and handling of fat thereafter. ASCs were isolated via a collagenase digestion solution as previously described [389]. Cells were then seeded at 5,000 cells/cm^2 and cultured in Lonza Mesenchymal Stem Cell Growth Medium [Lonza, Basel, Switzerland] up to second passage.

Alginate Bead and Microbead Fabrication

To test our hypotheses that alginate calcification can occur independently of how and where microbeads were implanted and that it could be eliminated by varying the crosslinking method, alginate microbeads were made in different crosslinking solutions. Medium molecular weight alginate (240,000 kDa) with a high guluronate to mannuronate ratio (69% guluronate) [FMC Biopolymer, Drammen, Norway] was UV light sterilized and dissolved in 155 mM sodium chloride [Ricca Chemical, Arlington, TX, USA] at a

concentration of 20 mg/ml. Alginate containing ASCs was initially seeded at 1×10^6 cells/ml, resulting in a final measured cell number of 40±7 cells per microbead (Figure 2B). Microspheres were created using a Nisco Encapsulator VAR V1 LIN-0043 [Nisco Engineering AG, Zurich, Switzerland] at a 4ml/hr flow rate, 0.175mm nozzle inner diameter, and 6kV electrostatic potential [390]. Microbeads were made in four different crosslinking solutions: (i) 50mM $CaCl_2$ and 150mM glucose (non-buffered); (ii) 50mM $CaCl_2$ and 150mM glucose with 25μM alendronate [Sigma] (bisphosphonate); (iii) 20mM $BaCl_2$ and 150mM glucose (barium); and (iv) 50mM $CaCl_2$ and 150mM glucose with 15mM 4-(2-hydroxyethyl)-1-piperazineethanesulfonic acid at pH 7.3 [Sigma] (HEPES-buffered). Microbeads made in non-buffered crosslinking solutions were washed and stored in 155 mM sodium chloride (saline) while microbeads made in the HEPES-buffered crosslinking solution were washed and stored in Dulbecco's modified eagle medium (DMEM) [Invitrogen, Carlsbad, CA, USA] at 37°C and 5% CO_2 prior to implantation to allow for longer term storage of ASC microbeads in future studies. Following microencapsulation, microbeads were implanted as described below.

Cell Viability

To determine whether ASCs were viable after microencapsulation in alginate and remained viable after injection delivery, microencapsulated ASCs suspended in DMEM were injected as described below and cultured for 0, 1, and 2 weeks in Lonza Mesenchymal Stem Cell Growth Medium. Microencapsulated ASCs that were not injected were also cultured for comparison (n=6 for each experimental group and time). Viability was measured using fluorescent confocal microscopy using a LIVE/DEAD Viability Kit following the manufacturer's protocol [Invitrogen]. Briefly, samples were

incubated for 30 minutes in a PBS solution containing 10 mM $CaCl_2$, 4 μM ethidium homodimer-1, and 2 μM calcein and imaged with a LSM 510 confocal microscope [Carl Zeiss MicroImaging Inc., Thornwood, NY].

Animal Surgeries

Male and female athymic nude (Nu/Nu) mice were housed in the vivarium in the Institute for Bioengineering and Bioscience at the Georgia Institute of Technology and handled under a protocol approved by the IACUC committee. Prior to surgeries, athymic mice were anesthetized using isoflurane gas. Both non-buffered and HEPES-buffered microbeads were directly implanted subcutaneously or intramuscularly or injected subcutaneously to determine if delivery method affected alginate calcification. Bisphosphonate and barium microbeads were only injected subcutaneously to reduce animal discomfort and to investigate how the crosslinking solution affects alginate calcification. For intramuscular implants, a small skin incision was made over the calf region of the hind limb, a pouch was prepared in the muscle by blunt dissection, and approximately 0.1 ml microbeads were inserted directly into the gastrocnemius muscle [391]. For all subcutaneous injections, 0.25 ml microbeads were mixed in 0.25 ml DMEM and injected via an 18 gauge needle. Animals were euthanized by CO_2 inhalation at various time points from 1 to 6 months. Each animal received either 2 injections or 2 implantations subcutaneously or 2 bilateral intramuscular implantations (n=4-6 for each experimental condition). Samples were harvested and processed for subsequent studies as described below.

Micro-computed Tomography

To assess the extent of alginate microbead mineralization, subcutaneous and intramuscular samples were excised from nude mice, immediately scanned using a μCT 40 (Scanco Medical, Switzerland) with a voxel size of 20μm, and analyzed as previously described [392]. Calcification was identified using a fixed threshold; individual samples were isolated with user-guided contours and three dimensional images were created. Samples were then fixed in 10% neutral buffered formalin [Sigma] for histological processing or frozen and lyophilized for subsequent materials characterization.

Histology

After 48 hours of fixation in formalin, representative undecalcified samples were embedded in plastic, and cut into 10-μm thick sections. Samples were stained with von Kossa with a nuclear fast red counter stain as previously described [295].

Fourier Transform-Infrared Spectroscopy (FTIR)

To test our hypothesis that alginate calcification mineral was similar to hydroxyapatite found in bone, infrared spectroscopy in attenuated total internal reflection (ATR) mode [Pike Technologies, Madison, WI, USA] was performed on lyophilized samples using a Nexus 870 FT-IR bench [Nicolet Instrument Corporation, Madison, WI, USA]. Each spectrum was the mean of two acquisitions (between 1800 and 800 cm-1) of at least 64 scans with a spectral resolution of 4 cm^{-1}.

X-Ray Diffraction

Crystal structure of the samples was identified using an X'Pert PRO Alpha-1 diffractometer [PANalytical, Almelo, The Netherlands]. X-ray diffraction (XRD) scans were collected using Cu Kα radiation. A 1° parallel plate collimator, ½ divergence slit

and 0.04 rad soller slit were used for controlled axial divergence. Bragg-Brentano parafocusing at 45 kV and 40 mA was used to analyze samples. The assignment of detected peaks to crystalline phases was performed using the database from the International Centre for Diffraction Data (ICDD, 2008).

Scanning Electron Microscopy and Energy Dispersive X-Ray Spectroscopy

Morphology of the microbeads was qualitatively evaluated using an Ultra 60 field emission scanning electron microscope (FESEM) [Carl Zeiss SMT Ltd., Cambridge, UK] at an accelerating voltage of 5 kV and different magnifications. Chemical composition of samples was determined using an INCAPentaFET-x3 energy dispersive x-ray spectrometer (EDS) [Oxford Instruments, Bucks, UK] at an accelerating voltage of 15 kV and a working distance of 8.5 mm.

RESULTS

In Vitro Calcification

Upon adding the calcium-crosslinked alginate beads to the phosphate buffer, the solution started to become cloudy. The phosphate concentration in the bath decreased by 20-35% over the first 4 hours and depended on the amount of alginate that was added (Figure 8.1A). The FTIR spectrum of the lyophilized alginate had peaks between 1600-1800cm^{-1}, 1370-1525cm^{-1}, and 900-1200cm^{-1} (Figure 8.1B) while the FTIR spectrum of the phosphate bath pellet had a similar peak between 900-1200cm^{-1} along with peaks centered around 1600 and 1400cm^{-1} (Figure 8.1C). Pure hydroxyapatite had characteristic peaks between 1400-1550cm^{-1} and 900-1200cm^{-1} (Figure 8.1D).
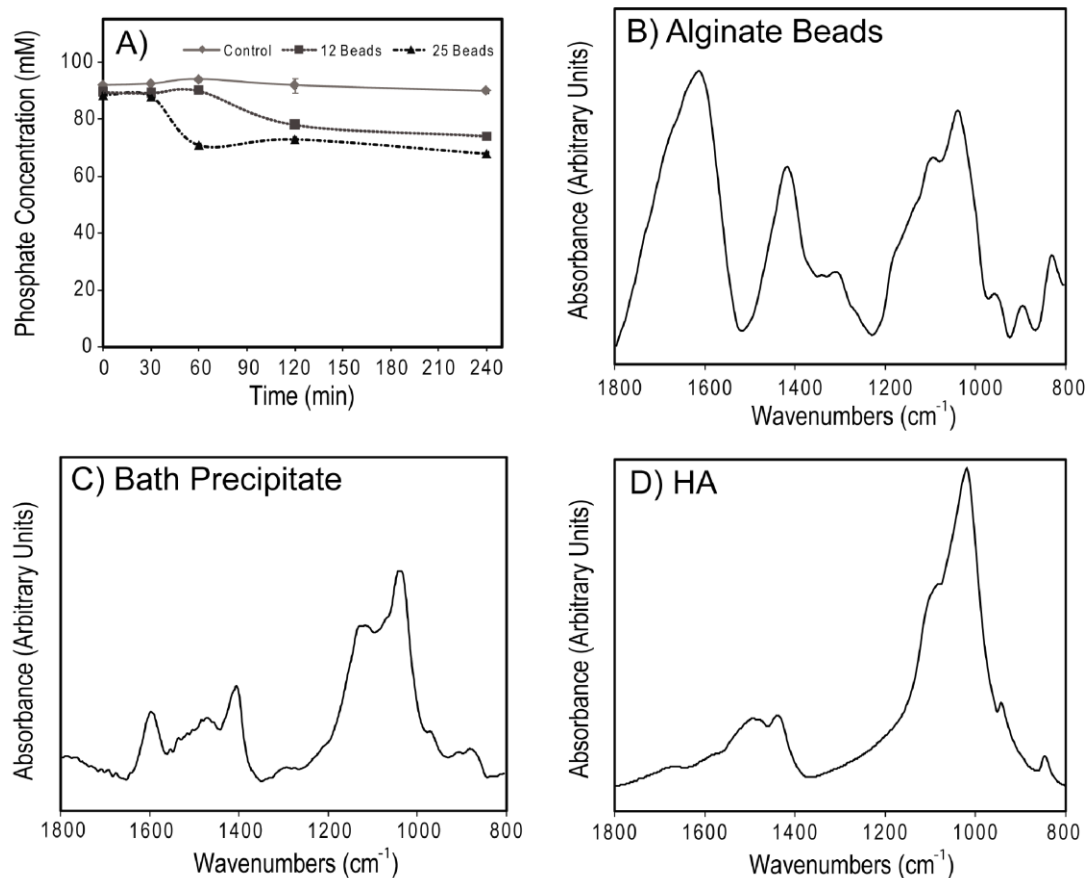
Figure 8.1: In vitro Study of Alginate Calcification
(A) Phosphate concentration of buffered bath over time for different amounts of alginate added to 25 mls of 4mM $(NH_4)_2HPO_4$ in 0.05 M Tris buffer at pH 7.4 (n=3 for each experimental group and time). FTIR spectra of (B) lyophilized alginate beads, (C) precipitate from the bath, and (D) pure hydroxyapatite.

<u>Visualization of In Vivo Calcification</u>

Microbeads formed in all crosslinking solutions ranged from 200-350μm in diameter (Figure 8.2A). When non-buffered microbeads were either implanted or injected subcutaneously into male nude mice, almost every sample showed the presence of mineral at all time points examined (1, 3, and 6 months; Table 8.1). Specifically, 24 of 24 implanted samples calcified whereas 21 of 24 injected samples calcified. ASC viability prior to implantation or injection was 70±3% (Figure 8.2B), and in vitro studies show cell viability increasing to 80±5% two weeks post injection (data not shown), yet

the presence of ASCs had no apparent effect on mineralization (Table 8.1). Mineralization was demonstrated by light microscopy (Figure 2C) or by visual inspection of implanted (Figure 8.2D) and injected (Figure 8.2E) microbeads.
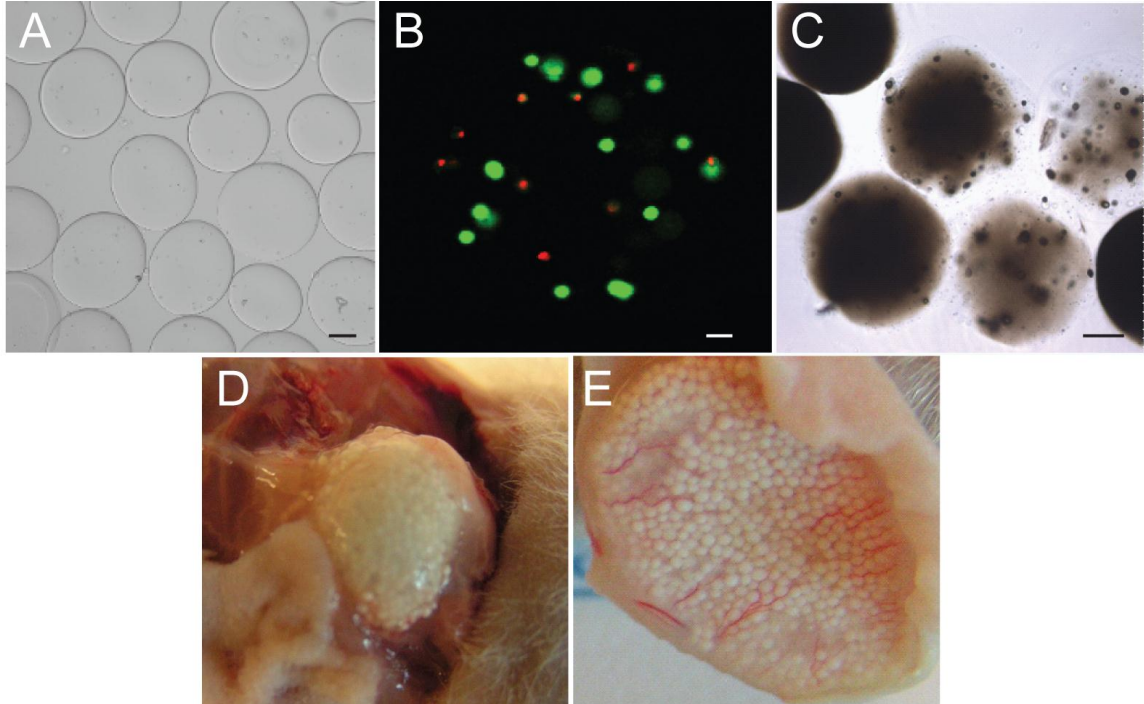
Figure 8.2: Gross-Visualization of Alginate Microbead Mineralization
(A) Microbeads before implantation or injection under a light microscope (Bar = 100µm). (B) Live/dead staining of human ASCs within a single microbead post injection (Bar = 25µm) (C) Visualization of mineralized microbeads 3 months post-implantation under a light microscope (Bar = 100µm). (D) Mineralized microbeads 3 months post-implantation. (E) Mineralized microbeads 1 month post-injection.

Table 8.1: Mineralization of Cellular and Acellular Microbeads

Months Post Op	Empty	ASC-seeded
1	*Implantation*: 4/4 Mineralized *Injection*: 3/4 Mineralized [1]	*Implantation*: 4/4 Mineralized *Injection*: 3/4 Mineralized
3	*Implantation*: 4/4 Mineralized *Injection*: 3/4 Mineralized [1]	*Implantation*: 4/4 Mineralized *Injection*: 4/4 Mineralized
6	*Implantation*: 4/4 Mineralized *Injection*: 4/4 Mineralized	*Implantation*: 4/4 Mineralized *Injection*: 4/4 Mineralized

[1]Microbeads for one sample disappeared and had no volume retention

Modifications to the crosslinking protocol reduced or eliminated calcification as detected by von Kossa staining (Table 8.2). When microbeads were injected subcutaneously, no visual calcification was evident when barium chloride was used as the crosslinker and the addition of the 25μM bisphosphonate to the crosslinking solution partially reduced mineralization. HEPES-buffered (pH 7.3) microbeads injected subcutaneously also had no apparent calcification. When HEPES-buffered samples were then directly implanted subcutaneously and intramuscularly, there was no visual mineralization. In contrast, when non-buffered microbeads were implanted a second time, all the subcutaneous and two-thirds of the intramuscular samples mineralized.

The intensity of von Kossa staining for phosphate was very strong in non-buffered samples as phosphate was present throughout almost every microbead (Figure 8.3A). Barium chloride-treated samples had no detectable presence of von Kossa staining with microbeads surrounded by endothelial tissue (Figure 8.3B). Bisphosphonate-treated samples that did calcify only had partially positive staining for phosphate as both the intensity of staining and the number of positively stained microbeads was lower compared to non-buffered samples (Figure 8.3C, Table 8.2). HEPES-buffered samples had no von Kossa staining and were surrounded by connective tissue (Figure 8.3D).

Cross-sectional x-ray sections of non-buffered samples via microCT showed extensive mineralization that was not just limited to the surfaces of individual microbeads or peripheral microbeads of the bolus (Figure 8.4A, B). Additionally, the intensity of X-ray attenuation seemed to be comparable to the adjacent bone. 3-D reconstructions further demonstrate the extent of calcification of both subcutaneous (Figure 8.4C) and

intramuscular (Figure 8.4D) samples. HEPES-buffered samples were undetectable by microCT (data not shown).

Table 8.2: Regulating Calcification by Modifying the Crosslinking Solution

	Non-buffered	Barium	Bisphosphonate	HEPES-Buffered
Implantation	*Subcutaneous*: 4/4 Calcified	-	-	*Subcutaneous*: 0/4 Calcified
	Intramuscular: 4/6 Calcified	-	-	*Intramuscular*: 0/4 Calcified
Injection	-	0/4 Calcified	2/4 Calcified	0/4 Calcified
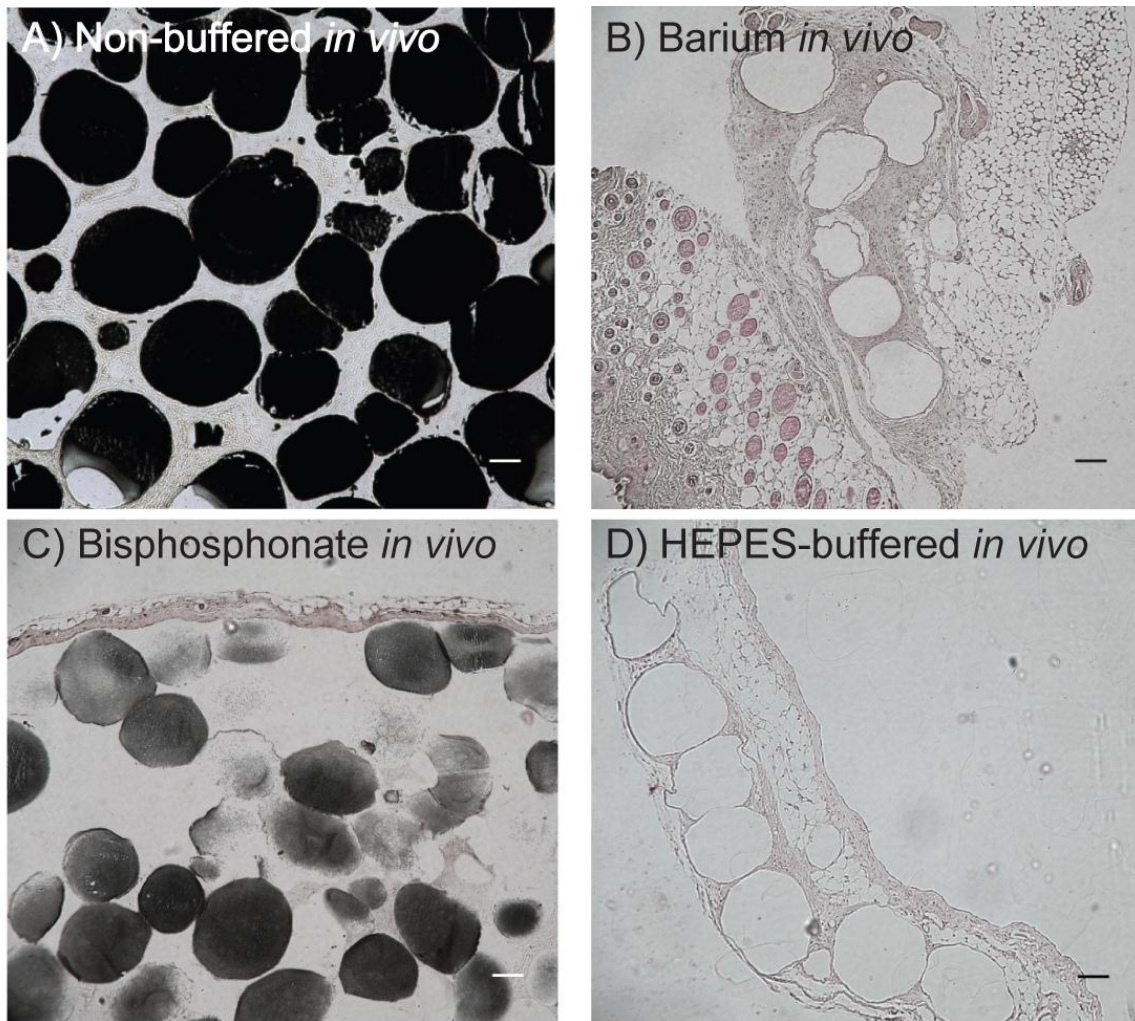
Figure 8.3: Histology of in vivo Microbead Samples
von Kossa with nuclear fast red counter stain to determine calcification for representative (A) non-buffered, (B) barium chloride, (C), bisphosphonate, (D) buffered samples in vivo after 2 months. Bar represents 100µm for all images.

153
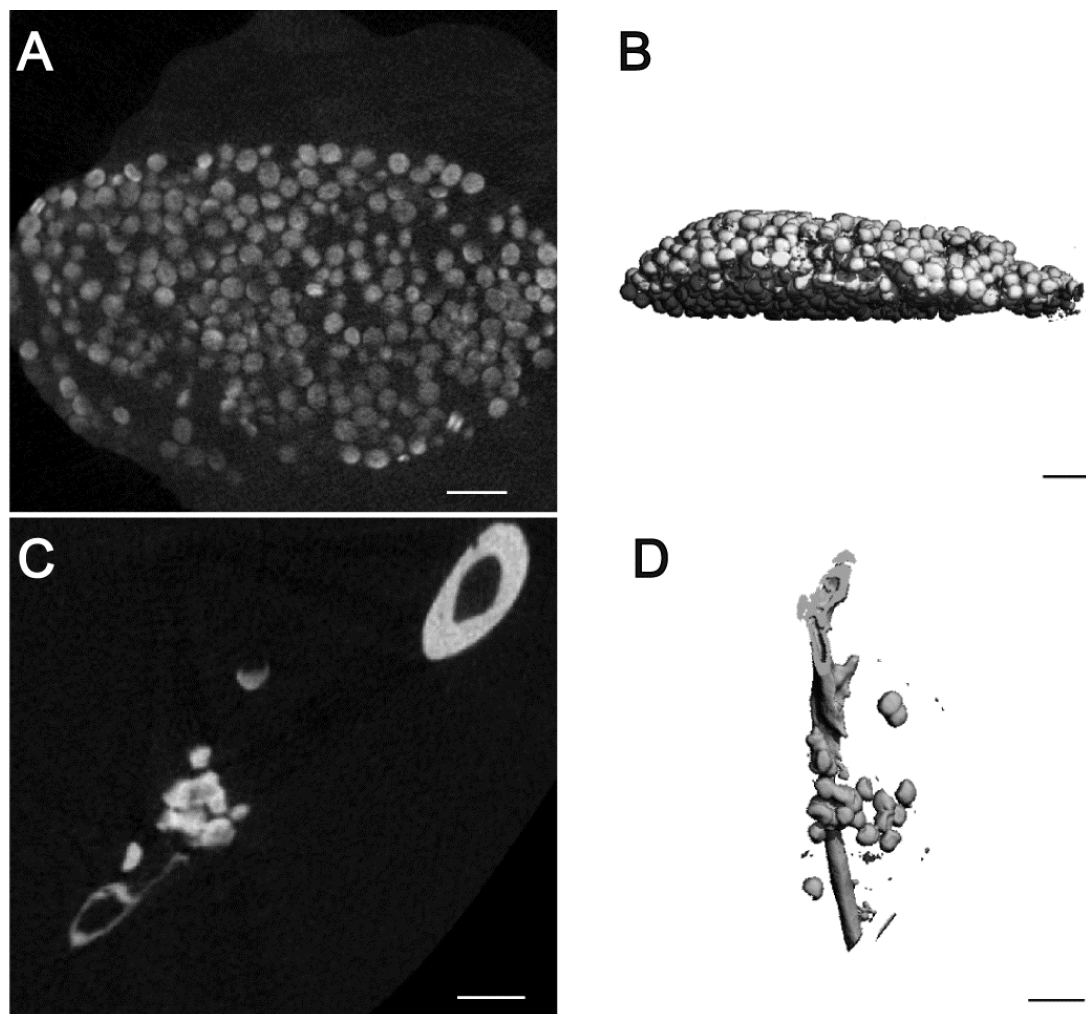
Figure 8.4: Micro-CT Images of in vivo Non-buffered Microbead Samples
(A) Representative X-ray cross-section of subcutaneously implanted non-buffered microbeads after 5 weeks in vivo. (B) 3-D reconstruction of subcutaneously implanted non-buffered microbeads after 5 weeks in vivo. (C) Representative sagittal X-ray cross-section of intramuscularly implanted non-buffered microbeads near the tibia after 5 weeks in vivo. (D) 3-D reconstruction of intramuscular implanted non-buffered microbeads along with the tibia after 5 weeks in vivo. Bar represents 1mm for all images.

Characterization of In Vivo Calcification

Comparison of FTIR spectra of the lyophilized explanted samples presented significant differences. The spectrum of the non-buffered sample (Figure 8.5A) showed the characteristic bands of hydroxyapatite around 1400-1550 cm^{-1} and 900-1200 cm^{-1} and corresponded well with the spectrum of the pure hydroxyapatite powder. The spectrum

154

of the HEPES-buffered sample (Figure 8.5B) had no traces of the HEPES spectrum (Figure 8.5C), but matched almost perfectly with the spectrum of the pure alginate powder (Figure 8.5D). No presence of hydroxyapatite was noted in the HEPES-buffered sample.
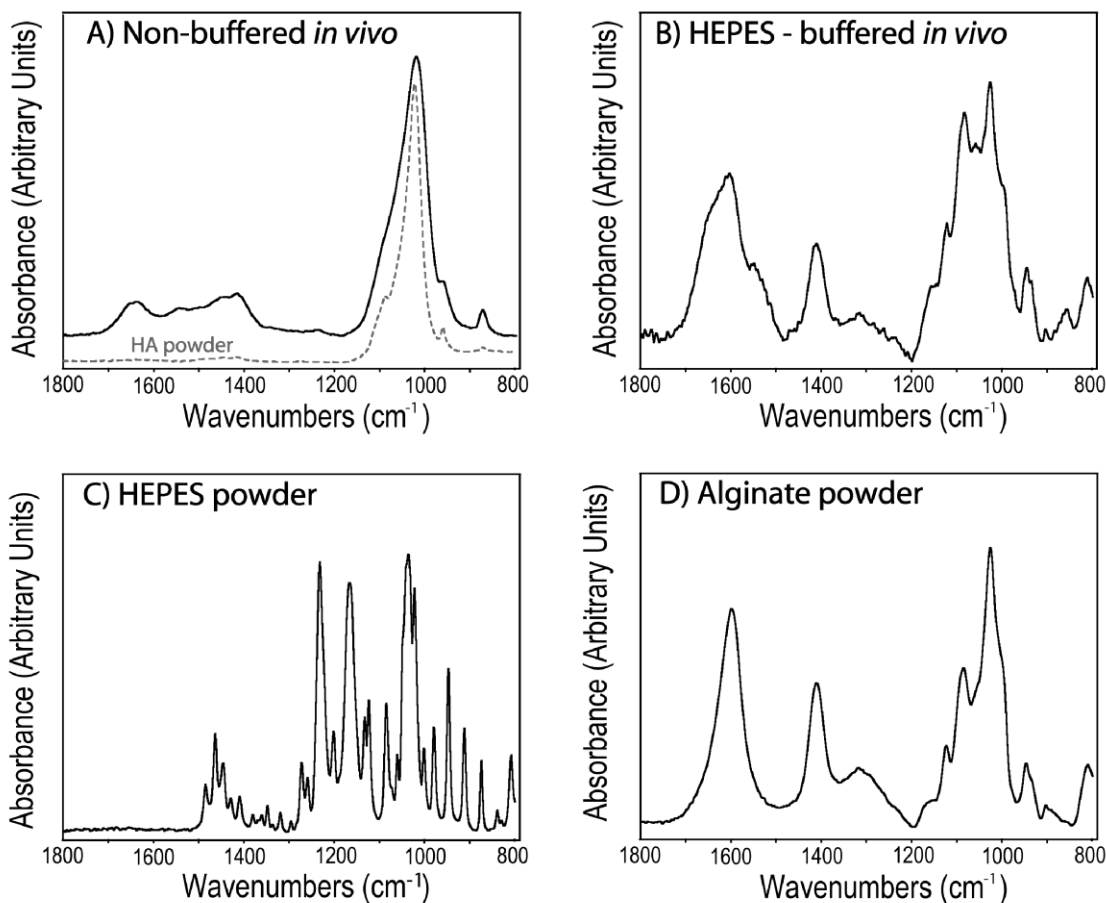
Figure 8.5: FTIR of in vivo Microbeads Samples
Spectra of (A) non-buffered microbeads after 5 weeks in vivo, (B) buffered microbeads after 5 weeks in vivo, (C) HEPES powder used to buffer the crosslinking solution, and (D) alginate powder used to make the microbeads.

The XRD spectra of the explanted samples showed the presence of monphasic crystalline structures (Figure 8.6). The alginate powder presented no diffraction pattern. The non-buffered sample appeared to have the crystal structure of hydroxyapatite, whereas the HEPES-buffered sample showed the main peaks of NaCl crystals and

incorporated none of the peaks of the HEPES buffer. The crystalline structures were further confirmed with the EDS spectra (Table 8.3), which showed the presence of 10.2 ± 1.3% Ca and 6.3 ± 0.8% P on the non-buffered sample (Ca/P ratio of 1.6±0.4), and only approximately 1% of each on the HEPES-buffered sample. Conversely, the HEPES-buffered sample included 14.3 ± 0.7% Na and 13.2 ± 1.8% Cl, and the non-buffered sample had < 1% of Na and no traces of Cl. The main components of both samples were C and O, primarily from the alginate polymer. SEM image of non-buffered microbeads that were lyophilized shows an intact spherical structure with surrounding tissue growth (Figure 8.7A) whereas HEPES-buffered microbeads that were lyophilized were clearly fragmented (Figure 8.7B).
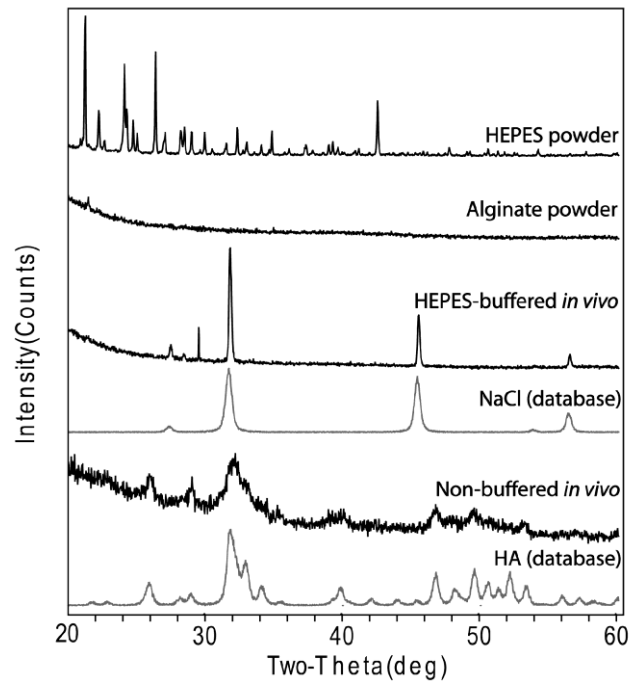
Figure 8.6 XRD of in vivo Microbead Samples
Spectra of HEPES powder used to buffer the crosslinking solution, alginate powder used to make the microbeads, buffered microbeads after 5 weeks in vivo, NaCl from the database, non-buffered microbeads after 5 weeks in vivo, and hydroxyapatite from the database.

Table 8.3: EDS Calculated Elemental Composition of *in vivo* Microbead Samples

	C	O	Na	Mg	Al	P	S	Cl	Ca	K
	: Concentration [atomic %][1,2]									
Non-buffered	34.0 ± 4.3	47.2 ± 2.0	< 1	< 1	1.2 ± 0.4	6.3 ± 0.8	< 1	-	10.2 ± 1.3	-
HEPES-Buffered	41.6 ± 1.0	27.5 ± 1.9	14.3 ± 0.7	-	< 1	1.15 ± 0.1	< 1	13.2 ± 1.8	< 1	< 1

[1] The values should be evaluated with an error of approximately ± 2% relative.
[2] Elements that were not present in all measurements of the same sample were not included in the table (e.g., Si).
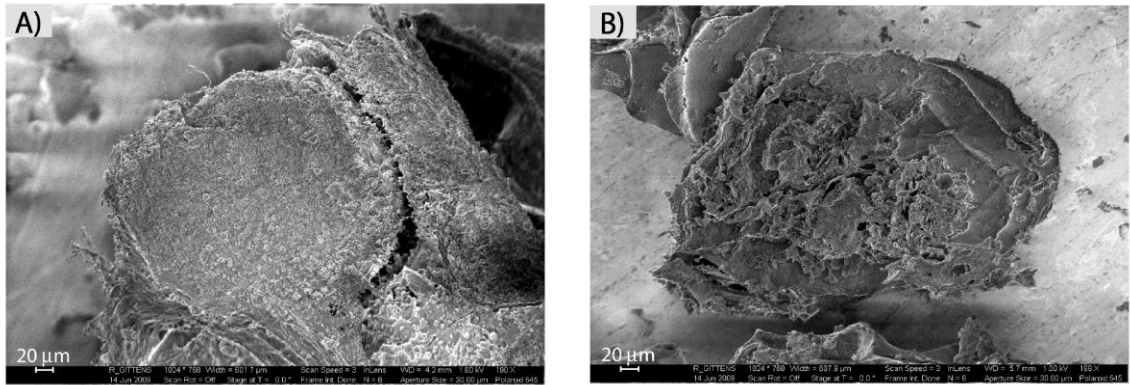
Figure 8.7: SEM Images of *in vivo* Microbead Samples
(A) Lyophilized non-buffered microbeads after 5 weeks in vivo. (B) Lyophilized buffered microbeads after 5 weeks in vivo.

DISCUSSION

Alginate mineralization has been sporadically reported when used for biomedical research and clinical applications [31, 385, 386]. The presence of such calcifications hinders soft tissue regeneration; therefore, effective strategies are needed to eliminate alginate calcification. This study is the first to characterize the mineralization that occurs, propose a mechanism behind alginate calcification, and develop strategies to modulate alginate calcification. It appears that alginate calcification both *in vitro* and *in vivo* occurs due to the alginate hydrogel providing a bolus of calcium ions that then interacts with surrounding phosphate ions to form calcium phosphate salts. This finding is confirmed by our *in vitro* results in which phosphate is sequestered from the solution into

the alginate and by our *in vivo* results where alginate crosslinked with barium - a divalent cation that does not readily interact with phosphate ions [348] - exhibited no mineralization, and the addition of alendronate - a bisphosphonate that prevents crystal growth at concentrations as low as 10^{-6}M [387] - reduced calcification. Although barium was effective at preventing calcification, it is known to be toxic at high levels [393] and hinders the ability for alginate to reabsorb while it significantly retards the delivery of soluble proteins [348]. Despite the alendronate's partial effectiveness, bisphosphonates are known to have a wide variety of side effects when treating osteoporosis [394] and have been shown to influence differentiation of stem cells [395]. Therefore, another method of regulating calcification induced by the alginate beads was investigated.

Hydroxyapatite crystals are stable to neutral to alkaline environments [388]. Therefore it was believed that buffering the pH of alginate hydrogels slightly below physiological levels with a non-phosphate buffer would help eliminate calcification *in vivo* while minimizing any biological side effects. HEPES was selected because it does not contain phosphate, is commonly used in cell culture, and is also effective for maintaining enzyme structure and function below physiological temperatures [396]. Additionally, instead of washing and storing microbeads in saline, which is the standard care for most medical implants, DMEM was used to allow for longer term storage of microbeads with encapsulated cells. MicroCT imaging along with von Kossa staining of precipitated phosphate showed extensive mineralization of non-buffered and saline-stored samples whereas buffering with HEPES and maintaining the pH of the crosslinking solution to pH 7.3, along with washing and storing samples in DMEM, completely eliminated mineralization. Both microCT and histology showed that calcification was

not limited to just the surface, suggesting that the calcium crosslinks throughout the microbeads play a major role in alginate calcification.

Further investigation using FTIR, XRD, and EDS showed that hydroxyapatite is the most stable crystal phase formed when alginate is calcified. Explanted non-buffered alginate microbeads had similar spectra to pure hydroxyapatite for both FTIR and XRD whereas buffered microbeads appeared to be a combination of alginate powder and salt crystals when both analytical modalities were used. Specifically, FTIR spectrum of non-buffered microbeads closely resembled that of 16-day-old rat calvaria with characteristic phosphate ($900\text{-}1180cm^{-1}$) and amide I ($1580\text{-}1750cm^{-1}$) peaks [397]. Although, the broad phosphate peak in the non-buffered microbeads does overlap with aryl-hydroxyl ($1030\text{-}1085$ cm^{-1}) and carboxylic acid ($915\text{-}995$ cm^{-1}) groups found in the HEPES-buffered microbeads and alginate powder, the disappearance of alginate peaks found at lower frequencies, the low intensities of the amide I and II peaks ($1405\text{-}1420$, $1600\text{-}1690$ cm^{-1}) in the non-buffered samples, and the XRD spectra suggest the formation of hydroxyapatite. To confirm these findings, the Ca/P ratio for non-buffered alginate was found to be 1.6 ± 0.4, which closely matches hydroxyapatite found in bone [398]. Non-buffered microbeads also had traces of Mg, which has been associated with facilitating the formation of calcified pathological cardiovascular deposits [399]. HEPES-buffered microbeads only had traces of calcium left, suggesting that these samples were starting to be reabsorbed. The presence of sulfur and higher content of carbon in HEPES-buffered microbeads compared to non-buffered samples suggest levels of tissue incorporation, which was also confirmed with histology. More studies though are needed to determine the ability of injectable microbeads to be used for tissue replacement or regeneration.

Cell-mediated mineralization is a complex process, and it is probable that multiple factors contribute to alginate calcification and its inhibition. It is not completely clear why buffering the calcium chloride bath with HEPES at a pH slightly below physiological levels (7.3) or washing and storing alginate microbeads in basal DMEM would prevent mineralization. Hydroxyapatite does not form de novo at pH less than 6.8 [388]. More soluble calcium phosphate phases form at lower pH values, hence the kinetics for hydroxyapatite mineral deposition would be lessened at the lower pH. It is possible that washing and storing microbeads in DMEM may have deposited amino acids such as glutamine or lysine that inhibited growth of any hydroxyapatite nuclei in a similar manner to how salivary proteins in supersaturated saliva prevent calcium phosphate mineral precipitation by adsorbing active sites of crystallite surfaces [388]. However, this explanation does not explain why non-buffered microbeads that were injected in DMEM still calcified. It is likely that making microbeads in HEPES-buffered calcium chloride at this lower pH and subsequent washing and storage in media was more effective than non-buffered saline alone in removing excess calcium ions and preventing hydroxyapatite nuclei from forming. Additionally, it has been shown that HEPES binds calcium ions with a maximum apparent binding of 1.24 ± 0.001 mmol of Ca^{2+}/L by HEPES at 10mM and pH 7.39 [400].

Although alginate microbead calcification did not strongly depend on the delivery method, delivery site, the presence of cells, or sex of the animal, biological factors can play a significant role in mineralizing alginate constructs *in vivo*. When bone marrow mesenchymal stem cells (MSCs) were treated with 10^{-7} dexamethasone and 10ng/ml TGF-β1 for more than 1 week, these cells were able to mineralize alginate scaffolds *in*

vivo whereas scaffolds with cells treated for only 1 day had no apparent calcification [31]. Osteogenic-induced adipose stem cells are able to calcify collagen scaffolds both in vitro and subcutaneously [401], and alginate microbeads containing a combination of osteoprogenitor and endothelial cells have been shown to mineralize in a metaphyseal femoral bone defect [349]. The final adipose stem cells concentration in our alginate microbeads is similar to MSC-seeded alginate constructs in Ma et al (2×10^6 cells/ml) [31] but significantly less than the microencapsulated osteoprogenitor and endothelial cells in Grellier et al (20×10^6 cells/ml) [349]. Regardless, to better utilize alginate microbeads for different tissue engineering strategies, more studies are needed to understand the exact mechanisms regulating *in vivo* mineralization of alginate.

Natural biomineralization systems and previous *in vitro* experiments have suggested that crystal nucleation and growth from organic templates occurs on surfaces that expose repetitive patterns of anionic groups [398, 402]. These negatively charged groups concentrate and create local supersaturation of inorganic cations, which leads to oriented nucleation of crystal formation. Alginate is a co-polymer with negatively charged blocks of (1-4)-linked β-D-mannuronate and (1-4)-linked α-L-guluronate residues. This structure may allow alginate polysaccharide chains to facilitate controlled calcification for bone tissue engineering. Peptide-amphiphile nanofibers modified with negatively charged peptides rich in phosphoserine groups have been shown to create hydroxyapatite *in vitro* that was aligned in the same manner as observed in bone [398]. Injectable, crosslinked-alginate that can then mineralize *in situ* without the presence of other biological or chemical factors may present an advantage over pre-mineralized scaffolds or bone morphogenetic proteins in that it avoids adverse immune responses,

limits systemic side effects, and is minimally-invasive for simple orthopaedic and reconstructive applications. However, in addition to hydroxyapatite formation and alignment, bone tissue engineering via mineralized alginate must also form constructs with high porosity and collagen content, osteoconductive properties, bioactivity, and mechanical integrity in order for this method of repair to be feasible.

CONCLUSION

In order to understand the mechanism behind alginate calcification and to develop ways to regulate it, studies *in vitro* and *in viv*o were performed. Non-buffered calcium crosslinked alginate beads placed in a phosphate buffered bath sequestered the surrounding phosphate and calcified, forming traces of hydroxyapatite. Non-buffered calcium crosslinked alginate microbeads with or without ASCs also mineralized when implanted subcutaneously or intramuscularly or injected subcutaneously after 1 to 6 months. More extensive analysis with microCT, FTIR, XRD, and EDS showed that the 1.6±0.4 Ca/P ratio of the mineral formed closely matched hydroxyapatite found in bone. Incorporating bisphosphonate helped regulate alginate calcification whereas using barium chloride as the crosslinking agent eliminated calcification. Buffering the crosslinking solution at pH 7.3 while washing and storing samples in basal media prior to implantation also eliminated calcification *in vivo.* This study effectively showed that calcium throughout the alginate is responsible for bulk hydroxyapatite formation and developed methods to partially regulate and eliminate alginate calcification.

CHAPTER 9

OPTIMIZING DELIVERY OF ADIPOSE STEM CELL

MICROBEADS FOR REPAIRING CARTILAGE FOCAL DEFECTS

INTRODUCTION

An effective therapy to treat articular cartilage lesions is needed because these injuries do not heal themselves [345]. The ineffectiveness of microfracture has been documented in human subjects as patients often experience short-term pain relief and develop progressive symptoms because of tissue failure [4-6]. Current cell therapies, such as autologous chondrocyte implantation, aim to directly regenerate cartilage by providing a source of cells that can synthesize new tissue. However, these therapies are used by a limited number of clinicians due to high variability in cartilage quality and functional outcomes [3, 4]. Therefore, a new paradigm has emerged in using stem cells, like adipose stem cells (ASCs), as growth factor production sources to stimulate diseased or damaged cartilage to regenerate itself [140, 148]. ASC microbeads are highly favorable for this new strategy because of their ability to maintain greater than 80% cell viability for at least 3 weeks post-injection and to be localized in the desired site *in vivo* for at least 3 months [223]. Additionally, previous studies have shown that ASC microbeads could be preconditioned to make growth factor secretion more favorable for cartilage regeneration.

To assess the potential of ASC microbeads to treat articular cartilage lesions, they first must be tested in focal cartilage defects. Additionally, methods need to be

developed to maintain the microbeads within the defect. Finally, a biomaterial approach may be needed to facilitate cartilage infiltration into critically-sized defects. Therefore, the objectives of this study were to determine if ASC microbeads could regenerate cartilage within a focal defect and if ASC microbeads needed to be combined with a functionalized biomaterial to promote cartilage ingrowth.

MATERIALS AND METHODS

Cell Isolation

ASCs were isolated from the inguinal fat pads of 125 g male Sprague-Dawley rats (Harlan Laboratories, Indianapolis, IN, USA) as previously described in detail [319, 320] and cultured in Lonza Mesenchymal Stem Cell Growth Medium (GM, Lonza, Walkersville, MD, USA). After one passage, these cells were negative for CD45 and positive for CD73 and CD271 [320].

Microencapsulation and Treatment

Once primary ASCs reached 90% confluence, cells were trypsinized and microencapsulated in 20 mg/mL low molecular weight (~150 kDa) alginate (FMC BioPolymer, Sandvika, Norway) with a high mannuronate to guluronate ratio (40% guluronate) dissolved in saline (Ricca Chemical, Arlington, TX, USA) at a cell concentration of 25×10^6 cells/mL as previously described [322], using a Nisco Encapsulator VAR V1 LIN-0043 (Nisco Engineering AG, Zurich, Switzerland) and a cross-linking solution of 50 mM CaCl2, 150 mM glucose, and 15 mM 4-(2-hydroxyethyl)-1-piperazineethanesulfonic acid (pH=7.3, Sigma, St. Louis, MO, USA). The microbeads were washed three times in GM and cultured in this medium for 5 days.

After 5 days of culture, microbeads were then treated for 5 days with either GM or chondrogenic medium (CM) consistent of 4.5 g/L glucose DMEM with 1 mM sodium pyruvate (Mediatech, Manassas, VA, USA), 40 µg/ml proline (Sigma), 50 µg/ml ascorbate-2-phosphate (Sigma), 1% ITS+ (Sigma), 100 nM dexamethasone (Sigma), 10 ng/ml recombinant human transforming growth factor beta-1 (TGF-β1, R&D Systems, Minneapolis, MN, USA) and 100 ng/ml recombinant human bone morphogenic protein-6 (BMP-6, PeproTech, Rocky Hill, NJ, USA). After 5 days of treatment, microbeads were washed in Dulbecco's modified Eagle's medium (DMEM) containing 1% penicillin and streptomyocin and stored at 4°C prior to implantation.

RGD-conjugated Hydrogel Preparation

One day before the surgeries, 20 mg/mL $CaSO_4$ (Sigma) was autoclaved and stored at 4°C. Prior to surgeries, sterile RGD-conjugated alginate (NOVATACH M RGD, FMC BioPolymer) was dissolved in DMEM containing 1% penicillin and streptomyocin at a concentration of 25 mg/mL. Using two syringes connected to a luer-lock 3-way connector the RGD-conjugated alginate and $CaSO_4$ were mixed at a 4:1 volume ratio.

Xiphoid Defect

To assess if ASC microbeads alone could promote cartilage regeneration, 3 mm cylindrical defects were made in the xiphoids of 125 g male Sprague-Dawley rats as previously described in detail [369] using a protocol approved by the Institutional Animal Care and Use Committee of the Georgia Institute of Technology. To assess if ASC microbeads could promote cartilage ingrowth along an RGD-conjugated hydrogel, 2 mm cylindrical defects were made in xiphoids. For both studies, ASC microbeads

preconditioned with MSCGM or CM were implanted into the defect, but were immobilized with the RGD-conjugated hydrogel mixture only in the 2 mm defect study. Empty defects and empty microbeads served as controls in the 3 mm defect study whereas empty defects with the hydrogel mixture and re-implanted excised cartilage (autografts) served as controls in the 2 mm study. All groups were tested in 7 rats.

35 days post operation, the xiphoids were excised and washed in saline and radiographic imaging (Faxitron Bioptics, Lincolnshire, IL, USA) was performed in the coronal plane at a voltage of 22 mV and exposure time of 16 s to visualize soft tissue penetration as previous described [369]. A blind observer then scored the presence of soft tissue penetration with a score of 0 representing no healing, a score of 0.5 representing partial healing, and a score of 1 representing full healing.

Equilibrium partitioning of an ionic contrast agent via micro-computed tomography (EPIC-μCT) was used to visualize the distribution of proteoglycans within the xiphoid defects as previously described [369, 370]. Xiphoids were incubated in 40% Hexabrix (Mallinckrodt, St. Louis, MO, USA) in saline containing 1% proteinase inhibitor cocktail (CalBiochem, Darmstadt, Germany) overnight and scanned using pre-determined settings [369]. Low X-ray attenuation (green/yellow) of three-dimensional color images corresponded to regions of high proteoglycan concentration and no or high X-ray attenuation (black and red/orange) indicated regions of low proteoglycan concentration. To determine cartilage volume, the 1 mm defect was isolated with user-guided contours and evaluated at a $100 - 250$ threshold range.

After scanning, samples were washed in saline for 2 hours at $37^{\circ}C$ to equilibrate out any excess Hexabrix. Samples were then fixed in 10% phosphate-buffered formalin

(Sigma) for 48 hours and embedded in paraffin. Sagittal sections of the defect were stained with safranin-O using a fast green counter stain to evaluate proteoglycan present.

RESULTS

<u>Effects of ASC Microbeads on Cartilage Regeneration</u>

X-ray scoring of defects with microbeads showed that although partial healing was observed, microbeads with encapsulated ASCs did not perform better than empty microbeads (Figure 9.1A). Histology confirmed these results, showing little to no apparent cell infiltration or extracellular matrix deposition (Figure 9.1C). There were also no differences in EPIC-μCT measured cartilage volume among all the groups (Figure 9.1B).

<u>Effect of ASC Microbeads and RGD-conjugated Hydrogel on Cartilage Regeneration</u>

X-ray scoring of defects showed that defects with GM or CM preconditioned ASC microbeads and hydrogel mixture performed better than empty defects with only the hydrogel (Figure 9.2A). Defects with only the hydrogel mixture had no apparent cell infiltration, new extracellular matrix (ECM) deposition, or perichondrium as indicated by the lack of fast green staining (Figure 9.2C). Defects with the ASC microbeads preconditioned in MSCGM had traces of fast green staining throughout the defect with cell infiltration and tissue deposition at the edges of the defect (Figure 9.2C). Defects with ASC microbeads preconditioned in CM had ECM deposition throughout the defect with cell infiltration, tissue resembling a perichondrium, and initial proteoglycan deposition (Figure 9.2C). Defects with the autograft had cell infiltration, a perichondrium that resembled that of the surrounding xiphoid and proteoglycan deposition between the edges of the defect and autograft (Figure 9.2C). EPIC-μCT

measured cartilage volume was highest for the autograft group, and no difference in cartilage volume was seen in any defect containing the hydrogel mixture (Figure 9.2B).
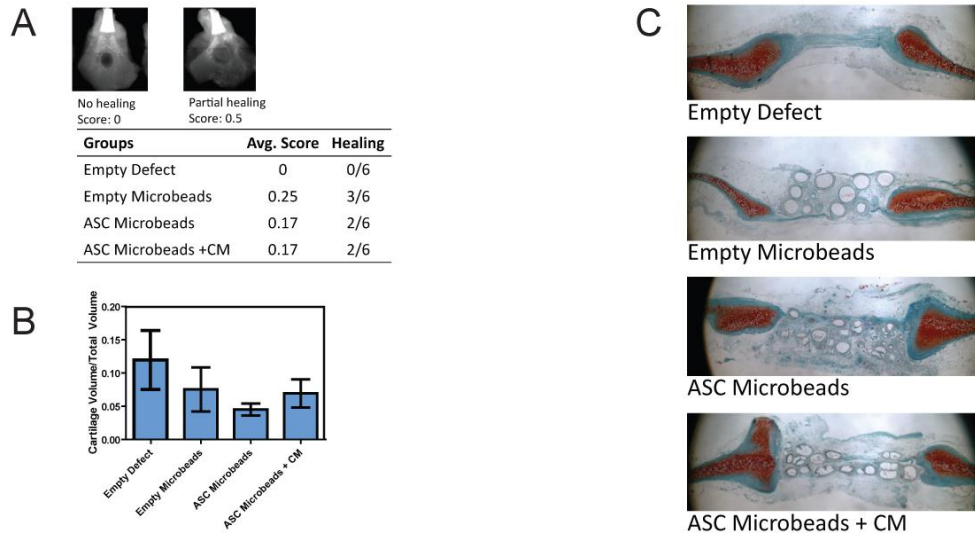
Figure 9.1: ASC Microbeads in Xiphoid Defect
(A) Radiographic scoring. (B) 3-D EPIC-µCT calculated cartilage volume within defects (n=6±SE). (C) Representative Safranin-O staining of 3 mm defects.
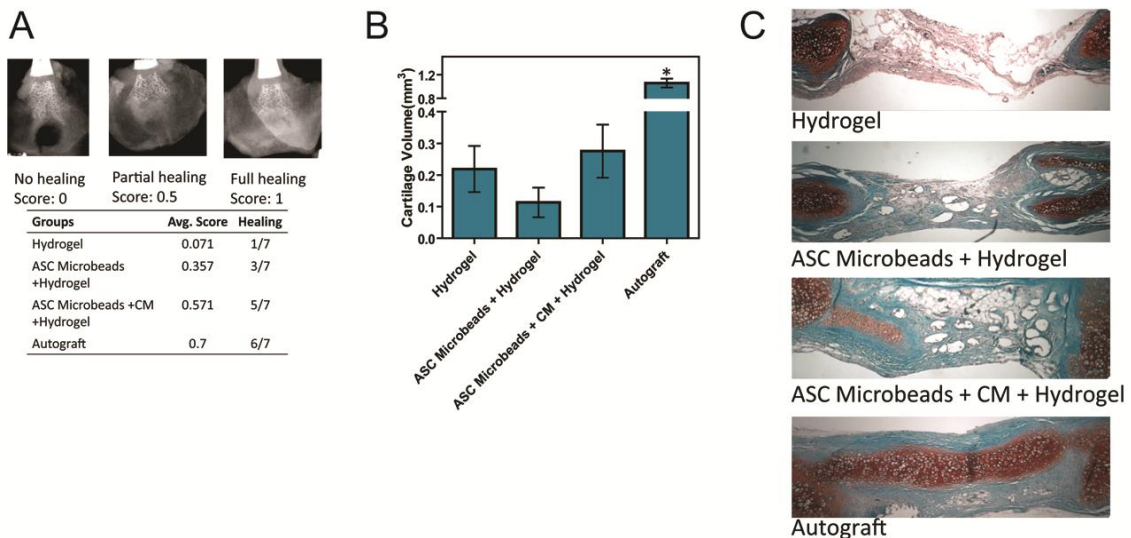
Figure 9.2: ASC Microbeads and RGD-Hydrogel Mixture in Xiphoid Defect
(A) Radiographic scoring. (B) 3-D EPIC-µCT calculated cartilage volume within defects (n=7±SE, *p<0.05 vs. all groups). (C) Representative Safranin-O staining of 2 mm defects.

DISCUSSION

When implanted in a focal cartilage defect, ASC microbeads alone were unable to regenerate tissue any better than empty microbeads. When ASC microbeads were immobilized in a RGD-conjugated hydrogel in a smaller defect, they were able to stimulate tissue infiltration from the defect edges and perichondrium while promoting proteoglycan deposition. Additionally ASC microbeads preconditioned with chondrogenic medium performed better than ASC microbeads preconditioned in growth medium. Despite these initial results, the full potential of the ASC microbeads and hydrogel mixture may have been better assessed at time periods longer than 35 days post-operation.

Alginate microbeads have previously been used to deliver progenitor cells in bone defects [349] and MSCs in the infarcted heart [169]. Additionally, RGD can increase expression of FGF-2 in microencapsulated MSCs, but has also been shown to inhibit chondrogenesis [238]. RGD's negative effects on chondrogeneis may be due to its ability to promote actin cytoskeleton reorganization. Actin cytoskeleton disruption via protein kinase C-dependent p38 mitogen-activated protein kinase signaling induced chondrogenesis [403], and inhibiting ROCK signaling, a well characterized regulator of cytoskeletal organization, elevated Sox9 expression and glycosaminoglycan synthesis [404]. Additionally, RGD is a biomimetic peptide derived from fibronectin, which is known to inhibit chondrogeneis [351]. Although the RGD-conjugated hydrogel did not appear to inhibit cartilage ingrowth, secreted factors from ASC microbeads may have counteracted this peptide's negative effects.

In these studies, the perichondrium appeared to be the main mediator for tissue infiltration and cartilaginous tissue deposition within the defect. This tissue is known to be a rich source of chondroprogenitors and has a central role in mediating the effects of TGF-β1 in endochondral bone formation [49]. Perichondrium transferred from ears and ribs have been used to resurface articular cartilage with varying levels of success [405, 406]. Additionally, chondroprogenitor cells isolated from the perichondrium have had promising results for cartilage tissue engineering and regeneration [407-409]. Although using the paracrine actions of ASCs to stimulate perichondrium-mediated tissue regeneration may be beneficial for regenerating hyaline cartilage, articular surfaces have no more than a peripheral rim of this tissue. Furthermore, isolating perichondrium from other hyaline surfaces to re-surface articular cartilage would lead to a significantly more complicated procedure, though periosteal flaps may provide a viable source of infiltrating progenitor cells. Therefore, when further optimizing ASC microbeads for cartilage regeneration, these factors will need to be taken into consideration.

EPIC-μCT was also performed in this study, but the results from 3-D evaluations were contradictory with results from radiographic imaging and histology. Subsequent investigation revealed that a noticeable amount of hexabrix was retained within alginate constructs after incubation overnight. This finding was highly surprising because of alginate polymer's negative charge and because of the ability of alginate microbeads to provide extended release of high pI proteins [410]. However, it may be possible that the negatively charged hexabrix may have interacted with the calcium crosslinks in alginate gels. Because the ability of EPIC-μCT to visualize and quantify proteoglycan

production is dependent on hexabrix exclusion from the anionic tissue, this method may not be optimal for detecting neocartilage formation within alginate constructs.

CONCLUSION

ASC microbeads were unable to facilitate any observable cartilage regeneration in 3 mm defects regardless of chondrogenic medium pretreatment. In 2 mm defects with only the RGD-conjugated hydrogel mixture, no apparent cell infiltration, new extracellular matrix deposition, or perichondrium formation was observed. Defects with the ASC microbeads preconditioned in GM and immobilized in RGD-conjugated hydrogel had cell infiltration and tissue deposition at the edges of the defect. Defects with ASC microbeads preconditioned in chondrogenic medium and RGD-conjugated hydrogel had extracellular matrix deposition throughout the defect with cell infiltration, tissue resembling a perichondrium, and initial proteoglycan deposition. Defects with the autograft had cell infiltration, a perichondrium that resembled that of the surrounding xiphoid, and proteoglycan deposition between the edges of the defect and autograft. These results suggest that ASC microbeads may serve as trophic factor production sources to stimulate cartilage regeneration along a biomimetic scaffold.

CHAPTER 10

CONCLUSION AND FUTURE PERSPECTIVES

In order to develop cartilage regeneration therapies that harness the paracrine actions of ASCs, the first step is to understand the signaling mechanisms that regulate temporal morphology and development of cartilaginous tissues. Tethers present in both the growth plates of long bones and synchondroses of the cranial base occurred in specific regions that could be mapped. These tethers thickened and accumulated in number with age as the tissue decreased in size. When the VDR was ablated, tether formation was nearly eliminated in both rachitic growth plates and synchondroses. Restoring mineral homeostasis with rescue diets restored the overall size of both growth centers but only partially restored growth center morphology and tether formation, suggesting that tether formation in both growth centers is partially regulated by VDR signaling via $1\alpha,25$-dihydroxy vitamin-D_3. Serial decalcified histological sections confirmed the findings from μCT analysis as parameters were significantly correlated between the two imaging and analytical techniques. During post-fetal development from 2 to 15 weeks of age, tether phenotype had significant relationships to animal weight. Synchondrosis and growth plate thicknesses were inversely correlated to weight in wild-type mice, whereas in both 2 to 15 week old normal mice and 10 week old VDR-/- mice with normal and abnormal mineral homeostasis, tether phenotype was tightly linked to growth center thickness. The strong association between tether formation and growth center morphology may have implications on normal skeletal development and

172

homeostasis, and further investigation may provide insight into strategies to regulate cartilage formation and bone growth.

Tailoring the secretory profile of ASCs is the next step in using the paracrine actions of these therapies to regenerate cartilage. Rat ASC cultures had high mRNA levels of TGF-β and MAPK signaling molecules, and preconditioning ASC cultures with chondrogenic medium and its individual components had distinct effects on trophic factor production. For rat ASC cultures in 2-D monolayer and 3-D alginate microbeads, chondrogenic medium increased the expression and secretion of IGF-I, TGF-β2, and TGF-β3 and decreased the expression and secretion of VEGF-A and FGF-2. Microencapsulation alone increased PTHrP expression and IGF-I, TGF-β2, and VEGF-A secretion in growth medium, but not necessarily in chondrogenic medium. Chondrogenic medium and microencapsulation had similar effects on human ASCs isolated from multiple donors as chondrogenic medium consistently decreased the expression of FGF-2 and secretion of VEGF-A from ASC microbeads derived from the same donor population. Additionally, microencapsulation alone increased gene expression of PTHrP and secretion of IGF-I and TGF-β3.

In subsequent studies with rat ASC monolayers cultured in growth and chondrogenic media, ascorbic acid 2-phosphate decreased FGF-18 expression and VEGF-A secretion but increased IGF-I and TGF-β2 secretion. Meanwhile, dexamethasone increased BMP-2 and FGF-18 expression, decreased FGF-2 expression, and decreased VEGF-A expression and secretion in growth and chondrogenic media. TGF-β1 and BMP-6 increased expression and secretion of TGF-β2 and FGF-18 expression while TGF-β1 also increased expression and secretion of FGF-2 and VEGF-

A. Crosslinking human ASC microbeads in $BaCl_2$ instead of $CaCl_2$ did not eliminate the beneficial effects of microencapsulation, but did decrease IGF-I gene expression and production. Increasing the guluronate content of the alginate microbead increased TGF-β3 expression and IGF-I maintained within. Decreasing the molecular weight of the alginate used eliminated the beneficial effects microencapsulation had on IGF-I secretion while increasing the molecular weight of alginate used decrease PTHrP gene expression. These studies demonstrated that different components of differentiation media and alginate microbeads can be used to tailor the secretome of stem cell therapies and that ASC microbeads may be a reliable source for delivering multiple growth factors to facilitate cartilage regeneration.

Before delivering these ASC therapies *in vivo,* the effect ASC-secreted factors have on chondrocyte behavior and cartilage regeneration needs to be determined. ASCs that were preconditioned in growth medium inhibited cartilage regeneration in a focal hyaline cartilage defect *in vivo*. *In vitro*, ASCs monolayers or microbeads cultured in growth medium secreted a large amount of VEGF-A which caused chondrocyte apoptosis and reduced proteoglycan synthesis. Additionally, these ASCs secrete factors that reduced chondrogenic gene expression and proliferation. Treating ASCs with chondrogenic medium reduced the secretion of VEGF-A, significantly reduced the deleterious effects ASC-secreted factors have on chondrocytes, and eliminated the inhibitory effect ASCs have on cartilage regeneration. Blocking VEGF-A in ASC-conditioned medium eliminated the deleterious effects ASC-secreted factors had on chondrocyte phenotype and apoptosis. Adding a high concentration of FGF-2 eliminated the apoptotic effect VEGF-A had on chondrocytes and adding both low and high

concentrations of FGF-2 eliminated the detrimental effects VEGF-A had on chondrocyte phenotype. These results have significant implications on how ASCs and possibly other stem cell therapies are used for repairing cartilage. Specifically, these therapies must be pre-treated or modified to reduce the inhibitory effects of VEGF-A and other secreted factors on cartilage regeneration.

The final step in exploiting the paracrine actions of ASCs to regenerate cartilage is to develop an effective method to deliver them *in vivo*. Initial studies showed that ASC alginate microbeads calcified after 1 to 6 months regardless if they were implanted intramuscularly or injected subcutaneously. Non-buffered calcium crosslinked alginate beads placed in a phosphate buffered bath sequestered the surrounding phosphate and calcified, forming traces of hydroxyapatite. More extensive analysis of calcified microbeads delivered *in vivo* showed that the 1.6±0.4 Ca/P ratio of the mineral formed closely matched hydroxyapatite found in bone. Incorporating bisphosphonate helped regulate alginate calcification whereas using barium chloride as the crosslinking agent eliminated calcification. Buffering the crosslinking solution at pH 7.3 while washing and storing samples in basal media prior to implantation also eliminated calcification *in vivo.* Once this formulation was optimized, ASC microbeads preconditioned with growth and chondrogenic media were implanted in 3 mm xiphoid cartilage defects but were unable to facilitate any observable cartilage regeneration. When ASC microbeads preconditioned in growth media were immobilized with an RGD-conjugated hydrogel in 2 mm defects, cell infiltration and tissue deposition at the edges of the defect were observed. Defects with ASC microbeads preconditioned in chondrogenic medium and immobilized in RGD-conjugated hydrogel had extracellular matrix deposition throughout the defect with

cell infiltration, tissue resembling a perichondrium, and initial proteoglycan deposition. These results suggest that modifying the crosslinking solution for alginate microbeads can regulate bulk hydroxyapatite formation and that ASC microbeads may serve as trophic factor production sources to stimulate cartilage regeneration along a biomimetic scaffold.

The strong correlations between tether formation and growth center thickness, animal weight, and tissue shrinkage during histological processing suggest that tethers may have a fundamental role in growth plate closure, mechanical stability, and their interrelationship. If confirmed, this revelation will contradict decades of growth plate development dogma because growth plate closure and changes in mechanical properties have long been thought to occur in layers corresponding to the tissue's different hierarchical zones. Tethers, however, traverse all developmental zones of the growth plate. The closest independent results that may confirm tethers' role in growth plate mechanical stability was disclosed by Sevenler and Bonassar et al. at the 2012 Annual Meeting of the Orthopaedic Research Society in San Francisco. They found that cyclic shear strain applied in the anteroposterior direction (γ_{yx}) on normal growth plates of Sprague-Dawley rats induced significant shear strain in the direction of growth (γ_{xy}) concentrated in bands located in the interterritorial matrix between chondrons. These bands of shear strain were similar to the periodic nature of tether formation within the growth plate. When the same shear strain was applied on growth plates of vitamin D deficient rats, the spacing between the peak strains were twice as large and not periodic, consistent with tether formation in VDR null mice. Whether tether formation forms in response to this shear strain or imparts the growth plate with this periodic mechanical

176

property is unknown. However, further elucidating the relationship between tissue microscale mechanical properties and tether formation during normal and abnormal growth plate development may revolutionize our understanding of growth plate biology and closure.

Although preconditioning with chondrogenic medium generally increased chondrogenic factors and decreased angiogenic ones, it is unknown what global effects it had on other cytokines, growth factors, and enzymes. Inflammatory cytokines, proteases, and inhibitors are important for cartilage regeneration and a better understanding of how preconditioning affects these factors is needed. Additionally, controlling the exact timing of different factors' secretion profiles is critically. Specifically, anti-inflammatory cytokines and growth factors that stimulate mesenchymal condensation and chondrogenesis may be critical for initial cartilage regeneration, but their presence during subsquent stages of regeneration may be detrimental. It is unknown whether ASCs preconditioned with different treatments will secrete temporally varying amounts of growth factors once delivered *in vivo*. Additionally, the exact role each ASC-secreted factor has in cartilage regeneration is unknown. To elucidate this may require several *in vivo* studies of varying lengths where multiple ASC populations that underwent different pretreatments are delivered.

Developing a novel ASC therapy that stimulates cartilage regeneration via its paracrine actions may take decades before it is clinically available to any patient. However, evaluating and tailoring stem cell therapies for tissue regeneration via its secretory profile are novel approaches that may lead to the next clinical breakthrough for regenerative medicine.

REFERENCES

1.   Rodkey WG, Steadman JR, Li ST. **A clinical study of collagen meniscus implants to restore the injured meniscus**. *Clin Orthop Relat Res* 1999:S281-92.

2.   Hunziker EB. **Articular cartilage repair: basic science and clinical progress. A review of the current status and prospects**. *Osteoarthritis Cartilage* 2002; 10:432-63.

3.   Creamer P, Hochberg MC. **Osteoarthritis**. *Lancet* 1997; 350:503-8.

4.   Johnson LL. **Arthroscopic abrasion arthroplasty historical and pathologic perspective: present status**. *Arthroscopy* 1986; 2:54-69.

5.   Mitchell N, Shepard N. **The resurfacing of adult rabbit articular cartilage by multiple perforations through the subchondral bone**. *J Bone Joint Surg Am* 1976; 58:230-3.

6.   Dhollander AA, Verdonk PC, Lambrecht S, Verdonk R, Elewaut D, Verbruggen G, Almqvist KF. **Midterm results of the treatment of cartilage defects in the knee using alginate beads containing human mature allogenic chondrocytes**. *Am J Sports Med* 2012; 40:75-82.

7.   Morrey BF. **Difficult complications after hip joint replacement. Dislocation**. *Clin Orthop Relat Res* 1997:179-87.

8.   Katz JN. **Total joint replacement in osteoarthritis**. *Best Pract Res Clin Rheumatol* 2006; 20:145-53.

9.   Safran MR, Seiber K. **The evidence for surgical repair of articular cartilage in the knee**. *J Am Acad Orthop Surg* 2010; 18:259-66.

10.   Brittberg M, Lindahl A, Nilsson A, Ohlsson C, Isaksson O, Peterson L. **Treatment of deep cartilage defects in the knee with autologous chondrocyte transplantation**. *N Engl J Med* 1994; 331:889-95.

11.   Minas T, Gomoll AH, Rosenberger R, Royce RO, Bryant T. **Increased failure rate of autologous chondrocyte implantation after previous treatment with marrow stimulation techniques**. *Am J Sports Med* 2009; 37:902-8.

12.   Panagopoulos A, van Niekerk L, Triantafillopoulos I. **Autologous Chondrocyte Implantation for Knee Cartilage Injuries: Moderate Functional Outcome and Performance in Patients With High-impact Activities**. *Orthopedics* 2012; 35:e6-e14.

13. Bachmann G, Basad E, Lommel D, Steinmeyer J. **[MRI in the follow-up of matrix-supported autologous chondrocyte transplantation (MACI) and microfracture]**. *Radiologe* 2004; 44:773-82.

14. Behrens P, Bitter T, Kurz B, Russlies M. **Matrix-associated autologous chondrocyte transplantation/implantation (MACT/MACI)--5-year follow-up**. *Knee* 2006; 13:194-202.

15. Saris DB, Vanlauwe J, Victor J, Haspl M, Bohnsack M, Fortems Y, Vandekerckhove B, Almqvist KF, Claes T, Handelberg F, Lagae K, van der Bauwhede J, Vandenneucker H, Yang KG, Jelic M, Verdonk R, Veulemans N, Bellemans J, Luyten FP. **Characterized chondrocyte implantation results in better structural repair when treating symptomatic cartilage defects of the knee in a randomized controlled trial versus microfracture**. *Am J Sports Med* 2008; 36:235-46.

16. Vanlauwe J, Saris DB, Victor J, Almqvist KF, Bellemans J, Luyten FP. **Five-year outcome of characterized chondrocyte implantation versus microfracture for symptomatic cartilage defects of the knee: early treatment matters**. *Am J Sports Med* 2011; 39:2566-74.

17. Copland IB, Lord-Dufour S, Cuerquis J, Coutu DL, Annabi B, Wang E, Galipeau J. **Improved autograft survival of mesenchymal stromal cells by plasminogen activator inhibitor 1 inhibition**. *Stem Cells* 2009; 27:467-77.

18. Coutu DL, Cuerquis J, El Ayoubi R, Forner KA, Roy R, Francois M, Griffith M, Lillicrap D, Yousefi AM, Blostein MD, Galipeau J. **Hierarchical scaffold design for mesenchymal stem cell-based gene therapy of hemophilia B**. *Biomaterials* 2011; 32:295-305.

19. Lin Z, Willers C, Xu J, Zheng MH. **The chondrocyte: biology and clinical application**. *Tissue Eng* 2006; 12:1971-84.

20. Niemeyer P, Pestka JM, Salzmann GM, Sudkamp NP, Schmal H. **Influence of cell quality on clinical outcome after autologous chondrocyte implantation**. *Am J Sports Med* 2012; 40:556-61.

21. Grogan SP, Barbero A, Diaz-Romero J, Cleton-Jansen AM, Soeder S, Whiteside R, Hogendoorn PC, Farhadi J, Aigner T, Martin I, Mainil-Varlet P. **Identification of markers to characterize and sort human articular chondrocytes with enhanced in vitro chondrogenic capacity**. *Arthritis Rheum* 2007; 56:586-95.

22. Lovice DB, Mingrone MD, Toriumi DM. **Grafts amd implants in rhinoplasty and nasal reconstruction**. *Otolaryngol Clin North Am* 1999; 32:113-41.

23. Phillips MI, Tang YL. **Genetic modification of stem cells for transplantation**. *Adv Drug Deliv Rev* 2008; 60:160-72.

24.   Locke M, Feisst V, Dunbar PR. **Concise review: human adipose-derived stem cells: separating promise from clinical need**. *Stem Cells* 2011; 29:404-11.

25.   Rada T, Reis RL, Gomes ME. **Adipose tissue-derived stem cells and their application in bone and cartilage tissue engineering**. *Tissue Eng Part B Rev* 2009; 15:113-25.

26.   Devine SM, Bartholomew AM, Mahmud N, Nelson M, Patil S, Hardy W, Sturgeon C, Hewett T, Chung T, Stock W, Sher D, Weissman S, Ferrer K, Mosca J, Deans R, Moseley A, Hoffman R. **Mesenchymal stem cells are capable of homing to the bone marrow of non-human primates following systemic infusion**. *Exp Hematol* 2001; 29:244-55.

27.   Devine SM, Cobbs C, Jennings M, Bartholomew A, Hoffman R. **Mesenchymal stem cells distribute to a wide range of tissues following systemic infusion into nonhuman primates**. *Blood* 2003; 101:2999-3001.

28.   Li F, Wang X, Niyibizi C. **Distribution of single-cell expanded marrow derived progenitors in a developing mouse model of osteogenesis imperfecta following systemic transplantation**. *Stem Cells* 2007; 25:3183-93.

29.   Niyibizi C, Wang S, Mi Z, Robbins PD. **The fate of mesenchymal stem cells transplanted into immunocompetent neonatal mice: implications for skeletal gene therapy via stem cells**. *Mol Ther* 2004; 9:955-63.

30.   Wang X, Li F, Niyibizi C. **Progenitors systemically transplanted into neonatal mice localize to areas of active bone formation in vivo: implications of cell therapy for skeletal diseases**. *Stem Cells* 2006; 24:1869-78.

31.   Smartt JM, Jr., Karmacharya J, Gannon FH, Teixeira C, Mansfield K, Hunenko O, Shapiro IM, Kirschner RE. **Intrauterine fetal constraint induces chondrocyte apoptosis and premature ossification of the cranial base**. *Plast Reconstr Surg* 2005; 116:1363-9.

32.   Baraniak PR, McDevitt TC. **Stem cell paracrine actions and tissue regeneration**. *Regen Med* 2010; 5:121-43.

33.   Hsiao ST, Asgari A, Lokmic Z, Sinclair R, Dusting GJ, Lim SY, Dilley RJ. **Comparative Analysis of Paracrine Factor Expression in Human Adult Mesenchymal Stem Cells Derived from Bone Marrow, Adipose, and Dermal Tissue**. *Stem Cells Dev* 2012.

34.   Reddi AH. **Morphogenesis and tissue engineering of bone and cartilage: inductive signals, stem cells, and biomimetic biomaterials**. *Tissue Eng* 2000; 6:351-9.

35. Abad V, Meyers JL, Weise M, Gafni RI, Barnes KM, Nilsson O, Bacher JD, Baron J. **The role of the resting zone in growth plate chondrogenesis**. *Endocrinology* 2002; 143:1851-7.

36. Brochhausen C, Lehmann M, Halstenberg S, Meurer A, Klaus G, Kirkpatrick CJ. **Signalling molecules and growth factors for tissue engineering of cartilage-what can we learn from the growth plate?** *J Tissue Eng Regen Med* 2009; 3:416-29.

37. Nilsson O, Parker EA, Hegde A, Chau M, Barnes KM, Baron J. **Gradients in bone morphogenetic protein-related gene expression across the growth plate**. *J Endocrinol* 2007; 193:75-84.

38. Weise M, De-Levi S, Barnes KM, Gafni RI, Abad V, Baron J. **Effects of estrogen on growth plate senescence and epiphyseal fusion**. *Proc Natl Acad Sci U S A* 2001; 98:6871-6.

39. Stevens DG, Boyer MI, Bowen CV. **Transplantation of epiphyseal plate allografts between animals of different ages**. *J Pediatr Orthop* 1999; 19:398-403.

40. Brighton CT, Heppenstall RB. **Oxygen tension in zones of the epiphyseal plate, the metaphysis and diaphysis. An in vitro and in vivo study in rats and rabbits**. *J Bone Joint Surg Am* 1971; 53:719-28.

41. Ballock RT, O'Keefe RJ. **The biology of the growth plate**. *J Bone Joint Surg Am* 2003; 85-A:715-26.

42. Wang W, Kirsch T. **Retinoic acid stimulates annexin-mediated growth plate chondrocyte mineralization**. *J Cell Biol* 2002; 157:1061-9.

43. Lewinson D, Silbermann M. **Chondroclasts and endothelial cells collaborate in the process of cartilage resorption**. *Anat Rec* 1992; 233:504-14.

44. Vu TH, Shipley JM, Bergers G, Berger JE, Helms JA, Hanahan D, Shapiro SD, Senior RM, Werb Z. **MMP-9/gelatinase B is a key regulator of growth plate angiogenesis and apoptosis of hypertrophic chondrocytes**. *Cell* 1998; 93:411-22.

45. Lee K, Lanske B, Karaplis AC, Deeds JD, Kohno H, Nissenson RA, Kronenberg HM, Segre GV. **Parathyroid hormone-related peptide delays terminal differentiation of chondrocytes during endochondral bone development**. *Endocrinology* 1996; 137:5109-18.

46. Maeda Y, Nakamura E, Nguyen MT, Suva LJ, Swain FL, Razzaque MS, Mackem S, Lanske B. **Indian Hedgehog produced by postnatal chondrocytes is essential for maintaining a growth plate and trabecular bone**. *Proc Natl Acad Sci U S A* 2007; 104:6382-7.

47. Vortkamp A, Lee K, Lanske B, Segre GV, Kronenberg HM, Tabin CJ. **Regulation of rate of cartilage differentiation by Indian hedgehog and PTH-related protein**. *Science* 1996; 273:613-22.

48. Serra R, Karaplis A, Sohn P. **Parathyroid hormone-related peptide (PTHrP)-dependent and -independent effects of transforming growth factor beta (TGF-beta) on endochondral bone formation**. *J Cell Biol* 1999; 145:783-94.

49. Alvarez J, Horton J, Sohn P, Serra R. **The perichondrium plays an important role in mediating the effects of TGF-beta1 on endochondral bone formation**. *Dev Dyn* 2001; 221:311-21.

50. Ballock RT, Heydemann A, Wakefield LM, Flanders KC, Roberts AB, Sporn MB. **TGF-beta 1 prevents hypertrophy of epiphyseal chondrocytes: regulation of gene expression for cartilage matrix proteins and metalloproteases**. *Dev Biol* 1993; 158:414-29.

51. Wozney JM. **Bone morphogenetic proteins**. *Prog Growth Factor Res* 1989; 1:267-80.

52. Polacek M, Bruun JA, Elvenes J, Figenschau Y, Martinez I. **The secretory profiles of cultured human articular chondrocytes and mesenchymal stem cells: implications for autologous cell transplantation strategies**. *Cell Transplant* 2010; 20:1381-3.

53. Goldring MB, Tsuchimochi K, Ijiri K. **The control of chondrogenesis**. *J Cell Biochem* 2006; 97:33-44.

54. Grimsrud CD, Romano PR, D'Souza M, Puzas JE, Schwarz EM, Reynolds PR, Roiser RN, O'Keefe RJ. **BMP signaling stimulates chondrocyte maturation and the expression of Indian hedgehog**. *J Orthop Res* 2001; 19:18-25.

55. Yoon BS, Pogue R, Ovchinnikov DA, Yoshii I, Mishina Y, Behringer RR, Lyons KM. **BMPs regulate multiple aspects of growth-plate chondrogenesis through opposing actions on FGF pathways**. *Development* 2006; 133:4667-78.

56. Ohlsson C, Nilsson A, Isaksson O, Lindahl A. **Growth hormone induces multiplication of the slowly cycling germinal cells of the rat tibial growth plate**. *Proc Natl Acad Sci U S A* 1992; 89:9826-30.

57. Pass C, MacRae VE, Ahmed SF, Farquharson C. **Inflammatory cytokines and the GH/IGF-I axis: novel actions on bone growth**. *Cell Biochem Funct* 2009; 27:119-27.

58. Sims NA, Clement-Lacroix P, Da Ponte F, Bouali Y, Binart N, Moriggl R, Goffin V, Coschigano K, Gaillard-Kelly M, Kopchick J, Baron R, Kelly PA. **Bone homeostasis in growth hormone receptor-null mice is restored by IGF-I but independent of Stat5**. *J Clin Invest* 2000; 106:1095-103.

59.   Liu JL, Yakar S, LeRoith D. **Conditional knockout of mouse insulin-like growth factor-1 gene using the Cre/loxP system**. *Proc Soc Exp Biol Med* 2000; 223:344-51.

60.   O'Keefe RJ, Crabb ID, Puzas JE, Rosier RN. **Effects of transforming growth factor-beta 1 and fibroblast growth factor on DNA synthesis in growth plate chondrocytes are enhanced by insulin-like growth factor-I**. *J Orthop Res* 1994; 12:299-310.

61.   Murakami S, Kan M, McKeehan WL, de Crombrugghe B. **Up-regulation of the chondrogenic Sox9 gene by fibroblast growth factors is mediated by the mitogen-activated protein kinase pathway**. *Proc Natl Acad Sci U S A* 2000; 97:1113-8.

62.   Kato Y, Iwamoto M. **Fibroblast growth factor is an inhibitor of chondrocyte terminal differentiation**. *J Biol Chem* 1990; 265:5903-9.

63.   Liu Z, Lavine KJ, Hung IH, Ornitz DM. **FGF18 is required for early chondrocyte proliferation, hypertrophy and vascular invasion of the growth plate**. *Dev Biol* 2007; 302:80-91.

64.   Robinson CJ, Stringer SE. **The splice variants of vascular endothelial growth factor (VEGF) and their receptors**. *J Cell Sci* 2001; 114:853-65.

65.   Connolly DT, Heuvelman DM, Nelson R, Olander JV, Eppley BL, Delfino JJ, Siegel NR, Leimgruber RM, Feder J. **Tumor vascular permeability factor stimulates endothelial cell growth and angiogenesis**. *J Clin Invest* 1989; 84:1470-8.

66.   Gerber HP, Vu TH, Ryan AM, Kowalski J, Werb Z, Ferrara N. **VEGF couples hypertrophic cartilage remodeling, ossification and angiogenesis during endochondral bone formation**. *Nat Med* 1999; 5:623-8.

67.   Horner A, Bord S, Kelsall AW, Coleman N, Compston JE. **Tie2 ligands angiopoietin-1 and angiopoietin-2 are coexpressed with vascular endothelial cell growth factor in growing human bone**. *Bone* 2001; 28:65-71.

68.   Pufe T, Harde V, Petersen W, Goldring MB, Tillmann B, Mentlein R. **Vascular endothelial growth factor (VEGF) induces matrix metalloproteinase expression in immortalized chondrocytes**. *J Pathol* 2004; 202:367-74.

69.   Hashimoto S, Creighton-Achermann L, Takahashi K, Amiel D, Coutts RD, Lotz M. **Development and regulation of osteophyte formation during experimental osteoarthritis**. *Osteoarthritis Cartilage* 2002; 10:180-7.

70.   Pfander D, Kortje D, Zimmermann R, Weseloh G, Kirsch T, Gesslein M, Cramer T, Swoboda B. **Vascular endothelial growth factor in articular cartilage of**

healthy and osteoarthritic human knee joints. *Ann Rheum Dis* 2001; 60:1070-3.

71.   Enomoto H, Inoki I, Komiya K, Shiomi T, Ikeda E, Obata K, Matsumoto H, Toyama Y, Okada Y. **Vascular endothelial growth factor isoforms and their receptors are expressed in human osteoarthritic cartilage**. *Am J Pathol* 2003; 162:171-81.

72.   Inada M, Wang Y, Byrne MH, Rahman MU, Miyaura C, Lopez-Otin C, Krane SM. **Critical roles for collagenase-3 (Mmp13) in development of growth plate cartilage and in endochondral ossification**. *Proc Natl Acad Sci U S A* 2004; 101:17192-7.

73.   Stickens D, Behonick DJ, Ortega N, Heyer B, Hartenstein B, Yu Y, Fosang AJ, Schorpp-Kistner M, Angel P, Werb Z. **Altered endochondral bone development in matrix metalloproteinase 13-deficient mice**. *Development* 2004; 131:5883-95.

74.   Ortega N, Behonick DJ, Werb Z. **Matrix remodeling during endochondral ossification**. *Trends Cell Biol* 2004; 14:86-93.

75.   Zhou Z, Apte SS, Soininen R, Cao R, Baaklini GY, Rauser RW, Wang J, Cao Y, Tryggvason K. **Impaired endochondral ossification and angiogenesis in mice deficient in membrane-type matrix metalloproteinase I**. *Proc Natl Acad Sci U S A* 2000; 97:4052-7.

76.   Breckon JJ, Hembry RM, Reynolds JJ, Meikle MC. **Regional and temporal changes in the synthesis of matrix metalloproteinases and TIMP-1 during development of the rabbit mandibular condyle**. *J Anat* 1994; 184 (Pt 1):99-110.

77.   Bertram H, Boeuf S, Wachters J, Boehmer S, Heisel C, Hofmann MW, Piecha D, Richter W. **Matrix metalloprotease inhibitors suppress initiation and progression of chondrogenic differentiation of mesenchymal stromal cells in vitro**. *Stem Cells Dev* 2009; 18:881-92.

78.   Burton DW, Foster M, Johnson KA, Hiramoto M, Deftos LJ, Terkeltaub R. **Chondrocyte calcium-sensing receptor expression is up-regulated in early guinea pig knee osteoarthritis and modulates PTHrP, MMP-13, and TIMP-3 expression**. *Osteoarthritis Cartilage* 2005; 13:395-404.

79.   Day TF, Guo X, Garrett-Beal L, Yang Y. **Wnt/beta-catenin signaling in mesenchymal progenitors controls osteoblast and chondrocyte differentiation during vertebrate skeletogenesis**. *Dev Cell* 2005; 8:739-50.

80.   Tamamura Y, Otani T, Kanatani N, Koyama E, Kitagaki J, Komori T, Yamada Y, Costantini F, Wakisaka S, Pacifici M, Iwamoto M, Enomoto-Iwamoto M. **Developmental regulation of Wnt/beta-catenin signals is required for growth**

plate assembly, cartilage integrity, and endochondral ossification. *J Biol Chem* 2005; 280:19185-95.

81.　Boyan BD, Hurst-Kennedy J, Denison TA, Schwartz Z. **24R,25-dihydroxyvitamin D3 [24R,25(OH)2D3] controls growth plate development by inhibiting apoptosis in the reserve zone and stimulating response to 1alpha,25(OH)2D3 in hypertrophic cells**. *J Steroid Biochem Mol Biol* 2010; 121:212-6.

82.　Hurst-Kennedy J, Zhong M, Gupta V, Boyan BD, Schwartz Z. **24R,25-Dihydroxyvitamin D3, lysophosphatidic acid, and p53: a signaling axis in the inhibition of phosphate-induced chondrocyte apoptosis**. *J Steroid Biochem Mol Biol* 2010; 122:264-71.

83.　Boyan BD, Jennings EG, Wang L, Schwartz Z. **Mechanisms regulating differential activation of membrane-mediated signaling by 1alpha,25(OH)2D3 and 24R,25(OH)2D3**. *J Steroid Biochem Mol Biol* 2004; 89-90:309-15.

84.　Akaogi J, Nozaki T, Satoh M, Yamada H. **Role of PGE2 and EP receptors in the pathogenesis of rheumatoid arthritis and as a novel therapeutic strategy**. *Endocr Metab Immune Disord Drug Targets* 2006; 6:383-94.

85.　Jakob M, Demarteau O, Suetterlin R, Heberer M, Martin I. **Chondrogenesis of expanded adult human articular chondrocytes is enhanced by specific prostaglandins**. *Rheumatology (Oxford)* 2004; 43:852-7.

86.　Guilak F, Fermor B, Keefe FJ, Kraus VB, Olson SA, Pisetsky DS, Setton LA, Weinberg JB. **The role of biomechanics and inflammation in cartilage injury and repair**. *Clin Orthop Relat Res* 2004:17-26.

87.　Xie C, Liang B, Xue M, Lin AS, Loiselle A, Schwarz EM, Guldberg RE, O'Keefe RJ, Zhang X. **Rescue of impaired fracture healing in COX-2-/- mice via activation of prostaglandin E2 receptor subtype 4**. *Am J Pathol* 2009; 175:772-85.

88.　Dean DD, Boyan BD, Schwart Z, Muniz OE, Carreno MR, Maeda S, Howell DS. **Effect of 1alpha,25-dihydroxyvitamin D3 and 24R,25-dihydroxyvitamin D3 on metalloproteinase activity and cell maturation in growth plate cartilage in vivo**. *Endocrine* 2001; 14:311-23.

89.　Schwartz Z, Sylvia VL, Dean DD, Boyan BD. **The synergistic effects of vitamin D metabolites and transforming growth factor-beta on costochondral chondrocytes are mediated by increases in protein kinase C activity involving two separate pathways**. *Endocrinology* 1998; 139:534-45.

90.　Schwartz Z, Schlader DL, Ramirez V, Kennedy MB, Boyan BD. **Effects of vitamin D metabolites on collagen production and cell proliferation of**

growth zone and resting zone cartilage cells in vitro. *J Bone Miner Res* 1989; 4:199-207.

91. Kinney RC, Schwartz Z, Week K, Lotz MK, Boyan BD. **Human articular chondrocytes exhibit sexual dimorphism in their responses to 17beta-estradiol**. *Osteoarthritis Cartilage* 2005; 13:330-7.

92. Raz P, Nasatzky E, Boyan BD, Ornoy A, Schwartz Z. **Sexual dimorphism of growth plate prehypertrophic and hypertrophic chondrocytes in response to testosterone requires metabolism to dihydrotestosterone (DHT) by steroid 5-alpha reductase type 1**. *J Cell Biochem* 2005; 95:108-19.

93. Maggini J, Mirkin G, Bognanni I, Holmberg J, Piazzon IM, Nepomnaschy I, Costa H, Canones C, Raiden S, Vermeulen M, Geffner JR. **Mouse bone marrow-derived mesenchymal stromal cells turn activated macrophages into a regulatory-like profile**. *PLoS One*; 5:e9252.

94. Zou L, Feng Y, Chen YJ, Si R, Shen S, Zhou Q, Ichinose F, Scherrer-Crosbie M, Chao W. **Toll-like receptor 2 plays a critical role in cardiac dysfunction during polymicrobial sepsis**. *Crit Care Med*; 38:1335-42.

95. Abarbanell AM, Wang Y, Herrmann JL, Weil BR, Poynter JA, Manukyan MC, Meldrum DR. **Toll-like receptor 2 mediates mesenchymal stem cell associated myocardial recovery and VEGF production following acute ischemia/reperfusion injury**. *Am J Physiol Heart Circ Physiol*.

96. Shi Y, Hu G, Su J, Li W, Chen Q, Shou P, Xu C, Chen X, Huang Y, Zhu Z, Huang X, Han X, Xie N, Ren G. **Mesenchymal stem cells: a new strategy for immunosuppression and tissue repair**. *Cell Res*.

97. Ren G, Zhao X, Zhang L, Zhang J, L'Huillier A, Ling W, Roberts AI, Le AD, Shi S, Shao C, Shi Y. **Inflammatory cytokine-induced intercellular adhesion molecule-1 and vascular cell adhesion molecule-1 in mesenchymal stem cells are critical for immunosuppression**. *J Immunol*; 184:2321-8.

98. Spaggiari GM, Capobianco A, Abdelrazik H, Becchetti F, Mingari MC, Moretta L. **Mesenchymal stem cells inhibit natural killer-cell proliferation, cytotoxicity, and cytokine production: role of indoleamine 2,3-dioxygenase and prostaglandin E2**. *Blood* 2008; 111:1327-33.

99. Selmani Z, Naji A, Zidi I, Favier B, Gaiffe E, Obert L, Borg C, Saas P, Tiberghien P, Rouas-Freiss N, Carosella ED, Deschaseaux F. **Human leukocyte antigen-G5 secretion by human mesenchymal stem cells is required to suppress T lymphocyte and natural killer function and to induce CD4+CD25highFOXP3+ regulatory T cells**. *Stem Cells* 2008; 26:212-22.

100. Selmani Z, Naji A, Gaiffe E, Obert L, Tiberghien P, Rouas-Freiss N, Carosella ED, Deschaseaux F. **HLA-G is a crucial immunosuppressive molecule**

secreted by adult human mesenchymal stem cells. *Transplantation* 2009; 87:S62-6.

101.   Spaggiari GM, Capobianco A, Becchetti S, Mingari MC, Moretta L. **Mesenchymal stem cell-natural killer cell interactions: evidence that activated NK cells are capable of killing MSCs, whereas MSCs can inhibit IL-2-induced NK-cell proliferation**. *Blood* 2006; 107:1484-90.

102.   English K, Barry FP, Mahon BP. **Murine mesenchymal stem cells suppress dendritic cell migration, maturation and antigen presentation**. *Immunol Lett* 2008; 115:50-8.

103.   Rasmusson I, Le Blanc K, Sundberg B, Ringden O. **Mesenchymal stem cells stimulate antibody secretion in human B cells**. *Scand J Immunol* 2007; 65:336-43.

104.   Ramasamy R, Fazekasova H, Lam EW, Soeiro I, Lombardi G, Dazzi F. **Mesenchymal stem cells inhibit dendritic cell differentiation and function by preventing entry into the cell cycle**. *Transplantation* 2007; 83:71-6.

105.   Spaggiari GM, Abdelrazik H, Becchetti F, Moretta L. **MSCs inhibit monocyte-derived DC maturation and function by selectively interfering with the generation of immature DCs: central role of MSC-derived prostaglandin E2**. *Blood* 2009; 113:6576-83.

106.   Nasef A, Chapel A, Mazurier C, Bouchet S, Lopez M, Mathieu N, Sensebe L, Zhang Y, Gorin NC, Thierry D, Fouillard L. **Identification of IL-10 and TGF-beta transcripts involved in the inhibition of T-lymphocyte proliferation during cell contact with human mesenchymal stem cells**. *Gene Expr* 2007; 13:217-26.

107.   English K, Barry FP, Field-Corbett CP, Mahon BP. **IFN-gamma and TNF-alpha differentially regulate immunomodulation by murine mesenchymal stem cells**. *Immunol Lett* 2007; 110:91-100.

108.   Sato K, Ozaki K, Oh I, Meguro A, Hatanaka K, Nagai T, Muroi K, Ozawa K. **Nitric oxide plays a critical role in suppression of T-cell proliferation by mesenchymal stem cells**. *Blood* 2007; 109:228-34.

109.   Meisel R, Zibert A, Laryea M, Gobel U, Daubener W, Dilloo D. **Human bone marrow stromal cells inhibit allogeneic T-cell responses by indoleamine 2,3-dioxygenase-mediated tryptophan degradation**. *Blood* 2004; 103:4619-21.

110.   Aggarwal S, Pittenger MF. **Human mesenchymal stem cells modulate allogeneic immune cell responses**. *Blood* 2005; 105:1815-22.

111.   Kilroy GE, Foster SJ, Wu X, Ruiz J, Sherwood S, Heifetz A, Ludlow JW, Stricker DM, Potiny S, Green P, Halvorsen YD, Cheatham B, Storms RW, Gimble JM.

Cytokine profile of human adipose-derived stem cells: expression of angiogenic, hematopoietic, and pro-inflammatory factors. *J Cell Physiol* 2007; 212:702-9.

112. Schinkothe T, Bloch W, Schmidt A. **In vitro secreting profile of human mesenchymal stem cells**. *Stem Cells Dev* 2008; 17:199-206.

113. Ren G, Zhang L, Zhao X, Xu G, Zhang Y, Roberts AI, Zhao RC, Shi Y. **Mesenchymal stem cell-mediated immunosuppression occurs via concerted action of chemokines and nitric oxide**. *Cell Stem Cell* 2008; 2:141-50.

114. Polchert D, Sobinsky J, Douglas G, Kidd M, Moadsiri A, Reina E, Genrich K, Mehrotra S, Setty S, Smith B, Bartholomew A. **IFN-gamma activation of mesenchymal stem cells for treatment and prevention of graft versus host disease**. *Eur J Immunol* 2008; 38:1745-55.

115. Augello A, Tasso R, Negrini SM, Cancedda R, Pennesi G. **Cell therapy using allogeneic bone marrow mesenchymal stem cells prevents tissue damage in collagen-induced arthritis**. *Arthritis Rheum* 2007; 56:1175-86.

116. Gerdoni E, Gallo B, Casazza S, Musio S, Bonanni I, Pedemonte E, Mantegazza R, Frassoni F, Mancardi G, Pedotti R, Uccelli A. **Mesenchymal stem cells effectively modulate pathogenic immune response in experimental autoimmune encephalomyelitis**. *Ann Neurol* 2007; 61:219-27.

117. Gonzalez-Rey E, Anderson P, Gonzalez MA, Rico L, Buscher D, Delgado M. **Human adult stem cells derived from adipose tissue protect against experimental colitis and sepsis**. *Gut* 2009; 58:929-39.

118. Gonzalez-Rey E, Gonzalez MA, Varela N, O'Valle F, Hernandez-Cortes P, Rico L, Buscher D, Delgado M. **Human adipose-derived mesenchymal stem cells reduce inflammatory and T cell responses and induce regulatory T cells in vitro in rheumatoid arthritis**. *Ann Rheum Dis* 2010; 69:241-8.

119. Haller MJ, Viener HL, Wasserfall C, Brusko T, Atkinson MA, Schatz DA. **Autologous umbilical cord blood infusion for type 1 diabetes**. *Exp Hematol* 2008; 36:710-5.

120. Gennery AR, Cant AJ. **Cord blood stem cell transplantation in primary immune deficiencies**. *Curr Opin Allergy Clin Immunol* 2007; 7:528-34.

121. Tyndall A, Gratwohl A. **Adult stem cell transplantation in autoimmune disease**. *Curr Opin Hematol* 2009; 16:285-91.

122. Tyndall A, Uccelli A. **Multipotent mesenchymal stromal cells for autoimmune diseases: teaching new dogs old tricks**. *Bone Marrow Transplant* 2009; 43:821-8.

123. Kinnaird T, Stabile E, Burnett MS, Lee CW, Barr S, Fuchs S, Epstein SE. **Marrow-derived stromal cells express genes encoding a broad spectrum of arteriogenic cytokines and promote in vitro and in vivo arteriogenesis through paracrine mechanisms**. *Circ Res* 2004; 94:678-85.

124. Hoffmann J, Glassford AJ, Doyle TC, Robbins RC, Schrepfer S, Pelletier MP. **Angiogenic effects despite limited cell survival of bone marrow-derived mesenchymal stem cells under ischemia**. *Thorac Cardiovasc Surg* 2010; 58:136-42.

125. Nguyen BK, Maltais S, Perrault LP, Tanguay JF, Tardif JC, Stevens LM, Borie M, Harel F, Mansour S, Noiseux N. **Improved function and myocardial repair of infarcted heart by intracoronary injection of mesenchymal stem cell-derived growth factors**. *J Cardiovasc Transl Res* 2010; 3:547-58.

126. Takahashi M, Li TS, Suzuki R, Kobayashi T, Ito H, Ikeda Y, Matsuzaki M, Hamano K. **Cytokines produced by bone marrow cells can contribute to functional improvement of the infarcted heart by protecting cardiomyocytes from ischemic injury**. *Am J Physiol Heart Circ Physiol* 2006; 291:H886-93.

127. Uemura R, Xu M, Ahmad N, Ashraf M. **Bone marrow stem cells prevent left ventricular remodeling of ischemic heart through paracrine signaling**. *Circ Res* 2006; 98:1414-21.

128. Xu M, Uemura R, Dai Y, Wang Y, Pasha Z, Ashraf M. **In vitro and in vivo effects of bone marrow stem cells on cardiac structure and function**. *J Mol Cell Cardiol* 2007; 42:441-8.

129. Gnecchi M, He H, Liang OD, Melo LG, Morello F, Mu H, Noiseux N, Zhang L, Pratt RE, Ingwall JS, Dzau VJ. **Paracrine action accounts for marked protection of ischemic heart by Akt-modified mesenchymal stem cells**. *Nat Med* 2005; 11:367-8.

130. Hinkel R, El-Aouni C, Olson T, Horstkotte J, Mayer S, Muller S, Willhauck M, Spitzweg C, Gildehaus FJ, Munzing W, Hannappel E, Bock-Marquette I, DiMaio JM, Hatzopoulos AK, Boekstegers P, Kupatt C. **Thymosin beta4 is an essential paracrine factor of embryonic endothelial progenitor cell-mediated cardioprotection**. *Circulation* 2008; 117:2232-40.

131. Sadat S, Gehmert S, Song YH, Yen Y, Bai X, Gaiser S, Klein H, Alt E. **The cardioprotective effect of mesenchymal stem cells is mediated by IGF-I and VEGF**. *Biochem Biophys Res Commun* 2007; 363:674-9.

132. Estrada R, Li N, Sarojini H, An J, Lee MJ, Wang E. **Secretome from mesenchymal stem cells induces angiogenesis via Cyr61**. *J Cell Physiol* 2009; 219:563-71.

133. Schenke-Layland K, Strem BM, Jordan MC, Deemedio MT, Hedrick MH, Roos KP, Fraser JK, Maclellan WR. **Adipose tissue-derived cells improve cardiac function following myocardial infarction**. *J Surg Res* 2009; 153:217-23.

134. Nie C, Yang D, Morris SF. **Local delivery of adipose-derived stem cells via acellular dermal matrix as a scaffold: a new promising strategy to accelerate wound healing**. *Med Hypotheses* 2009; 72:679-82.

135. Nambu M, Kishimoto S, Nakamura S, Mizuno H, Yanagibayashi S, Yamamoto N, Azuma R, Kiyosawa T, Ishihara M, Kanatani Y. **Accelerated wound healing in healing-impaired db/db mice by autologous adipose tissue-derived stromal cells combined with atelocollagen matrix**. *Ann Plast Surg* 2009; 62:317-21.

136. Xu L, Yan J, Chen D, Welsh AM, Hazel T, Johe K, Hatfield G, Koliatsos VE. **Human neural stem cell grafts ameliorate motor neuron disease in SOD-1 transgenic rats**. *Transplantation* 2006; 82:865-75.

137. Corti S, Locatelli F, Papadimitriou D, Del Bo R, Nizzardo M, Nardini M, Donadoni C, Salani S, Fortunato F, Strazzer S, Bresolin N, Comi GP. **Neural stem cells LewisX+ CXCR4+ modify disease progression in an amyotrophic lateral sclerosis model**. *Brain* 2007; 130:1289-305.

138. Lu P, Jones LL, Snyder EY, Tuszynski MH. **Neural stem cells constitutively secrete neurotrophic factors and promote extensive host axonal growth after spinal cord injury**. *Exp Neurol* 2003; 181:115-29.

139. Yan J, Welsh AM, Bora SH, Snyder EY, Koliatsos VE. **Differentiation and tropic/trophic effects of exogenous neural precursors in the adult spinal cord**. *J Comp Neurol* 2004; 480:101-14.

140. Crigler L, Robey RC, Asawachaicharn A, Gaupp D, Phinney DG. **Human mesenchymal stem cell subpopulations express a variety of neuro-regulatory molecules and promote neuronal cell survival and neuritogenesis**. *Exp Neurol* 2006; 198:54-64.

141. Kim YJ, Park HJ, Lee G, Bang OY, Ahn YH, Joe E, Kim HO, Lee PH. **Neuroprotective effects of human mesenchymal stem cells on dopaminergic neurons through anti-inflammatory action**. *Glia* 2009; 57:13-23.

142. Park HJ, Lee PH, Bang OY, Lee G, Ahn YH. **Mesenchymal stem cells therapy exerts neuroprotection in a progressive animal model of Parkinson's disease**. *J Neurochem* 2008; 107:141-51.

143. Chachques JC, Trainini JC, Lago N, Cortes-Morichetti M, Schussler O, Carpentier A. **Myocardial Assistance by Grafting a New Bioartificial Upgraded Myocardium (MAGNUM trial): clinical feasibility study**. *Ann Thorac Surg* 2008; 85:901-8.

144. Gamradt SC, Lieberman JR. **Genetic modification of stem cells to enhance bone repair**. *Ann Biomed Eng* 2004; 32:136-47.

145. Tai K, Pelled G, Sheyn D, Bershteyn A, Han L, Kallai I, Zilberman Y, Ortiz C, Gazit D. **Nanobiomechanics of repair bone regenerated by genetically modified mesenchymal stem cells**. *Tissue Eng Part A* 2008; 14:1709-20.

146. Waese EY, Kandel RA, Stanford WL. **Application of stem cells in bone repair**. *Skeletal Radiol* 2008; 37:601-8.

147. Jabbarzadeh E, Starnes T, Khan YM, Jiang T, Wirtel AJ, Deng M, Lv Q, Nair LS, Doty SB, Laurencin CT. **Induction of angiogenesis in tissue-engineered scaffolds designed for bone repair: a combined gene therapy-cell transplantation approach**. *Proc Natl Acad Sci U S A* 2008; 105:11099-104.

148. Li W, Ma N, Ong LL, Nesselmann C, Klopsch C, Ladilov Y, Furlani D, Piechaczek C, Moebius JM, Lutzow K, Lendlein A, Stamm C, Li RK, Steinhoff G. **Bcl-2 engineered MSCs inhibited apoptosis and improved heart function**. *Stem Cells* 2007; 25:2118-27.

149. Noiseux N, Gnecchi M, Lopez-Ilasaca M, Zhang L, Solomon SD, Deb A, Dzau VJ, Pratt RE. **Mesenchymal stem cells overexpressing Akt dramatically repair infarcted myocardium and improve cardiac function despite infrequent cellular fusion or differentiation**. *Mol Ther* 2006; 14:840-50.

150. Gnecchi M, He H, Noiseux N, Liang OD, Zhang L, Morello F, Mu H, Melo LG, Pratt RE, Ingwall JS, Dzau VJ. **Evidence supporting paracrine hypothesis for Akt-modified mesenchymal stem cell-mediated cardiac protection and functional improvement**. *FASEB J* 2006; 20:661-9.

151. Mirotsou M, Zhang Z, Deb A, Zhang L, Gnecchi M, Noiseux N, Mu H, Pachori A, Dzau V. **Secreted frizzled related protein 2 (Sfrp2) is the key Akt-mesenchymal stem cell-released paracrine factor mediating myocardial survival and repair**. *Proc Natl Acad Sci U S A* 2007; 104:1643-8.

152. Gu F, Amsden B, Neufeld R. **Sustained delivery of vascular endothelial growth factor with alginate beads**. *J Control Release* 2004; 96:463-72.

153. Spaeth E, Klopp A, Dembinski J, Andreeff M, Marini F. **Inflammation and tumor microenvironments: defining the migratory itinerary of mesenchymal stem cells**. *Gene Ther* 2008; 15:730-8.

154. Sharp FR, Ran R, Lu A, Tang Y, Strauss KI, Glass T, Ardizzone T, Bernaudin M. **Hypoxic preconditioning protects against ischemic brain injury**. *NeuroRx* 2004; 1:26-35.

155. Rehman J, Traktuev D, Li J, Merfeld-Clauss S, Temm-Grove CJ, Bovenkerk JE, Pell CL, Johnstone BH, Considine RV, March KL. **Secretion of angiogenic and**

antiapoptotic factors by human adipose stromal cells. *Circulation* 2004; 109:1292-8.

156.   He A, Jiang Y, Gui C, Sun Y, Li J, Wang JA. **The antiapoptotic effect of mesenchymal stem cell transplantation on ischemic myocardium is enhanced by anoxic preconditioning**. *Can J Cardiol* 2009; 25:353-8.

157.   Creagh EM, Sheehan D, Cotter TG. **Heat shock proteins--modulators of apoptosis in tumour cells**. *Leukemia* 2000; 14:1161-73.

158.   Mambula SS, Stevenson MA, Ogawa K, Calderwood SK. **Mechanisms for Hsp70 secretion: crossing membranes without a leader**. *Methods* 2007; 43:168-75.

159.   Haider H, Ashraf M. **Strategies to promote donor cell survival: combining preconditioning approach with stem cell transplantation**. *J Mol Cell Cardiol* 2008; 45:554-66.

160.   Lele Z, Krone PH. **Expression of genes encoding the collagen-binding heat shock protein (Hsp47) and type II collagen in developing zebrafish embryos**. *Mech Dev* 1997; 61:89-98.

161.   Christians ES, Zhou Q, Renard J, Benjamin IJ. **Heat shock proteins in mammalian development**. *Semin Cell Dev Biol* 2003; 14:283-90.

162.   Loones MT, Morange M. **Hsp and chaperone distribution during endochondral bone development in mouse embryo**. *Cell Stress Chaperones* 1998; 3:237-44.

163.   Favet N, Duverger O, Loones MT, Poliard A, Kellermann O, Morange M. **Overexpression of murine small heat shock protein HSP25 interferes with chondrocyte differentiation and decreases cell adhesion**. *Cell Death Differ* 2001; 8:603-13.

164.   Eberhard J, Zahl A, Dommisch H, Winter J, Acil Y, Jepsen S. **Heat shock induces the synthesis of the inflammatory mediator leukotriene B4 in human pulp cells**. *Int Endod J* 2005; 38:882-8.

165.   Olivares-Navarrete R, Hyzy SL, Hutton DL, Erdman CP, Wieland M, Boyan BD, Schwartz Z. **Direct and indirect effects of microstructured titanium substrates on the induction of mesenchymal stem cell differentiation towards the osteoblast lineage**. *Biomaterials* 2010; 31:2728-35.

166.   Olivares-Navarrete R, Hyzy SL, Park JH, Dunn GR, Haithcock DA, Wasilewski CE, Boyan BD, Schwartz Z. **Mediation of osteogenic differentiation of human mesenchymal stem cells on titanium surfaces by a Wnt-integrin feedback loop**. *Biomaterials* 2011; 32:6399-411.

167. Olivares-Navarrete R, Raz P, Zhao G, Chen J, Wieland M, Cochran DL, Chaudhri RA, Ornoy A, Boyan BD, Schwartz Z. **Integrin alpha2beta1 plays a critical role in osteoblast response to micron-scale surface structure and surface energy of titanium substrates**. *Proc Natl Acad Sci U S A* 2008; 105:15767-72.

168. Gittens RA, McLachlan T, Olivares-Navarrete R, Cai Y, Berner S, Tannenbaum R, Schwartz Z, Sandhage KH, Boyan BD. **The effects of combined micron-/submicron-scale surface roughness and nanoscale features on cell proliferation and differentiation**. *Biomaterials* 2011; 32:3395-403.

169. Yu J, Du KT, Fang Q, Gu Y, Mihardja SS, Sievers RE, Wu JC, Lee RJ. **The use of human mesenchymal stem cells encapsulated in RGD modified alginate microspheres in the repair of myocardial infarction in the rat**. *Biomaterials* 2010; 31:7012-20.

170. Bell BF, Schuler M, Tosatti S, Textor M, Schwartz Z, Boyan BD. **Osteoblast response to titanium surfaces functionalized with extracellular matrix peptide biomimetics**. *Clin Oral Implants Res* 2011; 22:865-72.

171. Kasper G, Glaeser JD, Geissler S, Ode A, Tuischer J, Matziolis G, Perka C, Duda GN. **Matrix metalloprotease activity is an essential link between mechanical stimulus and mesenchymal stem cell behavior**. *Stem Cells* 2007; 25:1985-94.

172. Mott JD, Werb Z. **Regulation of matrix biology by matrix metalloproteinases**. *Curr Opin Cell Biol* 2004; 16:558-64.

173. Skutek M, van Griensven M, Zeichen J, Brauer N, Bosch U. **Cyclic mechanical stretching modulates secretion pattern of growth factors in human tendon fibroblasts**. *Eur J Appl Physiol* 2001; 86:48-52.

174. Ito M, Azuma Y, Ohta T, Komoriya K. **Effects of ultrasound and 1,25-dihydroxyvitamin D3 on growth factor secretion in co-cultures of osteoblasts and endothelial cells**. *Ultrasound Med Biol* 2000; 26:161-6.

175. Ebisawa K, Hata K, Okada K, Kimata K, Ueda M, Torii S, Watanabe H. **Ultrasound enhances transforming growth factor beta-mediated chondrocyte differentiation of human mesenchymal stem cells**. *Tissue Eng* 2004; 10:921-9.

176. Emohare O, Hafez MI, Sandison A, Coombs RR, McCarthy ID. **Laser-induced thermal stress and the heat shock response in neural cells**. *Acta Orthop Scand* 2004; 75:610-7.

177. Greenberger S, Boscolo E, Adini I, Mulliken JB, Bischoff J. **Corticosteroid suppression of VEGF-A in infantile hemangioma-derived stem cells**. *N Engl J Med* 2010; 362:1005-13.

178. Hamidouche Z, Fromigue O, Nuber U, Vaudin P, Pages JC, Ebert R, Jakob F, Miraoui H, Marie PJ. **Autocrine fibroblast growth factor 18 mediates**

dexamethasone-induced osteogenic differentiation of murine mesenchymal stem cells**. *J Cell Physiol* 2010; 224:509-15.

179. Cizkova D, Rosocha J, Vanicky I, Radonak J, Galik J, Cizek M. **Induction of mesenchymal stem cells leads to HSP72 synthesis and higher resistance to oxidative stress**. *Neurochem Res* 2006; 31:1011-20.

180. Afzal MR, Haider H, Idris NM, Jiang S, Ahmed RP, Ashraf M. **Preconditioning promotes survival and angiomyogenic potential of mesenchymal stem cells in the infarcted heart via NF-kappaB signaling**. *Antioxid Redox Signal* 2010; 12:693-702.

181. Niagara MI, Haider H, Jiang S, Ashraf M. **Pharmacologically preconditioned skeletal myoblasts are resistant to oxidative stress and promote angiomyogenesis via release of paracrine factors in the infarcted heart**. *Circ Res* 2007; 100:545-55.

182. Giugliano G, Pasquali D, Notaro A, Brongo S, Nicoletti G, D'Andrea F, Bellastella A, Sinisi AA. **Verapamil inhibits interleukin-6 and vascular endothelial growth factor production in primary cultures of keloid fibroblasts**. *Br J Plast Surg* 2003; 56:804-9.

183. MacLeod RJ, Chattopadhyay N, Brown EM. **PTHrP stimulated by the calcium-sensing receptor requires MAP kinase activation**. *Am J Physiol Endocrinol Metab* 2003; 284:E435-42.

184. Tfelt-Hansen J, MacLeod RJ, Chattopadhyay N, Yano S, Quinn S, Ren X, Terwilliger EF, Schwarz P, Brown EM. **Calcium-sensing receptor stimulates PTHrP release by pathways dependent on PKC, p38 MAPK, JNK, and ERK1/2 in H-500 cells**. *Am J Physiol Endocrinol Metab* 2003; 285:E329-37.

185. Sato N, Meijer L, Skaltsounis L, Greengard P, Brivanlou AH. **Maintenance of pluripotency in human and mouse embryonic stem cells through activation of Wnt signaling by a pharmacological GSK-3-specific inhibitor**. *Nat Med* 2004; 10:55-63.

186. Zisa D, Shabbir A, Mastri M, Taylor T, Aleksic I, McDaniel M, Suzuki G, Lee T. **Intramuscular VEGF activates an SDF1-dependent progenitor cell cascade and an SDF1-independent muscle paracrine cascade for cardiac repair**. *Am J Physiol Heart Circ Physiol* 2011; 301:H2422-32.

187. Herrmann JL, Weil BR, Abarbanell AM, Wang Y, Poynter JA, Manukyan MC, Meldrum DR. **IL-6 and TGF-alpha costimulate mesenchymal stem cell vascular endothelial growth factor production by ERK-, JNK-, and PI3K-mediated mechanisms**. *Shock* 2011; 35:512-6.

188. Baliram R, Latif R, Berkowitz J, Frid S, Colaianni G, Sun L, Zaidi M, Davies TF. **Thyroid-stimulating hormone induces a Wnt-dependent, feed-forward loop**

for osteoblastogenesis in embryonic stem cell cultures. *Proc Natl Acad Sci U S A* 2011; 108:16277-82.

189.   Modder UI, Roforth MM, Hoey K, McCready LK, Peterson JM, Monroe DG, Oursler MJ, Khosla S. **Effects of estrogen on osteoprogenitor cells and cytokines/bone-regulatory factors in postmenopausal women**. *Bone* 2011; 49:202-7.

190.   Chang TM. **Semipermeable Microcapsules**. *Science* 1964; 146:524-5.

191.   Efrat S. **Beta-cell replacement for insulin-dependent diabetes mellitus**. *Adv Drug Deliv Rev* 2008; 60:114-23.

192.   Orive G, De Castro M, Ponce S, Hernandez RM, Gascon AR, Bosch M, Alberch J, Pedraz JL. **Long-term expression of erythropoietin from myoblasts immobilized in biocompatible and neovascularized microcapsules**. *Mol Ther* 2005; 12:283-9.

193.   Hortelano G, Chang PL. **Gene therapy for hemophilia**. *Artif Cells Blood Substit Immobil Biotechnol* 2000; 28:1-24.

194.   Hernandez RM, Orive G, Murua A, Pedraz JL. **Microcapsules and microcarriers for in situ cell delivery**. *Adv Drug Deliv Rev* 2010; 62:711-30.

195.   Amsden B, Turner N. **Diffusion characteristics of calcium alginate gels**. *Biotechnol Bioeng* 1999; 65:605-10.

196.   Orive G, De Castro M, Kong HJ, Hernandez RM, Ponce S, Mooney DJ, Pedraz JL. **Bioactive cell-hydrogel microcapsules for cell-based drug delivery**. *J Control Release* 2009; 135:203-10.

197.   Leddy HA, Awad HA, Guilak F. **Molecular diffusion in tissue-engineered cartilage constructs: effects of scaffold material, time, and culture conditions**. *J Biomed Mater Res B Appl Biomater* 2004; 70:397-406.

198.   Chang SC, Rowley JA, Tobias G, Genes NG, Roy AK, Mooney DJ, Vacanti CA, Bonassar LJ. **Injection molding of chondrocyte/alginate constructs in the shape of facial implants**. *J Biomed Mater Res* 2001; 55:503-11.

199.   Hott ME, Megerian CA, Beane R, Bonassar LJ. **Fabrication of tissue engineered tympanic membrane patches using computer-aided design and injection molding**. *Laryngoscope* 2004; 114:1290-5.

200.   Lee KY, Bouhadir KH, Mooney DJ. **Controlled degradation of hydrogels using multi-functional cross-linking molecules**. *Biomaterials* 2004; 25:2461-6.

201. Kong HJ, Kaigler D, Kim K, Mooney DJ. **Controlling rigidity and degradation of alginate hydrogels via molecular weight distribution**. *Biomacromolecules* 2004; 5:1720-7.

202. Boontheekul T, Kong HJ, Mooney DJ. **Controlling alginate gel degradation utilizing partial oxidation and bimodal molecular weight distribution**. *Biomaterials* 2005; 26:2455-65.

203. Hauselmann HJ, Fernandes RJ, Mok SS, Schmid TM, Block JA, Aydelotte MB, Kuettner KE, Thonar EJ. **Phenotypic stability of bovine articular chondrocytes after long-term culture in alginate beads**. *J Cell Sci* 1994; 107 (Pt 1):17-27.

204. Lim F, Sun AM. **Microencapsulated islets as bioartificial endocrine pancreas**. *Science* 1980; 210:908-10.

205. Alsberg E, Anderson KW, Albeiruti A, Franceschi RT, Mooney DJ. **Cell-interactive alginate hydrogels for bone tissue engineering**. *J Dent Res* 2001; 80:2025-9.

206. Rowley JA, Madlambayan G, Mooney DJ. **Alginate hydrogels as synthetic extracellular matrix materials**. *Biomaterials* 1999; 20:45-53.

207. Genes NG, Rowley JA, Mooney DJ, Bonassar LJ. **Effect of substrate mechanics on chondrocyte adhesion to modified alginate surfaces**. *Arch Biochem Biophys* 2004; 422:161-7.

208. Chang SC, Tobias G, Roy AK, Vacanti CA, Bonassar LJ. **Tissue engineering of autologous cartilage for craniofacial reconstruction by injection molding**. *Plast Reconstr Surg* 2003; 112:793-9; discussion 800-1.

209. Vacanti CA, Bonassar LJ, Vacanti MP, Shufflebarger J. **Replacement of an avulsed phalanx with tissue-engineered bone**. *N Engl J Med* 2001; 344:1511-4.

210. Robitaille R, Pariseau JF, Leblond FA, Lamoureux M, Lepage Y, Halle JP. **Studies on small (<350 microm) alginate-poly-L-lysine microcapsules. III. Biocompatibility Of smaller versus standard microcapsules**. *J Biomed Mater Res* 1999; 44:116-20.

211. Awad HA, Wickham MQ, Leddy HA, Gimble JM, Guilak F. **Chondrogenic differentiation of adipose-derived adult stem cells in agarose, alginate, and gelatin scaffolds**. *Biomaterials* 2004; 25:3211-22.

212. Buschmann MD, Gluzband YA, Grodzinsky AJ, Hunziker EB. **Mechanical compression modulates matrix biosynthesis in chondrocyte/agarose culture**. *J Cell Sci* 1995; 108 (Pt 4):1497-508.

213. Iwata H, Amemiya H, Matsuda T, Takano H, Hayashi R, Akutsu T. **Evaluation of microencapsulated islets in agarose gel as bioartificial pancreas by studies**

of hormone secretion in culture and by xenotransplantation. *Diabetes* 1989; 38 Suppl 1:224-5.

214. Ma J, Wang H, He B, Chen J. **A preliminary in vitro study on the fabrication and tissue engineering applications of a novel chitosan bilayer material as a scaffold of human neofetal dermal fibroblasts**. *Biomaterials* 2001; 22:331-6.

215. Aiedeh K, Gianasi E, Orienti I, Zecchi V. **Chitosan microcapsules as controlled release systems for insulin**. *J Microencapsul* 1997; 14:567-76.

216. Muzzarelli R, Baldassarre V, Conti F, Ferrara P, Biagini G, Gazzanelli G, Vasi V. **Biological activity of chitosan: ultrastructural study**. *Biomaterials* 1988; 9:247-52.

217. Rabanel JM, Banquy X, Zouaoui H, Mokhtar M, Hildgen P. **Progress technology in microencapsulation methods for cell therapy**. *Biotechnol Prog* 2009; 25:946-63.

218. Nuttelman CR, Rice MA, Rydholm AE, Salinas CN, Shah DN, Anseth KS. **Macromolecular Monomers for the Synthesis of Hydrogel Niches and Their Application in Cell Encapsulation and Tissue Engineering**. *Prog Polym Sci* 2008; 33:167-79.

219. Silva GA, Czeisler C, Niece KL, Beniash E, Harrington DA, Kessler JA, Stupp SI. **Selective differentiation of neural progenitor cells by high-epitope density nanofibers**. *Science* 2004; 303:1352-5.

220. Zhang S, Holmes T, Lockshin C, Rich A. **Spontaneous assembly of a self-complementary oligopeptide to form a stable macroscopic membrane**. *Proc Natl Acad Sci U S A* 1993; 90:3334-8.

221. Zhang S, Marini DM, Hwang W, Santoso S. **Design of nanostructured biological materials through self-assembly of peptides and proteins**. *Curr Opin Chem Biol* 2002; 6:865-71.

222. Kisiday J, Jin M, Kurz B, Hung H, Semino C, Zhang S, Grodzinsky AJ. **Self-assembling peptide hydrogel fosters chondrocyte extracellular matrix production and cell division: implications for cartilage tissue repair**. *Proc Natl Acad Sci U S A* 2002; 99:9996-10001.

223. Moyer HR, Kinney RC, Singh KA, Williams JK, Schwartz Z, Boyan BD. **Alginate microencapsulation technology for the percutaneous delivery of adipose-derived stem cells**. *Ann Plast Surg* 2010; 65:497-503.

224. Herrero EP, Del Valle EM, Galan MA. **Immobilization of mesenchymal stem cells and monocytes in biocompatible microcapsules to cell therapy**. *Biotechnol Prog* 2007; 23:940-5.

225. Iwata H, Takagi T, Amemiya H, Shimizu H, Yamashita K, Kobayashi K, Akutsu T. **Agarose for a bioartificial pancreas**. *J Biomed Mater Res* 1992; 26:967-77.

226. Poncelet D. **Production of alginate beads by emulsification/internal gelation**. *Ann N Y Acad Sci* 2001; 944:74-82.

227. Kobayashi T, Aomatsu Y, Kanehiro H, Hisanaga M, Nakajima Y. **Protection of NOD islet isograft from autoimmune destruction by agarose microencapsulation**. *Transplant Proc* 2003; 35:484-5.

228. Whitesides GM. **The origins and the future of microfluidics**. *Nature* 2006; 442:368-73.

229. Sugiura S, Oda T, Izumida Y, Aoyagi Y, Satake M, Ochiai A, Ohkohchi N, Nakajima M. **Size control of calcium alginate beads containing living cells using micro-nozzle array**. *Biomaterials* 2005; 26:3327-31.

230. Workman VL, Dunnett SB, Kille P, Palmer DD. **Microfluidic chip-based synthesis of alginate microspheres for encapsulation of immortalized human cells**. *Biomicrofluidics* 2007; 1:14105.

231. Zhang H, Tumarkin E, Peerani R, Nie Z, Sullan RM, Walker GC, Kumacheva E. **Microfluidic production of biopolymer microcapsules with controlled morphology**. *J Am Chem Soc* 2006; 128:12205-10.

232. Nie Z, Xu S, Seo M, Lewis PC, Kumacheva E. **Polymer particles with various shapes and morphologies produced in continuous microfluidic reactors**. *J Am Chem Soc* 2005; 127:8058-63.

233. Hong J, deMello AJ, Jayasinghe SN. **Bio-electrospraying and droplet-based microfluidics: control of cell numbers within living residues**. *Biomed Mater* 2010; 5:21001.

234. Qiu C, Chen M, Yan H, Wu HK. **Generation of uniformly sized alginate microparticles for cell encapsulation by using a soft-lithography approach**. *Advanced Materials* 2007; 19:1603-+.

235. Dendukuri D, Pregibon DC, Collins J, Hatton TA, Doyle PS. **Continuous-flow lithography for high-throughput microparticle synthesis**. *Nature Materials* 2006; 5:365-9.

236. Khademhosseini A, Eng G, Yeh J, Fukuda J, Blumling J, 3rd, Langer R, Burdick JA. **Micromolding of photocrosslinkable hyaluronic acid for cell encapsulation and entrapment**. *J Biomed Mater Res A* 2006; 79:522-32.

237. Rivest C, Morrison DWG, Ni B, Rubin J, Yadav V, Mahdavi A, Karp JM, Khademhosseini A. **Microscale hydrogels for medicine and biology: Synthesis,**

characteristics and applications. *Journal of Mechanics of Materials and Structures* 2007; 2:1103-19.

238. Connelly JT, Garcia AJ, Levenston ME. **Inhibition of in vitro chondrogenesis in RGD-modified three-dimensional alginate gels**. *Biomaterials* 2007; 28:1071-83.

239. Yamada KM. **Adhesive recognition sequences**. *J Biol Chem* 1991; 266:12809-12.

240. Ruoslahti E. **RGD and other recognition sequences for integrins**. *Annu Rev Cell Dev Biol* 1996; 12:697-715.

241. Pinkse GG, Bouwman WP, Jiawan-Lalai R, Terpstra OT, Bruijn JA, de Heer E. **Integrin signaling via RGD peptides and anti-beta1 antibodies confers resistance to apoptosis in islets of Langerhans**. *Diabetes* 2006; 55:312-7.

242. Chan G, Mooney DJ. **New materials for tissue engineering: towards greater control over the biological response**. *Trends Biotechnol* 2008; 26:382-92.

243. Kavalkovich KW, Boynton RE, Murphy JM, Barry F. **Chondrogenic differentiation of human mesenchymal stem cells within an alginate layer culture system**. *In Vitro Cell Dev Biol Anim* 2002; 38:457-66.

244. Fischbach C, Mooney DJ. **Polymeric systems for bioinspired delivery of angiogenic molecules**. *Polymers for Regenerative Medicine* 2006:191-221.

245. Richardson TP, Peters MC, Ennett AB, Mooney DJ. **Polymeric system for dual growth factor delivery**. *Nat Biotechnol* 2001; 19:1029-34.

246. Schultz-Cherry S, Lawler J, Murphy-Ullrich JE. **The type 1 repeats of thrombospondin 1 activate latent transforming growth factor-beta**. *J Biol Chem* 1994; 269:26783-8.

247. Schultz-Cherry S, Ribeiro S, Gentry L, Murphy-Ullrich JE. **Thrombospondin binds and activates the small and large forms of latent transforming growth factor-beta in a chemically defined system**. *J Biol Chem* 1994; 269:26775-82.

248. Babbitt BP, Allen PM, Matsueda G, Haber E, Unanue ER. **Binding of immunogenic peptides to Ia histocompatibility molecules**. *Nature* 1985; 317:359-61.

249. Nelson CA, Viner N, Young S, Petzold S, Benoist C, Mathis D, Unanue ER. **Amino acid residues on the I-Ak alpha-chain required for the binding and stability of two antigenic peptides**. *J Immunol* 1996; 156:176-82.

250. Zisch AH, Schenk U, Schense JC, Sakiyama-Elbert SE, Hubbell JA. **Covalently conjugated VEGF--fibrin matrices for endothelialization**. *J Control Release* 2001; 72:101-13.

251. Bouhadir KH, Lee KY, Alsberg E, Damm KL, Anderson KW, Mooney DJ. **Degradation of partially oxidized alginate and its potential application for tissue engineering**. *Biotechnol Prog* 2001; 17:945-50.

252. Fonseca KB, Bidarra SJ, Oliveira MJ, Granja PL, Barrias CC. **Molecularly designed alginate hydrogels susceptible to local proteolysis as three-dimensional cellular microenvironments**. *Acta Biomater* 2011; 7:1674-82.

253. Sarkar N, Banerjee J, Hanson AJ, Elegbede AI, Rosendahl T, Krueger AB, Banerjee AL, Tobwala S, Wang R, Lu X, Mallik S, Srivastava DK. **Matrix metalloproteinase-assisted triggered release of liposomal contents**. *Bioconjug Chem* 2008; 19:57-64.

254. Ashton RS, Banerjee A, Punyani S, Schaffer DV, Kane RS. **Scaffolds based on degradable alginate hydrogels and poly(lactide-co-glycolide) microspheres for stem cell culture**. *Biomaterials* 2007; 28:5518-25.

255. Boyan BD, Schwart Z, Howell DS, Naski M, Ranly DM, Sylvia VL, Dean DD, *The biology, chemistry, and biochemistry of the mammalian growth plate*, in *Disorders of bone and mineral metabolism*, F.L. Coe and M.J. Favus, Editors. 2001, Lippincott, Williams, and Wilkins, Inc: Philadelphia, Pennsylvania. p. 498-532.

256. Chen CH, Sakai Y, Demay MB. **Targeting expression of the human vitamin D receptor to the keratinocytes of vitamin D receptor null mice prevents alopecia**. *Endocrinology* 2001; 142:5386-9.

257. Kato S. **Genetic mutation in the human 25-hydroxyvitamin D3 1alpha-hydroxylase gene causes vitamin D-dependent rickets type I**. *Mol Cell Endocrinol* 1999; 156:7-12.

258. Li YC, Amling M, Pirro AE, Priemel M, Meuse J, Baron R, Delling G, Demay MB. **Normalization of mineral ion homeostasis by dietary means prevents hyperparathyroidism, rickets, and osteomalacia, but not alopecia in vitamin D receptor-ablated mice**. *Endocrinology* 1998; 139:4391-6.

259. Amling M, Priemel M, Holzmann T, Chapin K, Rueger JM, Baron R, Demay MB. **Rescue of the skeletal phenotype of vitamin D receptor-ablated mice in the setting of normal mineral ion homeostasis: formal histomorphometric and biomechanical analyses**. *Endocrinology* 1999; 140:4982-7.

260. DeLuca HF, *The metabolism and functions of vitamin D*, in *Vitamin D: chemical, biochemical and clinical update*, A.W. Norman, et al., Editors. 1985, Walter de Gruyter: New York. p. 361-75.

261. Boyan BD, Wong KL, Fang M, Schwartz Z. **1alpha,25(OH)2D3 is an autocrine regulator of extracellular matrix turnover and growth factor release via ERp60 activated matrix vesicle metalloproteinases**. *J Steroid Biochem Mol Biol* 2007; 103:467-72.

262. Martin EA, Ritman EL, Turner RT. **Time course of epiphyseal growth plate fusion in rat tibiae**. *Bone* 2003; 32:261-7.

263. Haines RW. **The histology of epiphyseal union in mammals**. *J Anat* 1975; 120:1-25.

264. Rogers LF, Poznanski AK. **Imaging of epiphyseal injuries**. *Radiology* 1994; 191:297-308.

265. Sailhan F, Chotel F, Guibal AL, Gollogly S, Adam P, Berard J, Guibaud L. **Three-dimensional MR imaging in the assessment of physeal growth arrest**. *Eur Radiol* 2004; 14:1600-8.

266. Reich A, Sharir A, Zelzer E, Hacker L, Monsonego-Ornan E, Shahar R. **The effect of weight loading and subsequent release from loading on the postnatal skeleton**. *Bone* 2008; 43:766-74.

267. Sergerie K, Lacoursiere MO, Levesque M, Villemure I. **Mechanical properties of the porcine growth plate and its three zones from unconfined compression tests**. *J Biomech* 2009; 42:510-6.

268. Villemure I, Cloutier L, Matyas JR, Duncan NA. **Non-uniform strain distribution within rat cartilaginous growth plate under uniaxial compression**. *J Biomech* 2007; 40:149-56.

269. Li YC, Pirro AE, Amling M, Delling G, Baron R, Bronson R, Demay MB. **Targeted ablation of the vitamin D receptor: an animal model of vitamin D-dependent rickets type II with alopecia**. *Proc Natl Acad Sci U S A* 1997; 94:9831-5.

270. Donohue MM, Demay MB. **Rickets in VDR null mice is secondary to decreased apoptosis of hypertrophic chondrocytes**. *Endocrinology* 2002; 143:3691-4.

271. Boyan BD, Sylvia VL, McKinney N, Schwartz Z. **Membrane actions of vitamin D metabolites 1alpha,25(OH)2D3 and 24R,25(OH)2D3 are retained in growth plate cartilage cells from vitamin D receptor knockout mice**. *J Cell Biochem* 2003; 90:1207-23.

272. Zar JH, *Biostatistical analysis*. 2nd ed. 1984, Englewood Cliffs, NJ: Prentice-Hall.

273. Nemere I, Farach-Carson MC, Rohe B, Sterling TM, Norman AW, Boyan BD, Safford SE. **Ribozyme knockdown functionally links a 1,25(OH)2D3 membrane binding protein (1,25D3-MARRS) and phosphate uptake in intestinal cells**. *Proc Natl Acad Sci U S A* 2004; 101:7392-7.

274. Nemere I, Schwartz Z, Pedrozo H, Sylvia VL, Dean DD, Boyan BD. **Identification of a membrane receptor for 1,25-dihydroxyvitamin D3 which mediates rapid activation of protein kinase C**. *J Bone Miner Res* 1998; 13:1353-9.

275. Dardenne O, Prud'homme J, Hacking SA, Glorieux FH, St-Arnaud R. **Correction of the abnormal mineral ion homeostasis with a high-calcium, high-phosphorus, high-lactose diet rescues the PDDR phenotype of mice deficient for the 25-hydroxyvitamin D-1alpha-hydroxylase (CYP27B1)**. *Bone* 2003; 32:332-40.

276. Aszodi A, Hunziker EB, Olsen BR, Fassler R. **The role of collagen II and cartilage fibril-associated molecules in skeletal development**. *Osteoarthritis Cartilage* 2001; 9 Suppl A:S150-9.

277. Kronenberg HM, Lee K, Lanske B, Segre GV. **Parathyroid hormone-related protein and Indian hedgehog control the pace of cartilage differentiation**. *J Endocrinol* 1997; 154 Suppl:S39-45.

278. Lanske B, Karaplis AC, Lee K, Luz A, Vortkamp A, Pirro A, Karperien M, Defize LH, Ho C, Mulligan RC, Abou-Samra AB, Juppner H, Segre GV, Kronenberg HM. **PTH/PTHrP receptor in early development and Indian hedgehog-regulated bone growth**. *Science* 1996; 273:663-6.

279. Schwartz Z, Ehland H, Sylvia VL, Larsson D, Hardin RR, Bingham V, Lopez D, Dean DD, Boyan BD. **1alpha,25-dihydroxyvitamin D(3) and 24R,25-dihydroxyvitamin D(3) modulate growth plate chondrocyte physiology via protein kinase C-dependent phosphorylation of extracellular signal-regulated kinase 1/2 mitogen-activated protein kinase**. *Endocrinology* 2002; 143:2775-86.

280. Chen J, Lee CS, Coleman RM, Yoon JY, Lohmann CH, Zustin J, Guldberg RE, Schwartz Z, Boyan BD. **Formation of tethers linking the epiphysis and metaphysis is regulated by vitamin d receptor-mediated signaling**. *Calcif Tissue Int* 2009; 85:134-45.

281. Boyan BD, Schwartz Z. **1,25-Dihydroxy vitamin D3 is an autocrine regulator of extracellular matrix turnover and growth factor release via ERp60-activated matrix vesicle matrix metalloproteinases**. *Cells Tissues Organs* 2009; 189:70-4.

282. Kimmel DB, Jee WS. **A quantitative histologic analysis of the growing long bone metaphysis**. *Calcif Tissue Int* 1980; 32:113-22.

283.   Ranly DM, *A Synopsis of Craniofacial Growth*. 2nd ed. 1988, Norwalk, Conneticut: Appleton and Lange.

284.   Proff P, Will F, Bokan I, Fanghanel J, Gedrange T. **Cranial base features in skeletal Class III patients**. *Angle Orthod* 2008; 78:433-9.

285.   Lei WY, Wong RW, Rabie AB. **Factors regulating endochondral ossification in the spheno-occipital synchondrosis**. *Angle Orthod* 2008; 78:215-20.

286.   Shum L, Wang X, Kane AA, Nuckolls GH. **BMP4 promotes chondrocyte proliferation and hypertrophy in the endochondral cranial base**. *Int J Dev Biol* 2003; 47:423-31.

287.   Rosenberg P, Arlis HR, Haworth RD, Heier L, Hoffman L, LaTrenta G. **The role of the cranial base in facial growth: experimental craniofacial synostosis in the rabbit**. *Plast Reconstr Surg* 1997; 99:1396-407.

288.   Cohen MM, Jr., Walker GF, Phillips C. **A morphometric analysis of the craniofacial configuration in achondroplasia**. *J Craniofac Genet Dev Biol Suppl* 1985; 1:139-65.

289.   Cohen MM, Jr., Kreiborg S. **Cranial size and configuration in the Apert syndrome**. *J Craniofac Genet Dev Biol* 1994; 14:153-62.

290.   Kreiborg S, Marsh JL, Cohen MM, Jr., Liversage M, Pedersen H, Skovby F, Borgesen SE, Vannier MW. **Comparative three-dimensional analysis of CT-scans of the calvaria and cranial base in Apert and Crouzon syndromes**. *J Craniomaxillofac Surg* 1993; 21:181-8.

291.   Tsukamoto Y, Kajii TS, Oonishi Y, Sugawara-Kato Y, Hirabayashi Y, Iida J. **Growth and development of the cranial base in mice that spontaneously develop anterior transverse crossbite**. *Am J Orthod Dentofacial Orthop* 2008; 134:676-83.

292.   Carinci F, Avantaggiato A, Curioni C. **Crouzon syndrome: cephalometric analysis and evaluation of pathogenesis**. *Cleft Palate Craniofac J* 1994; 31:201-9.

293.   Mundlos S, Otto F, Mundlos C, Mulliken JB, Aylsworth AS, Albright S, Lindhout D, Cole WG, Henn W, Knoll JH, Owen MJ, Mertelsmann R, Zabel BU, Olsen BR. **Mutations involving the transcription factor CBFA1 cause cleidocranial dysplasia**. *Cell* 1997; 89:773-9.

294.   Leonardi R, Cutrera A, Barbato E. **Rapid Maxillary Expansion Affects the Spheno-occipital Synchondrosis in Youngsters**. *Angle Orthod*; 80:106-10.

295. Rubin J, Schwartz Z, Boyan BD, Fan X, Case N, Sen B, Drab M, Smith D, Aleman M, Wong KL, Yao H, Jo H, Gross TS. **Caveolin-1 knockout mice have increased bone size and stiffness**. *J Bone Miner Res* 2007; 22:1408-18.

296. Hildebrand T, Laib A, Muller R, Dequeker J, Ruegsegger P. **Direct three-dimensional morphometric analysis of human cancellous bone: microstructural data from spine, femur, iliac crest, and calcaneus**. *J Bone Miner Res* 1999; 14:1167-74.

297. Coleman RM, Phillips JE, Lin A, Schwartz Z, Boyan BD, Guldberg RE. **Characterization of a small animal growth plate injury model using microcomputed tomography**. *Bone* 2010; 46:1555-63.

298. Mikic B, Amadei E, Rossmeier K, Bierwert L. **Sex matters in the establishment of murine tendon composition and material properties during growth**. *J Orthop Res* 2010; 28:631-8.

299. Ecklund K, Jaramillo D. **Imaging of growth disturbance in children**. *Radiol Clin North Am* 2001; 39:823-41.

300. van der Eerden BC, Gevers EF, Lowik CW, Karperien M, Wit JM. **Expression of estrogen receptor alpha and beta in the epiphyseal plate of the rat**. *Bone* 2002; 30:478-85.

301. Vanderschueren D, Vandenput L, Boonen S, Lindberg MK, Bouillon R, Ohlsson C. **Androgens and bone**. *Endocr Rev* 2004; 25:389-425.

302. Yuasa T, Kondo N, Yasuhara R, Shimono K, Mackem S, Pacifici M, Iwamoto M, Enomoto-Iwamoto M. **Transient activation of Wnt/{beta}-catenin signaling induces abnormal growth plate closure and articular cartilage thickening in postnatal mice**. *Am J Pathol* 2009; 175:1993-2003.

303. Zheng Q, Sebald E, Zhou G, Chen Y, Wilcox W, Lee B, Krakow D. **Dysregulation of chondrogenesis in human cleidocranial dysplasia**. *Am J Hum Genet* 2005; 77:305-12.

304. Estes BT, Diekman BO, Gimble JM, Guilak F. **Isolation of adipose-derived stem cells and their induction to a chondrogenic phenotype**. *Nat Protoc* 2010; 5:1294-311.

305. Gimble J, Guilak F. **Adipose-derived adult stem cells: isolation, characterization, and differentiation potential**. *Cytotherapy* 2003; 5:362-9.

306. Kim BS, Kang KS, Kang SK. **Soluble factors from ASCs effectively direct control of chondrogenic fate**. *Cell Prolif* 2010; 43:249-61.

307. Rubina K, Kalinina N, Efimenko A, Lopatina T, Melikhova V, Tsokolaeva Z, Sysoeva V, Tkachuk V, Parfyonova Y. **Adipose stromal cells stimulate**

angiogenesis via promoting progenitor cell differentiation, secretion of angiogenic factors, and enhancing vessel maturation. *Tissue Eng Part A* 2009; 15:2039-50.

308. Hanada K, Solchaga LA, Caplan AI, Hering TM, Goldberg VM, Yoo JU, Johnstone B. **BMP-2 induction and TGF-beta 1 modulation of rat periosteal cell chondrogenesis**. *J Cell Biochem* 2001; 81:284-94.

309. Takahashi T, Ogasawara T, Kishimoto J, Liu G, Asato H, Nakatsuka T, Uchinuma E, Nakamura K, Kawaguchi H, Chung UI, Takato T, Hoshi K. **Synergistic effects of FGF-2 with insulin or IGF-I on the proliferation of human auricular chondrocytes**. *Cell Transplant* 2005; 14:683-93.

310. Fischer J, Dickhut A, Rickert M, Richter W. **Human articular chondrocytes secrete parathyroid hormone-related protein and inhibit hypertrophy of mesenchymal stem cells in coculture during chondrogenesis**. *Arthritis Rheum* 2010; 62:2696-706.

311. Beier F, Ali Z, Mok D, Taylor AC, Leask T, Albanese C, Pestell RG, LuValle P. **TGFbeta and PTHrP control chondrocyte proliferation by activating cyclin D1 expression**. *Mol Biol Cell* 2001; 12:3852-63.

312. Minina E, Kreschel C, Naski MC, Ornitz DM, Vortkamp A. **Interaction of FGF, Ihh/Pthlh, and BMP signaling integrates chondrocyte proliferation and hypertrophic differentiation**. *Dev Cell* 2002; 3:439-49.

313. Im GI, Jung NH, Tae SK. **Chondrogenic differentiation of mesenchymal stem cells isolated from patients in late adulthood: the optimal conditions of growth factors**. *Tissue Eng* 2006; 12:527-36.

314. Awad HA, Halvorsen YD, Gimble JM, Guilak F. **Effects of transforming growth factor beta1 and dexamethasone on the growth and chondrogenic differentiation of adipose-derived stromal cells**. *Tissue Eng* 2003; 9:1301-12.

315. Pathi S, Rutenberg JB, Johnson RL, Vortkamp A. **Interaction of Ihh and BMP/Noggin signaling during cartilage differentiation**. *Dev Biol* 1999; 209:239-53.

316. Baum C, Dullmann J, Li Z, Fehse B, Meyer J, Williams DA, von Kalle C. **Side effects of retroviral gene transfer into hematopoietic stem cells**. *Blood* 2003; 101:2099-114.

317. Schumann D, Kujat R, Nerlich M, Angele P. **Mechanobiological conditioning of stem cells for cartilage tissue engineering**. *Biomed Mater Eng* 2006; 16:S37-52.

318. Kolambkar YM, Peister A, Soker S, Atala A, Guldberg RE. **Chondrogenic differentiation of amniotic fluid-derived stem cells**. *J Mol Histol* 2007; 38:405-13.

319. Dosier CR, Erdman CP, Park JH, Schwartz Z, Boyan BD, Guldberg RE. **Resveratrol effect on osteogenic differentiation of rat and human adipose derived stem cells in a 3-D culture environment**. *Journal of the Mechanical Behavior of Biomedical Materials* 2011; In Press.

320. Erdman CP, Dosier CR, Olivares-Navarrete R, Baile C, Guldberg RE, Schwartz Z, Boyan BD. **Effects of Resveratrol on Enrichment of Adipose-derived Stem Cells and their Differentiation to Osteoblasts in Two and Three Dimensional Cultures**. *Journal of Tissue Engineering and Regenerative Medicine* 2011; In Press.

321. Boyan BD, Schwartz Z, Swain LD, Carnes DL, Jr., Zislis T. **Differential expression of phenotype by resting zone and growth region costochondral chondrocytes in vitro**. *Bone* 1988; 9:185-94.

322. Lee CS, Moyer HR, Gittens RA, Williams JK, Boskey AL, Boyan BD, Schwartz Z. **Regulating in vivo calcification of alginate microbeads**. *Biomaterials* 2010; 31:4926-34.

323. Fitzgerald JB, Jin M, Dean D, Wood DJ, Zheng MH, Grodzinsky AJ. **Mechanical compression of cartilage explants induces multiple time-dependent gene expression patterns and involves intracellular calcium and cyclic AMP**. *J Biol Chem* 2004; 279:19502-11.

324. Takamizawa S, Maehata Y, Imai K, Senoo H, Sato S, Hata R. **Effects of ascorbic acid and ascorbic acid 2-phosphate, a long-acting vitamin C derivative, on the proliferation and differentiation of human osteoblast-like cells**. *Cell Biol Int* 2004; 28:255-65.

325. Hata R, Senoo H. **L-ascorbic acid 2-phosphate stimulates collagen accumulation, cell proliferation, and formation of a three-dimensional tissuelike substance by skin fibroblasts**. *J Cell Physiol* 1989; 138:8-16.

326. Tsutsumi K, Fujikawa H, Kajikawa T, Takedachi M, Yamamoto T, Murakami S. **Effects of L-ascorbic acid 2-phosphate magnesium salt on the properties of human gingival fibroblasts**. *J Periodontal Res* 2011.

327. Kwack MH, Shin SH, Kim SR, Im SU, Han IS, Kim MK, Kim JC, Sung YK. **l-Ascorbic acid 2-phosphate promotes elongation of hair shafts via the secretion of insulin-like growth factor-1 from dermal papilla cells through phosphatidylinositol 3-kinase**. *Br J Dermatol* 2009; 160:1157-62.

328. O'Keefe RJ, Puzas JE, Brand JS, Rosier RN. **Effects of transforming growth factor-beta on matrix synthesis by chick growth plate chondrocytes**. *Endocrinology* 1988; 122:2953-61.

329. Iruela-Arispe ML, Sage EH. **Endothelial cells exhibiting angiogenesis in vitro proliferate in response to TGF-beta 1**. *J Cell Biochem* 1993; 52:414-30.

330. Pepper MS, Vassalli JD, Orci L, Montesano R. **Biphasic effect of transforming growth factor-beta 1 on in vitro angiogenesis**. *Exp Cell Res* 1993; 204:356-63.

331. Grimsrud CD, Romano PR, D'Souza M, Puzas JE, Reynolds PR, Rosier RN, O'Keefe RJ. **BMP-6 is an autocrine stimulator of chondrocyte differentiation**. *J Bone Miner Res* 1999; 14:475-82.

332. Boden SD, Liu Y, Hair GA, Helms JA, Hu D, Racine M, Nanes MS, Titus L. **LMP-1, a LIM-domain protein, mediates BMP-6 effects on bone formation**. *Endocrinology* 1998; 139:5125-34.

333. Imabayashi H, Mori T, Gojo S, Kiyono T, Sugiyama T, Irie R, Isogai T, Hata J, Toyama Y, Umezawa A. **Redifferentiation of dedifferentiated chondrocytes and chondrogenesis of human bone marrow stromal cells via chondrosphere formation with expression profiling by large-scale cDNA analysis**. *Exp Cell Res* 2003; 288:35-50.

334. Loty S, Forest N, Boulekbache H, Sautier JM. **Cytochalasin D induces changes in cell shape and promotes in vitro chondrogenesis: a morphological study**. *Biol Cell* 1995; 83:149-61.

335. Demol J, Lambrechts D, Geris L, Schrooten J, Van Oosterwyck H. **Towards a quantitative understanding of oxygen tension and cell density evolution in fibrin hydrogels**. *Biomaterials* 2011; 32:107-18.

336. Lee EY, Xia Y, Kim WS, Kim MH, Kim TH, Kim KJ, Park BS, Sung JH. **Hypoxia-enhanced wound-healing function of adipose-derived stem cells: increase in stem cell proliferation and up-regulation of VEGF and bFGF**. *Wound Repair Regen* 2009; 17:540-7.

337. Shintani N, Hunziker EB. **Differential effects of dexamethasone on the chondrogenesis of mesenchymal stromal cells: influence of microenvironment, tissue origin and growth factor**. *Eur Cell Mater* 2011; 22:302-19; discussion 19-20.

338. Estes BT, Guilak F. **Three-dimensional culture systems to induce chondrogenesis of adipose-derived stem cells**. *Methods Mol Biol* 2011; 702:201-17.

339. Estes BT, Wu AW, Guilak F. **Potent induction of chondrocytic differentiation of human adipose-derived adult stem cells by bone morphogenetic protein 6**. *Arthritis Rheum* 2006; 54:1222-32.

340. Schweigerer L, Neufeld G, Friedman J, Abraham JA, Fiddes JC, Gospodarowicz D. **Capillary endothelial cells express basic fibroblast growth factor, a mitogen that promotes their own growth**. *Nature* 1987; 325:257-9.

341. Argun M, Oner M, Guney A, Halici M, Temizyurek O, Canoz O. **The healing of full-thickness articular cartilage defects in rabbits: successful results with fibroblast growth factor**. *Eklem Hastalik Cerrahisi* 2010; 21:147-52.

342. Coutu DL, Yousefi AM, Galipeau J. **Three-dimensional porous scaffolds at the crossroads of tissue engineering and cell-based gene therapy**. *J Cell Biochem* 2009; 108:537-46.

343. Dupont KM, Sharma K, Stevens HY, Boerckel JD, Garcia AJ, Guldberg RE. **Human stem cell delivery for treatment of large segmental bone defects**. *Proc Natl Acad Sci U S A* 2010; 107:3305-10.

344. Nerem RM. **Cell-based therapies: from basic biology to replacement, repair, and regeneration**. *Biomaterials* 2007; 28:5074-7.

345. Kim HK, Moran ME, Salter RB. **The potential for regeneration of articular cartilage in defects created by chondral shaving and subchondral abrasion. An experimental investigation in rabbits**. *J Bone Joint Surg Am* 1991; 73:1301-15.

346. Babensee JE, McIntire LV, Mikos AG. **Growth factor delivery for tissue engineering**. *Pharm Res* 2000; 17:497-504.

347. Aslani P, Kennedy RA. **Studies on diffusion in alginate gels .1. Effect of cross-linking with calcium or zinc ions on diffusion of acetaminophen**. *Journal of Controlled Release* 1996; 42:75-82.

348. Bhopatkar D, Anal AK, Stevens WF. **Ionotropic alginate beads for controlled intestinal protein delivery: effect of chitosan and barium counter-ions on entrapment and release**. *J Microencapsul* 2005; 22:91-100.

349. Grellier M, Granja PL, Fricain JC, Bidarra SJ, Renard M, Bareille R, Bourget C, Amedee J, Barbosa MA. **The effect of the co-immobilization of human osteoprogenitors and endothelial cells within alginate microspheres on mineralization in a bone defect**. *Biomaterials* 2009; 30:3271-8.

350. Hao X, Silva EA, Mansson-Broberg A, Grinnemo KH, Siddiqui AJ, Dellgren G, Wardell E, Brodin LA, Mooney DJ, Sylven C. **Angiogenic effects of sequential release of VEGF-A165 and PDGF-BB with alginate hydrogels after myocardial infarction**. *Cardiovasc Res* 2007; 75:178-85.

351. Swalla BJ, Solursh M. **Inhibition of limb chondrogenesis by fibronectin**. *Differentiation* 1984; 26:42-8.

352. Diekman BO, Rowland CR, Lennon DP, Caplan AI, Guilak F. **Chondrogenesis of adult stem cells from adipose tissue and bone marrow: induction by growth factors and cartilage-derived matrix**. *Tissue Eng Part A* 2010; 16:523-33.

353. Gagne TA, Chappell-Afonso K, Johnson JL, McPherson JM, Oldham CA, Tubo RA, Vaccaro C, Vasios GW. **Enhanced proliferation and differentiation of human articular chondrocytes when seeded at low cell densities in alginate in vitro**. *J Orthop Res* 2000; 18:882-90.

354. Estes BT, Wu AW, Storms RW, Guilak F. **Extended passaging, but not aldehyde dehydrogenase activity, increases the chondrogenic potential of human adipose-derived adult stem cells**. *J Cell Physiol* 2006; 209:987-95.

355. Schipper BM, Marra KG, Zhang W, Donnenberg AD, Rubin JP. **Regional anatomic and age effects on cell function of human adipose-derived stem cells**. *Ann Plast Surg* 2008; 60:538-44.

356. Aust L, Devlin B, Foster SJ, Halvorsen YD, Hicok K, du Laney T, Sen A, Willingmyre GD, Gimble JM. **Yield of human adipose-derived adult stem cells from liposuction aspirates**. *Cytotherapy* 2004; 6:7-14.

357. van Harmelen V, Skurk T, Rohrig K, Lee YM, Halbleib M, Aprath-Husmann I, Hauner H. **Effect of BMI and age on adipose tissue cellularity and differentiation capacity in women**. *Int J Obes Relat Metab Disord* 2003; 27:889-95.

358. Oedayrajsingh-Varma MJ, van Ham SM, Knippenberg M, Helder MN, Klein-Nulend J, Schouten TE, Ritt MJ, van Milligen FJ. **Adipose tissue-derived mesenchymal stem cell yield and growth characteristics are affected by the tissue-harvesting procedure**. *Cytotherapy* 2006; 8:166-77.

359. Ogawa R, Mizuno H, Watanabe A, Migita M, Hyakusoku H, Shimada T. **Adipogenic differentiation by adipose-derived stem cells harvested from GFP transgenic mice-including relationship of sex differences**. *Biochem Biophys Res Commun* 2004; 319:511-7.

360. Gimble JM, Guilak F. **Differentiation potential of adipose derived adult stem (ADAS) cells**. *Curr Top Dev Biol* 2003; 58:137-60.

361. Macchiarini P, Birchall M, Hollander A, Mantero S, Conconi MT. **Clinical transplantation of a tissue-engineered airway Authors' reply**. *Lancet* 2009; 373:718-9.

362. Mobasheri A, Csaki C, Clutterbuck AL, Rahmanzadeh M, Shakibaei M. **Mesenchymal stem cells in connective tissue engineering and regenerative medicine: applications in cartilage repair and osteoarthritis therapy**. *Histol Histopathol* 2009; 24:347-66.

363. Hou N, Cui P, Luo J, Ma R, Zhu L. **Tissue-engineered larynx using perfusion-decellularized technique and mesenchymal stem cells in a rabbit model**. *Acta Otolaryngol* 2011; 131:645-52.

364. Gomez-de-Antonio D, Zurita M, Santos M, Salas I, Vaquero J, Varela A. **Stem cells and bronchial stump healing**. *J Thorac Cardiovasc Surg* 2010; 140:1397-401.

365. McCarty RC, Xian CJ, Gronthos S, Zannettino AC, Foster BK. **Application of autologous bone marrow derived mesenchymal stem cells to an ovine model of growth plate cartilage injury**. *Open Orthop J* 2010; 4:204-10.

366. Endres M, Wenda N, Woehlecke H, Neumann K, Ringe J, Erggelet C, Lerche D, Kaps C. **Microencapsulation and chondrogenic differentiation of human mesenchymal progenitor cells from subchondral bone marrow in Ca-alginate for cell injection**. *Acta Biomater* 2010; 6:436-44.

367. Nasatzky E, Schwartz Z, Boyan BD, Soskolne WA, Ornoy A. **Sex-dependent effects of 17-beta-estradiol on chondrocyte differentiation in culture**. *J Cell Physiol* 1993; 154:359-67.

368. Raines AL, Olivares-Navarrete R, Wieland M, Cochran DL, Schwartz Z, Boyan BD. **Regulation of angiogenesis during osseointegration by titanium surface microstructure and energy**. *Biomaterials* 2010; 31:4909-17.

369. Moyer HR, Wang Y, Farooque T, Wick T, Singh KA, Xie L, Guldberg RE, Williams JK, Boyan BD, Schwartz Z. **A new animal model for assessing cartilage repair and regeneration at a nonarticular site**. *Tissue Eng Part A* 2010; 16:2321-30.

370. Palmer AW, Guldberg RE, Levenston ME. **Analysis of cartilage matrix fixed charge density and three-dimensional morphology via contrast-enhanced microcomputed tomography**. *Proc Natl Acad Sci U S A* 2006; 103:19255-60.

371. Deckers MM, Karperien M, van der Bent C, Yamashita T, Papapoulos SE, Lowik CW. **Expression of vascular endothelial growth factors and their receptors during osteoblast differentiation**. *Endocrinology* 2000; 141:1667-74.

372. Kim JH, Lee MC, Seong SC, Park KH, Lee S. **Enhanced proliferation and chondrogenic differentiation of human synovium-derived stem cells expanded with basic fibroblast growth factor**. *Tissue Eng Part A* 2011; 17:991-1002.

373. Perrier E, Ronziere MC, Bareille R, Pinzano A, Mallein-Gerin F, Freyria AM. **Analysis of collagen expression during chondrogenic induction of human bone marrow mesenchymal stem cells**. *Biotechnol Lett* 2011; 33:2091-101.

374. Nishizawa K, Imai S, Mimura T, Kubo M, Araki S, Shioji S, Takemura Y, Matsusue Y. **In-advance trans-medullary stimulation of bone marrow enhances spontaneous repair of full-thickness articular cartilage defects in rabbits**. *Cell Tissue Res* 2010; 341:371-9.

375. Matsumoto T, Cooper GM, Gharaibeh B, Meszaros LB, Li G, Usas A, Fu FH, Huard J. **Cartilage repair in a rat model of osteoarthritis through intraarticular transplantation of muscle-derived stem cells expressing bone morphogenetic protein 4 and soluble Flt-1**. *Arthritis Rheum* 2009; 60:1390-405.

376. Kubo S, Cooper GM, Matsumoto T, Phillippi JA, Corsi KA, Usas A, Li G, Fu FH, Huard J. **Blocking vascular endothelial growth factor with soluble Flt-1 improves the chondrogenic potential of mouse skeletal muscle-derived stem cells**. *Arthritis Rheum* 2009; 60:155-65.

377. Maes C, Stockmans I, Moermans K, Van Looveren R, Smets N, Carmeliet P, Bouillon R, Carmeliet G. **Soluble VEGF isoforms are essential for establishing epiphyseal vascularization and regulating chondrocyte development and survival**. *J Clin Invest* 2004; 113:188-99.

378. Ahmed N, Dreier R, Gopferich A, Grifka J, Grassel S. **Soluble signalling factors derived from differentiated cartilage tissue affect chondrogenic differentiation of rat adult marrow stromal cells**. *Cell Physiol Biochem* 2007; 20:665-78.

379. Bian L, Zhai DY, Mauck RL, Burdick JA. **Coculture of human mesenchymal stem cells and articular chondrocytes reduces hypertrophy and enhances functional properties of engineered cartilage**. *Tissue Eng Part A* 2011; 17:1137-45.

380. Hildner F, Concaro S, Peterbauer A, Wolbank S, Danzer M, Lindahl A, Gatenholm P, Redl H, van Griensven M. **Human adipose-derived stem cells contribute to chondrogenesis in coculture with human articular chondrocytes**. *Tissue Eng Part A* 2009; 15:3961-9.

381. Goosen MF. **Physico-chemical and mass transfer considerations in microencapsulation**. *Ann N Y Acad Sci* 1999; 875:84-104.

382. Mierisch CM, Cohen SB, Jordan LC, Robertson PG, Balian G, Diduch DR. **Transforming growth factor-beta in calcium alginate beads for the treatment of articular cartilage defects in the rabbit**. *Arthroscopy* 2002; 18:892-900.

383. Paek HJ, Campaner AB, Kim JL, Aaron RK, Ciombor DM, Morgan JR, Lysaght MJ. **In vitro characterization of TGF-beta1 release from genetically modified fibroblasts in Ca(2+)-alginate microcapsules**. *ASAIO J* 2005; 51:379-84.

384. Klokk TI, Melvik JE. **Controlling the size of alginate gel beads by use of a high electrostatic potential**. *J Microencapsul* 2002; 19:415-24.

385. Thornton AJ, Alsberg E, Hill EE, Mooney DJ. **Shape retaining injectable hydrogels for minimally invasive bulking**. *J Urol* 2004; 172:763-8.

386. Davey RB, Sparnon AL, Byard RW. **Unusual donor site reactions to calcium alginate dressings**. *Burns* 2000; 26:393-8.

387. Blumenthal NC. **Mechanisms of inhibition of calcification**. *Clin Orthop Relat Res* 1989:279-89.

388. Nancollas GH, Johnsson MA. **Calculus formation and inhibition**. *Adv Dent Res* 1994; 8:307-11.

389. Zuk PA, Zhu M, Ashjian P, De Ugarte DA, Huang JI, Mizuno H, Alfonso ZC, Fraser JK, Benhaim P, Hedrick MH. **Human adipose tissue is a source of multipotent stem cells**. *Mol Biol Cell* 2002; 13:4279-95.

390. Boyan BD, Kinney RC, Schwartz Z, *Microencapsulation of Cells in Hydrogels Using Electrostatic Potentials*, U.S.P.a.T. Office, Editor. 2008: United States. p. 1-11.

391. Ranly DM, McMillan J, Keller T, Lohmann CH, Meunch T, Cochran DL, Schwartz Z, Boyan BD. **Platelet-derived growth factor inhibits demineralized bone matrix-induced intramuscular cartilage and bone formation. A study of immunocompromised mice**. *J Bone Joint Surg Am* 2005; 87:2052-64.

392. Boyan BD, Wong KL, Wang L, Yao H, Guldberg RE, Drab M, Jo H, Schwartz Z. **Regulation of growth plate chondrocytes by 1,25-dihydroxyvitamin D3 requires caveolae and caveolin-1**. *J Bone Miner Res* 2006; 21:1637-47.

393. Dallas CE, Williams PL. **Barium: rationale for a new oral reference dose**. *J Toxicol Environ Health B Crit Rev* 2001; 4:395-429.

394. Recker RR, Lewiecki EM, Miller PD, Reiffel J. **Safety of bisphosphonates in the treatment of osteoporosis**. *Am J Med* 2009; 122:S22-32.

395. Yao S, McCarthy PL, Dunford LM, Roy DM, Brown K, Paplham P, Syta M, Lamonica D, Smiley S, Battiwalla M, Padmanabhan S, Hahn T. **High prevalence of early-onset osteopenia/osteoporosis after allogeneic stem cell transplantation and improvement after bisphosphonate therapy**. *Bone Marrow Transplant* 2008; 41:393-8.

396. Baicu SC, Taylor MJ. **Acid-base buffering in organ preservation solutions as a function of temperature: new parameters for comparing buffer capacity and efficiency**. *Cryobiology* 2002; 45:33-48.

397. Bonewald LF, Harris SE, Rosser J, Dallas MR, Dallas SL, Camacho NP, Boyan B, Boskey A. **von Kossa staining alone is not sufficient to confirm that mineralization in vitro represents bone formation**. *Calcif Tissue Int* 2003; 72:537-47.

398. Hartgerink JD, Beniash E, Stupp SI. **Self-assembly and mineralization of peptide-amphiphile nanofibers**. *Science* 2001; 294:1684-8.

399. Tomazic BB. **Physiochemical principles of cardiovascular calcification**. *Z Kardiol* 2001; 90 Suppl 3:68-80.

400. Crowell JA, Bowers GN, Jr. **Apparent binding of ionized calcium by various buffers**. *Clin Chem* 1985; 31:267-70.

401. Kakudo N, Shimotsuma A, Miyake S, Kushida S, Kusumoto K. **Bone tissue engineering using human adipose-derived stem cells and honeycomb collagen scaffold**. *J Biomed Mater Res A* 2008; 84:191-7.

402. Mann S, Archibald DD, Didymus JM, Douglas T, Heywood BR, Meldrum FC, Reeves NJ. **Crystallization at Inorganic-organic Interfaces: Biominerals and Biomimetic Synthesis**. *Science* 1993; 261:1286-92.

403. Lim YB, Kang SS, An WG, Lee YS, Chun JS, Sonn JK. **Chondrogenesis induced by actin cytoskeleton disruption is regulated via protein kinase C-dependent p38 mitogen-activated protein kinase signaling**. *J Cell Biochem* 2003; 88:713-8.

404. Woods A, Wang G, Beier F. **RhoA/ROCK signaling regulates Sox9 expression and actin organization during chondrogenesis**. *J Biol Chem* 2005; 280:11626-34.

405. Upton J, Sohn SA, Glowacki J. **Neocartilage derived from transplanted perichondrium: what is it?** *Plast Reconstr Surg* 1981; 68:166-74.

406. Engkvist O, Skoog V, Pastacaldi P, Yormuk E, Juhlin R. **The cartilaginous potential of the perichondrium in rabbit ear and rib. A comparative study in vivo and in vitro**. *Scand J Plast Reconstr Surg* 1979; 13:275-80.

407. Park J, Gelse K, Frank S, von der Mark K, Aigner T, Schneider H. **Transgene-activated mesenchymal cells for articular cartilage repair: a comparison of primary bone marrow-, perichondrium/periosteum- and fat-derived cells**. *J Gene Med* 2006; 8:112-25.

408. Van Osch GJ, Van Der Veen SW, Burger EH, Verwoerd-Verhoef HL. **Chondrogenic potential of in vitro multiplied rabbit perichondrium cells cultured in alginate beads in defined medium**. *Tissue Eng* 2000; 6:321-30.

409. Dounchis JS, Coutts RD, Amiel D. **Cartilage repair with autogenic perichondrium cell/polylactic acid grafts: a two-year study in rabbits**. *J Orthop Res* 2000; 18:512-5.

410. Wells LA, Sheardown H. **Extended release of high pI proteins from alginate microspheres via a novel encapsulation technique**. *Eur J Pharm Biopharm* 2007; 65:329-35.